Quantum Scattering Theory and Applications

A thesis presented

by

Adam Lupu-Sax

to

The Department of Physics

in partial fulfillment of the requirements

for the degree of

Doctor of Philosophy

in the subject of

Physics

Harvard University

Cambridge, Massachusetts

September 1998

Abstract

Scattering theory provides a convenient framework for the solution of a variety of problems. In this thesis we focus on the combination of boundary conditions and scattering potentials and the combination of non-overlapping scattering potentials within the context of scattering theory. Using a scattering t-matrix approach, we derive a useful relationship between the scattering t-matrix of the scattering potential and the Green function of the boundary, and the t-matrix of the combined system, effectively renormalizing the scattering t-matrix to account for the boundaries. In the case of the combination of scattering potentials, the combination of t-matrix operators is achieved via multiple scattering theory. We also derive methods, primarily for numerical use, for finding the Green function of arbitrarily shaped boundaries of various sorts.

These methods can be applied to both open and closed systems. In this thesis, we consider single and multiple scatterers in two dimensional strips (regions which are infinite in one direction and bounded in the other) as well as two dimensional rectangles. In 2D strips, both the renormalization of the single scatterer strength and the conductance of disordered many-scatterer systems are studied. For the case of the single scatterer we see non-trivial renormalization effects in the narrow wire limit. In the many scatterer case, we numerically observe suppression of the conductance beyond that which is explained by weak localization.

In closed systems, we focus primarily on the eigenstates of disordered many-scatterer systems. There has been substantial investigation and calculation of properties of the eigenstate intensities of these systems. We have, for the first time, been able to investigate these questions numerically. Since there is little experimental work in this regime, these numerics provide the first test of various theoretical models. Our observations indicate that the probability of large fluctuations of the intensity of the wavefunction are explained qualitatively by various field-theoretic models. However, quantitatively, no existing theory accurately predicts the probability of these fluctuations.

Acknowledgments

Doing the work which appears in this thesis has been a largely delightful way to spend the last five years. The financial support for my graduate studies was provided by a National Science Foundation Fellowship, Harvard University and the Harvard/Smithsonian Institute for Theoretical Atomic and Molecular Physics (ITAMP). Together, all of these sources provided me with the wonderful opportunity to study without being concerned about my finances.

My advisor, Rick Heller, is a wonderful source of ideas and insights. I began working with Rick four years ago and I have learned an immense amount from him in that time. From the very first time we spoke I have felt not only challenged but respected. One particularly nice aspect of having Rick as an advisor is his ready availability. More than one tricky part of this thesis has been sorted out in a marathon conversation in Rick's office. I cannot thank him enough for all of his time and energy.

In the last five years I have had the great pleasure of working not only with Rick himself but also with his post-docs and other students. Maurizio Carioli was a post-doc when I began working with Rick. There is much I cannot imagine having learned so quickly or so well without him, particularly about numerical methods. Lev Kaplan, a student and then post-doc in the group, is an invaluable source of clear thinking and uncanny insight. He has also demonstrated a nearly infinite patience in discussing our work. My class-mate Neepa Maitra and I began working with Rick at nearly the same time and have been partners in this journey. Neepa's emotional support and perceptive comments and questions about my work have made my last five years substantially easier. Alex Barnett, Bill Bies, Greg Fiete, Jesse Hersch, Bill Hosten and Areez Mody, all graduate students in Rick's group, have given me wonderful feedback on this and other work. The substantial post-doc contingent in the group, Michael Haggerty, Martin Naraschewski and Doron Cohen have been equally helpful and provided very useful guidance along the way.

At the time I began graduate school I was pleasantly surprised by the cooperative spirit among my classmates. Many of us spent countless hours discussing physics and sorting out problem sets. Among this crowd I must particularly thank Martin Bazant, Brian Busch, Sheila Kannappan, Carla Levy, Carol Livermore, Neepa Maitra, Ron Rubin and Glenn Wong for making many late nights bearable and, oftentimes, fun. I must particularly thank Martin, Carla and Neepa for remaining great friends and colleagues in the years that followed. I have had the great fortune to make good friends at various stages in my life and I am honored to count these three among them.

It is hard to imagine how I would have done all of this without my fiancée, Kiersten Conner. Our upcoming marriage has been a singular source of joy during the process of writing this thesis. Her unflagging support and boundless sense of humor have kept me centered throughout graduate school.

My parents, Chip Lupu and Jana Sax, have both been a great source of support and encouragement throughout my life and the last five years have been no exception. The rest of my family has also been very supportive, particularly my grandmothers, Sara Lupu and Pauline Sax and my step-mother Nancy Altman. It saddens me that neither of my grandfathers, Dave Lupu or N. Irving Sax, are alive to see this moment in my life but I thank them both for teaching me things that have helped bring me this far.

Citations to Previously Published Work

Portions of chapter 4 and Appendix B have appeared in

"Quantum scattering from arbitrary boundaries," M.G.E da Luz, A.S. Lupu-Sax and E.J. Heller, Physical Review B, **56**, no. 3, pages 2496-2507 (1997).

Contents

List of Figures

List of Tables

Chapter 1

Introduction and Outline of the Thesis

1.1 Introduction

"Scattering" evokes a simple image. We begin with separate objects which are far apart and moving towards each other. After some time they collide and then travel away from each other and, eventually, are far apart again. We don't necessarily care about the details of the collision except insofar as we can predict from it where and how the objects will end up. This picture of scattering is the first one we physicists learn and it is a beautiful example of the power of conservation laws [25]:

> In many cases the laws of conservation of momentum and energy alone can be used to obtain important results concerning the properties of various mechanical processes. It should be noted that these properties are independent of of the particular type of interaction between the particles involved.
>
> L.D. Landau, *Mechanics* (1976)

Quantum scattering is a more subtle affair. Even elastic scattering, which does not change the internal state of the colliding particles, is more complicated than its classical counterpart [26]:

> In classical mechanics, collisions of two particles are entirely determined by their velocities and impact parameter (the distance at which they would pass if they did not interact). In quantum mechanics, the very wording of the problem must be changed, since in motion with definite velocities the concept of the path

> is meaningless, and therefore so is the impact parameter. The purpose of the theory is here only to calculate the probability that, as a result of the collision, the particles will deviate (or, as we say, be *scattered*) through any given angle.
>
> L.D. Landau, *Quantum Mechanics* (1977)

This so-called "differential cross-section," the probability that a particle is scattered through a given angle, is the very beginning of any treatment of scattering, whether classical or quantum mechanical.

However, the cross-section is not the part of scattering theory upon which we intend to build. It is instead the separation between free propagation (motion without interaction) and collision. That this idea should lead to so much useful physics is at first surprising. However the Schrödinger equation, like any other wave equation does not make this split particularly obvious. It is indeed some work to recover the benefits of this division from the complications of wave mechanics.

In fact, the idea of considering separately the free or unperturbed motion of particles and their interaction is usually considered in the context of perturbation theory. Unsurprisingly then, the very first quantum mechanical scattering theory was Born's perturbative treatment of scattering [6] which he developed not to solve scattering problems but to address the completeness of the new quantum theory:

> Heisenberg's quantum mechanics has so far been applied exclusively to the calculation of stationary states and vibration amplitudes associated with transitions...
>
> Bohr has already directed attention to the fact that all difficulties of principle associated with the quantum approach...occur in the interactions of atoms at short distances and consequently in collision processes... I therefore attack the problem of investigating more closely the interaction of the free particle (α-ray or electron) and an arbitrary atom and of determining whether a description of a collision is not possible within the framework of existing theory.
>
> M. Born, *On The Quantum Mechanics of Collisions* (1926)

Later in the same note, the connection to perturbation theory is made clear: "One can then show with the help of a simple perturbation calculation that there is a uniquely determined solution of the Schrödinger equation with a potential V..."

Scattering theory has developed substantially since Born's note appeared. Still, we will take great advantage of one common feature of perturbations and scattering. The

division between perturbation and unperturbed motion is one of definition, not of physics. Much of the art in using perturbation theory comes from recognizing just what division of the problem will give a solvable unperturbed motion and a convergent perturbation series.

In scattering, the division between free motion and collision seems much more natural and less flexible. However, many of the methods developed in this thesis take advantage of what little flexibility there is in order to solve some problems not traditionally in the purview of scattering theory as well as attack some which are practically intractable by other means.

1.2 Outline of the Thesis

In chapter 2 we begin with a nearly traditional development of scattering theory. The development deviates from the traditional only in that it generalizes the usual definitions and calculations to arbitrary spatial dimension. This is done mostly because the applications in the thesis require two dimensional scattering theory but most readers will be familiar with the three dimensional version. A generalized derivation allows the reader to assume $d = 3$ and check that the results are what they expect and then use the $d = 2$ version when necessary. I have as much as possible followed standard textbook treatments of each piece of scattering theory. I am confident that the d-dimensional generalizations presented here exist elsewhere in the literature. For instance, work using so-called "hyper-spherical coordinates" to solve few-body problems certainly contains much of the same information, though perhaps not in the same form.

The final two sections of chapter 2 are a bit more specific. The first, section 2.4, deals with zero range interactions, a tool which will be used almost constantly throughout the remainder of the thesis. It is our hope that the treatment of the zero range interaction in this section is considerably simpler than the various formalisms which are typically used. After this section follows a short section explicitly covering some details of scattering in two dimensions.

After this introductory material, we move on to the central theoretical work in scattering theory. Chapter 3 covers two extensions of ordinary scattering theory. The first is multiple scattering theory. A system with two or more distinct scatterers can be handled by solving the problem one scatterer at a time and then combining those results. This is a nice example of the usefulness of the split between propagation and collision made

above. Multiple scattering theory takes this split and some very clever book-keeping and solves a very complex problem. Our treatment differs somewhat from Fadeev's in order to emphasize similarities with the techniques introduced in section 3.2.

A separation between free propagation and collision and its attendant book-keeping have more applications than multiple scattering. In section 3.2 we develop the central new theoretic tool of this work, the renormalized t-matrix. In multiple scattering theory, we used the separation between propagation and collision to piece together the scattering from multiple targets, in essence complicating the collision phase. With appropriate renormalization, we can also change what we mean by propagation. We derive the relevant equations and spend some time exploring the consequences of the transformation of propagation. The sort of change we have in mind will become clearer as we discuss the applications.

Both of the methods explained in chapter 3 involve combining solved problems and thus solving a more complicated problem. The techniques discussed in chapter 4 are used to solve some problems from scratch. In their simplest form they have been applied to mesoscopic devices and it is hoped that the more complex versions might be applied to look at dirty and clean superconductor normal metal junctions.

We begin working on applications in chapter 5 where we explore our first non-trivial example of scatterer renormalization, the change in scatterer strength of a scatterer placed in a wire. We begin with a fixed two-dimensional zero range interaction of known scattering amplitude. We place this scatterer in an infinite straight wire (channel of finite width). Both the scatterer in free space and the wire without scatterer are solved problems. Their combination is more subtle and brings to bear the techniques developed in 3.2. Much of the chapter is spent on necessary applied mathematics, but it concludes with the interesting case of a wire which is narrower than the cross-section of the scatterer (which has zero-range so can fit in any finite width wire). This calculation could be applied to a variety of systems, hydrogen confined on the surface of liquid helium for one.

Next, in chapter 6 we treat the case of the same scatterer placed in a completely closed box. While a wire is still open and so a scattering problem, it is at first hard to imagine how a closed system could be. After all, the differential cross-section makes no sense in a closed system. Wonderfully, the equations developed for scattering in open systems are still valid in a closed one and give, in some cases, very useful methods for examining properties of the closed system. As with the previous chapter, much of the work in this chapter is preliminary but necessary applied mathematics. Here, we first confront the oddity of using

the equations of scattering theory to find the energies of discrete stationary states. With only one scatterer and renormalization, this turns out to be mathematically straightforward. Still, this idea is important enough to the sequel that we do numerical computations on the case of ground state energies of a single scatterer in a rectangle with perfectly reflective walls. Using the methods presented here, this is simply a question of solving one non-linear equation. We compare the energies so calculated to numerically calculated ground state energies of hard disks in rectangles computed with a standard numerical technique. This is intended both as confirmation that we can extract discrete energies from these methods and as an illustration of the similarity between isolated zero range interactions and hard disks.

Having spent a substantial amount of time on examples of renormalization, we return multiple scattering to the picture as well. We will consider in particular disordered sets of fixed scatterers, motivated, for example, by quenched impurities in a metal. Before we apply these techniques to disordered systems, we consider disordered systems themselves in chapter 7. Here we define and explain some important concepts which are relevant to disordered systems as well as discuss some theoretical predictions about various properties of disordered systems.

We return to scattering in a wire in chapter 8. Instead of the single scatterer of chapter 5 we now place many scatterers in the same wire and consider the conductance of the disordered region of the wire. We use this to examine weak localization, a quantum effect present only in the presence of time-reversal symmetry. In the final chapter we use the calculations of this chapter as evidence that our disorder potential has the properties we would predict from a hard disk model, as we explored for the one scatterer case in chapters 5 and 6.

Our final application is presented in chapter 9. Here we examine some very specific properties of disordered scatterers in a rectangle. These calculations were in some sense the original inspiration for this work and are its most unique achievement. Here calculations are performed which are, apparently, out of reach of other numerical methods. These calculations both confirm some theoretical expectations and confound others leaving a rich set of new questions. At the same time, it is also the most specialized application we consider, and not one with the broad applicability of the previous applications.

In chapter 10 we present some conclusions and ideas for future extensions of the ideas in this work. This is followed (after the bibliography) by a variety of technical appen-

dices which are referred to throughout the body of the thesis.

Chapter 2

Quantum Scattering Theory in d-Dimensions

> The methods of progress in theoretical physics have undergone a vast change during the present century. The classical tradition has been to consider the world to be an association of observable objects (particles, fluids, fields, etc.) moving about according to definite laws of force, so that one could form a mental picture in space and time of the whole scheme. This led to a physics whose aim was to make assumptions about the mechanism and forces connecting these observable objects, to account for their behavior in the simplest possible way. It has become increasingly evident in recent times, however, that nature works on a different plan. Her fundamental laws do not govern the world as it appears in our mental picture in any very direct way, but instead they control a substratum of which we cannot form a mental picture without introducing irrelevancies.
>
> P.A.M. Dirac, *Quantum Mechanics* (1930)

Nearly all physics experiments measure the outcome of scattering events. This ubiquity has made scattering theory a crucial part of any standard quantum text. Not surprisingly, all the attention given to scattering processes has led to the invention of very powerful theoretical tools, many of which can be applied to problems which are not traditional scattering problems.

After this chapter, our use of scattering theory will involve mostly non-traditional uses of the tools of scattering theory. However, those tools are so important to what follows that we must provide at least a summary of the basic theory.

There are nearly as many approaches to scattering as authors of quantum mechanics textbooks. As is typical, we begin by defining the problem and the idea of the

scattering cross-section. We then make the somewhat lengthy calculation which relates the differential cross-section to the potential of the scatterer. We perform this calculation for arbitrary spatial dimension.

At first, this may seem like more work than necessary to review scattering theory. However, in what follows we will frequently use two dimensional scattering theory. While we could have derived everything in two dimensions, we would then have lost the reassuring feeling of seeing familiar three dimensional results. The arbitrary dimension derivation gives us both.

We proceed to consider the consequences of particle conservation, or unitarity, and derive the d-dimensional optical theorem. It is interesting to note that for both this calculation and the previous one, the dimensional dependence enters only through the asymptotic expansion of the plane wave.

Once we have this machinery in hand, we proceed to discuss point scatterers or "zero range interactions" as they will play a large role in various applications which follow. In the final section we focus briefly on two dimensions since two dimensional scattering theory is the stage on which all the applications play out.

2.1 Cross-Sections

At first, we will generalize to arbitrary spatial dimension a calculation from [28] (pp. 803-5) relating the scattering cross-section to matrix elements of the potential, V.

We consider a domain in which the stationary solutions of the Schrödinger equation are known, and we label these by $\phi_{\mathbf{k}}$. For example, in free space,

$$\phi_{\mathbf{k}}(\mathbf{r}) = e^{i\mathbf{k}\cdot\mathbf{r}}. \tag{2.1}$$

In the presence of a potential there will be new stationary solutions, labeled by $\psi_{\mathbf{k}}^{(\pm)}$ where superscript plus and minus labels the asymptotic behavior of ψ in terms of d-dimensional spherical waves. In particular

$$H\left|\psi_{\mathbf{k}}^{\pm}\right\rangle = E\left|\psi_{\mathbf{k}}^{\pm}\right\rangle, \tag{2.2}$$

and

$$\psi_{\mathbf{k}}^{\pm}(\mathbf{r}) \overset{r\to\infty}{\sim} \phi_{\mathbf{k}}(\mathbf{r}) + f_{\mathbf{k}}^{\pm}(\Omega)\frac{e^{\pm ikr}}{r^{\frac{d-1}{2}}}. \tag{2.3}$$

We assume the plane wave, $\phi_{\mathbf{k}}(\mathbf{r})$ is wide but finite so we may always go far enough away that scattering at any angle but $\Omega = 0$ involves only the scattered part of the wave. Since the flux of the *scattered* wave is $\mathbf{j} = \mathrm{Im}\{\psi^*_{\mathrm{scatt}} \nabla \psi_{\mathrm{scatt}}\} = \hat{\mathbf{r}} |f^{\pm}_{\mathbf{k}}(\Omega)|^2 / r^{d-1}$, the probability per unit time of a scattered particle to cross a surface element $d\mathbf{a}$ is

$$v \frac{\left| f^{\pm}_{\mathbf{k}}(\Omega) \right|^2}{r^{d-1}} d\mathbf{a} = v \left| f^{\pm}_{\mathbf{k}}(\Omega) \right|^2 d\Omega. \tag{2.4}$$

But the current density (flux per unit area) in the incident wave is v so

$$\frac{d\sigma_{a \to b}}{d\Omega} = |f^{+}_{\mathbf{k}_a}(\Omega_b)|^2 \tag{2.5}$$

If unambiguous, we will replace $\mathbf{k}_a$ and $\mathbf{k}_b$ by a and b respectively.

We proceed to develop a relationship between the scattering function f and matrix elements of the potential, $\hat{V}$. This will lead us to the definition of the so-called scattering t-matrix.

Consider two potentials, $U(\mathbf{r})$ and $\tilde{U}(\mathbf{r})$ (both of which fall off faster $1/r$). We will show

$$\left\langle \tilde{\psi}^-_b \left| \left(\hat{U} - \hat{\tilde{U}} \right) \right| \psi^+_a \right\rangle \equiv \int \tilde{\psi}^-_b(\mathbf{r}) \left[U(\mathbf{r}) - \tilde{U}(\mathbf{r}) \right] \psi^+_a(\mathbf{r}) \, d\mathbf{r} \tag{2.6}$$

$$= \frac{\hbar^2}{m} i^{\frac{d+1}{2}} (2\pi)^{\frac{d-1}{2}} k^{\frac{3-d}{2}} \left[f^+_a(\Omega_b) - \tilde{f}^-_b(\Omega_a)^* \right]. \tag{2.7}$$

We begin with the Schrödinger equation for the ψ's:

$$\left(-\frac{\hbar^2}{2m} \nabla^2 + \hat{\tilde{U}} \right) \tilde{\psi}^-_b = E \tilde{\psi}^-_b \tag{2.8}$$

$$\left(-\frac{\hbar^2}{2m} \nabla^2 + \hat{U} \right) \psi^+_a = E \psi^+_a. \tag{2.9}$$

We multiply (2.9) by $\left(\tilde{\psi}^-_b \right)^*$ and the complex conjugate of (2.8) by ψ^+_a and then subtract the latter equation from the former. Since $U(\mathbf{r})$ and $\tilde{U}(\mathbf{r})$ are real, we have (dropping the a's and b's when unambiguous)

$$-\frac{\hbar^2}{2m} \left\{ \left(\tilde{\psi}^- \right)^* \nabla^2 \psi^+ - \left[\nabla^2 \left(\tilde{\psi}^- \right)^* \right] \psi^{(+)} \right\}] + \left(\tilde{\psi}^- \right)^* \left(U - \hat{\tilde{U}} \right) \psi^{(+)} = 0. \tag{2.10}$$

We integrate over a sphere of radius R centered at the origin to get

$$\left\langle \tilde{\psi}^- \left| \left(\hat{U} - \hat{\tilde{U}} \right) \right| \psi^+ \right\rangle = \frac{\hbar^2}{2m} \lim_{R \to \infty} \int_{r<R} \left\{ \left(\tilde{\psi}^- \right)^* \nabla^2 \psi^+ - \left[\nabla^2 \left(\tilde{\psi}^- \right)^* \right] \psi^+ \right\} \, d\mathbf{r}. \tag{2.11}$$

For two functions of $\mathbf{r}$, ξ_1 and ξ_2 we define

$$W\left[\xi_1,\xi_2\right] \equiv \xi_1 \frac{\partial \xi_2}{\partial r} - \xi_2 \frac{\partial \xi_1}{\partial r}, \tag{2.12}$$

and its integral over the d-dimensional sphere

$$\begin{aligned} \left\{\xi_1,\xi_2\right\}_R &\equiv \int W\left[\xi_1,\xi_2\right]|_{r=R}\, R^{d-1}\, d\Omega \\ &= \int \left[\xi_1 \nabla \xi_2 - \xi_2 \nabla \xi_1\right] \cdot \, d\mathbf{a} \end{aligned}$$

Green's Theorem implies

$$\left\{\xi_1,\xi_2\right\}_R = \int_{r<R} \left[\xi_1(\nabla^2 \xi_2) - (\nabla^2 \xi_1)\xi_2\right] \, d\mathbf{r}, \tag{2.13}$$

and thus equation (2.11) may be written

$$\left\langle \tilde{\psi}^- \left| \left(\hat{U} - \hat{\tilde{U}}\right) \right| \psi^+ \right\rangle = \frac{\hbar^2}{2m} \lim_{R\to\infty} \left\{ \left(\tilde{\psi}^-\right)^*, \psi^+ \right\}_R. \tag{2.14}$$

To evaluate the surface integral, we substitute the asymptotic form of the ψ's:

$$\begin{aligned} \lim_{R\to\infty} \left\{ \left(\tilde{\psi}^-\right)^*, \psi^+ \right\}_R = & \overbrace{\lim_{R\to\infty} \left\{ e^{-i\mathbf{k}_b\cdot\mathbf{r}}, e^{i\mathbf{k}_a\cdot\mathbf{r}} \right\}_R}^{1} + \overbrace{\lim_{R\to\infty} \left\{ e^{-i\mathbf{k}_b\cdot\mathbf{r}}, f^+ \frac{e^{ikr}}{r^{\frac{d-1}{2}}} \right\}_R}^{2} + \\ & \underbrace{\lim_{R\to\infty} \left\{ (f^-)^* \frac{e^{ikr}}{r^{\frac{d-1}{2}}}, e^{i\mathbf{k}_a\cdot\mathbf{r}} \right\}_R}_{3} + \underbrace{\lim_{R\to\infty} \left\{ (f^-)^* \frac{e^{ikr}}{r^{\frac{d-1}{2}}}, f^+ \frac{e^{ikr}}{r^{\frac{d-1}{2}}} \right\}_R}_{4}. \end{aligned} \tag{2.15}$$

Since we are performing these integrals at large r, we require only the asymptotic form of the plane wave and only in a form suitable for integration. We find this form by doing a stationary phase integral [41] of an arbitrary function of solid angle against a plane wave at large $\mathbf{r}$. That is,

$$I = \lim_{\mathbf{r}\to\infty} \int e^{i\mathbf{k}\cdot\mathbf{r}} f(\Omega_r)\, d\Omega_r \tag{2.16}$$

We find the points where the exponential varies most slowly as a function of the integration variables, in this case the angles in Ω_r. Since $\mathbf{k}\cdot\mathbf{r} = kr\cos\left(\theta_{kr}\right)$ the stationary phase points will occur at $\theta_{kr} = 0, \pi$. We expand the exponential around each of these points to yield

$$\begin{aligned} I \approx & \int \exp\left(ikr \Pi_{i=1}^{d-1} \left[1 - \frac{1}{2}\left(\theta_k^{(i)} - \theta_r^{(i)}\right)^2 \right] \right) f(\Omega_r)\, d\Omega_r + \\ & \int \exp\left(ikr \Pi_{i=1}^{d-1} \left[-1 + \frac{1}{2}\left(\theta_k^{(i)} - \theta_r^{(i)}\right)^2 \right] \right) f(\Omega_r)\, d\Omega_r. \end{aligned}$$

We perform all the integrals using complex Gaussian integration to yield an asymptotic form for the plane wave (to be used only in an integral):

$$e^{i\mathbf{k}\cdot\mathbf{r}} \text{ “}\sim\text{”} \left(\frac{2\pi}{ikr}\right)^{\frac{d-1}{2}} \left[\delta\left(\Omega_r - \Omega_k\right) e^{ikr} + i^{d-1}\delta\left(\Omega_r + \Omega_k\right) e^{-ikr}\right], \tag{2.17}$$

where $\Omega_r + \Omega_k = 0$ (enforced by the second δ-function) means that $\hat{\mathbf{r}} = -\hat{\mathbf{k}}$.

We'll attack the integrals in equation (2.15) one at a time, beginning with

$$\lim_{R\to\infty} \left\{e^{-i\mathbf{k}_b\cdot\mathbf{r}}, e^{i\mathbf{k}_a\cdot\mathbf{r}}\right\}_R = \int iR^d \left(\mathbf{k}_a + \mathbf{k}_b\right)\cdot\hat{\mathbf{r}}\, e^{iR(\mathbf{k}_a - \mathbf{k}_b)\cdot\hat{\mathbf{r}}}\, d\Omega. \tag{2.18}$$

Since $\mathbf{k}_a$ and $\mathbf{k}_b$ have the same length, $\mathbf{k}_a + \mathbf{k}_b$ is orthogonal to $\mathbf{k}_a - \mathbf{k}_b$. Thus, we can always choose our angular integrals such that our innermost integral is exactly zero:

$$\left\{e^{-i\mathbf{k}_b\cdot\mathbf{r}}, e^{i\mathbf{k}_a\cdot\mathbf{r}}\right\}_R \sim \int_0^{2\pi} \cos\theta e^{ia\sin\theta}\, d\theta = \frac{1}{ia}\int_0^{2\pi} \frac{\partial}{\partial\theta}\left(e^{ia\sin\theta}\right) d\theta = \frac{1}{ia}\, e^{ia\sin\theta}\Big|_0^{2\pi} = 0. \tag{2.19}$$

Thus $\lim_{R\to\infty}\left\{e^{-i\mathbf{k}_b\cdot\mathbf{r}}, e^{i\mathbf{k}_a\cdot\mathbf{r}}\right\}_R = 0$.

We can do the second integral using the asymptotic form of the plane wave. The only contribution comes from the *incoming* part of the plane wave,

$$\lim_{R\to\infty}\left\{e^{-i\mathbf{k}_b\cdot\mathbf{r}}, f^+\frac{e^{ikr}}{r^{(d-1)/2}}\right\}_R = \pi^{\frac{d-1}{2}} k^{\frac{3-d}{2}} (2i)^{\frac{d+1}{2}} f^+\left(\Omega_b\right). \tag{2.20}$$

We can do the third integral exactly the same way. Again, only the incoming part of the plane wave contributes,

$$\lim_{R\to\infty}\left\{\left(f^-\right)^* \frac{e^{ikr}}{r^{\frac{d-1}{2}}}, e^{i\mathbf{k}_a\cdot\mathbf{r}}\right\}_R = -\pi^{\frac{d-1}{2}} k^{\frac{3-d}{2}} (2i)^{\frac{d+1}{2}} f^-\left(-\Omega_a\right)^*. \tag{2.21}$$

The fourth integral is zero since both waves are purely outgoing. Thus

$$\lim_{R\to\infty}\left\{\left(\hat{\psi}^-\right)^*, \psi^{(+)}\right\}_R = (2i)^{\frac{d+1}{2}} \pi^{\frac{d-1}{2}} k^{\frac{3-d}{2}} \left[f^+\left(\Omega_b\right) - f^-\left(-\Omega_a\right)^*\right], \tag{2.22}$$

which, when substituted into equation 2.14 gives the desired result.

Let's apply the result (2.7) to the case $\hat{U} = \hat{V}$, $\hat{\tilde{U}} = 0$. We have

$$\left\langle \phi_b \left| \hat{V} \right| \psi_a^+ \right\rangle = \frac{\hbar^2}{m}(2\pi)^{\frac{d-1}{2}} k^{\frac{3-d}{2}} i^{\frac{d+1}{2}} f_a^+\left(\Omega_b\right). \tag{2.23}$$

We also apply it to the case $\hat{U} = 0$, $\hat{\tilde{U}} = \hat{V}$, yielding

$$\left\langle \psi_b^- \left| \hat{V} \right| \phi_a \right\rangle = \frac{\hbar^2}{m}(2\pi)^{\frac{d-1}{2}} k^{\frac{3-d}{2}} i^{\frac{d+1}{2}} f_b^-\left(-\Omega_a\right)^*. \tag{2.24}$$

Finally, we apply (2.7) to the case $\hat{U} = \hat{V}$, $\hat{\tilde{U}} = \hat{V}$, yielding

$$f_a^+ (\Omega_b) = f_b^- (-\Omega_a)^* . \tag{2.25}$$

We now have

$$\frac{d\sigma_{a\to b}}{d\Omega} = \left| f_a^+ (\Omega_b) \right|^2 = \frac{m^2}{\hbar^4} (2\pi)^{1-d} k^{d-3} \left| \left\langle \phi_b \left| \hat{V} \right| \psi_a^+ \right\rangle \right|^2 . \tag{2.26}$$

Since the d-dimensional density of states per unit energy is

$$\varrho_d(E) = \frac{1}{(2\pi\hbar)^d} p^{d-1} \frac{dp}{dE} = \frac{1}{(\pi\hbar)^d} (\hbar k)^{d-1} \frac{m}{\hbar k} = \frac{m}{(2\pi\hbar)^d} (\hbar k)^{d-2} \tag{2.27}$$

and the initial velocity is $\hbar k/m$, we can write our final result for cross-section in a more useful form,

$$\frac{d\sigma_{a\to b}}{d\Omega} = \frac{2\pi}{\hbar v} \left| \left\langle \phi_b \left| \hat{V} \right| \psi_a^+ \right\rangle \right|^2 \varrho_d(E), \tag{2.28}$$

where all of the dimensional dependence is in the density of states and the matrix element.

For purposes which will become clear later, it is useful to define the so-called "t-matrix" operator, $\hat{t}^{\pm}(E)$ such that

$$\hat{t}^{\pm}(E) \left| \phi_a \right\rangle = \hat{V} \left| \psi_a^{\pm} \right\rangle , \tag{2.29}$$

and our result may be re-written as

$$\frac{d\sigma_{a\to b}}{d\Omega} = \frac{2\pi}{\hbar v} \left| \left\langle \phi_b \left| \hat{t}^{\pm}(E) \right| \phi_a \right\rangle \right|^2 \varrho_d(E). \tag{2.30}$$

2.2 Unitarity and the Optical Theorem

The fact that particles are neither created nor destroyed in the scattering process forces a specific relationship between the total cross-section, $\sigma = \int (d\sigma/d\Omega) d\Omega$ and $f(\Omega = 0)$. It is to this relationship that we now turn. This section closely follows a calculation from [26] (pp. 508-510) but, as in the previous section, generalizes it to arbitrary spatial dimension.

Suppose the incoming wave is a linear combination of plane waves, as in

$$\psi_{\text{incoming}} = \int F(\Omega') e^{i\mathbf{k}\cdot\mathbf{r}'} \, d\Omega' \tag{2.31}$$

So the asymptotic outgoing form of ψ is (where $f(\Omega_a, \Omega_b) = f_a^{(+)}(\Omega_b)$ is simply a more symmetric notation than used in the previous section)

$$\psi \sim \int F(\Omega') e^{i\mathbf{k}\cdot\mathbf{r}'} + \frac{e^{ikr}}{r^{\frac{d-1}{2}}} \int F(\Omega') f\left(\Omega', \Omega\right) d\Omega, \tag{2.32}$$

For large r we can use the asymptotic for of the plane wave (2.17) to perform the first integral. We then get

$$\psi \sim \left(\frac{2\pi}{ikr}\right)^{\frac{d-1}{2}} \left[F(\Omega)e^{ikr} + i^{d-1}F(-\Omega)e^{-ikr}\right] + \frac{e^{ikr}}{r^{\frac{d-1}{2}}} \int F(\Omega')f^{(+)}\left(\Omega', \Omega\right) d\Omega. \tag{2.33}$$

We can write this more simply (without the common factor $(2\pi/ik)^{(d-1)/2}$)

$$\frac{e^{-ikr}}{r^{\frac{d-1}{2}}}F(-\Omega) + i^{1-d}\frac{e^{ikr}}{r^{\frac{d-1}{2}}}\left(\hat{S}F\right)(\Omega) \tag{2.34}$$

where

$$\hat{S} = 1 + \left(\frac{ik}{2\pi}\right)^{\frac{d-1}{2}} \hat{f} \tag{2.35}$$

and $\hat{f}$ is an integral operator defined by

$$\left(\hat{f}F\right)(\Omega) = \int F(\Omega')f(\Omega', \Omega)\, d\Omega' \tag{2.36}$$

$\hat{S}$ is called the "scattering operator" or "S-matrix." Since the scattering process is elastic, we must have as many particles going into the center as there are going out of the center. and the normalization of these two waves must be the same. So $\hat{S}$ is unitary:

$$\hat{S}\hat{S}^{\dagger} = 1. \tag{2.37}$$

Substituting (2.35) we get

$$i^{\frac{d-1}{2}}\hat{f} + i^{\frac{1-d}{2}}\hat{f}^{\dagger} = -\left(\frac{k}{2\pi}\right)^{\frac{d-1}{2}} \hat{f}^{\dagger}\hat{f}, \tag{2.38}$$

then divide through by i:

$$i^{\frac{d-3}{2}}\hat{f} - i^{\frac{3-d}{2}}\hat{f}^{\dagger} = i\left(\frac{k}{2\pi}\right)^{\frac{d-1}{2}} \hat{f}^{\dagger}\hat{f}. \tag{2.39}$$

We apply the definition (2.36) and have

$$i^{\frac{d-3}{2}}f(\Omega, \Omega')\left[-i^{\frac{d-3}{2}}f(\Omega', \Omega)\right]^{*} = i\left(\frac{k}{2\pi}\right)^{\frac{d-1}{2}} \int f(\Omega, \Omega'')f^{*}(\Omega', \Omega'')d\Omega'', \tag{2.40}$$

the unitarity condition for scattering.

For $\Omega = \Omega'$ we have

$$\mathrm{Im}\left\{i^{\frac{d-3}{2}}f(\Omega, \Omega)\right\} = \frac{1}{2}\left(\frac{k}{2\pi}\right)^{\frac{d-1}{2}} \int |f(\Omega, \Omega)|^2 d\Omega = \frac{1}{2}\left(\frac{k}{2\pi}\right)^{\frac{d-1}{2}} \sigma \tag{2.41}$$

which is the optical theorem.

Invariance under time reversal (interchanging initial and final states and the direction of motion of each wave) implies

$$\begin{aligned} S(\Omega, \Omega') &= S(-\Omega', -\Omega) \\ f(\Omega, \Omega') &= f(-\Omega', -\Omega) \end{aligned}$$

which is called the "reciprocity theorem."

2.3 Green Functions

The cross-section is frequently the end result of a scattering calculation. However, for most of the applications considered here, we are concerned with more general properties of scattering solutions. For these applications, the machinery of Green functions is invaluable and is introduced in this section. Much of the material in this section is covered in greater detail in [10]. A more formal development, some examples and some useful Green function identities are given in appendix A.

The idea of a Green function operator is both simple and beautiful. Suppose a quantum system is initially (at $t = 0$) in state $|\psi\rangle$. What is the amplitude that the system will be found in state $|\psi'\rangle$ a time τ later? This information is contained in the time-domain Green function. We can take the Fourier transform of this function with respect to τ and get the energy-domain Green function. It is the energy domain Green function which we explore in some detail below.

We define an energy-domain Green function operator for the Hamiltonian H via

$$(z - \hat{H} \pm i\epsilon)\hat{G}^{(\pm)}(z) = \hat{1} \tag{2.42}$$

where "$\hat{1}$" is the identity operator. The $\pm i\epsilon$ is used to avoid difficulties when z is equal to an eigenvalue of $\hat{H}$. ϵ is always taken to zero at the end of a calculation. We frequently use the Green function operator, $\hat{G}_o^{\pm}(z)$ corresponding to $\hat{H} = \hat{H}_o = -\frac{\hbar^2}{2m}\nabla^2$.

Consider the Hamiltonian $\hat{H} = \hat{H}_o + \hat{V}$. As in the previous section, we denote the eigenstates of $\hat{H}_o$ by $|\phi_a\rangle$ and the eigenstates of $\hat{H}$ by $|\psi_a^{\pm}\rangle$. These satisfy

$$\hat{H}_o |\phi_a\rangle = E_a |\phi_a\rangle \tag{2.43}$$

$$\hat{H} |\psi_a^{\pm}\rangle = E_a |\psi_a^{\pm}\rangle , \tag{2.44}$$

We claim

$$\left|\psi_a^{\pm}\right\rangle = \left|\phi_a\right\rangle + \hat{G}_o^{\pm}(E_a)\hat{V}\left|\psi_a^{\pm}\right\rangle. \tag{2.45}$$

The claim is easily proved by applying the operator $(E_a - \hat{H}_o \pm i\epsilon)$ to the left of both sides of the equation since $(E_a - \hat{H}_o \pm i\epsilon)\left|\psi_a^{\pm}\right\rangle = \hat{V}\left|\psi_a^{\pm}\right\rangle$, $(E_a - \hat{H}_o \pm i\epsilon)\left|\phi_a\right\rangle = 0$ and $(E_a - \hat{H}_o \pm i\epsilon)G_o^{\pm}(E_a) = \hat{1}$. Using the t-matrix, we can re-write this as

$$\left|\psi_a^{\pm}\right\rangle = \left|\phi_a\right\rangle + \hat{G}_o^{\pm}(E_a)\hat{t}^{\pm}(E_a)\left|\phi_a\right\rangle, \tag{2.46}$$

but we can also re-write (2.45) by iterating it (inserting the right hand side into itself as $\left|\psi_a^{\pm}\right\rangle$) to give

$$\left|\psi_a^{\pm}\right\rangle = \left|\phi_a\right\rangle + \hat{G}_o^{\pm}(E_a)\hat{V}\left[\left|\phi_a\right\rangle + \hat{G}_o^{\pm}\hat{V}\left|\phi_a\right\rangle + \cdots\right]. \tag{2.47}$$

From (2.46, 2.47) we get a useful expression for the t-matrix:

$$\hat{t}^{\pm}(z) = \hat{V} + \hat{V}\hat{G}_o^{\pm}(z)\hat{V} + \hat{V}\hat{G}_o^{\pm}(z)\hat{V}\hat{G}_o^{\pm}(z)\hat{V} + \cdots. \tag{2.48}$$

We factor out the first $\hat{V}$ in each term and sum the geometric series to yield

$$\begin{aligned}
\hat{t}^{\pm}(z) &= \hat{V}\left[1 - \hat{V}\hat{G}_o^{\pm}(z)\right]^{-1} \\
&= \hat{V}\left\{\hat{G}_o^{\pm}(z)\left[\left\{\hat{G}_o^{\pm}\right\}^{-1}(z) - \hat{V}\right]\right\} \\
&= \hat{V}\left(z - \hat{H}_o - \hat{V} \pm i\epsilon\right)^{-1}\left\{\hat{G}_o^{\pm}\right\}^{-1}(z) \\
&= \hat{V}G^{\pm}(z)\left(z - \hat{H}_o \pm i\epsilon\right),
\end{aligned} \tag{2.49}$$

where (2.49) is frequently used as the *definition* of $\hat{t}^{\pm}(z)$.

We now proceed to develop an equation for the Green function itself.

$$G^{\pm}(z) = \left(z - \hat{H}_o - \hat{V} \pm i\epsilon\right)^{-1} \tag{2.50}$$

$$= \left\{\left(z - \hat{H}_o \pm i\epsilon\right)\left[1 - \left(z - \hat{H}_o \pm i\epsilon\right)^{-1}\hat{V}\right]\right\}^{-1} \tag{2.51}$$

$$= \left[1 - \left(z - \hat{H}_o \pm i\epsilon\right)^{-1}\hat{V}\right]^{-1}(z - H_o \pm i\epsilon)^{-1} \tag{2.52}$$

$$= \left[1 - \hat{G}_o^{\pm}(z)\hat{V}\right]^{-1}\hat{G}_o^{\pm}(z). \tag{2.53}$$

We expand $\left[1 - \hat{G}_o^{\pm}(z)\hat{V}\right]^{-1}$ in a power series to get

$$\hat{G}^{\pm}(z) = \hat{G}_o^{\pm}(z) + \hat{G}_o^{\pm}(z)\hat{V}\hat{G}_o^{\pm}(z) + \hat{G}_o^{\pm}(z)\hat{V}\hat{G}_o^{\pm}(z)\hat{V}\hat{G}_o^{\pm}(z) + \cdots, \tag{2.54}$$

which we can re-write as

$$\hat{G}^{\pm}(z) = \hat{G}_o^{\pm}(z) + \hat{G}_o^{\pm}(z)\hat{V}\left[\hat{G}_o^{\pm}(z) + \hat{G}_o^{\pm}(z)\hat{V}\hat{G}_o^{\pm}(z) + \cdots\right] \tag{2.55}$$

$$= \hat{G}_o^{\pm}(z) + \hat{G}_o^{\pm}(z)\hat{V}\hat{G}^{\pm}(z), \tag{2.56}$$

and, using (2.49) and the definition of $\hat{G}_o^{(\pm)}(z)$, we get a t-matrix version of this equation, namely

$$\hat{G}^{\pm}(z) = \hat{G}_o^{\pm}(z) + \hat{G}_o^{\pm}(z)\hat{t}^{\pm}(z)\hat{G}_o^{\pm}(z). \tag{2.57}$$

2.3.1 Green functions in the position representation

So far we have looked at Green functions only as operators rather than functions in a particular basis. Quite a few of the specific calculations which follow are performed in position representation and it is useful to identify some general properties of d-dimensional Green functions. We begin from the defining equation (2.42), re-written in position space:

$$\left[z + \frac{\hbar^2}{2m}\nabla_{\mathbf{r}}^2 - V(\mathbf{r}) \pm i\epsilon\right] G^{\pm}(\mathbf{r}, \mathbf{r}'; z) = \delta\left(\mathbf{r} - \mathbf{r}'\right). \tag{2.58}$$

We begin by considering an arbitrary point $\mathbf{r}_o$ and a small ball around it, $B(\mathbf{r}_o, \eta)$. We can move the origin to $\mathbf{r}_o$ and then integrate both sides of (2.58) over this volume:

$$\int_{B(\eta)} \left[z + \frac{\hbar^2}{2m}\nabla_{\mathbf{r}}^2 - V(\mathbf{r}_o - \mathbf{r}) \pm i\epsilon\right] G^{\pm}(\mathbf{r}_o - \mathbf{r}, \mathbf{0}; z)\, d\mathbf{r} = \int_{B(\eta)} \delta\left(\mathbf{r}\right)\, d\mathbf{r}. \tag{2.59}$$

We now consider the $\eta \to 0$ limit of this equation. We assume that the potential is finite and continuous at $\mathbf{r} = \mathbf{r}_o$ so $V(\mathbf{r}_o - \mathbf{r})$ can be replaced by $V(\mathbf{r}_o)$ in the integrand. We can safely assume that

$$\lim_{\eta \to 0} \int_{B(\mathbf{r}_o, \eta)} G^{\pm}(\mathbf{r}_o - \mathbf{r}, \mathbf{0}; z)\, d\mathbf{r} = 0 \tag{2.60}$$

since, if it weren't, the integral of the $\nabla^2 G$ term would be infinite. We are left with

$$\lim_{\eta \to 0} \int_{B(\mathbf{0}, \epsilon)} \nabla^2 G^{\pm}(\mathbf{r_o} - \mathbf{r}, \mathbf{0}; z)\, d\mathbf{r} = \frac{2m}{\hbar^2}. \tag{2.61}$$

We can apply Gauss's theorem to the integral and get

$$\lim_{\eta \to 0} \int_{\partial B(\mathbf{0}, \eta)} \frac{\partial}{\partial r} G^{\pm}(\mathbf{r}_o - \mathbf{r}, \mathbf{0}; z) \eta^{d-1} d\Omega = \frac{2m}{\hbar^2}. \tag{2.62}$$

So we have a first order differential equation for $G^{\pm}(\mathbf{r}, \mathbf{r}'; z)$ for small $\rho = |\mathbf{r} - \mathbf{r}_o|$:

$$\frac{\partial}{\partial \rho} G^{\pm}(\rho; z) = \frac{2m}{\hbar^2} \frac{\rho^{1-d}}{S_d}, \tag{2.63}$$

where

$$S_d = \frac{2\pi^{d/2}}{\Gamma(d/2)} \tag{2.64}$$

is the surface area of the unit sphere in d-dimensions (this is easily derived by taking the product of d Gaussian integrals and then performing the integral in radial coordinates, see e.g., [32], pp. 501-2).

In particular, in two dimensions the Green function has a logarithmic singularity "on the diagonal" where $\mathbf{r} \to \mathbf{r}'$. In $d > 2$ dimensions, the diagonal singularity goes as r^{2-d}. It is worth noting that in one dimension there is no diagonal singularity in G.

As a consequence of our derivation of the form of the singularity in G, we have proved that, as long as $V(\mathbf{r})$ is finite and continuous in the neighborhood of $\mathbf{r}*$, then

$$\lim_{\mathbf{r}\to\mathbf{r}*} G^{\pm}(\mathbf{r}, \mathbf{r}*; z) - G_o^{\pm}(\mathbf{r}, \mathbf{r}*; z) < \infty \tag{2.65}$$

This will prove useful in what follows.

2.4 Zero Range Interactions

For the sake of generality, up to now we have not mentioned a specific potential. However, in what follows we will frequently be concerned with potentials which interact with the particle only at one point. Such interactions are frequently called "zero range interactions" or "zero range potentials."

There is a wealth of literature about zero range interactions in two and three dimensions, including [7, 13, 2], their application to chaotic systems, for example [3, 38] and their applications in statistical mechanics, including [31, 22].

In one dimension, the Dirac delta function is just such a point interaction. However, in two or more dimensions, the Dirac delta function does not scatter incoming particles at all. This is shown for two dimensions in [7]. In more than one dimension, the wavefunction can be set to 0 at a single point without perturbing the wavefunction since an infinitesimal part of the singular solution to the Schrödinger equation can force ψ to be zero at a single point. Since there are no singular solutions to the Schrödinger equation in one dimension, the one dimensional Dirac δ-function does scatter, as is well known.

Trying to construct a potential corresponding to a zero-range interaction can be quite challenging. The formal construction of these interactions leads one to consider the Hamiltonian in a reduced space where some condition must be satisfied at the point of

interaction. Choosing the wave function to be zero at the interaction point leads to the mathematical formalism of "self-adjoint extension theory" so named because the restriction of the Hamiltonian operator to the space of functions which are zero at a point leaves a non self-adjoint Hamiltonian. The family of possible extensions which would make the Hamiltonian self-adjoint correspond to various scattering strengths [2].

Much of this complication arises because of an attempt to write the Hamiltonian explicitly or to make sure that every possible zero range interaction is included in the formalism. To avoid these details, we consider a very limited class of zero-range interactions, namely zero-range s-wave scatterers.

Consider a scatterer placed at the origin in two dimensions. We assume the physical scatterer being modeled is small compared to the wavelength, $lambda = 2\pi/\sqrt{E}$ and thus scatters only s-waves. So we can write the t-matrix (for a general discussion of t-matrices see, e. g., [35]),

$$\hat{t}^{\pm}(z) = |\mathbf{0}\rangle\, s^{\pm}(z)\, \langle \mathbf{0}|\,. \tag{2.66}$$

If, at energy E, $|\phi\rangle$ is incident on the scatterer, we write the full wave (incident plus scattered) as

$$|\psi^{\pm}\rangle = |\phi\rangle + \hat{G}_o^{\pm}(E)\hat{t}^{\pm}(E)\,|\phi\rangle\,, \tag{2.67}$$

which may be written more clearly in position space

$$\psi^{\pm}(\mathbf{r}) = \phi(\mathbf{r}) + G_o^{\pm}(\mathbf{r}, \mathbf{0}; E)s^{\pm}(E)\phi(\mathbf{0}). \tag{2.68}$$

At this point the scatterer strength, $s^{\pm}(z)$, is simply a complex constant. We can consider $s^{\pm}(E)$ as it relates to the cross-section. From equation (2.26) with $V\,|\psi_a^{\pm}\rangle$ replaced by $t^{\pm}\,|\phi_a\rangle$ we have (since $\left\langle \phi_b \left| \hat{t}^{\pm}(z) \right| \phi_a \right\rangle = s^{\pm}(z)$)

$$\sigma(E) = S_d \frac{m^2}{\hbar^4}(2\pi)^{1-d}k^{d-3}|s^{\pm}(E)|^2 \tag{2.69}$$

where S_d, the surface area of the unit sphere in d dimensions is given by (2.64).

We also consider another length scale, akin to the three-dimensional scattering length. Instead of looking at the asymptotic form of the wave function, we look at the s-wave component of the wave function by using $R_o(r)$, the regular part of the s-wave solution to the Schrödinger equation, as an incident wave. We then have

$$\psi^{+}(\mathbf{r}) = R_o(r) + G_o^{+}(r; E)s(E)R_o(0) \tag{2.70}$$

We define an effective radius, a_e, as the smallest positive real number solution of

$$R_o(x) + s^+(E)G_o^+(x,E) = 0. \tag{2.71}$$

We can reverse this line of argument and find $s^+(E)$ for a particular a_e

$$s^(E) = -\frac{R_o(a_e)}{G_o^+(a_e;E)} \tag{2.72}$$

The point interaction accounts for the s-wave part of the scattering from a hard disk of radius a_e. From equation 2.69 the cross section of a point interaction with effective radius a_e is

$$\sigma(E) = S_d \frac{m^2}{\hbar^4}(2\pi)^{1-d}k^{d-3}\left|\frac{R_o(a_a)}{G_o^+(a_e;E)}\right|^2 \tag{2.73}$$

but this is exactly the s-wave part of the cross-section of a hard disk in d-dimensions. Though zero range interactions have the cross-section of hard disks, depending on the dimension and the value of $s^+(E)$, the point interaction can be attractive or repulsive.

In three dimensions, the $E \to 0$ limit of a_e exists and is the scattering length as defined in the modern sense [36]. It is interesting to note that other authors, e.g., Landau and Lifshitz in their classic quantum mechanics text [26] define the scattering length as we have defined the effective radius, namely as the first node in the s-wave part of the wave function. These definitions are equivalent in three dimensions but quite different in two where the modern scattering length is not well defined but, for any finite energy, the effective radius is.

2.5 Scattering in two dimensions

While many of the techniques discussed in the following chapters are quite general, just as we will frequently use point interactions in applications due to their simplicity, we will usually work in two dimensions either because of intrinsic interest (as in chapter 9) or because numerical work is easier in two dimensions than three.

Since most people are familiar with scattering in three dimensions, some of the features of two dimensional scattering theory are, at first, surprising. For example

$$\frac{d\sigma_{a\to b}}{d\Omega} = \left|f_a^+(\Omega_b)\right|^2 = \frac{m^2}{\hbar^4}\frac{1}{2\pi k}\left|\langle\phi_b|V|\psi_a^+\rangle\right|^2, \tag{2.74}$$

implying that as $E \to 0$, $\sigma(E) \sim \lambda \to \infty$ which is very different from three dimensions. Also, the optical theorem in two dimensions is different than its three-dimensional counterpart:

$$\mathrm{Im}\left\{e^{-\frac{i\pi}{4}} f(\Omega,\Omega)\right\} = \sqrt{\frac{k}{8\pi}}\sigma. \tag{2.75}$$

We have already mentioned the difference in the diagonal behavior of the two and three dimensional Green functions. The logarithmic singularity in G prevents a simple idea of scattering length from making sense in two dimensions. This singularity comes from the form of the free-scattering solutions in two dimensions (the equivalent of the three-dimensional spherical harmonics). In two dimensions the free scattering solutions are Bessel and Neumann functions of integer order. The small argument and asymptotic properties of these functions are summarized in appendix E.

In two dimensions, we can write the specific form of the causal t-matrix for a zero range interaction with effective radius a_e located at $\mathbf{r}_s$: $\hat{t}^+(E) = |\mathbf{r}_s\rangle\, s^+(E)\, \langle \mathbf{r}_s|$ with

$$s^+(E) = -i\frac{4J_o(\sqrt{E}a)}{H_o^{(1)}(\sqrt{E}a)}, \tag{2.76}$$

where $J_o(x)$ is the Bessel function of zero$^{\text{th}}$ order and $H_o^{(1)}(x)$ is the Hankel function of zero$^{\text{th}}$ order.

Chapter 3

Scattering in the Presence of Other Potentials

In chapter 2 we presented scattering theory in its traditional form. We computed cross-sections and scattering wave functions. In this chapter, we focus more on the tools of scattering theory and broaden their applicability. Here we begin to see the great usefulness of the book-keeping associated with t-matrices. We will also begin to use scattering theory for closed systems, an idea which is confusing at the outset, but quite natural after some practice.

3.1 Multiple Scattering

Multiple scattering theory has been applied to many problems, from neutron scattering by atoms in a lattice to the scattering of electrons on surfaces [21]. In most applications, the individual scatterers are treated in the s-wave limit, i.e., they can be replaced by zero range interactions of appropriate strength. We begin our discussion of multiple scattering theory with this special case before moving on to the general case in the following section. This is done for pedagogical reasons. The general case involves some machinery which gets in the way of understanding important physical concepts.

3.1.1 Multiple Scattering of Zero Range Interactions

Consider a domain, with given boundary conditions and potential, in which the Green function operator, $\hat{G}_B^{\pm}(z)$ for the Schrödinger equation is known. Into this domain we place N zero range interactions located at the positions $\{\mathbf{r}_i\}$ and with t-matrices $\{\hat{t}_i^+(z)\}$ given by $\hat{t}_i^+(z) = s_i^+(z)\,|\mathbf{r}_i\rangle\,\langle\mathbf{r}_i|$. At energy E, $\phi(\mathbf{r})$ is incident on the set of scatterers and we want to find the outgoing solutions of the Schrödinger equation, $\psi^+(\mathbf{r})$, in the presence of the scatterers.

We define the functions $\alpha_i^+(\mathbf{r})$ via

$$\alpha_i^+(\mathbf{r}) = \phi(\mathbf{r}) + \sum_{j\neq i} G_B^+(\mathbf{r},\mathbf{r}_j;E)s_j^+(E)\alpha_j^+(\mathbf{r}_j). \tag{3.1}$$

The number $\alpha_i(\mathbf{r}_i)$ represents the amplitude of the wave that hits scatterer i last. That is, $\alpha_i^+(\mathbf{r})$ is determined by all the other $\alpha_j^+(\mathbf{r})$ $(j \neq i)$. The full solution can be written in terms of the $\alpha_i^+(\mathbf{r}_i)$:

$$\psi^+(\mathbf{r}) = \phi(\mathbf{r}) + \sum_{i} G_B^+(\mathbf{r},\mathbf{r}_i;E)s_i^+(E)\alpha_i^+(\mathbf{r}_i). \tag{3.2}$$

The expression (3.1) gives a set of linear equations for the $\alpha_i(\mathbf{r}_i)$. This can be seen more simply from the following substitution and rearrangement:

$$\alpha_i^+(\mathbf{r}_i) - \sum_{j\neq i} G_B^+(\mathbf{r}_i,\mathbf{r}_j;E)s_j^+(E)\alpha_j^+(\mathbf{r}_j) = \phi(\mathbf{r}_i). \tag{3.3}$$

We define the N-vectors $\mathbf{a}$ and $\mathbf{b}$ via $\mathbf{a}_i = \alpha_i^+(\mathbf{r}_i)$ and $\mathbf{b}_i = \phi(\mathbf{r}_i)$ and rewrite (3.3) as a matrix equation

$$\left[\mathbf{1} - \mathbf{t}^+(E)\bar{\mathbf{G}_\mathbf{B}}^+(E)\right]\mathbf{a} = \mathbf{b}, \tag{3.4}$$

where $\mathbf{1}$ is the $N \times N$ identity matrix, $\mathbf{t}(E)$ is a diagonal $N \times N$ matrix defined by $(\mathbf{t})_{ii} = s_i(E)$ and $\bar{\mathbf{G}}_B^+(E)$ is an off-diagonal propagation matrix given by

$$\left(\bar{\mathbf{G}}_B^+(E)\right)_{ij} = \begin{cases} G_B^+(\mathbf{r}_i,\mathbf{r}_j;E) & \text{for} \quad i \neq j \\ 0 & \text{for} \quad i = j. \end{cases} \tag{3.5}$$

More explicitly, $\mathbf{1} - \mathbf{t}^+(E)\bar{\mathbf{G}}_B^+(E)$ is given by (suppressing the "E" and "+"):

$$\mathbf{1} - \mathbf{t}\bar{\mathbf{G}}_B = \begin{pmatrix} 1 & -s_1G_B(\mathbf{r}_1,\mathbf{r}_2) & \cdots & -s_1G_B(\mathbf{r}_1,\mathbf{r}_N) \\ -s_2G(\mathbf{r}_2,\mathbf{r}_1) & 1 & \cdots & -s_2G_B(\mathbf{r}_2,\mathbf{r}_N) \\ \vdots & \vdots & \ddots & \vdots \\ -s_NG_B(\mathbf{r}_N,\mathbf{r}_1) & -s_NG_B(\mathbf{r}_N,\mathbf{r}_2) & \cdots & 1 \end{pmatrix}. \tag{3.6}$$

The off-diagonal propagator is required since the individual t-matrices account for the diagonal propagation. That is, the scattering events where the incident wave hits scatterer i, propagates freely and then hits scatterer i again are already counted in $\hat{t}_i$.

We can look at this diagrammatically. We use a solid line to indicate causal propagation and a dashed line ending with an "$\times_i$" to indicate scattering from the i^{th} scatterer. With this "dictionary," we can write the infinite series form of $\hat{t}_i$ as

$\hat{t}_i =$ 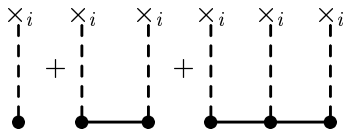 (3.7)

so $\hat{G}_o + \hat{G}_o \hat{t}_i \hat{G}_o$ has the following terms:

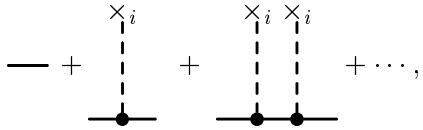 (3.8)

Now we consider multiple scattering from two scatterers. The Green function has the direct term, terms from just scatterer 1, terms from just scatterer 2 and terms involving both, i.e.,

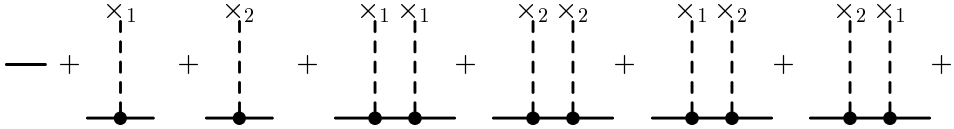 (3.9)

The off diagonal propagator appearing in multiple scattering theory allows to add only the terms involving more than one scatterer, since the one scatterer terms are already accounted for in each $\hat{t}_i^+$.

If, at energy E, $\mathbf{1} - \mathbf{t}^+ \bar{\mathbf{G}}_B$ is invertible, we can solve the matrix equation (3.4) for $\mathbf{a}$:

$$\mathbf{a} = \left[\mathbf{1} - \mathbf{t}\bar{\mathbf{G}}_B\right]^{-1} \mathbf{b}, \tag{3.10}$$

where the inverse is here is just ordinary matrix inversion. We substitute (3.10) into (3.2) to get

$$\psi^+(\mathbf{r}) = \phi(\mathbf{r}) + \sum_{ij} G_B^+(\mathbf{r}, \mathbf{r}_i; E) s_i^+(E) \left(\left[\mathbf{1} - \mathbf{t}^+(E)\bar{\mathbf{G}}_B^+(E)\right]^{-1} \right)_{ij} \phi(\mathbf{r}_j). \tag{3.11}$$

We can define a multiple scattering t-matrix

$$\hat{t}^+(E) = \sum_{ij} |\mathbf{r}_i\rangle \left(\mathbf{t}^+(E)\right)_{ii} \left(\left[\mathbf{1} - \mathbf{t}(E)\bar{\mathbf{G}}_B^+(E)\right]^{-1} \right)_{ij} \langle \mathbf{r}_j | , \tag{3.12}$$

and write the full solution in a familiar form

$$|\psi^+\rangle = |\phi\rangle + \hat{G}_B^+(E)\hat{t}^+(E)\,|\phi\rangle\,. \tag{3.13}$$

An analogous solution can be constructed for $|\psi^-\rangle$ by replacing all the outgoing solutions in the above with incoming solutions (superscript "+" goes to superscript "-").

We have shown that scattering from N zero range interactions is solved by the inversion of an $N \times N$ matrix. As we will see below, generalized multiple scattering theory is not so simple. It does, however, rely on the inversion of an operator on a smaller space than that in which the problem is posed.

3.1.2 Generalized Multiple Scattering Theory

We now consider placing N scatterers (not necessarily zero range), with t-matrices $\hat{t}_i^{\pm}(z)$, in a background domain with Green function operator $\hat{G}_B^{\pm}(z)$. In what follows, the argument z is suppressed.

We assume that each t-matrix is identically zero outside some domain $\mathcal{C}_i$ and we further assume that the $\mathcal{C}_i$ do not overlap, that is $\mathcal{C}_i \cap \mathcal{C}_j = \emptyset$ for all $i \neq j$. We define the scattering space, $\mathcal{S} = \bigcup_i \mathcal{C}_i$. In the case of N zero range scatterers, the scattering space is just N discrete points. The definition of the scattering space allows a separation between propagation and scattering events.

As in the point scatterer case, we consider the function, $\alpha_i(\mathbf{r}) = \langle \mathbf{r} \,|\alpha_i\rangle$, representing the amplitude which hits the i$^{\text{th}}$ scatterer last. We can write a set of linear equations for the α_i:

$$\left|\alpha_i^{\pm}\right\rangle = |\phi\rangle + \hat{G}_B^{\pm} \sum_{j \neq i} \hat{t}_j^{\pm} \left|\alpha_j^{\pm}\right\rangle, \tag{3.14}$$

where $\psi(\mathbf{r})$ is the incident wave. As in the simpler case above, the full solution can be written in terms of the $\alpha_i^{\pm}$ via

$$|\psi^{\pm}\rangle = |\phi\rangle + \hat{G}_B^{\pm} \sum_{i} \hat{t}_i^{\pm} \left|\alpha_i^{\pm}\right\rangle. \tag{3.15}$$

The derivation begins to get complicated here. Since the scattering space is not necessarily discrete, we cannot map our problem onto a finite matrix. We now begin to create a framework in which the results of the previous section can be generalized.

We define the projection operators, $\hat{P}_i$, which are projectors onto the ith scatterer, that is

$$\left\langle \mathbf{r} \left| \hat{P}_i \right| f \right\rangle = \begin{cases} f(\mathbf{r}) & \text{if} \quad \mathbf{r} \in \mathcal{C}_i \\ 0 & \text{if} \quad \mathbf{r} \notin \mathcal{C}_i \end{cases}. \tag{3.16}$$

Also we define a projection operator for the whole scattering space, $\hat{\mathbf{P}} = \sum_{i=1}^{N} \hat{P}_i$.

We can project our equations for the $\alpha_i^{\pm}(\mathbf{r})$ onto each scatterer in order to get equations analogous to the matrix equation we had for $\alpha_i(\mathbf{r}_i)$ in the previous section:

$$\hat{P}_i \left|\alpha_i^{\pm}\right\rangle = \hat{P}_i \left|\phi\right\rangle + \hat{P}_i \hat{G}_B^{\pm} \sum_{j\neq i} \hat{t}_j^{\pm} \left|\alpha_j^{\pm}\right\rangle, \tag{3.17}$$

and, fur purely formal reasons, we define a quantity analogous to the vector $\mathbf{a}$ in the zero range scatterer case:

$$\left|\Psi^{\pm}\right\rangle = \sum_i \hat{P}_i \left|\alpha_i^{\pm}\right\rangle. \tag{3.18}$$

We note that $\Psi(\mathbf{r})$ is non-zero on the scattering space only.

With these definitions, we can develop a linear equation for $|\Psi^{\pm}\rangle$. We begin by summing (3.17) over the N scatterers:

$$\left|\Psi^{\pm}\right\rangle = \hat{\mathbf{P}} \left|\phi\right\rangle + \sum_i \hat{P}_i \hat{G}_B^{\pm} \sum_{j\neq i} \hat{t}_j^{\pm} \left|\alpha_j^{\pm}\right\rangle. \tag{3.19}$$

Since $\hat{t}_i^{\pm}$ is unaffected by multiplication by $\hat{P}_i$, we have $\hat{t}_i^{\pm} = \hat{P}_i \hat{t}_i^{\pm}$ and $\hat{t}_i^{\pm} \left|\Psi^{\pm}\right\rangle = \hat{t}_i^{\pm} \left|\alpha_i^{\pm}\right\rangle$. Thus we can re-write (3.19) as

$$\left|\Psi^{\pm}\right\rangle = \hat{\mathbf{P}} \left|\phi\right\rangle + \sum_i \hat{P}_i \hat{G}_B^{\pm} \sum_{j\neq i} \hat{P}_j \hat{t}_j^{\pm} \left|\Psi^{\pm}\right\rangle, \tag{3.20}$$

or

$$\left|\Psi^{\pm}\right\rangle = \hat{\mathbf{P}} \left|\phi\right\rangle + \sum_i \sum_{j\neq i} \hat{P}_i \hat{G}_B^{\pm} \hat{P}_j \hat{t}_j^{\pm} \left|\Psi\right\rangle. \tag{3.21}$$

We can simplify this equation if, as in the zero range scatterer case, we define an off-diagonal background Green function operator,

$$\bar{\mathbf{G}}_B^{\pm} = \sum_i \sum_{j\neq i} \hat{P}_i \hat{G}_B^{\pm} \hat{P}_j = \hat{\mathbf{P}} \hat{G}_B^{\pm} \hat{\mathbf{P}} - \sum_{i=1}^{N} \hat{P}_i \hat{G}_B^{\pm} \hat{P}_i, \tag{3.22}$$

and a diagonal t-matrix operator,

$$\hat{\mathbf{t}}^{\pm} = \sum_m \hat{t}_m^{\pm}, \tag{3.23}$$

and note that

$$\bar{\mathbf{G}}_B^{\pm} \hat{\mathbf{t}}^{\pm} = \sum_i \sum_{j\neq i} \hat{P}_i \hat{G}_B^{\pm} \hat{P}_j \hat{t}_j^{\pm} \tag{3.24}$$

We can now re-write (3.19) as

$$\left|\Psi^{\pm}\right\rangle = \hat{\mathbf{P}} \left|\phi\right\rangle + \bar{\mathbf{G}}_B^{\pm} \hat{\mathbf{t}}^{\pm} \left|\Psi^{\pm}\right\rangle, \tag{3.25}$$

which we may formally solve for $|\Psi^{\pm}\rangle$:

$$|\Psi^{\pm}\rangle = \left[\hat{\mathbf{P}} - \bar{\mathbf{G}}_B^{\pm}\hat{\mathbf{t}}^{\pm}\right]^{-1}\hat{\mathbf{P}}\,|\phi\rangle\,. \tag{3.26}$$

The operator $\left[\hat{\mathbf{P}} - \bar{\mathbf{G}}_B^{\pm}\hat{\mathbf{t}}^{\pm}\right]$ is an operator on functions on the scattering space, $\mathcal{S}$, and the boldface $-\mathbf{1}$ superscript indicates inversion with respect to the scattering space only. In the case of zero range interactions the scattering space is a discrete set and the inverse is just ordinary matrix inversion. In general, finding this inverse involves solving a set of coupled linear integral equations.

We note that the projector, $\hat{\mathbf{P}}$, is just the identity operator on the scattering space so

$$\left[\hat{\mathbf{P}} - \bar{\mathbf{G}}_B^{\pm}\hat{\mathbf{t}}^{\pm}\right]^{-\mathbf{1}} = \left[\hat{\mathbf{1}} - \bar{\mathbf{G}}_B^{\pm}\hat{\mathbf{t}}^{\pm}\right]^{-\mathbf{1}}. \tag{3.27}$$

We can re-write (3.15), yielding

$$|\psi^{\pm}\rangle = |\phi\rangle + \hat{G}_B^{\pm}\hat{\mathbf{t}}^{\pm}\,|\Psi^{\pm}\rangle\,. \tag{3.28}$$

Substituting (3.26) into (3.28) gives

$$|\psi^{\pm}\rangle = |\phi\rangle + \hat{G}_B^{\pm}\hat{\mathbf{t}}^{\pm}\left[\hat{\mathbf{1}} - \bar{\mathbf{G}}_B^{\pm}\hat{\mathbf{t}}^{\pm}\right]^{-\mathbf{1}}\hat{\mathbf{P}}\,|\phi\rangle\,, \tag{3.29}$$

The identity

$$\hat{A}(1 - \hat{B}\hat{A})^{-1} = (1 - \hat{A}\hat{B})^{-1}\hat{A}, \tag{3.30}$$

implies

$$|\psi^{\pm}\rangle = |\phi\rangle + \hat{G}_B^{\pm}\left[\hat{\mathbf{1}} - \hat{\mathbf{t}}\bar{\mathbf{G}}_B\right]^{-\mathbf{1}}\hat{\mathbf{t}}\,|\phi\rangle\,. \tag{3.31}$$

We now define a multiple scattering t-matrix

$$\hat{t}^{\pm} = \left[\hat{\mathbf{1}} - \hat{\mathbf{t}}^{\pm}\bar{\mathbf{G}}_B^{\pm}\right]^{-\mathbf{1}}\hat{\mathbf{t}}^{\pm}, \tag{3.32}$$

which is zero outside the scattering space. Our wavefunction can now be written

$$|\psi^{\pm}\rangle = |\phi\rangle + \hat{G}_B^{\pm}\hat{t}^{\pm}\,|\phi\rangle\,. \tag{3.33}$$

This derivation seems much more complicated than the special case presented first. While this is true, the underlying concepts are exactly the same. The complications arise from the more complicated nature of the individual scatterers. Each scatterer now leads to a linear integral equation, rather than a linear algebraic equation; what was simply a

set of linear equations easily solved by matrix techniques, becomes a set of linear integral equations which are difficult to solve except in special cases.

The techniques in this section are also useful formally. We will use them later in this chapter to effect an alternate proof of the scatterer renormalization discussed in the next section.

3.2 Renormalized t-matrices

In the previous section we used the t-matrix formalism and some complicated book-keeping to combine many scatterers into one t-matrix. In this section we'd like to work with the propagation step. We'll start with a potential with known t-matrix in free space. We then imagine changing free space by adding boundaries for example. We then find the correct t-matrix, for the same physical potential, for use with this new propagator.

To begin we consider the scatterer in free space. It has known t-matrix $\hat{t}^{\pm}(z)$ which satisfies

$$G_s^{\pm}(z) = \hat{G}_o^{\pm}(z) + \hat{G}_o^{\pm}(z)\hat{t}^{\pm}(z)\hat{G}_o^{\pm}(z). \tag{3.34}$$

where the subscript "s" is used to denote that this Green function is for the scatterer in free space. Now, rather than free space, we suppose we have a more complicated background but one with a known Green function operator, $\hat{G}_B^{\pm}(z)$. We note that there exists a t-matrix, $\hat{t}_B^{\pm}(z)$, such that:

$$\hat{G}_B^{\pm}(z) = \hat{G}_o^{\pm}(z) + \hat{G}_o^{\pm}(z)\hat{t}_B^{\pm}(z)\hat{G}_o^{\pm}(z). \tag{3.35}$$

We will use the $\hat{t}_B^{\pm}(z)$ operator in the algebra which follows, but only as a formal tool. Frequently, the division between scatterer and background is arbitrary; we can often treat the background as a scatterer or a scatterer as part of the background.

As an example, we begin with a zero range scatterer, with effective radius a_e, in two dimensions. In section 2.5, we computed $\hat{t}^{+}(z)$ for this scatterer in free space. We place this scatterer into an infinite wire with periodic transverse boundary conditions. The causal Green function operator, $\hat{G}_B^{+}(\mathbf{r}, \mathbf{r}'; z)$, can be written as an infinite sum and can be calculated quite accurately using numerical techniques (see chapter 5).

Computing a t-matrix for the scatterer and boundary together is quite difficult. Also, such a t-matrix would be non-zero not only on the scatterer but on the entire infinite length boundary. This lacks the simplicity of a zero-range scatterer t-matrix. Instead, we'd

like to find a t-matrix, $\hat{T}^+(z)$, for the scatterer such that the full Green function, $\hat{G}^+(z)$, may be written

$$\hat{G}^+(z) = \hat{G}_B^+(z) + \hat{G}_B^+(z)\hat{T}^+(z)\hat{G}_B^+(z). \tag{3.36}$$

We'll call $\hat{T}^+(z)$ the "renormalized" t-matrix. This name will become clearer below.

Let's start with a guess. What can happen in our rectangle that couldn't happen in free-space? The answer is simple: amplitude may scatter off of the scatterer, hit the walls and return to the scatterer again. That is, there are multiple scattering events between the background and the scatterer. Diagrammatically, this is just like the two scatterer multiple scattering theory considered in the previous section where scatterer 1, instead of being another scatterer, is the background (see equation 3.9).

Naively we would expect to add up all the scattering events (dropping the z's):

$$\hat{T}^+ = \hat{t}^+ + \hat{t}^+\hat{G}_B^+\hat{t}^+ + \hat{t}^+\hat{G}_B^+\hat{t}^+\hat{G}_B^+\hat{t}^+ + \cdots = \left[\sum_{n=0}^{\infty}\left(\hat{t}^+\hat{G}_B^+\right)^n\right]\hat{t}. \tag{3.37}$$

This is perhaps clearer if we consider the position representation:

$$T^+(\mathbf{r},\mathbf{r}') = t^+(\mathbf{r},\mathbf{r}') + \int d\mathbf{r}''\, d\mathbf{r}'''t^+(\mathbf{r},\mathbf{r}'')G_B^+(\mathbf{r}'',\mathbf{r}''')t(\mathbf{r}''',\mathbf{r}') + \cdots, \tag{3.38}$$

and, since our scatterer is zero-range,

$$t^+(r,r') = s^+\delta(\mathbf{r}-\mathbf{r_s})\delta(\mathbf{r}'-\mathbf{r_s}), \tag{3.39}$$

which simplifies (3.38):

$$T^+(\mathbf{r},\mathbf{r}') = s^+\delta(\mathbf{r}-\mathbf{r_s})\delta(\mathbf{r}'-\mathbf{r_s}) + s^+G_B^+(\mathbf{r_s},\mathbf{r_s})\delta(\mathbf{r}-\mathbf{r_s})\delta(\mathbf{r}'-\mathbf{r_s}) + \cdots. \tag{3.40}$$

Summing the geometric series yields:

$$T^+(\mathbf{r},\mathbf{r}') = \delta(\mathbf{r}-\mathbf{r_s})\delta(\mathbf{r}'-\mathbf{r_s})\frac{s^+}{1-s^+G_B^+(\mathbf{r_s},\mathbf{r_s})}, \tag{3.41}$$

as an operator equation:

$$\hat{T}^+ = \frac{1}{1-\hat{t}^+\hat{G}_B^+}\hat{t}^+. \tag{3.42}$$

This is not quite right. With multiple scattering we had to define an off-diagonal Green function since the diagonal part was already accounted for by the individual t-matrices. Something similar is needed here or we will be double counting terms which scatter, propagate without hitting the boundary, and then scatter again.

We can correct this by subtracting $\hat{G}_o^+$ from $\hat{G}_B^+$ in the previous derivation:

$$\hat{T}^+ = \hat{t}^+ + \hat{t}^+(\hat{G}_B^+ - \hat{G}_o^+)\hat{t}^+ + \hat{t}^+(\hat{G}_B^+ - \hat{G}_o^+)\hat{t}^+(\hat{G}_B^+ - \hat{G}_o^+)\hat{t}^+ + \cdots = \frac{1}{1 - \hat{t}^+(\hat{G}_B^+ - \hat{G}_o^+)}\hat{t}^+. \tag{3.43}$$

For future reference, we'll state the final result:

$$\hat{T}^+(z) = \frac{1}{1 - \hat{t}^+(z)\left[\hat{G}_B^+(z) - \hat{G}_o^+(z)\right]}\hat{t}^+(z). \tag{3.44}$$

We haven't proven this but we can derive the same result more rigorously in at least two ways, both of which are shown below. The first proof follows from the expression (2.49) for the t-matrix derived in section 2.3. This is a purely formal derivation but it has the advantage of being relatively compact. Our second derivation uses the generalized multiple scattering theory of section 3.1.2. While this derivation is algebraically quite tedious, it emphasizes the arbitrariness of the split between scatterer and background by treating them on a completely equal footing.

We note that the free-space Green function operator, $\hat{G}_o^+(z)$, could be replaced by any Green function for which the t-matrix of the scatterer is known. That should be clear from the derivations below.

3.2.1 Derivation

Formal Derivation

Suppose we have $\hat{H} = \hat{H}_o + \hat{H}_B + \hat{H}_s$ where $\hat{H}_B$ is the Hamiltonian of the "background," and $\hat{H}_s$ is the "scatterer" Hamiltonian which may be any reasonable potential. There is a t-matrix for the scatterer without the background:

$$\hat{t}^\pm(z) = \hat{H}_s\hat{G}_s^\pm(z)(z - \hat{H}_o \pm i\epsilon), \tag{3.45}$$

and for the scatterer in the presence of the background where the background is treated as part of the propagator:

$$\hat{T}^\pm(z) = \hat{H}_s\hat{G}^\pm(z)(z - \hat{H}_o - \hat{H}_B \pm i\epsilon). \tag{3.46}$$

This yields an expression for the full Green function, $\hat{G}^\pm(z)$ operator:

$$\hat{G}^\pm(z) = \hat{G}_B^\pm(z) + \hat{G}_B^\pm(z)\hat{T}^\pm(z)\hat{G}_B^\pm(z), \tag{3.47}$$

where $G_B^{\pm}(z)$ solves

$$(z - \hat{H}_o - \hat{H}_B \pm i\epsilon)\hat{G}_B^{\pm}(z) = \hat{1}. \tag{3.48}$$

We wish to find $\hat{T}^{\pm}(z)$ in terms of $\hat{t}^{\pm}(z)$, $\hat{G}_o^{\pm}(z)$, and $\hat{G}_B^{\pm}(z)$. Formally, we can use (3.45) to solve for $\hat{H}_s$:

$$\hat{H}_s = \hat{t}^{\pm}(z)(z - \hat{H}_o \pm i\epsilon)^{-1}\left[\hat{G}_s^{\pm}(z)\right]^{-1} = \hat{t}^{\pm}(z)\hat{G}_o^{\pm}(z)(z - \hat{H}_o - \hat{H}_s \pm i\epsilon). \tag{3.49}$$

We substitute this into (3.46)

$$\hat{T}^{\pm}(z) = \hat{t}^{\pm}(z)\hat{G}_o^{\pm}(z)\left[\hat{G}_s^{\pm}(z)\right]^{-1}\hat{G}^{\pm}(z)(z - \hat{H}_o - \hat{H}_B \pm i\epsilon), \tag{3.50}$$

which we can re-write

$$\begin{aligned}\hat{T}^{\pm}(z) &= \hat{t}^{\pm}(z)\hat{G}_o^{\pm}(z)\left[\hat{G}_o^{\pm}(z) + \hat{G}_o^{\pm}(z)\hat{t}^{\pm}(z)\hat{G}_o^{\pm}(z)\right]^{-1} \\ &\quad \left[\hat{G}_B^{\pm}(z) + \hat{G}_B^{\pm}(z)\hat{T}^{\pm}(z)\hat{G}_B^{\pm}(z)\right]\left[\hat{G}_B^{\pm}(z)\right]^{-1},\end{aligned} \tag{3.51}$$

and, canceling a few inverses, we have

$$\hat{T}^{\pm}(z) = \hat{t}^{\pm}(z)\left[1 + \hat{G}_o^{\pm}(z)\hat{t}^{\pm}(z)\right]^{-1}\left[1 + \hat{G}_B^{\pm}(z)\hat{T}^{\pm}(z)\right]. \tag{3.52}$$

We re-write this as

$$\left[1 - \hat{t}^{\pm}(z)\left[1 + \hat{G}_o^{\pm}(z)\hat{t}^{\pm}(z)\right]^{-1}\hat{G}_B^{\pm}(z)\right]\hat{T}^{\pm}(z) = \hat{t}^{\pm}(z)\left[1 + \hat{G}_o^{\pm}(z)\hat{t}^{\pm}(z)\right]^{-1}, \tag{3.53}$$

which we solve for $\hat{T}^{\pm}(z)$:

$$\hat{T}^{\pm}(z) = \left[1 - \hat{t}^{\pm}(z)\left[1 + \hat{G}_o^{\pm}(z)\hat{t}^{\pm}(z)\right]^{-1}\hat{G}_B^{\pm}(z)\right]^{-1}\hat{t}^{\pm}(z)\left[1 + \hat{G}_o^{\pm}(z)\hat{t}^{\pm}(z)\right]^{-1}. \tag{3.54}$$

To proceed we'll need the operator identity

$$(1 - \hat{A}\hat{B})^{-1}\hat{A} = \hat{A}(1 - \hat{B}\hat{A})^{-1}, \tag{3.55}$$

Which we apply to yield

$$\begin{aligned}\hat{T}^{\pm}(z) &= \left[1 - \left[1 + \hat{t}^{\pm}(z)\hat{G}_o^{\pm}(z)\right]^{-1}\hat{t}^{\pm}(z)\hat{G}_B^{\pm}(z)\right]^{-1}\left[1 + \hat{t}^{\pm}(z)\hat{G}_o^{\pm}(z)\right]^{-1}\hat{t}^{\pm}(z) \\ &= \left\{\left[1 + \hat{t}^{\pm}(z)\hat{G}_o^{\pm}(z)\right]\left[1 - \left[1 + \hat{t}^{\pm}(z)\hat{G}_o^{\pm}(z)\right]^{-1}\hat{t}^{\pm}(z)\hat{G}_B^{\pm}(z)\right]\right\}^{-1}\hat{t}^{\pm}(z) \\ &= \left\{1 + \hat{t}^{\pm}(z)\hat{G}_o^{\pm}(z) - \hat{t}^{\pm}(z)\hat{G}_B^{\pm}(z)\right\}^{-1}\hat{t}^{\pm}(z) \\ &= \frac{1}{1 - \hat{t}^{\pm}(z)\left[\hat{G}_B^{\pm}(z) - \hat{G}_o^{\pm}(z)\right]}\hat{t}^{\pm}(z).\end{aligned} \tag{3.56}$$

Thus we have verified our guess, albeit in an exceedingly formal way.

Derivation Using Generalized Multiple Scattering Theory

Consider a situation with two scatterers in free space. One, the background, with a scattering t-matrix $\hat{t}_1^{\pm}$ which is identically zero outside the domain $\mathcal{C}_1$ and the other a scattering t-matrix $\hat{t}_2^{\pm}$ which is zero outside the domain $\mathcal{C}_2$. They may each be point scatterers or extended scatterers. We assume that the scatterers do not overlap, i.e., $\mathcal{C}_1 \cap \mathcal{C}_2 = \emptyset$. The scattering space, $\mathcal{S}$, is simply the union of $\mathcal{C}_1$ and $\mathcal{C}_2$, $\mathcal{S} = \mathcal{C}_1 \cup \mathcal{C}_2$. From this point on in the derivation, we drop the superscript "$\pm$" since we carried it through the previous derivation and it should be clear here that there is a superscript "$\pm$" on every t-matrix and every Green function. We also drop the argument "z".

Now we apply the generalized multiple scattering theory of section 3.1.2 where the background Green function operator is just $\hat{G}_o$. We have an explicit form for $\hat{\mathbf{t}}$:

$$\left[\hat{\mathbf{t}}\right]_{ij} = \hat{t}_i \delta_{ij}, \tag{3.57}$$

and $\bar{\mathbf{G}}_o$:

$$\left[\bar{\mathbf{G}}_\mathbf{o}\right]_{ij} = \begin{cases} 0 & i = j \\ \hat{G}_B & i \neq j \end{cases} \tag{3.58}$$

According to our derivation of section 3.1.2, the t-matrix may be written

$$\hat{t} = \left[\hat{\mathbf{1}} - \hat{\mathbf{t}}\bar{\mathbf{G}}_o\right]^{-\mathbf{1}} \hat{\mathbf{t}}. \tag{3.59}$$

Painful as it is, let's write out all of the terms in the above expression for $\hat{t}$. We drop the "hats" on all the operators since everything in sight is an operator. First we have to invert $\mathbf{1} - \hat{\mathbf{t}}\bar{\mathbf{G}}_o$ and we have to do it carefully because none of these operators necessarily commute.

$$1 - \hat{\mathbf{t}}\bar{\mathbf{G}}_o = \begin{pmatrix} 1 & -t_1 G_o \\ -t_2 G_o & 1 \end{pmatrix}, \tag{3.60}$$

so

$$\left(1 - \hat{\mathbf{t}}\bar{\mathbf{G}}_o\right)^{-1} = \begin{pmatrix} (1 - t_1 G_o t_2 G_o)^{-1} & t_1 G_o (1 - t_2 G_o t_1 G_o)^{-1} \\ t_2 G_o (1 - t_1 G_o t_2 G_o)^{-1} & (1 - t_2 G_o t_1 G_o)^{-1} \end{pmatrix}, \tag{3.61}$$

and thus

$$\left(\mathbf{1} - \hat{\mathbf{t}}\bar{\mathbf{G}}_o\right)^{-1} \hat{\mathbf{t}} = \begin{pmatrix} (1 - t_1 G_o t_2 G_o)^{-1} t_1 & t_1 G_o (1 - t_2 G_o t_1 G_o)^{-1} t_2 \\ t_2 G_o (1 - t_1 G_o t_2 G_o)^{-1} t_1 & (1 - t_2 G_o t_1 G_o)^{-1} t_2 \end{pmatrix}. \tag{3.62}$$

So, in detail,

$$\begin{aligned} G &= G_o \\ &\quad + G_o(1 - t_1 G_o t_2 G_o)^{-1} t_1 G_o + G_o(1 - t_2 G_o t_1 G_o)^{-1} t_2 G_o \\ &\quad + G_o t_1 G_o (1 - t_2 G_o t_1 G_o)^{-1} t_2 G_o + G_o t_2 G_o (1 - t_1 G_o t_2 G_o)^{-1} t_1 G_o \end{aligned} \quad . \tag{3.63}$$

We want to rewrite this in the form

$$G = G_1 + G_1 T_2 G_1, \tag{3.64}$$

where T_2 is the renormalized t-matrix operator for scatterer 2 in the presence of scatterer 1.

First we add and subtract $G_o t_1 G_o$:

$$\begin{aligned} G &= G_o + G_o t_1 G_o \\ &\quad - G_o t_1 G_o + G_o(1 - t_1 G_o t_2 G_o)^{-1} t_1 G_o + G_o(1 - t_2 G_o t_1 G_o)^{-1} t_2 G_o \\ &\quad + G_o t_1 G_o (1 - t_2 G_o t_1 G_o)^{-1} t_2 G_o + G_o t_2 G_o (1 - t_1 G_o t_2 G_o)^{-1} t_1 G_o, \end{aligned} \tag{3.65}$$

or

$$\begin{aligned} G &= G_o + G_o t_1 G_o + G_o \left[(1 - t_1 G_o t_2 G_o)^{-1} - 1\right] t_1 G_o \\ &\quad + G_o(1 - t_2 G_o t_1 G_o)^{-1} t_2 G_o \\ &\quad + G_o t_1 G_o (1 - t_2 G_o t_1 G_o)^{-1} t_2 G_o + G_o t_2 G_o (1 - t_1 G_o t_2 G_o)^{-1} t_1 G_o, \end{aligned} \tag{3.66}$$

but

$$\Big[(1 - t_1 G_o t_2 G_o)^{-1} - 1\Big] = (1 - t_1 G_o t_2 G_o)^{-1} t_1 G_o t_2 G_o. \tag{3.67}$$

So

$$\begin{aligned} G &= G_o + G_o t_1 G_o + G_o(1 - t_1 G_o t_2 G_o)^{-1} t_1 G_o t_2 G_o t_1 G_o \\ &\quad + G_o(1 - t_2 G_o t_1 G_o)^{-1} t_2 G_o \\ &\quad + G_o t_1 G_o (1 - t_2 G_o t_1 G_o)^{-1} t_2 G_o + G_o t_2 G_o (1 - t_1 G_o t_2 G_o)^{-1} t_1 G_o \end{aligned} \quad . \tag{3.68}$$

We use the operator identity (3.55) to rewrite G:

$$\begin{aligned} G &= G_o + G_o t_1 G_o + G_o t_1 G_o (1 - t_2 G_o t_1 G_o)^{-1} t_2 G_o t_1 G_o \\ &\quad + G_o(1 - t_2 G_o t_1 G_o)^{-1} t_2 G_o \\ &\quad + G_o t_1 G_o (1 - t_2 G_o t_1 G_o)^{-1} t_2 G_o + G_o(1 - t_2 G_o t_1 G_o)^{-1} t_2 G_o t_1 G_o. \end{aligned} \tag{3.69}$$

Several terms now have the common factor, $(1 - t_2 G_o t_1 G_o)$. This allows us to collapse several terms:

$$G = (G_o + G_o t_1 G_o) + (G_o + G_o t_1) \frac{1}{1 - t_2 G_o t_1 G_o} t_2 (G_o + G_o t_1 G_o), \tag{3.70}$$

but $G_o + G_o t_1 G_o = G_1$ is the Green function for scatterer 1 alone. Also, $t_2(G_o t_1 G_o) = t_2(G_1 - G_o)$, so we have

$$G = G_1 + G_1 \frac{1}{1 - t_2 (G_1 - G_o)} t_2 G_1. \tag{3.71}$$

Now we see that equation 3.71 has exactly the same form as equation 2.49. So we have derived (restoring the "$\pm$" and the "z")

$$\hat{T}_2^{\pm}(z) = \frac{1}{1 - \hat{t}_2^{\pm}(z) \left[\hat{G}_1^{\pm}(z) - \hat{G}_o^{\pm}(z)\right]} \hat{t}_2^{\pm}(z), \tag{3.72}$$

which is identical to equation 3.44 as was to be shown. In the notation of the previous derivation, $T_2(z) = T(z)$, $t_2(z) = t(z)$ and $G_1(z) = G_B(z)$.

3.2.2 Consequences

Free Space Background

What happens if $\hat{G}_B^{\pm}(z) = \hat{G}_o^{\pm}(z)$? Our formula should reduce to $\hat{T}^{\pm}(z) = \hat{t}^{\pm}(z)$. And it does:

$$\hat{T}^{\pm}(z) = \frac{1}{1 - \hat{t}^{\pm}(z)[\hat{G}^{\pm}(z)_B - \hat{G}_o^{\pm}(z)]} \hat{t}^{\pm}(z) = \hat{t}^{\pm}(z). \tag{3.73}$$

Closed Systems

Suppose G_B comes from a finite domain, e.g., a rectangular domain in two dimensions. Then we have

$$\hat{T} = \frac{1}{1 - \hat{t}^{\pm}(\hat{G}_B - \hat{G}_o^{\pm})} \hat{t}^{\pm} = \frac{1}{1 - \hat{t}^{\pm}(\hat{G}_o^{\pm} \hat{t}_B \hat{G}_o^{\pm})} \hat{t}^{\pm}. \tag{3.74}$$

It is not obvious from this that $\hat{T}$ doesn't depend on the choice if incoming or outgoing solutions in the above equation. However, it is clear from physical considerations that a closed system only has one class of solutions. In fact, the above equation is independent of the choice of incoming or outgoing solutions for the free space quantities. We can show this in a non-rigorous way by observing that

$$\hat{T} = \frac{1}{\left(\hat{t}^{\pm}\right)^{-1} - \left[\hat{G}_B - \hat{G}_o^{\pm}\right]}, \tag{3.75}$$

and that

$$\left(\hat{t}^{\pm}\right)^{-1} = \hat{H}_s^{-1} - \hat{G}_o^{\pm}, \tag{3.76}$$

so

$$\hat{T}^{-1} = \hat{H}_s^{-1} - \hat{G}_B. \tag{3.77}$$

To show this rigorously would require a careful definition of what these various inverses mean since many of the operators can be singular. We need to properly define the space on which these operators act. This would be similar to the definition of the scattering space used in section 3.1.2.

The Green function operator of a closed system has poles at the eigenenergies. That is, $\hat{t}_B(z)$ and $\hat{G}_B(z)$ have poles at $z = E_n^o$ for $n \in \{1 \ldots \infty\}$. For z near E_n^o

$$\hat{t}_B(z) \approx \frac{\hat{R}'_n}{z - E_n}, \tag{3.78}$$

and

$$\hat{G}_B(z) \approx \frac{\hat{G}_o^{\pm}(z)\hat{R}'_n\hat{G}_o^{\pm}(z)}{z - E_n}. \tag{3.79}$$

$\hat{G}_o^{\pm}(z)$ has no poles (though it may have other sorts of singularities). So we define

$$\hat{R}_n = \hat{G}_o^{\pm}(E_o^n)\hat{R}'_n\hat{G}_o^{\pm}(E_o^n). \tag{3.80}$$

Since we have added a scatterer, in general none of the poles of $\hat{G}_B(z)$ should be poles of $\hat{G}(z)$. This is something we can check explicitly. Suppose $z = E_n^o + \epsilon$ where $|\epsilon| << 1$. Then

$$\hat{G}(z) = \hat{G}(E_n^0 + \epsilon) = \frac{\hat{R}_n}{\epsilon} + \frac{\hat{R}_n}{\epsilon}\frac{1}{1 - \frac{\hat{t}^{\pm}(z)\hat{R}_n}{\epsilon}}\hat{t}^{\pm}(z)\frac{\hat{R}_n}{\epsilon}, \tag{3.81}$$

which is easily simplified:

$$\hat{G}(z) = \frac{\hat{R}_n}{\epsilon}\left(1 - \frac{1}{1 - \frac{\epsilon}{\hat{t}^{\pm}(z)\hat{R}_n}}\right). \tag{3.82}$$

We assume that $\hat{t}^{\pm}(E_n^o) \neq 0$ and we know that $\hat{R}_n \neq 0$ because E_n is a *simple* pole of $G_B(z)$. So there exists ϵ such that

$$\frac{\epsilon}{\hat{t}^{\pm}(z)\hat{R}_n} << 1. \tag{3.83}$$

So we have

$$\frac{1}{1 - \frac{\epsilon}{\hat{t}^{\pm}(z)\hat{R}_n}} \approx 1 + \frac{\epsilon}{\hat{t}^{\pm}(z)\hat{R}_n}, \tag{3.84}$$

and thus

$$\hat{G}(z) = \frac{1}{\hat{t}^{\pm}(z)} + \mathcal{O}(\epsilon). \tag{3.85}$$

Therefore, the poles of $\hat{G}_B(z)$ are not poles of $\hat{G}(z)$ unless $\hat{t}(E_n^0) = 0$.

So Where are the Poles in $\hat{G}(z)$?

As we expect, the analytic structure of $\hat{G}(z)$ and $\hat{T}(z)$ coincide (at least for the most part, see [10], p. 52). More simply, since the poles of $\hat{G}_B(z)$ are not poles of $\hat{G}(z)$, only poles of $\hat{T}(z)$ will contribute poles to $\hat{G}(z)$.

Recall

$$\hat{T}(z) = \frac{1}{1 - \hat{t}^{\pm}(z)\left[\hat{G}_B(z) - \hat{G}_o^{\pm}(z)\right]}\hat{t}^{\pm}(z), \tag{3.86}$$

so poles of $\hat{T}(z)$ occur at $E_n (\neq E_n^o)$ satisfying

$$\hat{t}^{\pm}(E_n)\left[\hat{G}_B(E_n) - \hat{G}_o^{\pm}(E_n)\right] = 1, \tag{3.87}$$

or

$$\hat{t}^{\pm}(E_n) = \left[\hat{G}_B(E_n) - \hat{G}_o^{\pm}(E_n)\right]^{-1} = \frac{1}{\hat{G}_o^{\pm}(E_n)\hat{t}_B^{\pm}(E_n)\hat{G}_o^{\pm}(E_n)}. \tag{3.88}$$

This is a simple equation to use when $\hat{G}_B$ comes from scatterers added to free space so $\hat{t}_B^{\pm}$ is known. When $\hat{G}_B$ is a Green function given a-priori, e.g., the Green function of an infinite wire in 2 dimensions, the above equation becomes somewhat more difficult to evaluate. We'll address this issue in a later chapter (5) about scattering in 2-dimensional wires.

Perturbatively small scatterers

For small $\hat{t}(z)$ the only way to satisfy equation 3.88 is for $\hat{G}_B(z)$ to be very large. But $\hat{G}_B(z)$ is large only near a pole, E_n^o of $\hat{G}_B(z)$. This is a nice result. It implies that for small $\hat{t}(z)$, i.e., a small scatterer, the poles, E_n of $\hat{G}(z)$ are close to the poles E_n^o of $\hat{G}_B(z)$ as we might expect. This idea has been used (see [11]) to explore the possibility that an atomic force microscope, used as a small scatterer, can probe the structure of the wavefunction of a quantum dot.

Renormalization of a zero range t-matrix

A zero range t-matrix provides a simple but subtle challenge for the application of this renormalization. Since

$$\hat{t}^{\pm}(z) = s^{\pm}(z)\left|\mathbf{r_s}\right\rangle\left\langle\mathbf{r_s}\right|, \tag{3.89}$$

we have,

$$\hat{T}^{\pm}(z) = \frac{1}{\frac{1}{s^{\pm}(z)} - \left[G_B(\mathbf{r_s}, \mathbf{r_s}; z) - G_o^{\pm}(\mathbf{r_s}, \mathbf{r_s}; z)\right]}\left|\mathbf{r_s}\right\rangle\left\langle\mathbf{r_s}\right|. \tag{3.90}$$

But, as we have already discussed in section 2.3, in more than one dimension, the Green function, $G(\mathbf{r}, \mathbf{r}'; z)$ for the Schrödinger equation is singular in the $\mathbf{r} \to \mathbf{r}'$ limit. So, we have to define $T(z)$ a bit more formally:

$$\hat{T}^{\pm}(z) = \lim_{\mathbf{r}' \to \mathbf{r_s}} \frac{1}{\frac{1}{s^{\pm}(z)} - \left[G_B(\mathbf{r_s}, \mathbf{r}'; z) - G_o^{\pm}(\mathbf{r_s}, \mathbf{r}'; z)\right]} |\mathbf{r_s}\rangle \langle \mathbf{r_s}| . \tag{3.91}$$

This limit can be quite difficult to evaluate. Four particular cases are dealt with in chapters 5 and 6.

Chapter 4

Scattering From Arbitrarily Shaped Boundaries

4.1 Introduction

In the previous chapter we developed some powerful tools for solving complicated scattering problems. All of them were built upon one or more Green functions. In this chapter we consider a variety of techniques for computing Green functions in various geometries. The techniques discussed in this chapter are useful when we have a problem which involves scattering on a surface of co-dimension one (one dimension less than the dimension of the system), for example scattering from a set of one dimensional curves in two dimensions.

We begin by computing the Green function of an arbitrary number of arbitrarily shaped smooth Dirichlet ($\psi = 0$) boundaries placed in free-space. The method is constructed by finding a potential which forces ψ to satisfy the Dirichlet boundary condition. The technique is somewhat more general. It can enforce an arbitrary linear combination of Dirichlet and Neumann boundary conditions. The more general case is dealt with in appendix B.

We then re-derive the fundamental results by considering certain expansions of ψ rather than a potential. This lends itself nicely to the generalizations which follow in the next two sections. We can use expansions of ψ to simply match boundary conditions. The first generalization is a small but useful step from Dirichlet boundary conditions to periodic boundary conditions.

We next consider scattering from a boundary between two regions with different known Green functions. This cannot be handled as a boundary condition but, nonetheless, all the scattering takes place at the interface. This method could be used to scatter from a potential barrier of fixed height; that was the original motivation for its development. It could also be used to scatter from a superconductor embedded in a normal metal or vice-versa since each has its own known Green function (see A.6). This idea is being actively pursued.

4.2 Boundary Wall Method I

Consider

$$V(\mathbf{r}) = \int_{\mathcal{C}} ds\, \lambda(s)\, \delta\left(\mathbf{r} - \mathbf{r}(s)\right) \tag{4.1}$$

where the integral runs over the surface $\mathcal{C}$. Here we will assume a pragmatic point of view by supposing that our mathematical problem is well posed, i.e., there does exist a solution for the Schrödinger equation satisfying the boundary conditions considered. Obviously, the method has no meaning when this is not so.) The boundary condition

$$\psi(\mathbf{r}(s)) = 0 \tag{4.2}$$

emerges as the limit of the potential's parameters ($\lambda \to \infty$). For finite λ, the potential has the effect of a penetrable or "leaky" wall. A similar idea has been used to incorporate Dirichlet boundary conditions into certain classes of *solvable* potentials in the context of the path integral formalism [19]. Here we use the delta wall more generally, resulting in a widely applicable and accurate procedure to solve boundary condition problems for arbitrary shapes.

Consider the Schrödinger equation for a d-dimensional system, $H(\mathbf{r})\psi(\mathbf{r}) = E\psi(\mathbf{r})$, with $H = H_0 + V$. As is well known, the solution for $\psi(\mathbf{r})$ is given by

$$\psi(\mathbf{r}) = \phi(\mathbf{r}) + \int d\mathbf{r}'\, G_0^E(\mathbf{r}, \mathbf{r}')V(\mathbf{r}')\psi(\mathbf{r}'), \tag{4.3}$$

where $\phi(\mathbf{r})$ solves $H_0(\mathbf{r})\phi(\mathbf{r}) = E\phi(\mathbf{r})$ and $G_0^E(\mathbf{r}, \mathbf{r}')$ is the Green function for H_0. Hereafter, for notational simplicity, we will suppress the superscript E in G_0^E.

Now, we introduce a δ-type potential

$$V(\mathbf{r}) = \lambda \int_{\mathcal{C}} ds\, \delta\left(\mathbf{r} - \mathbf{r}(s)\right), \tag{4.4}$$

where the integral is over $\mathcal{C}$, a connected or disconnected surface. $\mathbf{r}(s)$ is the vector position of the point s on $\mathcal{C}$ (we will call the set of all such vectors $\mathcal{S}$), and λ is the potential's strength. Clearly, $V(\mathbf{r}) = 0$ for $\mathbf{r} \notin \mathcal{S}$.

In the limit $\lambda \to \infty$, the wavefunction will satisfy (4.2) (with $\alpha(s) = 1$) as shown below. For finite λ, a wave function subject to the potential (4.4) will satisfy a "leaky" form of the boundary condition.

Inserting the potential (4.4) into (4.3), the volume integral is trivially performed with the delta function, yielding

$$\psi(\mathbf{r}) = \phi(\mathbf{r}) + \lambda \int_{\mathcal{C}} ds'\, G_0(\mathbf{r}, \mathbf{r}(s'))\, \psi(\mathbf{r}(s')) = \phi(\mathbf{r}) + \int_{\mathcal{C}} ds'\, G_0(\mathbf{r}, \mathbf{r}(s'))\, T_\phi(\mathbf{r}(s')). \tag{4.5}$$

Thus, if $\lambda\, \psi(\mathbf{r}(s)) = T_\phi(\mathbf{r}(s))$ is known for all s, the wave function everywhere is obtained from (4.5) by a single definite integral. For $\mathbf{r} = \mathbf{r}(s'')$ some point of $\mathcal{S}$

$$\psi(\mathbf{r}(s'')) = \phi(\mathbf{r}(s'')) + \lambda \int_{\mathcal{C}} ds'\, G_0(\mathbf{r}(s''), \mathbf{r}(s'))\, \psi(\mathbf{r}(s')), \tag{4.6}$$

which may be abbreviated unambiguously as

$$\psi(s'') = \phi(s'') + \lambda \int ds'\, G_0(s'', s')\, \psi(s'). \tag{4.7}$$

We can formally solve this equation, getting

$$\tilde{\psi} = \left[\tilde{\mathrm{I}} - \lambda\, \tilde{G}_0\right]^{-1} \tilde{\phi}, \tag{4.8}$$

where $\tilde{\psi}, \tilde{\phi}$ stand for the vectors of $\psi(s)$'s and $\phi(s)$'s on the boundary, and $\tilde{\mathrm{I}}$ for the identity operator. The tildes remind us that the free Green function operator and the wave-vectors are evaluated only on the boundary.

We define

$$T = \lambda \left[\tilde{\mathrm{I}} - \lambda\, \tilde{G}_0\right]^{-1}, \tag{4.9}$$

and then it is easy to see that T_ϕ in (4.5) is given from (4.8)-(4.9) by

$$T_\phi(\mathbf{r}(s')) = \int ds\, T(s', s)\, \phi(s). \tag{4.10}$$

In order to make contact with the standard t-matrix formalism in scattering theory [35], we note that a T operator for the whole space may be written as

$$t(\mathbf{r}_f, \mathbf{r}_i) = \int ds''\, ds'\, \delta(\mathbf{r}_f - \mathbf{r}(s''))\, T(s'', s')\, \delta(\mathbf{r}_i - \mathbf{r}(s')). \tag{4.11}$$

Finally, we observe that (4.6) can be written as

$$\tilde{\psi} = \left[\tilde{\mathrm{I}} + \tilde{G}_0\, T\right] \tilde{\phi}. \tag{4.12}$$

For $\lambda \to \infty$, the operator T converges to $-\left[\tilde{G}_0\right]^{-1}$. Inserting this into (4.12), we have

$$\tilde{\psi} = \left[\tilde{\mathrm{I}} - \tilde{G}_0 \left[\tilde{G}_0\right]^{-1}\right] \tilde{\phi} = 0. \tag{4.13}$$

So, ψ satisfies a Dirichlet boundary condition on the surface $\mathcal{C}$ for $\lambda = \infty$.

4.3 Boundary Wall Method II

We can simplify the previous derivation considerably if we *assume* that there exists an operator

$$\hat{t}(E) = \int ds\, ds'\, |\mathbf{r}(s)\rangle\, T(s, s'; E)\, \langle \mathbf{r}(s')|\,, \tag{4.14}$$

such that the solution of our scattering problem, $|\psi\rangle$, may be written

$$|\psi\rangle = |\phi\rangle + \hat{G}_o(E)\hat{t}(E)\,|\phi\rangle\,, \tag{4.15}$$

or, in position space,

$$\psi(\mathbf{r}) = \phi(\mathbf{r}) + \int d\mathbf{r}'\, d\mathbf{r}'' G_o(\mathbf{r}, \mathbf{r}'; E) t(\mathbf{r}', \mathbf{r}''; E)\phi(\mathbf{r}''), \tag{4.16}$$

which we can simplify to

$$\psi(\mathbf{r}) = \phi(\mathbf{r}) + \int ds'\, ds'' G_o(\mathbf{r}, \mathbf{r}(s'); E) T(s', s''; E)\phi(\mathbf{r}(s'')). \tag{4.17}$$

The solution is a bit simpler if we make a notational switch:

$$t[\phi](s) = \int ds'\, T(s, s'; E)\phi(\mathbf{r}(s')) \tag{4.18}$$

Now we enforce the dirichlet boundary condition $\psi(\mathbf{r}(\mathbf{s})) = 0$. That gives us a Fredholm integral equation of the first kind:

$$\int ds'\, G_o(\mathbf{r}, \mathbf{r}(s'); E) t[\phi](s') = -\phi(\mathbf{r}(s)) \tag{4.19}$$

which we may solve for $t[\phi](s)$ (e.g., using standard numerical methods.) Formally, we can solve this with

$$t[\phi](s) = -\int ds'\, G_o^{-1}(s, s'; E)\phi(s') \tag{4.20}$$

where the new notation reminds us that the inverse is calculated only on the boundary. That is $G_o^{-1}(s, s')$ satisfies

$$\int ds''\, G_o(\mathbf{r}(s), \mathbf{r}(s''); E) G_o^{-1}(s'', s'; E) = \delta(s - s'). \tag{4.21}$$

4.4 Periodic Boundary Conditions

We can generalize this for other sorts of boundary conditions. In this section, we'll deal with periodic boundary conditions. As with Dirichlet/Neumann boundary conditions we may write the solution in terms of an expansion in free-space solutions to the wave-equation. However, first we should properly characterize our periodic boundaries. We'll consider a kind of generalized periodic boundaries.

Consider two surfaces, $\mathcal{C}_1$ and $\mathcal{C}_2$ both parameterized by functions of a generalized parameter s. We insist that the surfaces are parameterized such that both parameter functions have the same domain. We define "periodic boundary conditions" as any set of conditions of the form

$$\begin{aligned} \psi(\mathbf{r_1}(s)) &= \psi(\mathbf{r_2}(s)) && (4.22) \\ \partial_{\mathbf{n}(\mathbf{r_1}(s))}\psi(\mathbf{r_1}(s)) &= \partial_{\mathbf{n}(\mathbf{r_2}(s))}\psi(\mathbf{r_2}(s)), && (4.23) \end{aligned}$$

where $\partial_{\mathbf{n}(\mathbf{r}(s))}$ denotes the partial derivative in the direction normal to the curve $\mathbf{r}(s)$. We note that different parameterizations of the surfaces may yield different solutions.

For example, consider the unit square in two-dimensions. Standard periodic boundary conditions specify that

$$\begin{aligned} \psi(0,y) &= \psi(1,y)\ \forall y \in [0,1] \\ \frac{\partial}{\partial x}\psi(0,y) &= \frac{\partial}{\partial x}\psi(1,y)\ \forall y \in [0,1] \\ \psi(x,0) &= \psi(x,1)\ \forall x \in [0,1] \\ \frac{\partial}{\partial y}\psi(x,0) &= \frac{\partial}{\partial y}\psi(x,1)\ \forall x \in [0,1]. \end{aligned} \tag{4.24}$$

We choose the surface $\mathcal{C}_1$ as the left side and top of the square and $\mathcal{C}_2$ as the right side and bottom of the box. We may choose a real parameter, $s \in [0,2]$, where $s \in [0,1]$ parameterizes the sides of the box from top to bottom and $s \in (1,2]$ parameterizes the top and bottom from right to left. However, twisted periodic boundaries may also be considered:

$$\begin{aligned} \psi(0,y) &= \psi(1,1-y)\ \forall y \in [0,1] \\ \frac{\partial}{\partial x}\psi(0,y) &= \frac{\partial}{\partial x}\psi(1,1-y)\ \forall y \in [0,1] \\ \psi(x,0) &= \psi(1-x,1)\ \forall x \in [0,1] \\ \frac{\partial}{\partial y}\psi(x,0) &= \frac{\partial}{\partial y}\psi(1-x,1)\ \forall x \in [0,1]. \end{aligned} \tag{4.25}$$

In our language, this simply means choosing a different parameterization of the two pieces of the box.

To solve this problem, we now expand ψ in terms of the free-space Green function on the boundary:

$$\psi(\mathbf{r}) = \phi(\mathbf{r}) + \int \left[G(\mathbf{r}, \mathbf{r}_1(s); E) f_1(s) + G(\mathbf{r}, \mathbf{r}_2(s); E) f_2(s)\right] ds \tag{4.26}$$

We insert the expansion (4.26) into equations (4.22-4.23):

$$\phi(\mathbf{r}_1(s)) + \int \left[G(\mathbf{r}_1(s), \mathbf{r}_1(s'); E) f_1(s') + G(\mathbf{r}_1(s), \mathbf{r}_2(s'); E) f_2(s')\right] ds' =$$
$$\phi(\mathbf{r}_2(s)) + \int \left[G(\mathbf{r}_2(s), \mathbf{r}_1(s'); E) f_1(s') + G(\mathbf{r}_2(s), \mathbf{r}_2(s'); E) f_2(s')\right] ds'$$

$$\partial_{\mathbf{n}(\mathbf{r}_1(s))} \phi(\mathbf{r}_1(s)) + \tag{4.27}$$
$$\int \left[\partial_{\mathbf{n}(\mathbf{r}_1(s))} G(\mathbf{r}_1(s), \mathbf{r}_1(s'); E) f_1(s') + \partial_{\mathbf{n}(\mathbf{r}_1(s))} G(\mathbf{r}_1(s), \mathbf{r}_2(s'); E) f_2(s')\right] ds' =$$

$$\partial_{\mathbf{n}(\mathbf{r}_2(s))} \phi(\mathbf{r}_2(s)) + \tag{4.28}$$
$$\int \left[\partial_{\mathbf{n}(\mathbf{r}_2(s))} G(\mathbf{r}_2(s), \mathbf{r}_1(s'); E) f_1(s') + \partial_{\mathbf{n}(\mathbf{r}_2(s))} G(\mathbf{r}_2(s), \mathbf{r}_2(s'); E) f_2(s')\right] ds' \tag{4.29}$$

This is a set of coupled Fredholm equations of the first type. To make this clearer we define:

$$\begin{aligned}
a(s) &= \phi(\mathbf{r}_2(s)) - \phi(\mathbf{r}_1(s)) \\
a'(s) &= \partial_{\mathbf{n}(\mathbf{r}_2(s))} \phi(\mathbf{r}_1(s)) - \partial_{\mathbf{n}(\mathbf{r}_1(s))} \phi(\mathbf{r}_2(s)), \qquad (4.30) \\
G_1(s, s'; E) &= G_o(\mathbf{r}_1(s), \mathbf{r}_1(s'); E) - G_o(\mathbf{r}_2(s), \mathbf{r}_1(s'); E) \\
G_2(s, s'; E) &= G_o(\mathbf{r}_1(s), \mathbf{r}_2(s'); E) - G_o(\mathbf{r}_2(s), \mathbf{r}_2(s'); E) \\
G_1'(s, s'; E) &= \partial_{\mathbf{n}(\mathbf{r}_1(s))} G_o(\mathbf{r}_1(s), \mathbf{r}_1(s'); E) - \partial_{\mathbf{n}(\mathbf{r}_2(s))} G_o(\mathbf{r}_2(s), \mathbf{r}_1(s'); E) \\
G_2'(s, s'; E) &= \partial_{\mathbf{n}(\mathbf{r}_1(s))} G_o(\mathbf{r}_1(s), \mathbf{r}_2(s'); E) - \partial_{\mathbf{n}(\mathbf{r}_2(s))} G_o(\mathbf{r}_2(s), \mathbf{r}_2(s'); E). \qquad (4.31)
\end{aligned}$$

and then re-write the equations at the boundary:

$$\begin{aligned}
\int \left[G_1(s, s') f_1(s') + G_2(s, s') f_2(s')\right] ds' &= a(s) \\
\int \left[G_1'(s, s') f_1(s') + G_2'(s, s') f_2(s')\right] ds' &= a'(s) \qquad (4.32)
\end{aligned}$$

which we can write, at least schematically, as a matrix equation

$$\begin{pmatrix} \mathcal{G}_1 & \mathcal{G}_2 \\ \mathcal{G}_1' & \mathcal{G}_2' \end{pmatrix} \begin{pmatrix} \mathbf{f}_1 \\ \mathbf{f}_2 \end{pmatrix} = \begin{pmatrix} \mathbf{a} \\ \mathbf{a}' \end{pmatrix} \tag{4.33}$$

where the $\mathcal{G}$'s are linear integral operators in the space of functions on the boundary and the $\mathbf{f}$'s and $\mathbf{a}$'s are vectors (functions) in that space.

Formally, we can solve this equation:

$$\begin{pmatrix} \mathbf{f}_1 \\ \mathbf{f}_2 \end{pmatrix} = \begin{pmatrix} \mathcal{G}_1 & \mathcal{G}_2 \\ \mathcal{G}_1' & \mathcal{G}_2' \end{pmatrix}^{-1} \begin{pmatrix} \mathbf{a} \\ \mathbf{a}' \end{pmatrix} \tag{4.34}$$

While we cannot usually invert this operator analytically, we can sample our boundary at a discrete set of points. We then construct and invert this operator in this finite dimensional space and, using this finite basis, construct an approximate solution to our scattering problem.

4.5 Green Function Interfaces

In this section we'll deal with scattering from an arbitrarily shaped potential step. Though this is not purely a boundary condition, the problem is solved, as in the previous two cases, if sums of solutions to "free-space" equations satisfy certain conditions on a boundary.

We consider an object with potenial V_o embedded in free-space (we could consider an object with one Green function embedded in a space with another Green function as long as the asymptotic solutions of the wave equation are known in both regions but we'll be a bit more specific) where the boundary between the two regions is parameterized by s via $\mathbf{r}(\mathbf{s})$ as the Dirichlet boundary was in section 4.3.

It is immediately clear that an expansion of the form (4.16) cannot work for the wavefunction inside the dielectric (though it may work for the wavefunction outside) since the Green function used in the expansion *does not* solve the wave equation inside. We need a separate expansion for the inside wavefunction. This is no surprise since at a potential step boundary we have twice as many boundary conditions: continuity of ψ *and* it's first derivative. We expand the inside and outside solutions separately to get

$$\psi_{\text{out}}(\mathbf{r}) \quad = \quad \phi_{\text{out}}(\mathbf{r}) + \int G_{\text{out}}(\mathbf{r}, \mathbf{r}(\mathbf{s}); E)\, t_{\text{out}}[\phi_{\text{in}}, \phi_{\text{out}}](s)\, ds, \tag{4.35}$$

$$\psi_{\rm in}(\mathbf{r}) \;\; = \;\; \phi_{\rm in}(\mathbf{r}) + \int G_{\rm in}(\mathbf{r},\mathbf{r}(\mathbf{s});E)\, t_{\rm in}[\phi_{\rm in},\phi_{\rm out}](s)\, ds, \tag{4.36}$$

where $\phi(\mathbf{r}) = \phi_{\rm out}(\mathbf{r}) - \phi_{\rm in}(\mathbf{r})$.

The incoming wave inside the potential step is puzzling at first. Because the basis in which we are expanding the solutions is not orthogonal, we have some freedom in choosing $\phi_{\rm in}(\mathbf{r}) = 0$.

i) We can choose $\phi_{\rm in}(\mathbf{r}) = 0$ which corresponds to the entire inside wavefunction being produced at the boundary sources. This is mathematically correct but a little awkward when the potential step is small compared to the incident energy.. When the step is small, the wavefunction inside and outside will be much like the incoming wave which leads us to

ii) A more physical but harder to define choice is to choose $\phi_{\rm in}(\mathbf{r})$ to be a solution to the wave equation inside the step and which has the property

$$\lim_{V_o\to 0} \phi_{\rm in}(\mathbf{r}(\mathbf{s})) = \phi_{\rm out}(\mathbf{r}(\mathbf{s})). \tag{4.37}$$

Though this seems ad hoc, it is mathematically as valid as choice (i) and has the nice property that

$$\lim_{V_o\to 0} t_{\rm in,out}[\phi](s) = 0, \tag{4.38}$$

which is appealing.

Now we write our boundary conditions:

$$\begin{aligned} \psi_{\rm out}(\mathbf{r}(s)) &= \psi_{\rm in}(\mathbf{r}(s)) \\ \partial_{\mathbf{n}(s)}\psi_{\rm out}(\mathbf{r}(s)) &= \partial_{\mathbf{n}(s)}\psi_{\rm in}(\mathbf{r}(s)), \end{aligned} \tag{4.39}$$

or

$$\begin{aligned} &\phi_{\rm out}(\mathbf{r}(s)) + \int G_{\rm out}(\mathbf{r}(s),\mathbf{r}(s');E)\, t_{\rm out}[\phi](s')\, ds' = \\ &\quad \phi_{\rm in}(\mathbf{r}(s)) + \int G_{\rm in}(\mathbf{r}(s),\mathbf{r}(s');E)\, t_{\rm in}[\phi](s')\, ds' \end{aligned} \tag{4.40}$$

$$\begin{aligned} &\partial_{\mathbf{n}(s)}\phi_{\rm out}(\mathbf{r}(s)) + \int \partial_{\mathbf{n}(s)} G_{\rm out}(\mathbf{r}(s),\mathbf{r}(s');E)\, t_{\rm out}[\phi](s')\, ds' = \\ &\quad \partial_{\mathbf{n}(s)}\phi_{\rm in}(\mathbf{r}(s)) + \int \partial_{\mathbf{n}(s)} G_{\rm in}(\mathbf{r}(s),\mathbf{r}(s');E)\, t_{\rm in}[\phi](s')\, ds', \end{aligned} \tag{4.41}$$

where $\partial_{\mathbf{n}(\mathbf{s})}$ is the normal derivative at the boundary point $\mathbf{r}(\mathbf{s})$.

The above is a set of coupled Fredholm equations of the first type. To make this clearer we define:

$$\begin{aligned} a(s) &= \phi_{\rm in}(\mathbf{r}(s)) - \phi_{\rm out}(\mathbf{r}(s)) \\ a'(s) &= \partial_{\mathbf{n}(s)}\phi_{\rm in}(\mathbf{r}(s)) - \partial_{\mathbf{n}(s)}\phi_{\rm out}(\mathbf{r}(s)) \end{aligned}$$

$$v(s) = t_{\rm out}[\phi](s)$$

$$w(s) = t_{\rm in}[\phi](s)$$

$$\begin{aligned} G_o(s,s';E) &= G_{\rm out}(\mathbf{r}(s),\mathbf{r}(s');E) \\ G_i(s,s';E) &= G_{\rm in}(\mathbf{r}(s),\mathbf{r}(s');E) \\ G'_o(s,s';E) &= \partial_{\mathbf{n}(s)}G_{\rm out}(\mathbf{r}(s),\mathbf{r}(s');E) \\ G'_i(s,s';E) &= \partial_{\mathbf{n}(s)}G_{\rm in}(\mathbf{r}(s),\mathbf{r}(s');E). \end{aligned} \tag{4.42}$$

Now we have the following system of integral equations

$$\begin{aligned} \int \left[G_o(s,s';E)v(s') - G_i(s,s';E)w(s')\right]\, ds' &= a(s) \\ \int \left[G'_o(s,s';E)v(s') - G'_i(s,s';E)w(s')\right]\, ds' &= a'(s), \end{aligned} \tag{4.43}$$

with all the G's and ϕ's given.

We may schematically represent this as a matrix equation:

$$\begin{pmatrix} \mathcal{G}_o & -\mathcal{G}_i \\ \mathcal{G}'_o & -\mathcal{G}'_i \end{pmatrix} \begin{pmatrix} \mathbf{v} \\ \mathbf{w} \end{pmatrix} = \begin{pmatrix} \mathbf{a} \\ \mathbf{a}' \end{pmatrix} \tag{4.44}$$

which we may formally solve:

$$\begin{pmatrix} \mathbf{v} \\ \mathbf{w} \end{pmatrix} = \begin{pmatrix} \mathcal{G}_o & -\mathcal{G}_i \\ \mathcal{G}'_o & -\mathcal{G}'_i \end{pmatrix}^{-1} \begin{pmatrix} \mathbf{a} \\ \mathbf{a}' \end{pmatrix} \tag{4.45}$$

This formal solution is not much use except perhaps in a special geometry. However, it does lead directly to a numerical scheme. Simply discretize the boundary by breaking it into N pieces $\{\mathcal{C}_i\}$ of length Δ. Label the center of each piece by s_i and change all the integrals in the integral equations to sums over i. Now the schematic matrix equation actually becomes

a $2N \times 2N$ matrix problem which can be solved by LU decomposition techniques or the like.

We might also worry about mutliple step edges or different steps inside each other. All this will work as well but we will get a set of equations for each interface so the problem may get quite costly. This would not be a sensible way to handle a smoothly varying potential. However, as noted at the beginning, the formalism here works for any known G_{in} and G_{out} and so certain smooth potentials may be handled if their Green function's are known.

4.6 Numerical Considerations and Analysis

4.6.1 Discretizing The Boundary Wall Equations

As discussed in Section 4.2, the key idea in our method is to calculate T and/or T_ϕ on $\mathcal{C}$, and then to perform the integral (4.5). Unfortunately, in the great majority of cases the analytical treatment is too hard to be applied. In such cases we consider the problem numerically.

We divide the region $\mathcal{C}$ into N parts, $\{\mathcal{C}_j\}_{j=1\ldots N}$. Then, we approximate

$$\begin{aligned}\psi(\mathbf{r}) &= \phi(\mathbf{r}) + \sum_{j=1}^{N} \int_{\mathcal{C}_j} ds\, \lambda\, G_0(\mathbf{r}, \mathbf{r}(s))\, \psi(\mathbf{r}(s)) \\ &\approx \phi(\mathbf{r}) + \sum_{j=1}^{N} \psi(\mathbf{r}(s_j)) \int_{\mathcal{C}_j} ds\, \lambda\, G_0(\mathbf{r}, \mathbf{r}(s)),\end{aligned} \tag{4.46}$$

with s_j the middle point of $\mathcal{C}_j$ and $\mathbf{r}_j = \mathbf{r}(s_j)$. Now, considering $\mathbf{r} = \mathbf{r}_i$ we write $\psi(\mathbf{r}_i) = \phi(\mathbf{r}_i) + \sum_{j=1}^{N} \lambda M_{ij} \psi(\mathbf{r}_j)$ (for M, see discussion below). If $\Psi = (\psi(\mathbf{r}_1), \ldots, \psi(\mathbf{r}_N))$, and $\Phi = (\phi(\mathbf{r}_1), \ldots, \phi(\mathbf{r}_N))$, we have $\Psi = \Phi + \lambda \mathbf{M} \Psi$, and thus $\lambda \Psi = \mathbf{T} \Phi$, with $\mathbf{T} = \lambda(\mathbf{I} - \lambda \mathbf{M})^{-1}$, which is the discrete T matrix. So

$$\lambda \Psi_i = (\mathbf{T}\Phi)_i = \lambda \sum_{j=1}^{N} \left[(\mathbf{I} - \lambda \mathbf{M})^{-1} \right]_{ij} \Phi_j, \tag{4.47}$$

and

$$\psi(\mathbf{r}) \approx \phi(\mathbf{r}) + \sum_{j=1}^{N} G_0(\mathbf{r}, \mathbf{r}_j)\, \Delta_j\, (\mathbf{T}\Phi)_j, \tag{4.48}$$

where we have used a mean value approximation to the last integral in (4.46) and defined Δ_j the volume of $\mathcal{C}_j$.

It follows from (4.46) that

$$M_{ij} = \int_{\mathcal{C}_j} ds\, G_0(\mathbf{r}_i, \mathbf{r}(s)). \tag{4.49}$$

We can approximate

$$M_{ij} \approx G_0(\mathbf{r}_i, \mathbf{r}_j)\, \Delta_j. \tag{4.50}$$

However, $G_0(\mathbf{r}_i, \mathbf{r}_j)$ may diverge for $i = j$ (e.g., the free particle Green functions in two or more dimensions). We discuss these approximations in detail in Section 4.6.3.

If we consider $\lambda \to \infty$, it is easy to show from the above results that

$$\psi(\mathbf{r}) \approx \phi(\mathbf{r}) - \sum_{j=1}^{N} G_0(\mathbf{r}, \mathbf{r}_j)\, \Delta_j\, (\mathbf{M}^{-1}\Phi)_j. \tag{4.51}$$

Equation (4.51) is then the approximated wave function of a particle under H_0 interacting with an impenetrable region $\mathcal{C}$.

4.6.2 The Many Scatterer Limit

The boundary wall method is a sort of multiple scattering approach to building boundaries. In the many scatterer limit, we can make this connection explicit.

Recall that the inverse of the multiple scattering t-matrix for point scatterers has the form

$$(\mathbf{M}_{ms})_{ij} = \begin{cases} 1/T_i(E) & \text{if} \quad i = j, \\ G_o(\mathbf{r}_i, \mathbf{r}_j; E) & \text{if} \quad i \neq j. \end{cases} \tag{4.52}$$

We assume that the discretization of the boundary wall method is uniform with spacing $\delta_i = l \ \forall i$. If, for the boundary wall M-matrix, we define $\mathbf{B} = -(1/l)\mathbf{M}$, we get a simpler version of the discretized equation:

$$\psi(\mathbf{r}) \approx \phi(\mathbf{r}) + \sum_{j=1}^{N} G_0(\mathbf{r}, \mathbf{r}_j)\, (\mathbf{B}^{-1}\Phi)_j. \tag{4.53}$$

we notice that $\mathbf{B}$ has the same off-diagonal elements as $\mathbf{M}_{ms}$. The diagonal elements of $\mathbf{B}$ have the form (where $k = \sqrt{E}$)

$$\mathbf{B}_{ii} = \frac{1}{l} \int_{-l/2}^{l/2} G\left(\mathbf{r}_i, \mathbf{r}(s_i + x); E\right)\, dx \approx \frac{1}{\pi} \int_0^{l/2} \ln(kx)\, dx = \frac{1}{2\pi} \left[\ln \frac{kl}{2} - 1\right] = \frac{1}{2\pi} \ln \frac{kl}{2e}. \tag{4.54}$$

If we want to identify this with a multiple scattering problem we must have $1/T_i(E) = \frac{1}{2\pi}\ln\frac{kl}{2e}$ which is the low energy form of the point interaction t-matrix discussed in section 2.4 for a scatterer of scattering length $l/2e$.

Thus, in the many scatterer limit ($kl << 1$), the Dirichlet boundary wall method becomes the multiple scattering of many pointlike scatterers along the boundaries where each scatterer has scattering length $l/2e$.

4.6.3 Quality of the Numerical Method

The numerical solution (4.53) approaches the solution (4.5) as $N \to \infty$. In practice, we choose N to be some finite but large number. In this section we explain how to choose N for a given problem and how the approximation (4.50) affects this choice.

In order to analyze the performance of the numerical solution, we must define some measure of the quality of the solution. We measure how well a Dirichlet boundary blocks the flow of current directed at it. Thus we measure the current,

$$\mathbf{j} = \Im\{\psi^*(\mathbf{r})\nabla\psi(\mathbf{r})\}, \tag{4.55}$$

behind a straight wall of length l. To simplify the analysis we integrate $\mathbf{j}\cdot\mathbf{n}$ over a "detector" located on one side of a wall with a normally incident plane wave on the other side. We divide this integrated current by the current which would have been incident on the detector without the wall present. We call this ratio, $\mathcal{T}$, the transmission coefficient of the wall. Instead of $\mathcal{T}$ as a function of N, we consider $\mathcal{T}$ vs. ρ, where $\rho = 2\pi N/(lk)$ is the number of boundary pieces per wavelength.

We consider three methods of constructing the matrix $\mathbf{M}$ for each value of ρ. The first is the simplest approximation:

$$M_{ij} = \begin{cases} \int_{\mathcal{C}_i} ds\, G_0(\mathbf{r}_i, \mathbf{r}(s)) & i = j \\ \\ \Delta G_0(\mathbf{r}_i, \mathbf{r}_j) & i \neq j, \end{cases} \tag{4.56}$$

which we call the "fully-approximated" $\mathbf{M}$. The next is a more sophisticated approximation with

$$M_{ij} = \begin{cases} \int_{\mathcal{C}_j} ds\, G_0(\mathbf{r}_i, \mathbf{r}(s)) & |s_i - s_j| < \frac{\kappa}{k} \\ \\ \Delta G_0(\mathbf{r}_i, \mathbf{r}_j) & |s_i - s_j| \geq \frac{\kappa}{k}, \end{cases} \tag{4.57}$$

which we call the "band-integrated" $\mathbf{M}$ because we perform the integrals only inside a band of $\kappa/(2\pi)$ wavelengths. Finally, we consider

$$M_{ij} = \int_{\mathcal{C}_j} ds\, G_0(\mathbf{r}_i, \mathbf{r}(s)) \quad \forall ij, \tag{4.58}$$

which we call the "integrated" $\mathbf{M}$.

Numerically, the "band-integrated" and "integrated" $\mathbf{M}$ require far more computational work than the "fully-approximated" $\mathbf{M}$ which requires the fewest integrals. All methods of calculating $\mathbf{M}$ scale as $\mathcal{O}(N^2)$. The calculation of $\mathbf{T}$ or $\mathbf{T}\Phi$ from $\mathbf{M}$ scales as $\mathcal{O}(N^3)$ and the calculation of $\psi(\mathbf{r})$ for a particular $\mathbf{r}$ from a given $\mathbf{T}\Phi$ scales as $\mathcal{O}(N)$. Which of these various calculations dominates the computation time depends on what sort of computation is being performed. When computing wavefunctions, computation time is typically dominated by the large number of $\mathcal{O}(N)$ vector multiplications. However, when calculating $\psi(\mathbf{r})$ in only a small number of places, e.g., when performing a flux calculation, computation time is often dominated by the $\mathcal{O}(N^3)$ construction of $\mathbf{T}\Phi$.

In Figure 4.1 we plot $\log_{10}\mathcal{T}$ vs. ρ for the three methods above and $2 \leq \rho \leq 30$. We see that all three methods block more than 99% of the current for $\rho > 5$. However, it is clear from the Figure that the "integrated" $\mathbf{M}$ and to a lesser extent the "band-integrated" $\mathbf{M}$ strongly outperform the "fully-approximated" $\mathbf{M}$ for all ρ plotted.

4.7 From Wavefunctions to Green Functions

We pause in the development of these various boundary conditions to explain how to get Green functions (which we'll need to use these boundary conditions in more complex scattering problems) from the wavefunctions we've been computing.

All the above methods compute wavefunctions from given boundary conditions and incoming waves. In several cases, the idea of an incoming wave is somewhat strange. For example, what is an incoming wave on a periodic boundary? However, we include the incoming wave only to allow the computation of Green functions as we outline below. When we have an eigenstate of the boundary condition, the incoming wave must be become unimportant and we will show that below.

One simple way to form a Green function from a *general* solution for wavefunctions is to recall that $G(\mathbf{r}, \mathbf{r}'; E)$ is the wavefunction at $\mathbf{r}$ given that the incoming wave is a free-space point-source at $\mathbf{r}'$, $\phi(\mathbf{r}) = G_o(\mathbf{r}, \mathbf{r}'; E)$. This yields an expression for the Green function

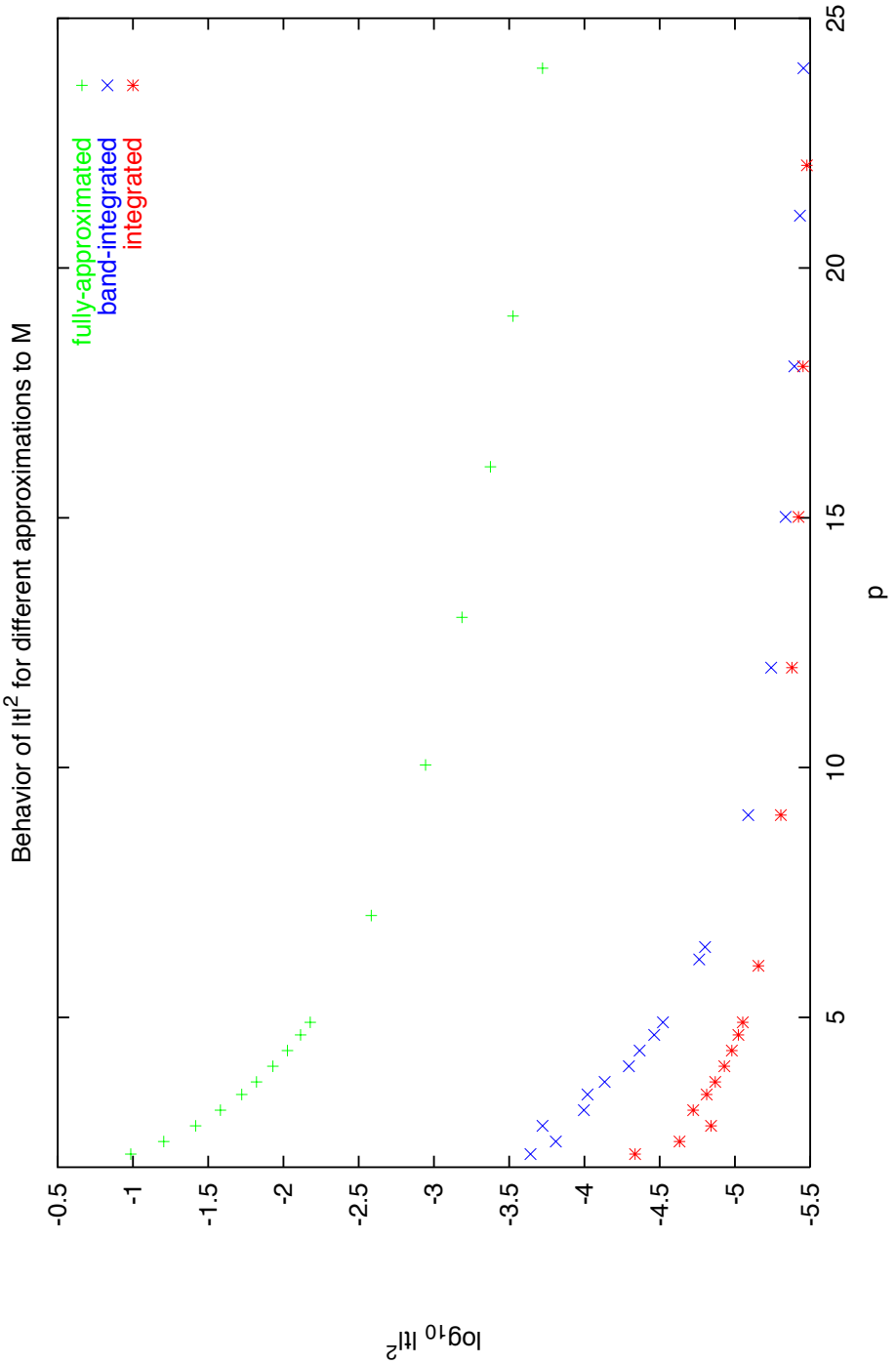

Figure 4.1: Transmission (at normal incidence) through a flat wall via the Boundary Wall method.

everywhere as a linear function of G_o.

4.7.1 Example I: Dirichlet Boundaries

For Dirichlet boundaries we had

$$\psi(\mathbf{r}) = \phi(\mathbf{r}) + \int G_o(\mathbf{r}, \mathbf{r}(s); E) T(s, s') \phi(\mathbf{r}(s'))\, ds\, ds'$$

where $T(s, s') = [G_o(s, s')]^{-1}$. So

$$G(\mathbf{r}, \mathbf{r}'; E) = G_o(\mathbf{r}, \mathbf{r}'; E) + \int G_o(\mathbf{r}, \mathbf{r}(s); E) T(s, s') G_o(\mathbf{r}(s'), \mathbf{r}'; E)\, ds\, ds'$$

4.7.2 Example II: Periodic Boundaries

For periodic boundaries we had

$$\psi(\mathbf{r}) = \phi(\mathbf{r}) + \int \left[G_o(\mathbf{r}, \mathbf{r}_1(s); E) f_1(s) + G_o(\mathbf{r}, \mathbf{r}_2(s); E) f_2(s) \right]\, ds\, ds'$$

where f_1 and f_2 are determined from

$$\begin{pmatrix} \mathbf{f}_1 \\ \mathbf{f}_2 \end{pmatrix} = \begin{pmatrix} \mathcal{G}_1 & \mathcal{G}_2 \\ \mathcal{G}_1' & \mathcal{G}_2' \end{pmatrix}^{-1} \begin{pmatrix} \mathbf{a} \\ \mathbf{a}' \end{pmatrix}$$

If we define

$$\begin{aligned} F_1(s, \mathbf{r}') = f_1(s) \quad &\text{given} \quad \phi(\mathbf{r}) = G_o(\mathbf{r}, \mathbf{r}'; E) \\ F_2(s, \mathbf{r}') = f_2(s) \quad &\text{given} \quad \phi(\mathbf{r}) = G_o(\mathbf{r}, \mathbf{r}'; E) \end{aligned}$$

we have

$$G(\mathbf{r}, \mathbf{r}'; E) = G_o(\mathbf{r}, \mathbf{r}'; E) + \int \left[G_o(\mathbf{r}, \mathbf{r}_1(s); E) F_1(s, \mathbf{r}') + G_o(\mathbf{r}, \mathbf{r}_2(s); E) F_2(s, \mathbf{r}') \right]\, ds$$

Though this looks like we have to solve many more equations than just to get the wavefunction, we note that the operator inverse which we need to get the wavefunction is sufficient to get the Green function, just as in the Dirichlet case. We simply apply that inverse to more vectors. Thus for all boundary conditions, the Green function requires extra matrix-vector multiplication work but the same amount of matrix inversion work.

4.8 Eigenstates

It is also useful to be able to use the above methods to identify eigenenergies and eigenstates (if they exist) of the above boundary conditions. This is actually quite simple. All of the various cases involved inverting some sort of generalized Green function operator on the boundary. This inverse is a generalized t-matrix and its poles correspond to eigenstates. Poles of t correspond to linear zeroes of G and so we may use standard techniques to check for a singular operator. If the operator we are inverting is singular, its nullspace holds the coefficients required to form the eigenstate. A more concrete explanation of this can be found in section 9.1.

Chapter 5

Scattering in Wires I: One Scatterer

In this section we consider the renormalization of the scatterer strength due to the presence of infinite length boundaries. The picture we have in mind is that of two dimensional wire (one dimensional free motion) with periodic boundary conditions in the transverse direction and a single scattering center. This will be our first example of scatterer renormalization by an external boundary.

5.1 One Scatterer in a Wide Wire

It seems intuitively clear that the scattering off a small object in the middle of a big wire should be much like scattering in free space. After all, if the confining walls are further away than any other length scale in the problem, they ought to play a small role. In this section we attempt to make this similarity explicit by computing the transmission coefficient for a wide wire with one small scatterer in its center. We will simply be making the connection between cross-section and transmission in the ballistic limit.

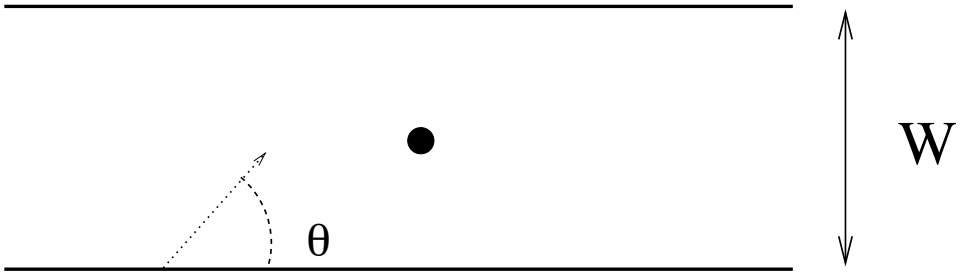

Figure 5.1: A Periodic wire with one scatterer and an incident particle.

We begin with a simple classical argument. Suppose a particle in the wire is incident with angle θ with respect to the walls, as in figure 5.1. What is the probability that such a particle scatters? For a small scatterer, the probability is approximately $P(\theta) = \frac{\sigma}{W} \times \frac{1}{\cos\theta}$. Of course, this must break down before $P(\theta) > 1$ but for $\sigma << W$ this will a small range of θ.

We now need to know how the various incident angles are populated in a particular scattering process. For this, we must think more carefully about the physical system we have in mind. In our case, this is a "two probe" conductance measurement on our wire, as pictured in figure 5.2. Our physical system involves connecting our wire to contacts which serve as reservoirs of scattering particles (e.g., electrons), running a fixed current, I, through the system and then measuring the voltage, V. Theoretically, it is the ratio of current to voltage which is interesting, thus we define the unitless conductance of this system,$g = (h/e^2)I/V$.

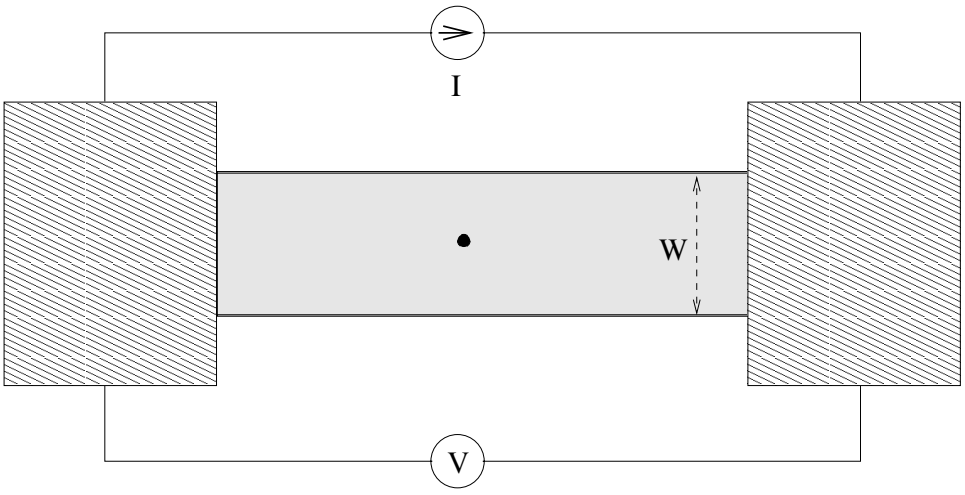

Figure 5.2: "Experimental" setup for a conductance measurement. The wire is connected to ideal contacts and the voltage drop at fixed current is measured.

In such a setup all of the transverse *quantum* channels are populated with equal probability. Since the quantum channels are uniformly distributed in momentum we have for the probability density of finding a particular transverse wavenumber, $\rho(k_y)dk_y = \frac{1}{2\sqrt{E}}dk_y$. We also know that $k_y = \sqrt{E}\sin\theta$ and together these give the density of incoming angles in the plane of the scatterer. $\rho(\theta)d\theta = \frac{1}{2}\cos\theta$. We'll also assume the scattering is isotropic; half of the scattered wave scatters backward. So, we have

$$R = \frac{1}{2}\int_{-\pi/2}^{\pi/2} P(\theta)\rho(\theta)\,d\theta = \frac{\pi\sigma}{4W}. \tag{5.1}$$

The maximum cross section of a zero range interaction in two dimensions is $4/\sqrt{E}$ (see 2.4) and corresponds to scattering all incoming s-waves. If we put this into (5.1), we get $R = \frac{\pi}{\sqrt{E}W}$. Interestingly, this is exactly one quantized channel of reflection. The wire has as many channels as half wavelengths fit across it, $N_c = \frac{\sqrt{E}W}{\pi}$ and the reflection coefficient is simply $1/N_c$, indicating that one channel of reflection in free space (the s-wave channel) is also one channel of reflection in the wire, though no longer one specific channel.

We can check this conclusion numerically (the numerical techniques will be discussed later in the chapter) as a check on the renormalization technique and the numerical method. In figure 5.3 we plot the numerically computed reflection coefficient and the theoretical value of $1/N_c$ for wires of varying widths, from 15 half wavelengths to 150 half wavelengths. The expected behavior is nicely confirmed, although there is a noticeable

discrete jump at a couple of widths where new channels have just opened.

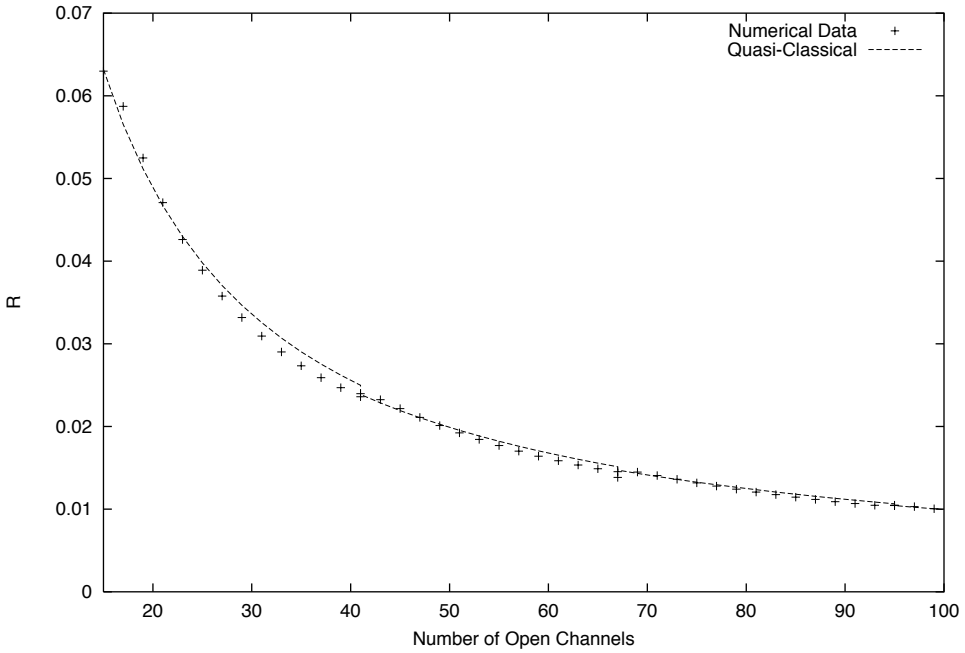

Figure 5.3: Reflection coefficient of a single scatterer in a wide periodic wire.

As the wire becomes narrower (at the left of the figure) we see that the agreement between the measured value and the quasi-classical theory is poorer. This is no surprise since our quasi-classical argument is bound to break down as the height of the wire becomes comparable to the wavelength and scatterer size. This is a hint of what we will see in section 5.6 where the limit of the narrow wire is considered. Before we consider that problem, we develop some necessary machinery. First we compute the Green function of the empty periodic wire, we then consider the renormalization of the scattering amplitude in a wire and the connection between Green functions and transmission coefficients.

It is interesting to watch the transition from wide to narrow in terms of scattering channels. Above, we saw that the scattering from one scatterer in a wide wire can be understood classically. As we will see later in the chapter, scattering in the narrow wire ($W < a \ll \lambda$) is much more complex. If we shrink the wire from wide to narrow we can watch this transition occur. This is shown in figure 5.4.

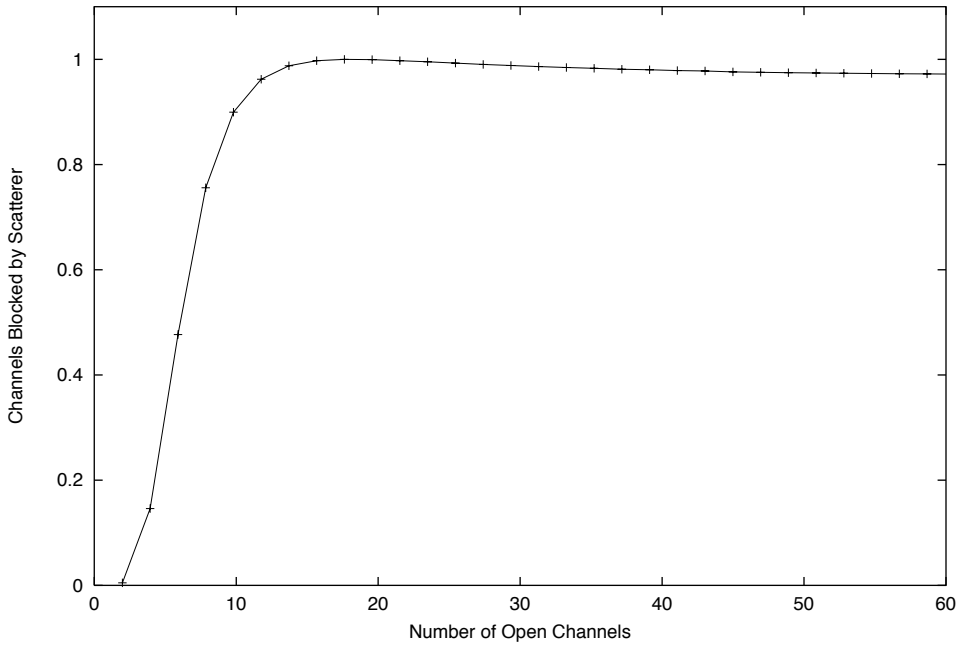

Figure 5.4: Number of scattering channels blocked by one scatterer in a periodic wire of varying width.

5.2 The Green function of an empty periodic wire

We now proceed to do some tedious but necessary mathematical work necessary to apply the methods of chapter 3 to this system. We begin by computing the Green function of the wire without the scatterer.

The state $|k, a\rangle$ defined by

$$\langle x, y\,|k, a\,\rangle = e^{ikx}\chi_a(y), \tag{5.2}$$

where $\chi_a(y)$ satisfies

$$-\frac{d^2}{dy^2}\chi_a(y) = \varepsilon_a\chi_a(y), \tag{5.3}$$

$$\chi_a(0) = \chi_a(W), \tag{5.4}$$

$$\left.\frac{d\chi_a}{dy}\right|_{y=0} = \left.\frac{d\chi_a}{dy}\right|_{y=W} \tag{5.5}$$

$$\int_0^W \chi_a^2(y)\,dy = 1, \tag{5.6}$$

is an eigenstate of the infinite ordered periodic wire. We can write the Green function of the infinite ordered wire as (see, e.g.,[10], or appendix A)

$$\hat{G}_B^+(z) = \sum_a \int_{-\infty}^{\infty} \frac{|k,a\rangle \langle k,a|}{z - \varepsilon_a - k^2 + i\epsilon}\, dk, \tag{5.7}$$

In order to perform the diagonal subtraction required to renormalize the single scatterer t-matrices (see section 3.2) we need to compute the Green function in position representation.

Equations 5.3-5.6 are satisfied by

$$\begin{array}{rlll} \chi_0(y) = \sqrt{\frac{1}{h}} & \text{with} & \varepsilon_0 = 0 & \\ \chi_a^{(0)}(y) = \sqrt{\frac{2}{W}} \sin\left(\frac{2\pi a}{W} y\right) & \text{with} & \varepsilon_a = \left(\frac{2\pi a}{W}\right)^2 & \\ \chi_a^{(1)}(y) = \sqrt{\frac{2}{W}} \cos\left(\frac{2\pi a}{W} y\right) & \text{with} & \varepsilon_a = \left(\frac{2\pi a}{W}\right)^2, & \end{array} \tag{5.8}$$

where the cos and sin solutions are degenerate for each a.

Since the eigenbasis of the wire is a product basis (the system is separable) we can apply the result of appendix A, section A.4 and we have:

$$\hat{G}_B^+(z) = \sum_a |a\rangle \langle a| \otimes \hat{g}_o^{(\pm)}(E - \varepsilon_a) \tag{5.9}$$

or, in the position representation (we will switch between the vector $\mathbf{r}$ and the pair x, y frequently in what follows),

$$G_B^+(\mathbf{r}, \mathbf{r}'; E) = G_B^+(x, y, x', y'; z) = \sum_a \chi_a(y)\chi_a(y') g_o^+(x, x'; E - \varepsilon_a), \tag{5.10}$$

where the one dimensional free Green function is

$$\begin{aligned} g_o^+(x, x'; z) &= \int_{-\infty}^{\infty} \frac{e^{ik(x-x')}}{z - k^2 + i\epsilon}\, dk \\ &= \begin{cases} \frac{-i}{2\sqrt{z}} \exp\left(i\sqrt{z}\,|x - x'|\right) & \text{if } \mathrm{Im}\{\sqrt{z}\} \geq 0, \mathrm{Re}\{z\} > 0 \\ \frac{-1}{2\sqrt{|\lambda|}} \exp\left(-\sqrt{|\lambda|}\,|x - x'|\right) & \text{if } z = -|\lambda| \end{cases}. \end{aligned}$$

When doing the Green function sum, we have to sum over all of the degenerate states at each energy. Thus, for all but the lowest energy mode (which is non-degenerate), the y-part of the sum looks like:

$$\sin\frac{2\pi a}{W} y \sin\frac{2\pi a}{W} y' + \cos\frac{2\pi a}{W} y \cos\frac{2\pi a}{W} y' = \cos\frac{2\pi a(y - y')}{W}, \tag{5.11}$$

which is sensible since the Green function of the periodic wire can depend only on $y - y'$. So, at this point, we have

$$G_B^+(x,y,x',y';z) = \frac{1}{W} g_o^{(+)}(x,x';z) + \frac{2}{W}\sum_{a=1}^{\infty} \cos\frac{2\pi a(y-y')}{W} g_o^+\left(x,x';z-\frac{4\pi^2a^2}{W^2}\right). \quad (5.12)$$

As nice as this form for G_B is, we need to do some more work. To renormalize free space scattering matrices we need to perform the diagonal subtraction discussed in section 3.2.2. In order for that subtraction to yield a finite result, G_B must have a logarithmic diagonal singularity. The next bit of work is to make this singularity explicit.

It is easy to see where the singularity will come from. Since $g_o^+(x,x;-|\lambda|) \sim \frac{1}{\sqrt{\lambda}}$ for E real there exists an M such that,

$$G_B^+(x,y,x,y;E) \approx \text{const.} + \frac{1}{2\pi}\sum_{a=M}^{\infty}\frac{1}{a}, \quad (5.13)$$

which diverges. We now proceed to extract the singularity more systematically.

We begin by substituting the definition of g_o and explicitly splitting the sum into two parts. The first part is a finite sum and includes energetically allowed transverse modes (open channels). For these modes the energy argument to g_o is positive and waves can propagate down the wire. The rest of the sum is over energetically forbidden transverse modes (closed channels). For these modes, waves in the x direction are evanescent. We define N, the greatest integer such that $E - 4\pi^2N^2/W > 0$, $k_a = \sqrt{E - 4\pi^2a^2/W^2}$ and $\kappa_a = \sqrt{4\pi^2a^2/W^2 - E}$ and have

$$\begin{aligned} G_B^+(x,y,x',y';E) &= \frac{-ie^{i\sqrt{E}|x-x'|}}{2W\sqrt{E}} - \frac{i}{W}\sum_{a=1}^{N}\cos\frac{2\pi a(y-y')}{W}\times\frac{e^{ik_a|x-x'|}}{k_a} \\ &\quad -\frac{1}{W}\sum_{a>N}^{\infty}\cos\frac{2\pi a(y-y')}{W}\times\frac{e^{-\kappa_a|x-x'|}}{\kappa_a}. \end{aligned} \quad (5.14)$$

In order to extract the singularity, we add and subtract a simpler infinite sum (see D.1),

$$\begin{aligned} &\frac{1}{2\pi}\sum_{a=1}^{\infty}\cos\frac{2\pi a(y-y')}{W}\times\frac{\exp\left(-\frac{2\pi a}{W}|x-x'|\right)}{a} \\ &= \frac{1}{4\pi}\ln\left\{\frac{\exp[2\pi(x-x')/W]}{2\cosh[2\pi(x-x')/h]-2\cos[2\pi(y-y')/W]}\right\}, \end{aligned} \quad (5.15)$$

to G_B. This gives

$$G_B^+(x,y,x',y';E) = \frac{-ie^{i\sqrt{E}|x-x'|}}{2W\sqrt{E}} - \frac{i}{W}\sum_{a=1}^{N}\cos\frac{2\pi a(y-y')}{W}$$
$$\times\left[\frac{e^{ik_a|x-x'|}}{k_a} - \frac{W\exp\left(-\frac{2\pi a}{W}|x-x'|\right)}{2i\pi a}\right]$$
$$-\frac{1}{W}\sum_{a>N}\cos\frac{2\pi a(y-y')}{W}\times\left[\frac{e^{-\kappa_a|x-x'|}}{\kappa_a} - \frac{W\exp\left(-\frac{2\pi a}{W}|x-x'|\right)}{2\pi a}\right]$$
$$-\frac{1}{4\pi}\ln\left\{\frac{\exp[2\pi(x-x')/W]}{2\cosh[2\pi(x-x')/W]-2\cos[2\pi(y-y')/W]}\right\}. \tag{5.16}$$

This is an extremely useful form for numerical work. For $x \neq x'$ or $y \neq y'$ we have transformed a slowly converging sum into a much more quickly converging sum. This is dealt with in detail in D.2.2.

In this form, the singular part of the sum is in the logarithm term and the rest of the expression is convergent for all $x-x', y-y'$. In fact, the remaining infinite sum is *uniformly* convergent for all $x-x'$, as shown in (D.2.2). We can now perform the diagonal subtraction of G_o. We begin by considering the $x \to x', y \to y'$ limit of G:

$$\lim_{x\to x',y\to y'} G^+(x,y,x',y';E) = \frac{-i}{2W\sqrt{E}} - \frac{i}{W}\sum_{a=1}^{N}\left[\frac{1}{k_a} - \frac{W}{2i\pi a}\right]$$
$$-\frac{1}{W}\sum_{a>N}\left[\frac{1}{\kappa_a} - \frac{W}{2\pi a}\right]$$
$$-\frac{1}{4\pi}\lim_{x\to x',y\to y'}\ln\left\{\frac{\exp[2\pi(x-x')/W]}{2\cosh[2\pi(x-x')/W]-2\cos[2\pi(y-y')/W]}\right\}. \tag{5.17}$$

We can use equation D.6 to simplify the limit of the logarithm:

$$\frac{1}{4\pi}\lim_{x\to x',y\to y'}\ln\left\{\frac{\exp[2\pi(x-x')/W]}{2\cosh[2\pi(x-x')/W]-2\cos[2\pi(y-y')/W]}\right\}$$
$$= \frac{1}{4\pi}\lim_{x\to x',y\to y'}\ln\left\{\left(\frac{2\pi}{W}\right)^2\left[(x-x')^2+(y-y')^2\right]\right\}$$
$$= \frac{1}{4\pi}\ln\left[\left(\frac{2\pi}{W}\right)^2\right] + \frac{1}{2\pi}\lim_{\mathbf{r}\to\mathbf{r}'}\ln\left(|\mathbf{r}-\mathbf{r}'|\right). \tag{5.18}$$

Since (from A.5.1)

$$\lim_{\mathbf{r}\to\mathbf{r}'} G_o(\mathbf{r},\mathbf{r}';z) = \frac{-i}{4} + \frac{1}{4}Y_o^{(R)}(0) + \frac{1}{2\pi}\ln(\sqrt{E}) + \frac{1}{2\pi}\ln\left(|\mathbf{r}-\mathbf{r}'|\right), \tag{5.19}$$

we have

$$\begin{aligned}\bar{G}_B^+(x,y;E) &= \lim_{\mathbf{r}\to\mathbf{r}'} G_B^+(x,y,x',y';E) - G_o^{(+)}(\mathbf{r},\mathbf{r}';E) \\ &= \frac{-i}{2W\sqrt{E}} - \frac{i}{W}\sum_{a=1}^{N}\left[\frac{1}{k_a} - \frac{W}{2i\pi a}\right] \\ &\quad -\frac{1}{W}\sum_{a>N}\left[\frac{1}{\kappa_a} - \frac{W}{2\pi a}\right] + \frac{1}{2\pi}\ln\left(\frac{2\pi}{W\sqrt{E}}\right) + \frac{i}{4} - \frac{1}{4}Y_o^{(R)}(0),\end{aligned} \tag{5.20}$$

which is independent of x and y as it must be for a translationally invariant system and finite, as proved in section 2.3.1.

The case of a Dirichlet bounded wire is very similar and so there's no need to repeat the calculation. For the sake of later calculations, we state the results here. We have

$$\begin{aligned}&G_B^+(x,y,x',y';E) = \\ &\quad -\frac{i}{W}\sum_{a=1}^{N}\sin\left(\frac{\pi a}{W}y\right)\sin\left(\frac{\pi a}{W}y'\right)\left[\frac{e^{ik_a|x-x'|}}{k_a} - \frac{e^{-\frac{2\pi}{W}a|x-x'|}}{2i\pi a}\right] \\ &\quad -\frac{1}{W}\sum_{a>N}\sin\left(\frac{\pi a}{W}y\right)\sin\left(\frac{\pi a}{W}y'\right)\left[\frac{e^{-\kappa_a|x-x'|}}{\kappa_a} - \frac{e^{-\frac{2\pi}{W}a|x-x'|}}{2\pi a}\right] \\ &\quad -\frac{1}{4\pi}\ln\left[\frac{\sin^2\frac{\pi(y+y')}{2W} + \sinh^2\frac{\pi(x-x')}{2W}}{\sin^2\frac{\pi(y-y')}{2W} + \sinh^2\frac{\pi(x-x')}{2W}}\right],\end{aligned} \tag{5.21}$$

and

$$\begin{aligned}&\bar{G}_B^+(x,y;E) = \\ &\quad -\frac{i}{W}\sum_{a=1}^{N}\sin^2\left(\frac{\pi a}{W}y\right)\left[\frac{1}{k_a} - \frac{1}{2i\pi a}\right] - \frac{1}{W}\sum_{a>N}\sin^2\left(\frac{\pi a}{W}y\right)\left[\frac{1}{\kappa_a} - \frac{1}{2\pi a}\right] \\ &\quad -\frac{1}{4\pi}\ln\left[\sin^2\frac{\pi y}{W}\right] + \frac{1}{2\pi}\ln\left(\frac{\pi}{2W\sqrt{E}}\right) + \frac{i}{4} - \frac{1}{4}Y_o^{(R)}(0).\end{aligned} \tag{5.22}$$

5.3 Renormalization of the ZRI Scattering Strength

Recall that the full Green function may be written

$$G^+(E) = G_B^+(E) + G_B^+(E)T^+(E)G_B^+(E) \tag{5.23}$$

where $T^+(E)$ is computed via the techniques in chapter 3, namely renormalization of the free space t-matrices.

We begin with a single scatterer in free space at $x = y = 0$. The t-matrix of that scatterer is (see section 2.4)

$$t^+(E) = s^+(E)\,|\mathbf{0}\rangle\,\langle\mathbf{0}| \tag{5.24}$$

which is renormalized by scattering from the boundaries of the wire:

$$T^+(E) = S^+(E)\,|\mathbf{0}\rangle\,\langle\mathbf{0}| \tag{5.25}$$

where

$$S^+(E) = s^+(E)\left[1 - s^+(E)\bar{G}_B^+(0,0;E)\right]^{-1} = \left[1/s^+(E) - \bar{G}_B^+(0,0;E)\right]^{-1}. \tag{5.26}$$

Thus, for a periodic wire,

$$1/S^+(E) = 1/s^+(E) + \frac{i}{2W\sqrt{E}} + \frac{i}{W}\sum_{a=1}^{N}\left[\frac{1}{k_a} - \frac{W}{2i\pi a}\right]$$

$$+\frac{1}{W}\sum_{a>N}\left[\frac{1}{\kappa_a} - \frac{W}{2\pi a}\right] - \frac{1}{2\pi}\ln\left(\frac{2\pi}{W\sqrt{E}}\right) + \frac{1}{4}Y_o^{(R)}(0), \tag{5.27}$$

and in the Dirichlet bounded wire,

$$\begin{aligned} 1/S^+(E) \;=\; & 1/s^+(E) + \frac{i}{2W\sqrt{E}} + \frac{i}{W}\sum_{a=1}^{N}\sin^2\left(\frac{\pi a}{y}\right)\left[\frac{1}{k_a} - \frac{W}{2i\pi a}\right] \\ & +\frac{1}{W}\sum_{a>N}\sin^2\left(\frac{\pi a}{y}\right)\left[\frac{1}{\kappa_a} - \frac{W}{2\pi a}\right] \\ & +\frac{1}{4\pi}\ln\left[\sin^2\frac{\pi y}{W}\right] - \frac{1}{2\pi}\ln\left(\frac{\pi}{h\sqrt{E}}\right) + \frac{1}{4}Y_o^{(R)}(0). \end{aligned} \tag{5.28}$$

So we have

$$G^+(x,y,x',y';E) = G_B^+(x,y,x',y';E) + G_B^+(x,y,0,0;E)S^+(E)G_B^+(0,0,x',y';E). \tag{5.29}$$

with $S^+(E)$ defined above.

5.4 From the Green function to Conductance

Since we now have the full Green function in the position representation, we can compute it between any two points in the wire. We can use this to compute the unitless conductance, g, of the wire via the Fisher-Lee relation [16, 40],

$$g = \mathrm{Tr}(\mathcal{T}^\dagger\mathcal{T}) \tag{5.30}$$

where $\mathcal{T}$ is the transmission matrix, i. e., $(\mathcal{T})_{ab}$ is the amplitude for transmitting from channel a in the left lead to channel b in the right lead. $\mathcal{T}$ is constructed from $G^+(\mathbf{r},\mathbf{r}';E)$ via

$$(\mathcal{T})_{ab} = -iv_a\sqrt{\frac{k_b}{k_a}}G^+_{ab}(x,x';E)\exp[-i(k_b x - k_a x')], \tag{5.31}$$

where

$$G^+_{ab}(x,x';E) = \left\langle x,a\left|\hat{G}^+(E)\right|x',b\right\rangle = \int \chi^*_a(y)G^+(x,y,x',y';E)\chi_b(y')\,dy\,dy', \tag{5.32}$$

is the Green function projected onto the channels of the leads. Since the choice of x and x' are arbitrary, we can choose them large enough that all the evanescent modes are arbitrarily small and thus we can ignore the closed channels. So there are only a finite number of propagating modes and the trace in the Fisher-Lee relation is a finite sum. We note that the prefactor $v_a\sqrt{k_a/k_b}$ is there simply because we have normalized our channels via $\int_0^h |\chi_a(y)|\,dy = 1$ rather than to unit flux. More detail on this is presented in [16] and even more in the review [40].

5.5 Computing the channel-to-channel Green function

We write the Green function of the infinite ordered wire as (see, e.g.,[10])

$$\hat{G}^+_B(z) = \sum_a \int_{-\infty}^{\infty} \frac{|k,a\rangle\langle k,a|}{z-\varepsilon_a-k^2+i\epsilon}\,dk, \tag{5.33}$$

so

$$\left\langle x,a\left|\hat{G}^+_B(z)\right|x',b\right\rangle = \delta_{ab}\int_{-\infty}^{\infty}\frac{e^{ik(x-x')}}{z-\varepsilon_a-k^2+i\epsilon}\,dk. \tag{5.34}$$

Since

$$\hat{G}^+(z) = \hat{G}^+_B(z) + \hat{G}^+_B(z)\hat{T}^+(z)\hat{G}^+_B(z), \tag{5.35}$$

and $T(z) = S(z)\,|r_s\rangle\langle r_s|$ we have

$$\begin{aligned} G^+_{ab}(x,x';z) &= \delta_{ab}\,g^+_o(x,x';z) \\ &\quad + g^+_o(x,x_s;z-\varepsilon_a)\,\chi_a(y_s)\,S^+(z)\chi_b(y_s)\,g^+_o(x_s,x';z-\varepsilon_b), \end{aligned}$$

If the t-matrix comes from the multiple scattering of many zero range interactions the t-matrix can be written:

$$\hat{t}(z) = \sum_{ij}|\mathbf{r_i}\rangle\,(\mathbf{t}(z))_{ij}\,\langle\mathbf{r_j}|\,. \tag{5.36}$$

In that case we will have a slightly more complicated expression for the channel-to-channel Green function:

$$\begin{aligned} G^+_{ab}(x,x';z) &= \delta_{ab}\, g^+_o\,(x,x';z) \\ &\quad + \sum_{ij} g^+_o\,(x,x_i;z-\varepsilon_a)\,\chi_a\,(y_i)\,(\mathbf{t}(z))_{ij}\,\chi_b\,(y_j)\,g^+_o\,(x_j,x';z-\varepsilon_b)\,, \end{aligned} \tag{5.37}$$

5.6 One Scatterer in a Narrow Wire

Whereas the wide wire can be modeled classically, the narrow wire is essentially quantum mechanical. In fact, what we mean by a narrow wire is a wire with fewer than one half-wavelength across it.

When the wire becomes narrow, the renormalization of the scattering amplitude due to the presence of the wire walls becomes significant. This is immediately apparent when we consider the case of a wire which is narrower than the scattering length of the scatterer. In essence, we consider reducing a two-dimensional scattering problem to a one-dimensional one by shrinking the width of the wire.

We'd like to consider the case where the wavelength, λ, is much larger than the width of the wire. This cannot be done for a wire with Dirichlet boundary conditions since there the lowest energy with one open channel gives a half wavelength across the wire. We will instead use a wire with periodic boundary conditions to consider this case. If the wide wire result remains valid, we would expect the transmission coefficient to be zero when there is only one open channel since, in the wide wire, our scatterer reflected exactly one channel. However, as we already saw in figure 5.4 this is not the case. As we see in more detail in figure 5.5, the transmission coefficient has a surprisingly non-trivial behavior when the width of the wire shrinks below a wavelength.

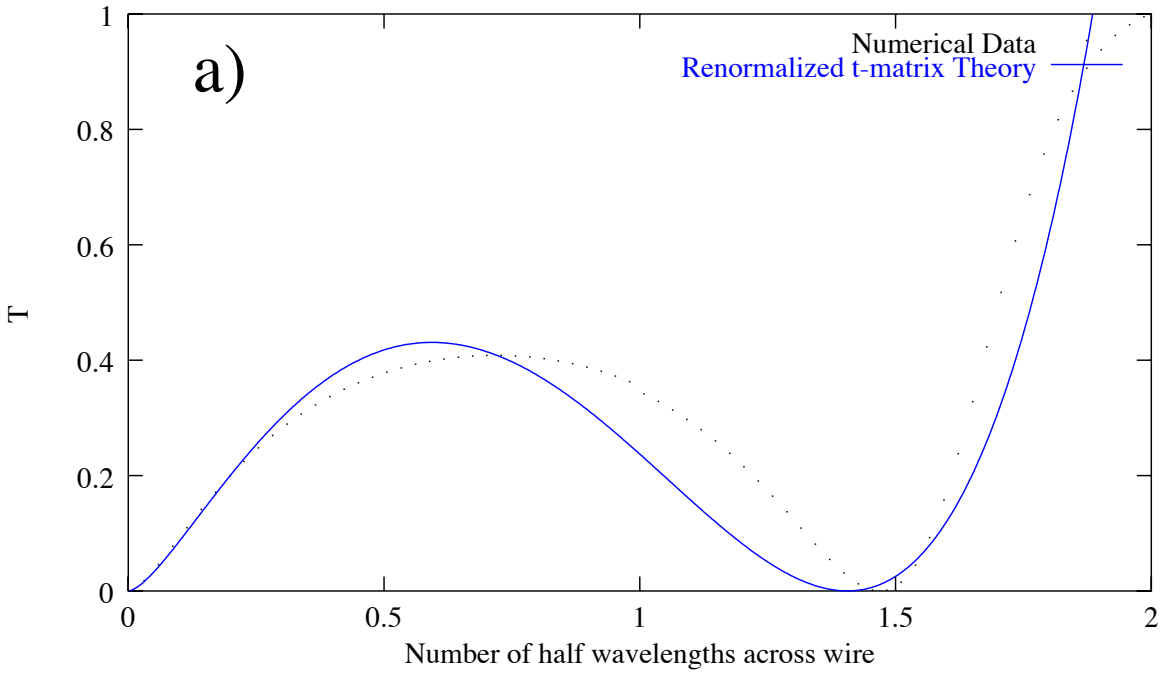

Figure 5.5: Transmission coefficient of a single scatterer in a narrow periodic wire.

It is possible to define a sort of cross-section in one dimension, for instance via the $d = 1$ optical theorem from section 2.2. In figure 5.6, we plot the cross-section of the scatterer rather than the transmission coefficient.

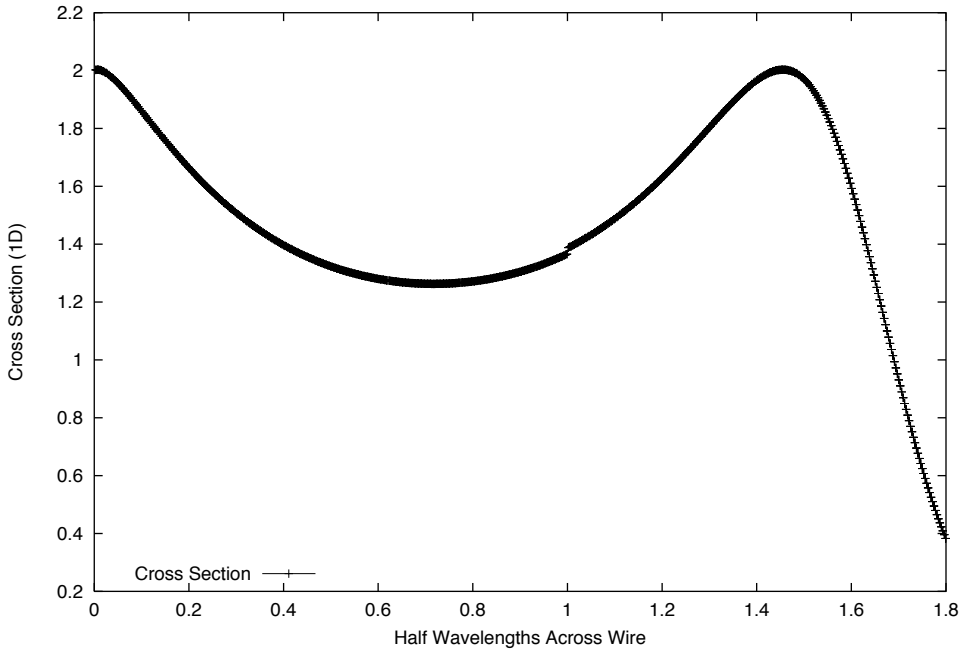

Figure 5.6: Cross-Section of a single scatterer in a narrow periodic wire.

There are various unexpected features of this transmission. In particular, why should the transmission go to 0 at some finite wire width? Also, why should the transmission go to 0 for a zero width wire? A less obvious feature, but one which is perhaps more interesting, is that for very small widths the behavior of the transmission coefficient is independent of the original scattering strength.

These features are consequences of the renormalization of the scattering amplitude. To see how this transmission occurs, we compute the full channel-to channel Green function for one scatterer in the center ($x = 0$) of a narrow ($h \to 0$) periodic wire. Since the wire is narrow, there is only one open channel so the channel to channel Green function has only one term.

$$\begin{aligned} \lim_{W\to 0} G^+_{00}(x,y,x',y';E) &= g^+_o(x,x';E) \\ &\quad + g^+_o(x,0;E)\frac{1}{\sqrt{W}}\left[\lim_{W\to 0} S^+(E)\right]\frac{1}{\sqrt{W}}\, g^+_o(0,x';E). \end{aligned}$$

The small W limit of $S^+(E)$ is straightforward. Using the result (5.27), we have

$$S^+(E) = \left\{ \frac{i}{2W\sqrt{E}} - \frac{1}{2\pi} \ln\left(\frac{2\pi a}{W}\right) + \frac{1}{W} \sum_{a=1}^{\infty} \left[\frac{1}{\kappa_a} - \frac{W}{2\pi a} \right] \right\}^{-1}. \tag{5.38}$$

For small W,

$$1/\kappa_a \approx \frac{W}{2\pi a} \left(1 + \frac{EW^2}{8\pi^2 a^2} \right), \tag{5.39}$$

and so the closed-channel sum may be approximated

$$\frac{1}{2\pi} \sum_{a=1}^{\infty} \frac{1}{a} \left(\frac{EW^2}{8\pi^2 a^2} \right) = \frac{EW^2}{16\pi^3} \sum_{a=1}^{\infty} \frac{1}{a^3} = \frac{EW^2}{16\pi^3} \zeta(3) \approx 1.2 \frac{EW^2}{16\pi^3}. \tag{5.40}$$

So

$$S^+(E) \overset{W<<1/\sqrt{E}}{=} \left[\frac{i}{2W\sqrt{E}} - \frac{1}{2\pi} \ln\left(\frac{2\pi a}{W}\right) + 1.2 \frac{EW^2}{16\pi^3} \right]^{-1}. \tag{5.41}$$

Using the definition of g_o and factoring out the large $i/2W\sqrt{E}$ in S^+ we have

$$\begin{aligned} \lim_{W\to 0} G_{00}^+(x,y,x',y';E) \quad \approx \quad & \frac{-i}{2\sqrt{E}} e^{i\sqrt{E}|x-x'|} \\ & + \frac{-i}{2\sqrt{E}} e^{i\sqrt{E}|x|} \frac{1}{\sqrt{W}} \\ & \times \frac{2W\sqrt{E}}{i} \left[1 + \frac{W\sqrt{E}}{i\pi} \ln\left(\frac{2\pi a}{W}\right) - 1.2 \frac{E^{3/2}W^3}{8i\pi^3} \right] \\ & \times \frac{1}{\sqrt{W}} \frac{-i}{2\sqrt{E}} e^{i\sqrt{E}|x'|} \end{aligned} \tag{5.42}$$

which, after the dust settles, can be re-written as

$$\begin{aligned} \lim_{W\to 0} G_{00}^{(+)}(x,y,x',y';E) \quad \approx \quad & \frac{-i}{2\sqrt{E}} e^{i\sqrt{E}|x-x'|} \\ & + \frac{i}{2\sqrt{E}} e^{i\sqrt{E}(|x|+|x'|)} \left[1 + \frac{W\sqrt{E}}{i\pi} \ln\left(\frac{2\pi a}{W}\right) - 1.2 \frac{E^{3/2}W^3}{8i\pi^3} \right] \end{aligned} \tag{5.43}$$

Since we are interested only in transmission, we can assume $x < 0$ and $x' > 0$ so $|x - x'| = |x| + |x'|$. With this caveat, we have

$$\lim_{W\to 0} G_{00}^+(x,y,x',y';E) \approx e^{i\sqrt{E}(|x|+|x'|)} \left[\frac{h}{2\pi} \ln\left(\frac{2\pi a}{W}\right) - 1.2 \frac{EW^3}{16\pi^3} \right]. \tag{5.44}$$

Finally, from (5.31), we have

$$(\mathcal{T})_{00} = -i \left[\frac{W\sqrt{E}}{\pi} \ln\left(\frac{2\pi a}{W}\right) - 1.2 \frac{E^{3/2}W^3}{8\pi^3} \right], \tag{5.45}$$

since, in units where $\hbar^2/2m = 1$, $v = 2\sqrt{E}$. We have plotted this small W approximation $|(\mathcal{T})_{00}|^2$ in figure 5.5. We see that there is good quantitative agreement for widths of fewer than $1/4$ wavelength. What is perhaps more surprising is the reasonably good qualitative agreement for the entire range of one wavelength.

Chapter 6

Scattering in Rectangles I: One Scatterer

In this section we begin the discussion of closed systems and eigenstates. As with the scatterer in a wire problem, we have quite a bit of preliminary work to do. We first compute the Background Green function, G_B and the diagonal difference $\langle \mathbf{r} | G_B - G_o | \mathbf{r} \rangle$ for the Dirichlet rectangle.

We then perform a simple numerical check on this result by using it to compute the ground state energy of a 1×1 square with a single zero range interaction at the center. We compare these energies with those computed by successive-over-relaxation (a standard lattice technique [33]) for a hard disk of the same effective radius as specified for the scatterer. This provides the simplest illustration of the somewhat subtle process of extracting discrete spectra from scattering theory.

We then compute the background Green function and diagonal difference for the periodic rectangle (a torus), as we will need that in 9.

6.1 Dirichlet boundaries

6.1.1 The Background Green Function

We consider a rectangular domain, $\mathbf{D}$, in R^2 defined by

$$\mathbf{D} = [0, l] \times [0, W] = \{(x, y) | 0 < x < l, 0 < y < W\}. \tag{6.1}$$

We wish to solve Schrödinger's equation

$$\left[\frac{\hbar^2}{2m}\nabla^2 + E\right]\psi(\vec{r}) = 0, \tag{6.2}$$

in the domain $\mathbf{D}$ subject to the boundary condition

$$\vec{r} \in \partial\mathbf{D} \Rightarrow \psi(\vec{r}) = 0, \tag{6.3}$$

where $\partial\mathbf{D}$ is the boundary of $\mathbf{D}$.

As in the previous chapter we set $\frac{\hbar^2}{2m} = 1$. Our equation reads

$$\left(\frac{\partial^2}{\partial x^2} + \frac{\partial^2}{\partial y^2} + E\right)\psi(x,y) = 0. \tag{6.4}$$

The eigen-functions of $\mathcal{L} = -\left(\frac{\partial^2}{\partial x^2} + \frac{\partial^2}{\partial y^2}\right)$ in the above domain with given boundary condition are

$$\phi_{nm}(x,y) = \frac{2}{\sqrt{lW}}\sin\left(\frac{n\pi x}{l}\right)\sin\left(\frac{m\pi y}{W}\right), \tag{6.5}$$

which satisfy

$$-\left(\frac{\partial^2}{\partial x^2} + \frac{\partial^2}{\partial y^2}\right)\phi_{nm}(x,y) = \left(\frac{n^2\pi^2}{l^2} + \frac{m^2\pi^2}{W^2}\right)\phi_{nm}(x,y). \tag{6.6}$$

We can thus write down a box Green function in the position representation

$$G_B(x,y,x',y';E) = \frac{4}{lW}\sum_{n,m=1}^{\infty}\frac{\sin\left(\frac{n\pi x}{l}\right)\sin\left(\frac{n\pi x'}{l}\right)\sin\left(\frac{m\pi y}{W}\right)\sin\left(\frac{m\pi y'}{W}\right)}{E - \frac{n^2\pi^2}{l^2} - \frac{m^2\pi^2}{W^2}}, \tag{6.7}$$

which satisfies

$$\left(z + \frac{\partial^2}{\partial x^2} + \frac{\partial^2}{\partial y^2}\right)G_B(x,y,x',y';z) = \delta(x-x')\delta(y-y'). \tag{6.8}$$

6.1.2 Re-summing the Dirichlet Green Function

As in the previous chapter, we'd like to rewrite this double sum as a single sum. We can do this by rearranging the sum and recognizing a Fourier series. First we re-arrange 6.7 as follows:

$$G_B(x,y,x',y';E) = \frac{2}{l}\sum_{n=1}^{\infty}\sin\left(\frac{n\pi x}{l}\right)\sin\left(\frac{n\pi x'}{l}\right)\frac{2}{W}\sum_{m=1}^{\infty}\frac{\sin\left(\frac{m\pi y}{h}\right)\sin\left(\frac{m\pi y'}{W}\right)}{\left(E - \frac{n^2\pi^2}{l^2}\right) - \frac{m^2\pi^2}{W^2}}. \tag{6.9}$$

We define

$$k_n = \sqrt{E - \frac{n^2\pi^2}{l^2}} \tag{6.10}$$

$$N = \left[\frac{l}{\pi}\sqrt{E}\right] \tag{6.11}$$

$$\kappa_n = \sqrt{\frac{n^2\pi^2}{l^2} - E}, \tag{6.12}$$

where $[x]$ is the greatest integer less than equal or equal to x. and then apply a standard trigonometric identity to the product of sines in the inner sum to yield

$$G_B(x,y,x',y';E) = \frac{2}{l}\sum_{n=1}^{\infty}\sin\left(\frac{n\pi x}{l}\right)\sin\left(\frac{n\pi x'}{l}\right)\frac{W}{\pi^2}\sum_{m=1}^{\infty}\frac{\cos\left(\frac{m\pi(y-y')}{W}\right)-\cos\left(\frac{m\pi(y+y')}{W}\right)}{\frac{W^2}{\pi^2}k_n^2 - m^2}. \tag{6.13}$$

We now need the Fourier series (see, e.g.,[18])

$$\sum_{n=1}^{\infty}\frac{\cos nx}{a^2-n^2} = \frac{\pi}{2}\frac{\cos\left[a(\pi-x)\right]}{a\sin\pi a} - \frac{1}{2a^2}, \tag{6.14}$$

for $0 \le x \le 2\pi$. So we have

$$\begin{aligned} G_B(x,y,x',y';E) &= \frac{2}{l}\sum_{n=1}^{\infty}\sin\left(\frac{n\pi x}{l}\right)\sin\left(\frac{n\pi x'}{l}\right) \\ &\quad\times\frac{1}{2}\frac{\cos\left[k_n\left(W-(y-y')\right)\right]-\cos\left[k_n\left(W-(y+y')\right)\right]}{k_n\sin hk_n}, \end{aligned}$$

and, after applying trigonometric identities, we have

$$\begin{aligned} G_B(x,y,x',y';E) &= -\frac{2}{l}\sum_{n=1}^{\infty}\sin\left(\frac{n\pi x}{l}\right)\sin\left(\frac{n\pi x'}{l}\right) \\ &\quad\times\frac{\sin\left[k_n\left(W-y\right)\right]\sin\left[k_n y'\right]}{k_n\sin k_n W}. \end{aligned}$$

We now re-write our expression for G_B yet again:

$$\begin{aligned} G_B(x,y,x',y';E) &= \frac{2}{l}\sum_{n=1}^{N}\frac{\sin\left(\frac{n\pi x}{l}\right)\sin\left(\frac{n\pi x'}{l}\right)\sin(k_n y')\sin\left[k_n\left(y-W\right)\right]}{k_n\sin\left(k_n W\right)} \\ &\quad+\frac{2}{l}\sum_{n=N+1}^{\infty}\frac{\sin\left(\frac{n\pi x}{l}\right)\sin\left(\frac{n\pi x'}{l}\right)\sinh(\kappa_n y')\sinh\left[\kappa_n\left(y-W\right)\right]}{\kappa_n\sinh\left(\kappa_n W\right)} \end{aligned} \tag{6.15}$$

6.1.3 Properties of the Re-summed G_B

As we will show below, the sum in (6.15) is not uniformly convergent as $y \to y'$. However, this limit is essential for calculation of renormalized t-matrices. We can, however, add and subtract something from each term so that we are left with convergent sums and singular sums with limits we understand.

Since the sum is symmetric under $y \leftrightarrow y'$ (this is obvious from the physical symmetry as well as the original double sum, equation 6.7), we may choose $y < y'$. We define $\delta = y' - y > 0$. and re-write the sum (6.15) as follows:

$$\begin{aligned} G_B(x,y,x',y';k^2) &= \frac{2}{l}\sum_{n=1}^{N}\frac{\sin\left(\frac{n\pi x}{l}\right)\sin\left(\frac{n\pi x'}{l}\right)\sin(k_n y')\sin\left[k_n\left(y-W\right)\right]}{k_n\sin\left(k_n W\right)} \\ &\quad +\frac{1}{l}\sum_{n=N+1}^{\infty}u_n, \end{aligned} \tag{6.16}$$

where

$$u_n = 2\sin\left(\frac{n\pi x}{l}\right)\sin\left(\frac{n\pi x'}{l}\right)\frac{\sinh\left(\kappa_n y\right)\sinh\left[\kappa_n(W-y-\delta)\right]}{\kappa_n\sinh\left(\kappa_n W\right)}. \tag{6.17}$$

We rewrite u_n to simplify the following analysis.

$$\begin{aligned} u_n &= -\sin\left(\frac{n\pi x}{l}\right)\sin\left(\frac{n\pi x'}{l}\right)\frac{\left(1-e^{-2\kappa_n W}\right)^{-1}}{\kappa_n}\times \\ &\quad \left[e^{-\kappa_n\delta}-e^{-\kappa_n(2y+\delta)}+e^{-\kappa_n(2W-\delta)}-e^{-\kappa_n(2W-2y+\delta)}\right]. \end{aligned} \tag{6.18}$$

We define

$$g_n(\xi) = \sin\left(\frac{n\pi x}{l}\right)\sin\left(\frac{n\pi x'}{l}\right)\frac{\left(1-e^{-2\kappa_n W}\right)^{-1}}{\kappa_n}e^{-\kappa_n\xi}. \tag{6.19}$$

We observe that for $M < n$

$$\begin{aligned} |g_n(\xi)| &\leq \frac{\left[1-\exp(-2\kappa_n W)\right]^{-1}}{\kappa_n}\exp\left(-\kappa_n\xi\right) \\ &\leq \frac{\left[1-\exp(-2\kappa_M W)\right]^{-1}}{\kappa_M}\exp\left(-\kappa_n\xi\right) \\ &< \frac{\left[1-\exp(-2\kappa_M W)\right]^{-1}}{\kappa_M}\exp\left(-\frac{\pi n}{l}\xi\right)\exp\left(\frac{El}{2n\pi}\xi\right) \\ &< \frac{\left[1-\exp(-2\kappa_M W)\right]^{-1}}{\kappa_M}\exp\left(\frac{El}{2M\pi}\xi\right)\exp\left(-\frac{\pi n}{l}\xi\right), \end{aligned} \tag{6.20}$$

and therefore

$$\sum_{n=M}^{\infty} g_n(\xi) < \frac{\left[1-\exp\left(-2\kappa_M W\right)\right]^{-1}}{\kappa_M} \exp\left(\frac{El}{2M\pi}\xi\right) \exp\left(\frac{-M\pi\xi}{l}\right) \frac{1}{1-\exp\left(\frac{-\pi\xi}{l}\right)}, \quad (6.21)$$

which converges for $\xi > 0$ but not uniformly. Thus we cannot take the $\xi \to 0$ limit inside the sum. However, if we can subtract off the diverging part, we may be able to find a uniformly converging sum as a remainder. With that in mind, we define

$$h_n(\xi) = \sin\left(\frac{n\pi x}{l}\right) \sin\left(\frac{n\pi x'}{l}\right) \frac{l}{n\pi} \exp\left(-\frac{n\pi}{l}\xi\right) \quad (6.22)$$

We first note that the sum $\sum_{n=1}^{\infty} h_n(\xi)$ may be performed exactly (see appendix D) yielding:

$$\sum_{n=1}^{\infty} h_n(\xi) = \frac{l}{4\pi} \ln\left\{\frac{\sin^2\left[\frac{\pi(x+x')}{2l}\right] + \sinh^2\left(\frac{\pi\xi}{2l}\right)}{\sin^2\left[\frac{\pi(x-x')}{2l}\right] + \sinh^2\left(\frac{\pi\xi}{2l}\right)}\right\}. \quad (6.23)$$

We now subtract $h_n(\xi)$ from $g_n(\xi)$ to get

$$\begin{aligned} g_n(\xi) - h_n(\xi) = & \\ & \sin\left(\frac{n\pi x}{l}\right) \sin\left(\frac{n\pi x'}{l}\right) \frac{l}{n\pi} \times \\ & \left[\left(1-e^{-2\kappa_n W}\right)^{-1} \left(1-\frac{El^2}{n^2\pi^2}\right)^{-1/2} \exp\left(-\frac{n\pi}{l}\xi\sqrt{1-\frac{El^2}{\pi^2 n^2}}\right) - \exp\left(-\frac{n\pi}{l}\xi\right)\right] \end{aligned} \quad (6.24)$$

As we show in appendix D, we can place a rigorous upper bound on $\sum_{n=M}^{\infty}\left[g_n(\xi) - h_n(\xi)\right]$ for sufficiently large M.

More precisely, given

$$M > \max\left\{\frac{l}{\pi}\sqrt{2E}, \frac{l}{\pi}\sqrt{E + \left[\frac{1}{2W}\ln\left(\frac{El^2}{\pi^2}\right)\right]^2}\right\}, \quad (6.25)$$

then

$$\sum_{n=M}^{\infty}\left[g_n(\xi) - h_n(\xi)\right] < \frac{El^2}{\pi^2 M^2}\left(h + \frac{4l}{3\pi}\right)\exp\left(-\frac{M\pi}{2l}\xi\right). \quad (6.26)$$

and $\sum_{n=M}^{\infty}\left[g_n(\xi) - h_n(\xi)\right]$ is uniformly convergent in $\xi \in [0, W]$.

We now have

$$\begin{aligned} G_B(x,y,x',y';E) = & \\ & 2\sum_{n=1}^{N} \frac{\sin\left(\frac{n\pi x}{l}\right)\sin\left(\frac{n\pi x'}{l}\right)\sin(k_n y')\sin\left[k_n\left(y-W\right)\right]}{k_n \sin\left(k_n W\right)} \end{aligned}$$

$$
\begin{aligned}
&-\frac{1}{l}\sum_{n=1}^{N}\left[-h_n(\delta)+h_n(2y+\delta)-h_n(2W-\delta)+h_n(2W-2y+\delta)\right]\\
&+\frac{1}{l}\sum_{n=1}^{\infty}\left[-h_n(\delta)+h_n(2y+\delta)-h_n(2W-\delta)+h_n(2W-2y+\delta)\right]\\
&+\frac{1}{l}\sum_{n=N+1}^{\infty}-\left[g_n(\delta)-h_n(\delta)\right]\\
&+\frac{1}{l}\sum_{n=N+1}^{\infty}\left[g_n(2y+\delta)-h_n(2y+\delta)\right]\\
&-\frac{1}{l}\sum_{n=N+1}^{\infty}\left[g_n(2h-\delta)-h_n(2h-\delta)\right]\\
&+\frac{1}{l}\sum_{n=N+1}^{\infty}\left[g_n(2W-2y+\delta)-h_n(2W+2y-\delta)\right] \qquad (6.27)
\end{aligned}
$$

The infinite sums of h's can be performed (see appendix D) so we have

$$
\begin{aligned}
&G_B(x,y,x',y';E)=\\
&\quad 2\sum_{n=1}^{N}\frac{\sin\left(\frac{n\pi x}{l}\right)\sin\left(\frac{n\pi x'}{l}\right)\sin(k_n y')\sin\left[k_n\left(y-W\right)\right]}{k_n\sin\left(k_n W\right)}\\
&\quad -\frac{1}{l}\sum_{n=1}^{N}\left[-h_n(\delta)+h_n(2y+\delta)-h_n(2W-\delta)+h_n(2W-2y+\delta)\right]\\
&\quad -\frac{1}{4\pi}\ln\left\{\frac{\sin^2\left[\frac{\pi(x+x')}{2l}\right]+\sinh^2\left(\frac{\pi\delta}{2l}\right)}{\sin^2\left[\frac{\pi(x-x')}{2l}\right]+\sinh^2\left(\frac{\pi\delta}{2l}\right)}\right\}+\frac{1}{4\pi}\ln\left\{\frac{\sin^2\left[\frac{\pi(x+x')}{2l}\right]+\sinh^2\left(\frac{\pi(2y+\delta)}{2l}\right)}{\sin^2\left[\frac{\pi(x-x')}{2l}\right]+\sinh^2\left(\frac{\pi(2y+\delta)}{2l}\right)}\right\}\\
&\quad -\frac{1}{4\pi}\ln\left\{\frac{\sin^2\left[\frac{\pi(x+x')}{2l}\right]+\sinh^2\left(\frac{\pi(2W-\delta)}{2l}\right)}{\sin^2\left[\frac{\pi(x-x')}{2l}\right]+\sinh^2\left(\frac{\pi(2W-\delta)}{2l}\right)}\right\}+\frac{1}{4\pi}\ln\left\{\frac{\sin^2\left[\frac{\pi(x+x')}{2l}\right]+\sinh^2\left(\frac{\pi(2W-2y+\delta)}{2l}\right)}{\sin^2\left[\frac{\pi(x-x')}{2l}\right]+\sinh^2\left(\frac{\pi(2W-2y+\delta)}{2l}\right)}\right\}\\
&\quad +\sum_{n=N+1}^{\infty}-\left[g_n(\delta)-h_n(\delta)\right]\\
&\quad +\sum_{n=N+1}^{\infty}\left[g_n(2y+\delta)-h_n(2y+\delta)\right]\\
&\quad +\sum_{n=N+1}^{\infty}-\left[g_n(2h-\delta)-h_n(2h-\delta)\right] \qquad (6.28)\\
&\quad +\sum_{n=N+1}^{\infty}\left[g_n(2h-2y+\delta)-h_n(2h+2y-\delta)\right]. \qquad (6.29)
\end{aligned}
$$

When using these expressions we truncate the infinite sums at some finite M. The analysis in appendix D allows us to bound the truncation error. With this in mind we define a

quantity which contains the non-singular part of G_B truncated at the M^{th} term:

$$
\begin{aligned}
&S_M(x,y,x',y';E) = \\
&\quad 2\sum_{n=1}^{N} \frac{\sin\left(\frac{n\pi x}{l}\right)\sin\left(\frac{n\pi x'}{l}\right)\sin(k_n y')\sin\left[k_n\,(y-W)\right]}{k_n \sin\left(k_n W\right)} \\
&\quad -\frac{1}{l}\sum_{n=1}^{N}\left[-h_n(\delta)+h_n(2y+\delta)-h_n(2W-\delta)+h_n(2W-2y+\delta)\right] \\
&\quad -\frac{1}{4\pi}\ln\left\{\frac{\sin^2\left[\frac{\pi(x+x')}{2l}\right]+\sinh^2\left(\frac{\pi(2y+\delta)}{2l}\right)}{\sin^2\left[\frac{\pi(x-x')}{2l}\right]+\sinh^2\left(\frac{\pi(2y+\delta)}{2l}\right)}\right\} - \frac{1}{4\pi}\ln\left\{\frac{\sin^2\left[\frac{\pi(x+x')}{2l}\right]+\sinh^2\left(\frac{\pi(2W-\delta)}{2l}\right)}{\sin^2\left[\frac{\pi(x-x')}{2l}\right]+\sinh^2\left(\frac{\pi(2W-\delta)}{2l}\right)}\right\} \\
&\quad +\frac{1}{4\pi}\ln\left\{\frac{\sin^2\left[\frac{\pi(x+x')}{2l}\right]+\sinh^2\left(\frac{\pi(2W-2y+\delta)}{2l}\right)}{\sin^2\left[\frac{\pi(x-x')}{2l}\right]+\sinh^2\left(\frac{\pi(2W-2y+\delta)}{2l}\right)}\right\} \\
&\quad +\sum_{n=N+1}^{M} -\left[g_n(\delta)-h_n(\delta)\right] \\
&\quad +\sum_{n=N+1}^{M}\left[g_n(2y+\delta)-h_n(2y+\delta)\right] \\
&\quad +\sum_{n=N+1}^{M} -\left[g_n(2h-\delta)-h_n(2h-\delta)\right] \\
&\quad +\sum_{n=N+1}^{M}\left[g_n(2h-2y+\delta)-h_n(2h+2y-\delta)\right]. \qquad (6.30)
\end{aligned}
$$

So

$$
G_B(x,y,x',y';E) \approx S_M(x,y,x',y';E) - \frac{1}{4\pi}\ln\left\{\frac{\sin^2\left[\frac{\pi(x+x')}{2l}\right]+\sinh^2\left[\frac{\pi(y'-y)}{2l}\right]}{\sin^2\left[\frac{\pi(x-x')}{2l}\right]+\sinh^2\left[\frac{\pi(y'-y)}{2l}\right]}\right\}. \qquad (6.31)
$$

We now have an approximate form for G_B which involves only *finite* sums and straightforward function evaluations. This will be analytically useful when we subtract G_o from G_B. It will also prove numerically useful in computing G_B.

6.1.4 Explicit Expression for $\bar{G}_B(\mathbf{r};k^2)$

Within the dressed-t formalism, we often need to calculate $G_B(\mathbf{r},\mathbf{r};z)-G_o(\mathbf{r},\mathbf{r};z)$. This quantity deserves special attention because it involves a very sensitive cancellation of infinities. Recall that

$$
\lim_{\mathbf{r}\to\mathbf{r}'} G_o(\mathbf{r},\mathbf{r}';k^2) = \lim_{\mathbf{r}\to\mathbf{r}'}\frac{1}{2\pi}\ln\left(k|\mathbf{r}-\mathbf{r}'|\right)+\frac{1}{4}Y_o^{(R)}(0)-\frac{i}{4}, \qquad (6.32)
$$

where $Y_o^{(R)}$ is the regular part of Y_o as defined in equation A.48 of section A.5.1.

If $G_B - G_o$ is to be finite, we need a canceling logarithmic singularity in G_B. Equation 6.31 makes it apparent that just such a singularity is also present in G_B. The logarithm term in that equation has a denominator which goes to 0 as $\mathbf{r} \to \mathbf{r}'$. We carefully manipulate the logarithms and write an explicitly finite expression for $G_B - G_o$

$$\begin{aligned} \bar{G}_B(\mathbf{r};E) \quad = \quad & \\ & S_M(x,y,x,y;E) + \tfrac{1}{\pi}\textstyle\sum_{n=1}^{M} \frac{\sin^2 \frac{n\pi x}{l}}{n} \qquad (6.33) \\ & -\tfrac{1}{2\pi}\ln kl - Y_o^{(R)}(0) + \tfrac{1}{2\pi}\ln\left(\tfrac{\pi}{2}\right) - \tfrac{1}{4\pi}\ln\left(\sin\tfrac{\pi x}{l}\right) + \tfrac{i}{4} \end{aligned}$$

6.1.5 Ground State Energies

One nice consequence of equation 3.44 is that it predicts a simple formula for the ground state energy of one scatterer with a known Green function background. Specifically, (3.44) implies that poles of $T(E)$ occur when

$$\frac{1}{s(E)} = \bar{G}_B(\mathbf{r_s};E) \qquad (6.34)$$

From section 2.4 we have

$$\frac{1}{s(E)} = \frac{1}{4}\left(i - \frac{Y_o(ka)}{J_o(ka)}\right) \qquad (6.35)$$

for $ka < 8$ we have

$$\frac{1}{s(E)} = \frac{i}{4} - \frac{1}{2\pi}\ln(\kappa\beta) - \frac{1}{4}Y_o^{(R)}(\kappa\beta) = \frac{i}{4} - \frac{1}{2\pi}\ln kl - \frac{1}{2\pi}\ln\beta. \qquad (6.36)$$

We define $F(E) = \frac{1}{s(E)} - \bar{G}_B(\mathbf{r};E)$ so

$$\begin{aligned} F(E) \quad = \quad & -\frac{Y_o(ka)}{4J_o(ka)} + \frac{1}{2\pi}\ln kl + \frac{1}{4}Y_o^{(R)}(0) \\ & -S_M(X,Y,X,Y) - \frac{1}{\pi}\sum_{n=1}^{\infty}\frac{\sin^2\frac{n\pi x}{l}}{n} \\ & -\frac{1}{2\pi}\ln\frac{\pi}{2} + \frac{1}{4\pi}\ln\sin\pi X \end{aligned}$$

We can use the $ka < 8$ expansion of the Neumann function to simplify F a bit:

$$F(E) \quad = \quad -\frac{1}{2\pi}\ln a/l - \frac{1}{4}\left[Y_o^{(R)}(ka) - Y_o^{(R)}(0)\right]$$

$$-S_M(x,y,x,y) - \frac{1}{\pi}\sum_{n=1}^{\infty}\frac{\sin^2\frac{n\pi x}{l}}{n}$$
$$-\frac{1}{2\pi}\ln\frac{\pi}{2} + \frac{1}{4\pi}\ln\sin\frac{\pi x}{l}$$

In figure 6.1 we compare the numerical solution of the equation $F(E) = 0$ with a numerical simulation performed with a standard method (Successive Over Relaxation [33]).

6.2 Periodic boundaries

6.2.1 The Background Green Function

We consider a rectangular domain, $\mathbf{\Omega}$, in R^2 defined by

$$\mathbf{\Omega} = [0,l]\times[0,W] = \{(x,y)|0<x<l, 0<y<W\}. \tag{6.37}$$

We wish to solve Schrödinger's equation

$$\left[\frac{\hbar^2}{2m}\nabla^2 + E\right]\psi(\vec{r}) = 0 \tag{6.38}$$

in the domain $\mathbf{\Omega}$ subject to the boundary conditions

$$\begin{aligned}
\psi(0,y) &= \psi(l,y),\\
\frac{\partial}{\partial x}\psi(x,y)\Big|_{x=0} &= \frac{\partial}{\partial x}\psi(x,y)\Big|_{x=l},\\
\psi(x,0) &= \psi(x,W),\\
\frac{\partial}{\partial y}\psi(x,y)\Big|_{y=0} &= \frac{\partial}{\partial y}\psi(x,y)\Big|_{y=W}.
\end{aligned}$$

We set $\frac{\hbar^2}{2m} = 1$. Our equation reads

$$\left(\frac{\partial^2}{\partial x^2} + \frac{\partial^2}{\partial y^2} + E\right)\psi(x,y) = 0. \tag{6.39}$$

The eigen-functions of $\mathcal{L} = -\left(\frac{\partial^2}{\partial x^2} + \frac{\partial^2}{\partial y^2}\right)$ in the above domain with given boundary condition are

$$\phi^{(1)}_{nm}(x,y) = \frac{2}{\sqrt{lW}}\sin\left(\frac{2n\pi x}{l}\right)\sin\left(\frac{2m\pi y}{W}\right), \tag{6.40}$$
$$\phi^{(2)}_{nm}(x,y) = \frac{2}{\sqrt{lW}}\cos\left(\frac{2n\pi x}{l}\right)\cos\left(\frac{2m\pi y}{W}\right), \tag{6.41}$$

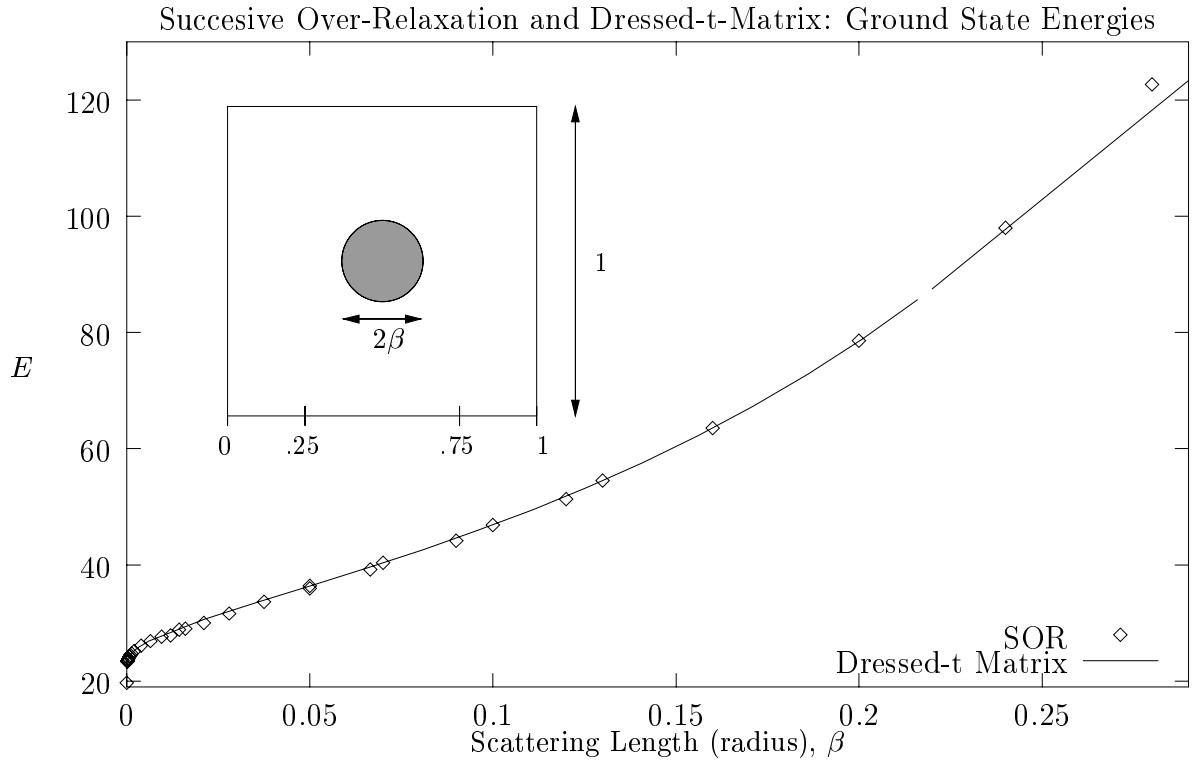

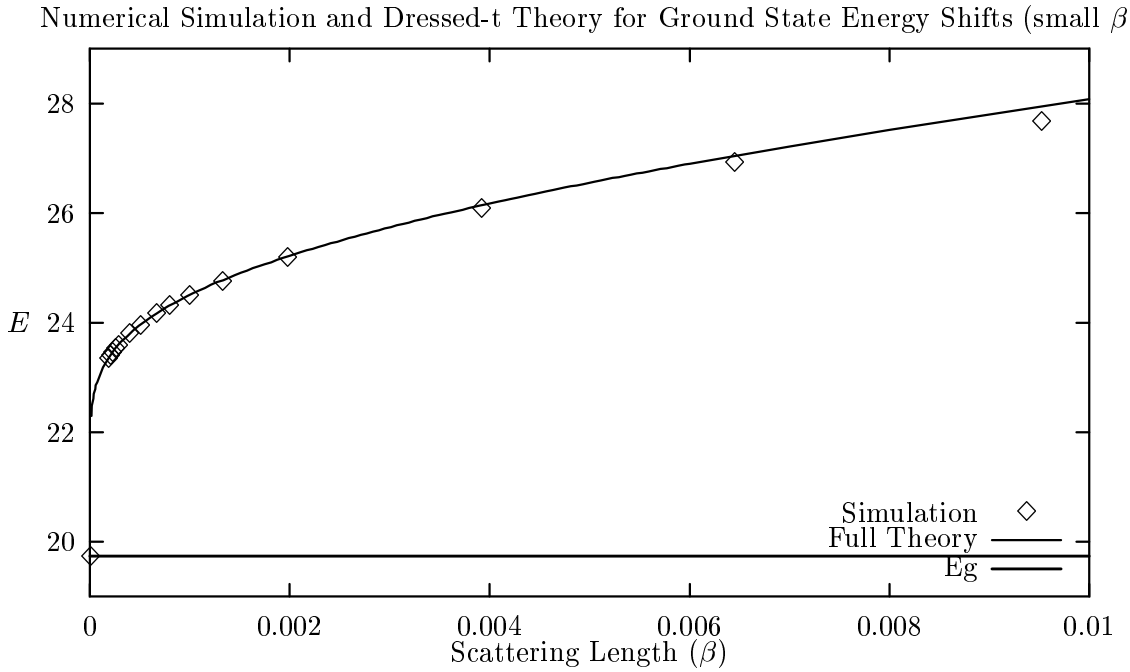

Figure 6.1: Comparison of Dressed-t Theory with Numerical Simulation

$$\phi^{(3)}_{nm}(x,y) = \frac{2}{\sqrt{lW}} \sin\left(\frac{2n\pi x}{l}\right) \cos\left(\frac{2m\pi y}{W}\right), \tag{6.42}$$

$$\phi^{(2)}_{nm}(x,y) = \frac{2}{\sqrt{lW}} \cos\left(\frac{2n\pi x}{l}\right) \sin\left(\frac{2m\pi y}{W}\right), \tag{6.43}$$

$$\tag{6.44}$$

all of which satisfy

$$-\left(\frac{\partial^2}{\partial x^2} + \frac{\partial^2}{\partial y^2}\right)\phi_{nm}(x,y) = \left(\frac{n^2\pi^2}{l^2} + \frac{m^2\pi^2}{W^2}\right)\phi_{nm}(x,y). \tag{6.45}$$

Note that the $m = 0$ and $n = 0$ is permissible but only the cosine state survives so there is no degeneracy. We can thus write down a box Green function in the position representation

$$G_B(x,y,x',y';E) = \frac{2}{lWE} + \frac{4}{lW}\sum_{n,m=1}^{\infty} \frac{\cos\left(\frac{n\pi|x-x'|}{l}\right)\cos\left(\frac{m\pi|y-y'|}{W}\right)}{E - \frac{n^2\pi^2}{l^2} - \frac{m^2\pi^2}{W^2}}, \tag{6.46}$$

where trigonometric identities have been applied to collapse the sines and cosines into just two cosines. We note that this Green function depends only on $|x - x'|$ and $|y - y'|$ as it must.

6.2.2 Re-summing G_B

As with the Dirichlet case, we'd like to re-sum this Green function to make it a single sum and to create an easier form for numerical use and the $G_o - G_B$ subtraction.

We begin by reorganizing G_B as follows:

$$G_B(x,y,x',y';E) = \frac{2}{lWE} + \frac{4}{lW}\sum_{n=1}^{\infty} \cos\left(\frac{n\pi|y-y'|}{W}\right) \sum_{m=1}^{\infty} \frac{\cos\left(\frac{m\pi|x-x'|}{l}\right)}{E - \frac{n^2\pi^2}{l^2} - \frac{m^2\pi^2}{W^2}}, \tag{6.47}$$

and then apply the following Fourier series identity (see, e.g.,[18]) to the inner sum:

$$\sum_{k=1}^{\infty} \frac{\cos kx}{a^2 - k^2} = \frac{\pi}{2}\frac{\cos\left[a(\pi - x)\right]}{a \sin a\pi} - \frac{1}{2a^2}, \tag{6.48}$$

for $0 \le x \le 2\pi$.

We define

$$N = \left[\frac{W}{2\pi}\sqrt{E}\right] \tag{6.49}$$

$$k_n = \sqrt{E - \frac{4\pi^2 n^2}{W^2}} \tag{6.50}$$

$$\kappa_n = \sqrt{\frac{4\pi^2 n^2}{W^2} - E} \tag{6.51}$$

$$X = |x - x'| \tag{6.52}$$

$$Y = |y - y'| \tag{6.53}$$

where $[x]$ is the greatest integer equal to or less than x. We now have

$$\begin{aligned} G_B(X,Y;E) &= \frac{\cos\left[\sqrt{E}\left(\frac{l}{2}-X\right)\right]}{2h\sqrt{E}\sin\left(\sqrt{E}\frac{l}{2}\right)} + \frac{1}{W}\sum_{n=1}^{N}\frac{\cos\left(\frac{2\pi}{W}nY\right)\cos\left[k_n\left(\frac{l}{2}-X\right)\right]}{k_n\sin\left(k_n\frac{l}{2}\right)} \\ &\quad -\frac{1}{W}\sum_{n=N+1}^{\infty}\frac{\cos\left(\frac{2\pi}{W}nY\right)\cosh\left[\kappa_n\left(\frac{l}{2}-X\right)\right]}{\kappa_n\sinh\left(\kappa_n\frac{l}{2}\right)}. \end{aligned} \tag{6.54}$$

We now follow a similar derivation to the one for Dirichlet boundaries. We choose an $M > N$ such that we may approximate $\kappa_n \sim \frac{2\pi n}{l}$. We can then approximate G_B by a finite sum plus a logarithm term arising from the highest energy terms in the sum. That sum looks like

$$\frac{1}{2\pi}\sum_{n=M+1}^{\infty}\frac{\cos\left(\frac{2\pi}{l}nY\right)e^{-\frac{2\pi}{l}n\bar{X}}}{n}, \tag{6.55}$$

where $\bar{X} = X\left(\mathrm{mod}\,\frac{l}{2}\right)$. We can sum this using (see e.g.,[18])

$$\sum_{k=1}^{\infty}\frac{x^k}{k} = \ln\left(\frac{1}{1-x}\right). \tag{6.56}$$

We define

$$\begin{aligned} S_p^{(M)}(X,Y,E) &= \frac{\cos\left[\sqrt{E}\left(\frac{l}{2}-X\right)\right]}{2h\sqrt{E}\sin\left(\sqrt{E}\frac{l}{2}\right)} + \frac{1}{W}\sum_{n=1}^{N}\frac{\cos\left(\frac{2\pi}{W}nY\right)\cos\left[k_n\left(\frac{l}{2}-X\right)\right]}{k_n\sin\left(k_n\frac{l}{2}\right)} \\ &\quad -\frac{1}{W}\sum_{n=N+1}^{M}\frac{\cos\left(\frac{2\pi}{W}nY\right)\cosh\left[\kappa_n\left(\frac{l}{2}-X\right)\right]}{\kappa_n\sinh\left(\kappa_n\frac{l}{2}\right)}. \end{aligned} \tag{6.57}$$

and write our approximate G_B as

$$\begin{aligned} G_B(X,Y;E) &\approx S_p^{(M)}(X,Y,E) + \frac{1}{4\pi}\ln\left[1 - 2e^{-\frac{2\pi}{W}\bar{X}}\cos\frac{2\pi}{W}Y + e^{-\frac{4\pi}{W}\bar{X}}\right] \\ &\quad +\frac{1}{2\pi}\sum_{n=1}^{M}\frac{\cos\left(\frac{2\pi}{W}nY\right)e^{-\frac{2\pi}{W}\bar{X}}}{n} \end{aligned} \tag{6.58}$$

6.2.3 Explicit Expression for $\bar{G}_B(\mathbf{r};E)$

With this re-summed version of G_B we can write an explicitly finite expression for

$$\bar{G}_B(\mathbf{r};E) = G_B(\mathbf{r},\mathbf{r};E) - G_o(\mathbf{r},\mathbf{r};E), \tag{6.59}$$

though both $G_B(\mathbf{r},\mathbf{r};E)$ and $G_o(\mathbf{r},\mathbf{r};E)$ are (logarithmically) infinite.

As with the Dirichlet case, all we need to do is carefully manipulate the logarithm in G_B in the $X, Y \to 0$ limit. Our answer is

$$\bar{G}_B(\mathbf{r};E) = S_p^{(M)}(0,0;E) - \frac{1}{2\pi}\ln\frac{kW}{2\pi} + \frac{1}{2\pi}\sum_{n=1}^{M}\frac{1}{n} - Y_o^{(R)}(0) + \frac{i}{4}X \tag{6.60}$$

Chapter 7

Disordered Systems

7.1 Disorder Averages

7.1.1 Averaging

When working with disordered systems we are rarely interested a particular realization of the disorder but instead in average properties. The art in calculating quantities in such systems is cleverly approximating these averages in ways which are appropriate for specific questions. In this section we will consider only the average Green function of a disordered system, $\langle G \rangle$ (rather than, for instance, higher moments of G). Good treatments of these approximations and more powerful approximation schemes may be found in [10, 34, 9].

Suppose, at fixed energy, we have N ZRI's with individual t-matrices $\hat{t}_i(E) = s_i \left|\mathbf{r}_i\right\rangle \left\langle \mathbf{r}_j\right|$. Any property of the system depends, at least in principle, on all the variables $s_i, \mathbf{r}_i$. We imagine that there are no correlations between different scatterers (location or strength) and that each has the same distribution of locations and strengths. Thus we can define the ensemble average of the Green function operator $G(E)$:

$$\langle G \rangle = \left[\prod_{i=1}^{N} \int d\mathbf{r}_i \, ds_i \, \rho_{\mathbf{r}} \left(\mathbf{r}_i\right) \, \rho_s(s_i) \right] G \tag{7.1}$$

We will typically use uniformly distributed scatterers and fixed scattering strengths. In this case $\rho_{\mathbf{r}} \left(\mathbf{r}_i\right) = \frac{1}{\mathcal{V}}$ where $\mathcal{V}$ is the volume of the system and $\rho_s(s_i) = s_o \delta \left(s_i - s_o\right)$ where s_o is the fixed scatterer strength.

We can write G as $G_o + G_o T G_o$ and, since G_o is independent of the disorder,

$$\langle G \rangle = G_o + G_o \langle T \rangle G_o. \tag{7.2}$$

Thus we must compute $\langle T \rangle$. This is such a useful quantity, there is quite a bit of machinery developed just for this computation.

7.1.2 Self-Energy

The self-energy, Σ, is a sort of average potential (though it is *not* $\langle V \rangle$) defined via

$$\langle G \rangle = G_o + G_o \Sigma \langle G \rangle , \tag{7.3}$$

and thus

$$\langle G \rangle^{-1} = G_o^{-1} - \Sigma. \tag{7.4}$$

This last equation explains why we call $\Sigma(E)$ the self-energy,

$$G_o^{-1} - \Sigma = [E - \Sigma] - H_o. \tag{7.5}$$

Within the first two approximations we discuss, the self-energy is just proportional to the identity operator so it can be thought of as just shifting the energy.

We can also use (7.3) to find Σ in terms of $\langle T \rangle$:

$$\Sigma = \langle T \rangle \left(1 + G_o \langle T \rangle\right)^{-1}, \tag{7.6}$$

or for $\langle T \rangle$ in terms of Σ:

$$\langle T \rangle = \Sigma \left(1 - \Sigma G_o\right)^{-1}. \tag{7.7}$$

Thus knowledge of either $\langle T \rangle$ or Σ is equivalent.

Recall that $G = G_o + G_o T G_o = G_o + G_o V G_o + G_o V G_o V G_o + \cdots$ means that the amplitude for a particle to propagate from one point to another is the sum of the amplitude for it to propagate from the initial point to the final point without interacting with the potential and the amplitude for it to propagate from the initial point to the potential, interact with the potential one or more times and then propagate to the final point. We can illustrate this diagrammatically:

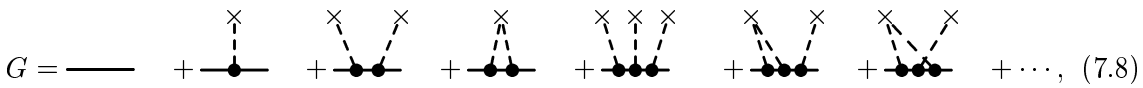

(7.8)

where solid lines represent free propagation (G_o) and a dashed line ending in an "$\times$" indicates an interaction with the impurity potential (V). Each different "$\times$" represents an interaction with the impurity potential at a different impurity. When multiple lines connect

to the same interaction vertex, the particle has interacted with the same impurity multiple times.

An *irreducible* diagram is one which cannot be divided into two sub-diagrams just by cutting a solid line (a free propagator). The self-energy, Σ, is equivalent to a sum over only irreducible diagrams (with the incoming and outgoing free propagators removed):

$\Sigma =$ 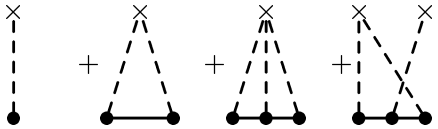 $+ \cdots,$ (7.9)

which is enough to evaluate G since we can build all the diagrams from the irreducible ones by adding free propagators:

$$\langle G \rangle = G_o + G_o \Sigma G_o + G_o \Sigma G_o \Sigma G_o + \cdots = G_o \left(1 - \Sigma G_o\right)^{-1} \tag{7.10}$$

There are a variety of standard techniques for evaluating the self-energy. The simplest approximation used is known as the "Virtual Crystal Approximation" (VCA). This is equivalent to replacing the sum over irreducible diagrams by the first diagram in the sum, i.e., $\Sigma = \langle V \rangle$. Since we don't use the potential itself, this approximation is actually more complicated to apply then the more accurate "average t-matrix approximation' (ATA). We note that, in a system where the impurity potential is known, $\langle V \rangle$ is just a real number and so the VCA just shifts the energy by the average value of the potential.

The ATA is a more sophisticated approximation that replaces the sum (7.9) by a sum of terms that involve a single impurity,

$\Sigma \approx$ 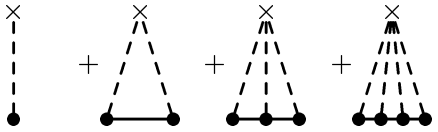 $+ \cdots,$ (7.11)

but this is, up to averaging, the same as the single scatterer t-matrix, t_i. Thus the ATA is equivalent to $\Sigma = \langle \sum_i t_i \rangle$. This approximation neglects diagrams like

which involve scattering from two or more impurities. We note that scattering from two or more impurities is included in G, just not in Σ. Of course while scattering from several impurities is accounted for in G, interference between scattering from various impurities is

neglected since diagrams which scatter from one impurity than other impurities and then the first impurity again are neglected. That is,

is included but

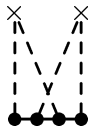

is not. At low concentrations, such terms are quite small. However, as the concentration increases, these diagrams contribute important corrections to G. One such correction comes from coherent backscattering which we'll discuss in greater detail in section 7.5.

We will use the ATA below to show that the classical limit of the quantum mean free path is equal to the classical mean free path. For N uniformly distributed fixed strength scatterers, the average is straightforward:

$$\left\langle \sum_{i=1}^{N} \hat{t}_i \right\rangle = \left[\prod_{i=1}^{N} \frac{1}{\mathcal{V}} \int d\mathbf{r}_i \, ds_i \, \delta(s_i - s_o) \right] \sum_i s_i \delta\left(\mathbf{r}_i - \mathbf{r}\right). \tag{7.12}$$

For each term in the sum, the $\mathbf{r}$ delta function will do one of the volume integrals and the rest will simply integrate to Ω, canceling the factors of $1/\mathcal{V}$ out front. The s delta functions will do all of the s integrals, leaving

$$\Sigma \approx \left\langle \sum_{i=1}^{N} \hat{t}_i \right\rangle = \frac{N}{\mathcal{V}} s_o = n s_o. \tag{7.13}$$

Thus the self energy is simply proportional to the scattering strength multiplied by the concentration. We note that s_o is in general complex and this will make the poles of the Green function complex, implying an exponential decay of amplitude as a wave propagates. We will interpret this decay as the wave-mechanical mean free time.

7.2 Mean Free Path

7.2.1 Classical Mechanics

Consider a domain of volume V in d-dimensions with reflective walls. V has units of [length]^d. Suppose we place N scattering centers in this domain at random (uniformly distributed), each with classical cross section σ. σ has units of [length]$^{d-1}$. Now suppose

we have a point particle that has just scattered off of one of the scattering centers. It now points in a random direction. What is the probability that it can travel a distance ℓ without scattering again?

If the particle travels a distance x without scattering, then there must be a tube of volume $x\sigma$ which is empty of scattering centers. The probability of that is given by the product of the chances that each of the N scatterers (without the reflective walls this would be $N-1$ but since we will take N large and we do have reflective walls, we'll leave it as N) is not in the volume $x\sigma$. That chance is $1-\frac{x\sigma}{V}$ so

$$P_\sigma^{(N)}(x) = \left(1 - \frac{x\sigma}{V}\right)^N \tag{7.14}$$

More precisely $1 - P_\sigma^{(N)}(x)$ is the probability that the free path-length is less than or equal to x. We define $n = N/V$, the concentration. So

$$P_\sigma^{(N)}(x) = \left(1 - \frac{x\sigma n}{N}\right)^N \tag{7.15}$$

We take the $N \to \infty$ while $n = \text{const.}$ limit which is valid for infinite systems and a good approximation when the mean free path is smaller than the system size. We have

$$P_\sigma(x) = \lim_{N\to\infty} P_\sigma^{(N)}(x) = e^{-n\sigma x}, \tag{7.16}$$

and thus the quasi-classical mean free path is

$$\ell_{\text{qc}} = \langle x \rangle = \int_0^\infty x \frac{\partial}{\partial x}\left(1 - P_\sigma(x)\right)\, dl = \int_0^\infty P_\sigma(x)\, dl = \frac{1}{n\sigma}. \tag{7.17}$$

Quasi-classical (indicated by the subscript "qc") here means that the transport between scattering events is classical but the cross-section of each scatterer is computed from quantum mechanics.

7.2.2 Quantum Mechanics

The mean free path is not so simple to define for a quantum mechanical system. After all, a particle no longer has a trajectory or a well defined distribution of path lengths. What then do we mean by the mean free path in a quantum mechanical system?

One possibility is simply to replace the classical cross-section in the expression (7.17) with the quantum mechanical cross-section, σ (we'll refer to this as the "quasi-classical"

mean free path). In what follows we'll show that this is equivalent to the low-density weak-scattering approximation to the self-energy discussed above.

We begin by noting that the free Green function takes a particularly simple form in the momentum representation:

$$G_o(\mathbf{p},\mathbf{p}';E) = \frac{\delta(\mathbf{p}-\mathbf{p}')}{E-E_{\mathbf{p}}}. \tag{7.18}$$

From this and the low-density weak-scattering approximation to Σ we have

$$\langle G(\mathbf{p},\mathbf{p}';E)\rangle = \frac{\delta(\mathbf{p}-\mathbf{p}')}{E-\Sigma-E_{\mathbf{p}}}. \tag{7.19}$$

If we write $\Sigma = \Delta - i\Gamma$ we have

$$\langle G(\mathbf{p},\mathbf{p}';E)\rangle = \frac{\delta(\mathbf{p}-\mathbf{p}')}{E-\Delta+i\Gamma-E_{\mathbf{p}}}. \tag{7.20}$$

Now we consider the Fourier transform of this Green function with respect to energy which gives us the time-domain Green function in the momentum representation (we are ignoring the energy dependence of Σ only for simplicity):

$$\begin{aligned}
\langle G(\mathbf{p},\mathbf{p}';t)\rangle &= \int_{-\infty}^{\infty} dE\, e^{-iEt}\,\langle G(\mathbf{p},\mathbf{p}';E)\rangle \\
&= \int_{-\infty}^{\infty} dE\, e^{-iEt}\frac{\delta(\mathbf{p}-\mathbf{p}')}{E-\Delta+i\Gamma-E_{\mathbf{p}}} \\
&= -i\delta(\mathbf{p}-\mathbf{p}')e^{-i(E_p+\Delta)t}e^{-\Gamma t},
\end{aligned}$$

which implies an exponential attenuation of the wave if $-\Gamma = \mathrm{Im}\{\Sigma\}$ is negative.

For the ATA, we have $\Sigma = ns_o$ which, for a two dimensional ZRI with scattering length a, is $n\frac{-4iJ_o(\sqrt{E}a)}{H_o(\sqrt{E}a)}$ and thus

$$-\Gamma = -4n\frac{J_o^2(\sqrt{E}a)}{\left|H_o(\sqrt{E}a)\right|^2} \tag{7.21}$$

which is manifestly negative.

We can associate the damping with a mean free time, τ via $\Gamma = 1/2\tau$. Since, at fixed energy, the velocity (in units where $\hbar^2/2m = 1$ is $v = 2\sqrt{E}$) we have for the mean free path, ℓ

$$\ell = v\tau = \frac{\sqrt{E}}{4n}\frac{\left|H_o(\sqrt{E}a)\right|^2}{J_o^2(\sqrt{E}a)} = \frac{1}{n\sigma}, \tag{7.22}$$

reproducing the quasi-classical result.

7.3 Properties of Randomly Placed ZRI's as a Disordered Potential

In this section we will be concerned with averages of T in the momentum representation. As in 7.2.2 we will assume the validity of the low-density weak-scattering approximation to T:

$$T \approx \sum_{i=1}^{N} s_i \left|\mathbf{r}_i\right\rangle \left\langle \mathbf{r}_i\right| . \tag{7.23}$$

In momentum space, this can be written

$$\left\langle \mathbf{k}\left|T\right|\mathbf{k}'\right\rangle = T(\mathbf{k},\mathbf{k}') \approx \sum_{i=1}^{N} s_i e^{-i(\mathbf{k}-\mathbf{k}')\cdot\mathbf{r}_i}. \tag{7.24}$$

Using the average (7.1), we have

$$\left\langle T(\mathbf{k},\mathbf{k}')\right\rangle \approx N\left\langle s\right\rangle f(\mathbf{k}-\mathbf{k}'), \tag{7.25}$$

where

$$f(\mathbf{q}) = \frac{1}{\Omega}\int_{\Omega} e^{-i(\mathbf{q})\cdot\mathbf{r}} d\mathbf{r}. \tag{7.26}$$

The function f, has a two important properties. Firstly, $f(0) = 1$ which implies, as we saw in 7.1.1, that $\langle T\rangle = N\langle s\rangle$. Also, when the bounding region, Ω, is all of space we have

$$f(\mathbf{q}) = \frac{1}{\Omega}\delta(q) = \delta_{\mathbf{q0}} \tag{7.27}$$

Together, these properties imply that the *average* ATA t-matrix cannot change the momentum of a scattered particle except insofar as the system is finite. A finite system will give a region of low momentum where momentum transfer can occur but for momenta larger than $1/L_o$, momentum transfer will still be suppressed.

We now consider the second moment of T or, more specifically,

$$\left\langle \left|T(\mathbf{k},\mathbf{k}')\right|^2 - \left|\left\langle T(\mathbf{k},\mathbf{k}')\right\rangle\right|^2 \right\rangle . \tag{7.28}$$

Since

$$\left|T(\mathbf{k},\mathbf{k}')\right|^2 \approx \sum_{i,j=1}^{N} s_i s_j^* e^{-i(\mathbf{k}-\mathbf{k}')\cdot\mathbf{r}_i} e^{i(\mathbf{k}-\mathbf{k}')\cdot\mathbf{r}_j}, \tag{7.29}$$

we have

$$\begin{aligned}\left\langle \left|T(\mathbf{k},\mathbf{k}')\right|^2 \right\rangle &\approx \sum_{i=1}^{N}\left\langle \left|s\right|^2\right\rangle + \sum_{i\neq j}^{N}\left|\left\langle s\right\rangle\right|^2\left|f(\mathbf{k}-\mathbf{k}')\right|^2 \\ &= N\left\langle \left|s\right|^2\right\rangle + \left(N^2-N\right)\left|\left\langle s\right\rangle\right|^2\left|f(\mathbf{k}-\mathbf{k}')\right|^2 .\end{aligned} \tag{7.30}$$

Thus

$$\left\langle \left|T(\mathbf{k},\mathbf{k}')\right|^2 - \left|\langle T(\mathbf{k},\mathbf{k}')\rangle\right|^2 \right\rangle \approx N\left[\left\langle |s|^2\right\rangle - \left|\langle s\rangle\right|^2 \left|f(\mathbf{k}-\mathbf{k}')\right|^2\right] \tag{7.31}$$

We note that if $s_i = s_o \ \forall i$ we have

$$\left\langle \left|T(\mathbf{k},\mathbf{k}')\right|^2 - \left|\langle T(\mathbf{k},\mathbf{k}')\rangle\right|^2 \right\rangle \approx N|s_o|^2\left[1 - \left|f(\mathbf{k}-\mathbf{k}')\right|^2\right]. \tag{7.32}$$

In this case,

$$\left\langle \left|T(\mathbf{k},\mathbf{k})\right|^2 - \left|\langle T(\mathbf{k},\mathbf{k})\rangle\right|^2 \right\rangle \approx 0 \tag{7.33}$$

At this point it is worth considering our geometry and computing f explicitly. We'll assume we are placing scatterers in a rectangle with length (x-direction) a and width (y-direction) b. Then we have, up to an arbitrary phase,

$$f(\mathbf{q}) = \operatorname{sinc}\frac{q_x x}{2a}\operatorname{sinc}\frac{q_y y}{2b}, \tag{7.34}$$

where

$$\operatorname{sinc} x = \frac{\sin x}{x}. \tag{7.35}$$

Thus $1 - \left|f(\mathbf{k}-\mathbf{k}')\right|^2$ is zero for $\mathbf{k} = \mathbf{k}'$ and then grows to 1 for larger momentum transfer. The zero momentum transfer "hole" in the second moment of T is an artifact of a potential made up of a fixed number of fixed size scatterers. To make contact with the standard condensed matter theory of disordered potentials, we should allow those fixed numbers to vary, thus making a more nearly constant second moment of T. We can do this easily enough by allowing the size of the scatterers to vary as well. Then $< |s|^2 > - |< s >|^2 \neq 0$. In fact we should choose a distribution of scatterer sizes such that $< |s|^2 > - |< s >|^2 \approx < |s|^2 >$.

Of course, the scatterer strength, s, is not directly proportional to the scattering length. For example, if the scattering length varies uniformly over a small range δa. It is straightforward to show that, for small δa,

$$< |s|^2 > - |< s >|^2 \approx \frac{(k\delta a)^2}{12}\left|\frac{ds}{d(ka)}\right|^2. \tag{7.36}$$

7.4 Eigenstate Intensities and the Porter-Thomas Distribution

One interesting quantity in a bounded quantum system with discrete spectrum (e.g., a Dirichlet square with random scatterers inside) is the distribution of wavefunction

intensities, t, at fixed energy E,

$$P(t) = \Delta \left\langle \sum_\alpha \delta\left(t - |\psi(\mathbf{r}_o)|^2\right) \delta\left(E - E_\alpha\right) \right\rangle \tag{7.37}$$

where Δ is the mean level spacing and $\mathbf{r}_o$ is a specific point in the system. Since $P(t)$ is a probability distribution, we have $\int_0^\infty P(t)\,dt = 1$ and since the integrated square wavefunction is normalized to 1, we also have $\int_0^\infty tP(t)\,dt = 1/\Omega$.

Though computing this quantity in general is quite hard, we can, as a baseline, compute it in one special case. As a naive guess at the form of the wavefunction in a disordered system, we conjecture that the wavefunction is a Gaussian random variable at each point in the system. That is, we assume that the distribution of values of ψ, $\rho(\psi)$ is

$$\rho(\psi) = ae^{-b|\psi|^2}, \tag{7.38}$$

where a and b are constants to be determined. We note that in a bounded system, we can make all the wavefunctions real. We proceed to determine the constants a and b. First, we use the fact that ρ is a probability distribution so $\int_{-\infty}^\infty \rho(x)\,dx = 1$ which gives

$$1 = a\int_{-\infty}^\infty e^{-bx^2}\,dx = a\sqrt{\frac{\pi}{b}} \tag{7.39}$$

implying $b = a^2\pi$. We also know that the normalization of ψ implies $\int_{-\infty}^\infty x^2\rho(x)\,dx = 1/\Omega$ which implies

$$\frac{1}{\Omega} = a\int_{-\infty}^\infty x^2 e^{-a^2\pi x^2}\,dx = \frac{1}{2\pi a^2}, \tag{7.40}$$

implying $a = \sqrt{\Omega/2\pi}$. So we have

$$\rho(\psi) = \sqrt{\frac{\Omega}{2\pi}} e^{-\Omega|\psi|^2/2}. \tag{7.41}$$

From this, we can compute $P(t)$ via

$$P(t) = \int_{-\infty}^\infty \delta\left(t - x^2\right)\rho(x)\,dx = \int_{-\infty}^\infty \frac{\delta(x-\sqrt{t}) + \delta(x+\sqrt{t})}{2|x|}\rho(x)\,dx. \tag{7.42}$$

We use the delta functions to do the integral and have

$$P(t) = \frac{\rho(\sqrt{t})}{\sqrt{t}}. \tag{7.43}$$

After substituting our previous result for ρ, we have

$$P(t) = \sqrt{\frac{\Omega}{2\pi t}} e^{-\Omega t/2}, \tag{7.44}$$

which is known as the "Porter-Thomas" distribution.

If time-reversal symmetry is broken, e.g., by a magnetic field, the wavefunction will, in general, be complex. In that case we can use the same argument where the real part and imaginary part of ψ are each Gaussian random variables. In that case we get

$$P(t) = e^{-\Omega t}. \tag{7.45}$$

This difference between time-reversal symmetric systems and their non-symmetric counterparts is a recurring motif in disordered quantum systems.

A derivation of the above results from Random Matrix Theory (using the assumption that the Hamiltonian is a random matrix with the symmetries of the system) is available many places, for example [14]. In this language, the Hamiltonian of time-reversal invariant systems are part of the "Gaussian Orthogonal Ensemble" (GOE) whereas Hamiltonians for systems without time-reversal symmetry are part of the "Gaussian Unitary Ensemble" (GUE). We will adopt this bit of terminology in what follows.

Of course, most systems do not behave exactly as the appropriate random matrix ensemble would indicate. These differences manifest themselves in a variety of properties of the system. In the numerical simulations which follow in chapters 8 and 9 we will see these departures quite clearly.

For disordered systems, GOE behavior is expected when there are many weak scattering events in every path which traverses the disordered region, guaranteeing diffusive transport without significant quantum effects from scattering phases. More precisely, to see GOE behavior, we expect to need a mean free path which is much smaller than the system size ($\ell << L$) but much larger than the wavelength ($\ell >> \lambda$). We will see this limit emerge in wavefunction statistics in chapter 9.

7.5 Weak Localization

In the previous section, we discussed one consequence of the assumption of a random wavefunction. Of course, the wavefunction is not random, it shows the consequences of the underlying classical dynamics. In the next few sections we explore some consequences of the underlying dynamics for the quantum properties.

Weak localization is a generic name for enhanced probability of finding a particle in a given region due to *short time* classical return probability. In quantized classically

chaotic (but not disordered) systems, wavefunction scarring [20] is the best known form of weak localization. In disordered systems, the most important consequence of of weak localization is the reduction of conductance due to coherent back-scattering.

It is not difficult to estimate the coherent back-scattering correction to the conductance. We begin by noting the conductance we expect for a wire with no coherent backscattering. Specifically, when $L >> \ell >> \lambda$ we expect the DC conductivity of a disordered wire to satisfy the Einstein relation

$$\Gamma = e^2 \nu_d D, \tag{7.46}$$

where Γ is the conductivity, e is the charge of the electron, ν_d is the d-dimensional density of states per unit volume and D is the classical diffusion constant.

The DC conductivity, Γ is proportional to $P(\mathbf{r}_1, \mathbf{r}_2)$, the probability that a particle starting at point $\mathbf{r}_1$ on one side of the system reaches $\mathbf{r}_2$ on the other side. Quantum mechanically, this quantity can be evaluated semiclassically by a sum over classical paths, p,

$$P(\mathbf{r}_1, \mathbf{r}_2) = \left| \sum_p A_p \right|^2, \tag{7.47}$$

where $A_p = |A_p| e^{iS_p}$ and S_p is the integral of the classical action over the path. The quantum probability differs from the classical in the interference terms:

$$P(\mathbf{r}_1, \mathbf{r}_2) = P(\mathbf{r}_1, \mathbf{r}_2)_{\text{classical}} + \sum_{p \neq p'} A_p A^*_{p'}. \tag{7.48}$$

Typically, disorder averaging washes out the interference term. However, when $\mathbf{r}_1 = \mathbf{r}_2$, the terms arising from paths which are time-reversed partners will have strong interference even after averaging since they will always have canceling phases. Since every path has a time reversed partner, we have

$$\langle P(\mathbf{r}, \mathbf{r}) \rangle = 2 \langle P(\mathbf{r}, \mathbf{r})_{\text{classical}} \rangle . \tag{7.49}$$

But this enhanced return probability implies a suppressed conductance since $\int P(\mathbf{r}, \mathbf{r}') d\mathbf{r}' = 1$ by conservation of probability. Thus $\frac{\delta\Gamma}{\Gamma}$ must be smaller by a factor of $- \langle P(\mathbf{r}, \mathbf{r})_{\text{classical}} \rangle$ due to this interference effect.

But $\langle P(\mathbf{r}, \mathbf{r})_{\text{classical}} \rangle$ is something we can compute straightforwardly. If we define $R(t)$ to be the probability that a particle which left the point $\mathbf{r}$ at time $t = 0$ returns at

time t, we have

$$\langle P(\mathbf{r},\mathbf{r})_{\text{classical}}\rangle = \int_{\tau}^{t_c} R(t)dt. \tag{7.50}$$

The lower cutoff, $\tau = v/\ell$ is there since our particle must scatter at least once to return and that takes a time of order the mean free time. The upper cutoff is present since we have only a finite disordered region and so, after a time $t_c = L_o^2/D$ the particle has diffused out and will not return. For a square sample, L_o is ambiguous up to a factor of $\sqrt{2}$. The upper cutoff can also be provided by a phase coherence time τ_ϕ. If particles lose phase coherence, for instance by interaction with a finite temperature heat bath, only paths which take less time than τ_ϕ will interfere. In this case the expression for the classical return probability is slightly modified:

$$\langle P(\mathbf{r},\mathbf{r})_{\text{classical}}\rangle = \int_{\tau}^{\infty} e^{-t/\tau_\phi} R(t)dt. \tag{7.51}$$

The return probability, $R(t)dt$, can be estimated for a diffusive system. Of all the trajectories that scatter, only those that pass within a volume $\sigma v\, dt$ of the origin contribute. The probability that a scattered particle falls within that volume is just the ratio of it to the total volume of diffusing trajectories, $(Dt)^{d/2}V_d$ where d is the effective number of dimensions (the number of dimensions of the disordered sample $>> \ell$) and $V_d = \pi^{d/2}/(d/2)!$ is the volume of the unit sphere in d-dimensions (this is easily calculated using products of Gaussian integrals, see e.g., [32] pp. 501-2) and $D = v\ell/d$. So

$$R(t)dt = \frac{\sigma v\, dt}{(Dt)^{d/2}V_d}. \tag{7.52}$$

With this expression for $R(t)dt$ in hand, we can do the integral (7.50) and get

$$\langle P(\mathbf{r},\mathbf{r})_{\text{classical}}\rangle = \frac{\sigma v}{D^{d/2}V_d}\begin{cases} 2\left[\sqrt{t_c}-\sqrt{\tau}\right] & d=1, \\ \ln(t_c/\tau) & d=2, \\ \left(1-\frac{d}{2}\right)^{-1} t^{1-\frac{d}{2}} & d>2. \end{cases} \tag{7.53}$$

For future reference we state the specific results for one and two dimensions. Rather than state the result of the estimation above, we give the correct leading order results (computed by diagrammatic perturbation theory, see, e.g., [4, 12]). These results have the same dependence on ℓ and L_o but slightly different prefactors than our estimate.

$$\delta\bar{\Gamma} = -\frac{e^2}{h}\begin{cases} \frac{2}{3}\left(\sqrt{2}L_o - \ell\right) & d=1 \\ \frac{2}{\pi}\ln\frac{\sqrt{2}L_o}{\ell} & d=2 \end{cases} \tag{7.54}$$

7.6 Strong Localization

Strong localization, characterized by the exponential decay of the wavefunction around some localization site, has dramatic consequences for both transport and wavefunction statistics. Strong enough disorder can always exponentially localize the wavefunction. Weak disorder can sometimes localize the wavefunction but this depends on the strength of the disorder and the dimensionality of the system. Below, we sketch out an argument, originally due to Thouless, which clarifies how strong localization occurs as well as its dimensional dependence.

The idea is simple. As a wavepacket diffuses we consider, at each instant of time, a d-dimensional box of volume $\Omega = Cr^d = (Dt)^{\frac{d}{2}}$ which surrounds it. At each moment we can project the wavepacket onto the eigenstates of the surrounding box. The average energy level spacing in that box is

$$\delta E = \frac{1}{\Omega \nu_d} = (Dt)^{-\frac{d}{2}} E^{1-\frac{d}{2}}. \tag{7.55}$$

However, the wavepacket has been diffusing for a time t and so we can use its autocorrelation function, $A(t)$, defined by

$$A(t) = \langle \psi(0) \, | \psi(t) \, \rangle) = \sum_n \langle \psi(0) \, | n \, \rangle \, e^{-iE_n t}, \tag{7.56}$$

to look at the spectrum of the wavepacket. If we can completely resolve the spectrum, no more dynamics occurs except the phase evolution of the eigenstates of the box. Thus the wavepacket has localized. After a time t, we can resolve levels with spacing $\Delta E = \frac{h}{t}$. We define the "Thouless Conductance" g via

$$g = \frac{\Delta E}{\delta E} = h D^{d/2} E^{\frac{d}{2}-1} t^{\frac{d}{2}-1}. \tag{7.57}$$

If $g < 1$ we can resolve the levels of the wavepacket and it localizes. Conversely, if $g > 1$, we cannot resolve the eigenstates making up the wavepacket and diffusion continues.

The first conclusion we can draw from this argument is the dimensional dependence of the $t \to \infty$ limit of g. In one dimension, it is apparent that $\lim_{t\to\infty} g = 0$ and thus all states in a weakly disordered one dimensional system localize. In two dimensions, this argument is inconclusive and seems to depend on the strength of the disorder. In fact, it is believed that all states in weakly disordered two dimensional systems localize as well but

with exponentially large localization lengths. For $d > 2$, $\lim_{t\to\infty} g = \infty$ and we expect the states to be extended.

When measuring conductance, the difference between localized and extended states in the disordered region is dramatic. If the state is exponentially localized in the disordered region, it will not couple well to the leads and the conductance will be suppressed. We can look for this effect by looking at the conductance of a disordered wire as a function of the length of the disordered region. If the states are extended, we expect the conductance to vary as $1/L$ whereas if the states are localized we expect the conductance to vary as $e^{-L/\xi}$ where ξ is the localization length.

The effect of exponential localization on wavefuntion statistics is equally dramatic. For instance, in two dimensions, since we know that

$$\psi(\mathbf{r}) = \sqrt{\frac{2}{\pi\xi^2}} e^{-|\mathbf{r}-\mathbf{r}_o|/\xi}, \tag{7.58}$$

we can compute

$$P(t) = \frac{2\pi}{\Omega}\int r\,dr\delta\left(t - \Omega|\psi(\mathbf{r})|^2\right) = \frac{2\pi}{\Omega}\int r\,dr\delta\left(t - \frac{2\Omega}{\pi\xi^2}e^{-2r/\xi}\right) = \frac{\pi\xi^2}{2\Omega}\frac{\ln\frac{2\Omega}{\pi\xi^2 t}}{t}. \tag{7.59}$$

In figure 7.1 we plot the Porter-Thomas distribution and the exponential localization distribution for a localization length $\xi = \sqrt{\Omega}/10$ and $\xi = \sqrt{\Omega}/100$ so we can see just how stark this effect is.

7.7 Anomalous Wavefunctions in Two Dimensions

The description above does not explain much about how strong localization occurs, either in the time-domain or as a function of disorder. This transition is particularly interesting in two dimensions since even the existence of strongly localized states in weakly disordered systems is subtle.

While it is not at all obvious that large fluctuations in wavefunction intensity in extended states is related to strong localization, it seems an interesting place to look. While this was perhaps the original reason these large fluctuations were studied, they have spawned an independent set of questions. The simplest of those questions is the one answered by $P(t)$, namely, how often do these large fluctuations occur?

Various field-theoretic techniques have been brought to bear on this problem [39, 15, 29]. All predict the same qualitative behavior of $P(t)$. Namely, that for large values of

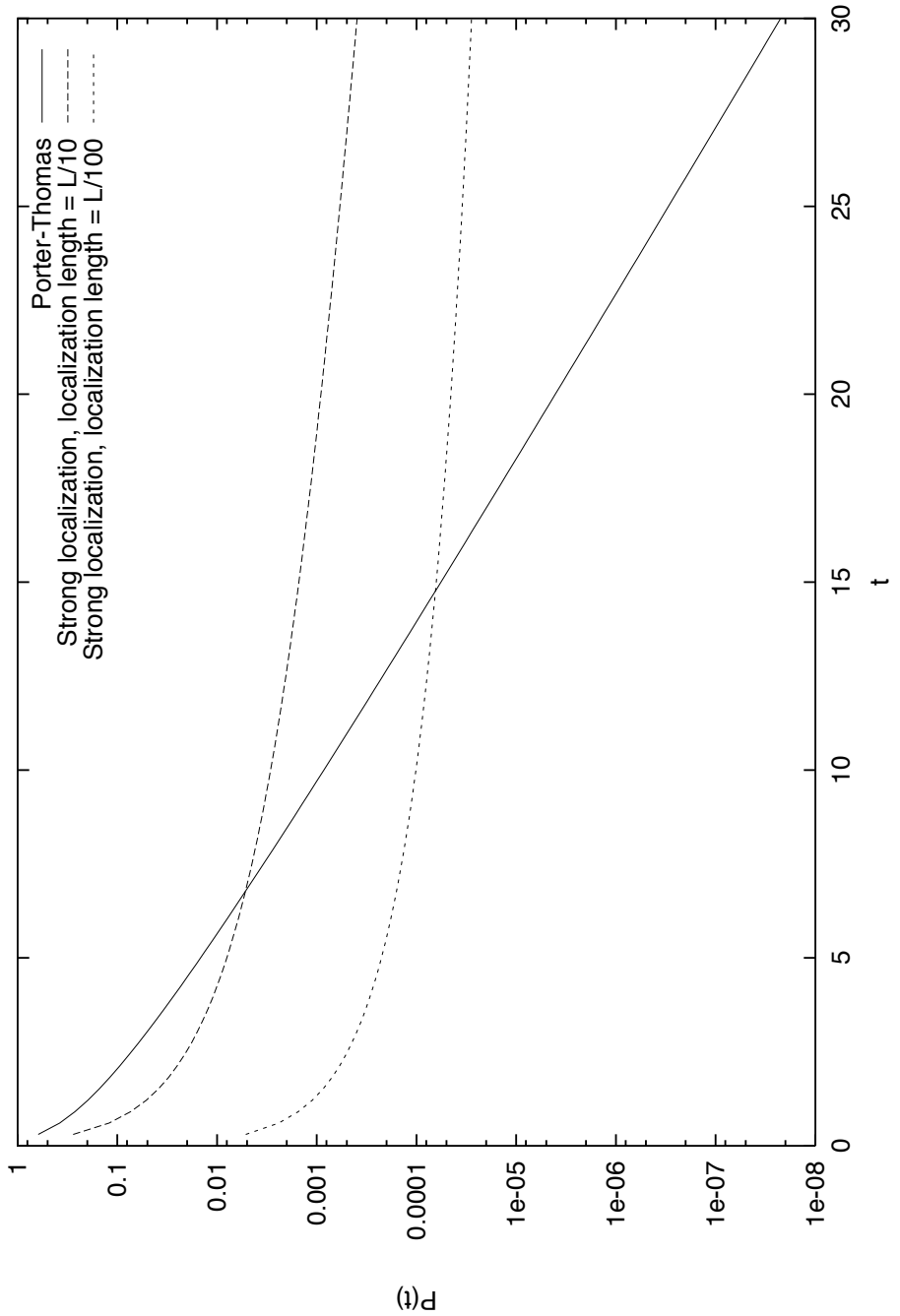

Figure 7.1: Porter-Thomas and exponential localization distributions compared.

t, $P(t)$ has a log-normal form:

$$P(t) \sim e^{-C_2 \ln^2 t}. \tag{7.60}$$

Various workers have argued for different forms for C_2 which depends on the energy E, the mean free path, ℓ, the system size, L_o and the symmetry class of the system (existence of time-reversal symmetry). The log-normal distribution looks strikingly different from either the Porter-Thomas distribution or the strong localization distribution. In figure 7.2 we plot all of these distributions for an example choice of μ for $t > 20$. We only consider large values of t because for small values of t, $P(t)$ will have a different form. For small enough values of t these calculations predict that $P(t)$ has the Porter-Thomas form. This allows them to be trivially distinguished from the strong-localization form which is very different from Porter-Thomas for small t.

We will focus in particular on two different calculations. The first, appearing in [39], uses the direct optimal fluctuation method (DOFM) and predicts

$$C_2^{(1)} = \frac{\pi k \ell}{4 \ln(F_1 k L_o)} \tag{7.61}$$

where D_1 is an $\mathcal{O}(1)$ constant. Another calculation, appearing in [15] and using the supersymmetric sigma model (SSSM) predicts

$$C_2^{(2)} = \frac{\beta \pi k \ell}{4 \ln(F_2 L_o/\ell)} \tag{7.62}$$

where $\beta = 1$ for time-reversal invariant systems and $\beta = 2$ for systems without time-reversal symmetry and D_2 is an $\mathcal{O}(1)$ constant.

In order to see the differences between $C_2^{(1,2)}$, in figure 7.3 we plot both of these coefficients versus both wavelength and mean free path for various values of D_1 and D_2.

7.8 Conclusions

In this chapter we reviewed material on quenched disorder in open and closed metallic systems. In the chapters that follow we will often compare to these results or try to verify them with numerical calculations.

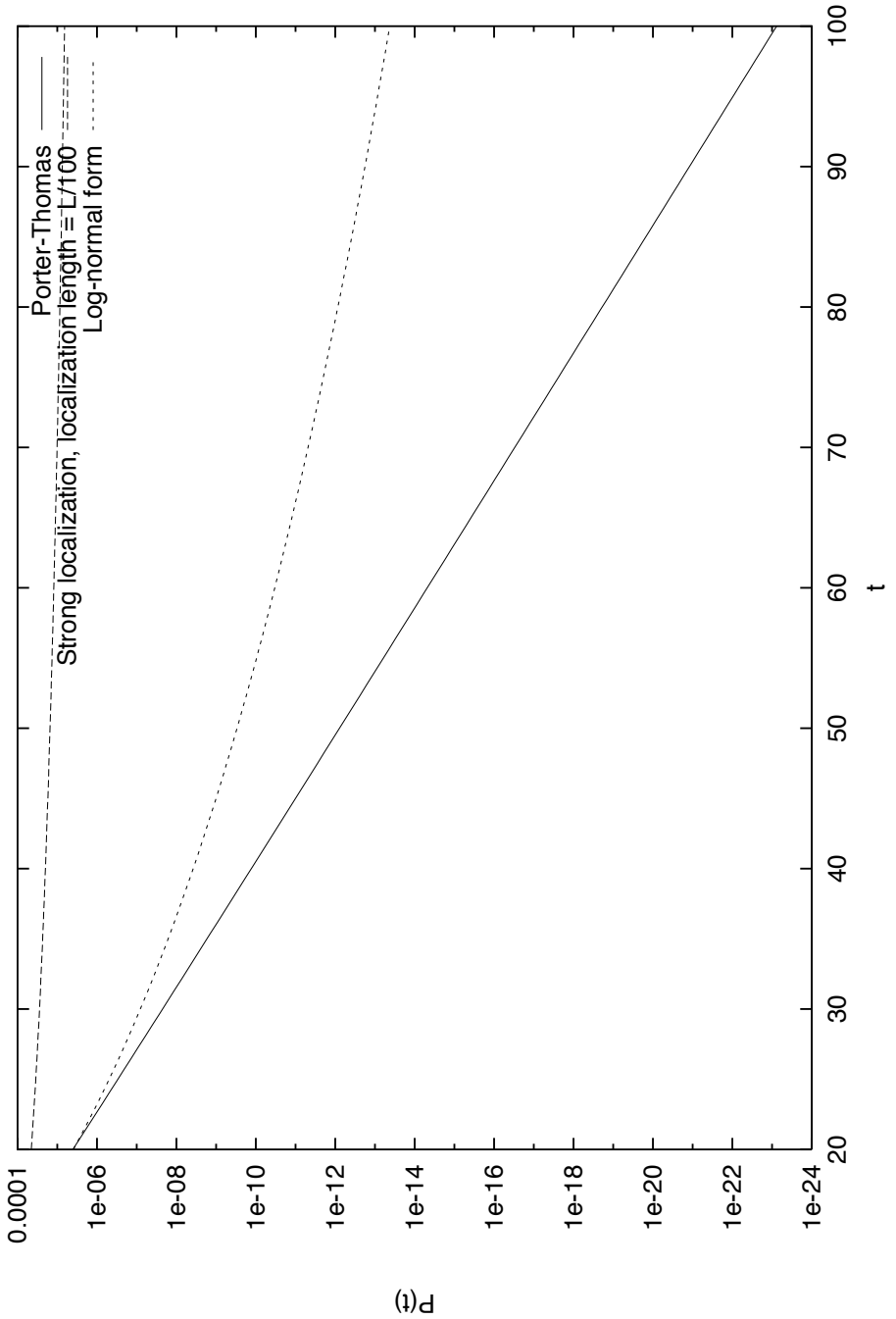

Figure 7.2: Porter-Thomas,exponential localization and log-normal distributions compared.

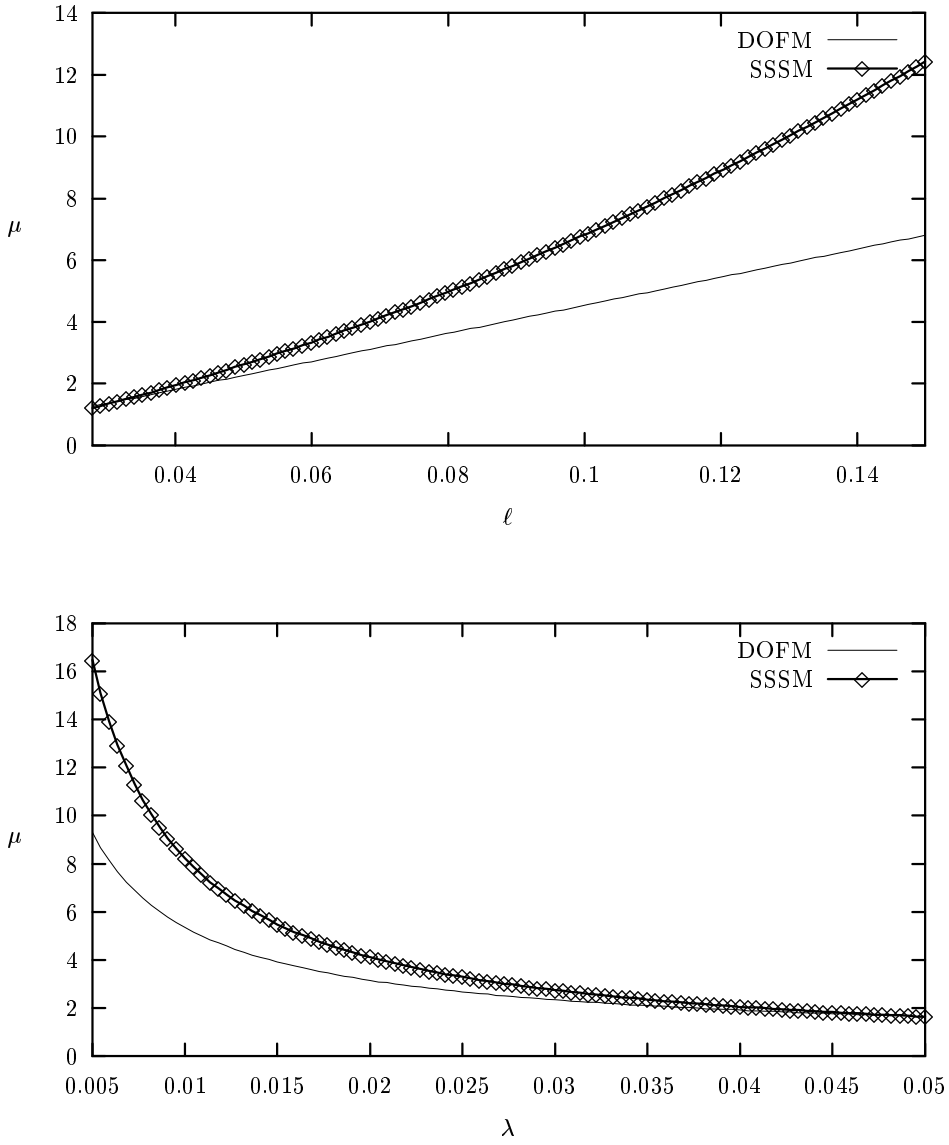

Figure 7.3: Comparison of log-normal coefficients for the DOFM and SSSM.

Chapter 8

Quenched Disorder in 2D Wires

We consider an infinite wire of width W with a disordered segment of length L as in Fig. 8.1. This wire will be taken to have periodic boundary conditions in the transverse (y) direction.

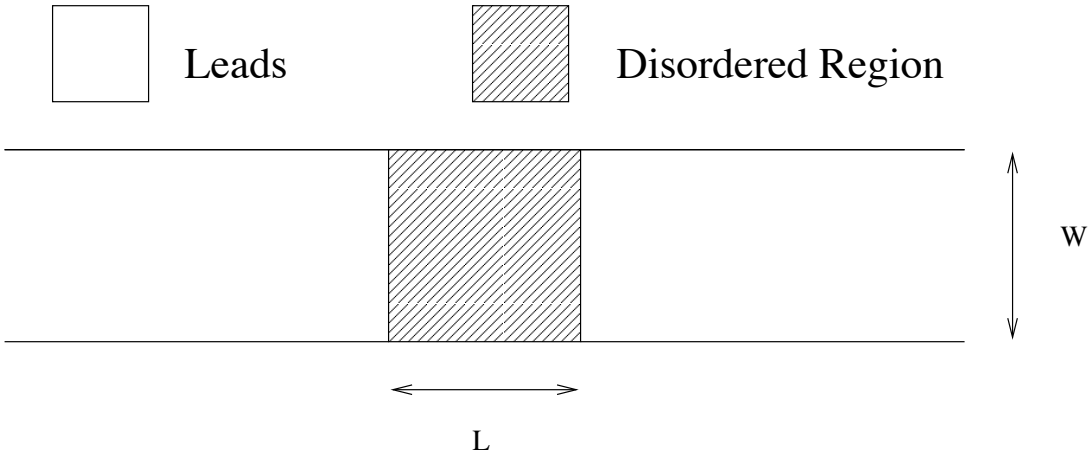

Figure 8.1: The wire used in open system scattering calculations.

To connect with the language of mesoscopic systems, we may think of the disordered region as a mesoscopic sample and the semi-infinite ordered regions on each side as perfectly conducting leads. For example, one can imagine realizing this system with an AlGaAs "quantum dot." [27].

We can measure many properties of this system. For instance, we have used renormalized scattering techniques to model a particular quantum dot [23]. Typical quantum

dot experiments involve measuring the conductance of the quantum dot as a function of various system parameters (e.g., magnetic field, dot shape or temperature). Thus we should consider how to extract conductance from a Green function.

In this section we discuss numerically computed transport coefficients. This allows us to verify that our disorder potential has the properties that we expect classically. Since we are interested in intensity statistics and how they depend on transport properties, it is important to compute these properties in the same model we use to gather statistics. For instance, as discussed in the previous chapter, the ATA breaks down when coherent back-scattering contributes a significant weak localization correction to the diffusion coefficient. In this regime it is useful to verify that the corrections to the transport are still small enough to use an expansion in λ/ℓ. When the disorder is strong enough, strong localization occurs and a different approximation is appropriate.

Of course, transport in disordered systems is interesting in its own right. Our method allows a direct exploration of the theory of weak localization in a disordered two dimensional systems.

8.1 Transport in Disordered Systems

8.1.1 Diffusion from Conductance

Computing the conductance of a disordered wire is not much different than computing the conductance of the one scatterer system. We use (5.37) to compute the channel-to-channel Green function, G_{ab}, from the multiple scattering t-matrix, find the transmission matrix $\mathcal{T}_{ab}$ from (5.31) and compute the conductance, $\Gamma = (e^2/h)\gamma$ using the Fisher-Lee relation (5.30).

In chapter 5, we assumed the (classical) transport to and from the scatterer was ballistic and derived an expression which related the intensity reflection coefficient (which can be trivially related to the observed conductance) to the scattering cross section of an obstacle in the wire. When many scatterers are placed randomly in the wire, this assumption is no longer valid. Most scattering events occur after other scattering events and thus the probability of various incident angles is uniform rather than determined by the channels of the wire. Also, there will typically be many scattering events. So, when we have many randomly placed scatterers, we will assume that the transport is *diffusive*. This will give

us a different relationship between the reflection coefficient and the cross-section of each obstacle.

It is instructive to compute the expected reflection coefficient as a function of the concentration and cross-section under the diffusion assumption and compare that result, R_D, to $R_B = \frac{\pi\sigma}{4W}$ computed under the ballistic assumption.

We begin from the relation between the intensity transmission coefficient, T_D, Γ and the number of open channels, N_c:

$$T_D = \frac{(h/e^2)\Gamma}{N_c}, \tag{8.1}$$

i.e., the transmission coefficient is just the unitless conductance per channel. From this we see that Γ does not go to ∞ for an empty wire as we might expect. Only a finite amount of flux can be carried in a wire with a finite number of open channels and this gives rise to a so-called "contact resistance" [8]. We thus split the unitless conductance into a disordered region dependent part (Γ_s) and a contact part:

$$\frac{h}{e^2}\Gamma = \left(\frac{e^2/h}{\Gamma_s} + \frac{1}{N_c}\right)^{-1}, \tag{8.2}$$

where the contact part is chosen so that $\lim_{T\to 1}\Gamma_s = \infty$.

At this point we invoke the assumption of diffusive transport. This allows us to use the Einstein relation [8] to relate the conductivity of the sample $\frac{L}{W}\Gamma_s$ to the diffusion constant via

$$\frac{L}{W}\Gamma_s = e^2\nu D, \tag{8.3}$$

where ν is the density of states per unit volume; $\nu = 1/(4\pi)$ in two dimensions. The L/W in front of Γ_s relates conductivity to conductance in two dimensions.

We now have

$$\frac{h}{e^2}\Gamma = \left(\frac{L}{hW\nu D} + \frac{1}{N_c}\right)^{-1} = \frac{hW\nu DN_c}{LN_c + hW\nu D}. \tag{8.4}$$

If we substitute this into (8.1) we have

$$T_D = \frac{hW\nu D}{LN_c + hW\nu D}. \tag{8.5}$$

As in the previous chapters, we choose units where $\hbar = 1$ and $m = 1/2$, so $\hbar^2/(2m) = 1$. We also choose units where the electron charge, $e = 1$. We now use $D = v\ell/d = k\ell$ [37] and $N_c \approx kW/\pi$ and get

$$T_D = \frac{\frac{\pi\ell}{2}}{L + \frac{\pi\ell}{2}}, \tag{8.6}$$

and

$$R_D = 1 - T_D = \frac{L}{L + \frac{\pi \ell}{2}}. \tag{8.7}$$

Finally, we use $l = LW/(N\sigma)$ to get

$$R_D = \frac{1}{1 + \frac{\pi W}{2N\sigma}}. \tag{8.8}$$

For very few scatterers we usually have $N\sigma << \pi W/2$ and thus

$$R_D = N\frac{2\sigma}{W\pi}. \tag{8.9}$$

Compare this to the ballistic result and we see that they are related by $R_B/R_D = \pi^2/8$. This factor arises from the different distributions of the incoming angles. In practice, there can be a large crossover region between these two behaviors, when the non-uniform distribution of the incoming angles can make a significant difference in the observed conductance.

We note that (8.7) can be rearranged to yield:

$$\ell = \frac{2L}{\pi}\left(\frac{1}{R_D} - 1\right) = L\frac{2}{\pi}\left(\frac{T_D}{R_D}\right), \tag{8.10}$$

which we will use as a way to compare numerical results with the assumption of quasi-classical diffusion.

8.1.2 Numerical Results

As our first numerical calculation we look at the mean free path as a function of scatterer concentration at fixed energy. In figure 8.2 we plot ℓ vs. n for a periodic wire of width 1 with a length 1 disordered region. There are about 35 wavelengths across the wire is and thus the wire has 71 open channels. We use scatterers with maximum s-wave cross section of $\frac{2}{\pi}\lambda$. We consider concentrations from 50 to 700 scatterers per unit area. At each concentration we compute the conductance of 20 realizations of the scatterers and average them. This range of concentrations corresponds to a range of quasi-classical mean free path from 1.1 to .069. We plot both the quasi-classical mean free path and the numerical result computed via (8.10).

From the figure, we see that the numerical result is noticeably smaller than the quasi-classical result, though it differs by at most 20% over the range of concentrations studied. This difference is partially explained by two things. At low concentrations, the numerically observed mean free path is smaller than the quasi-classical because the transport

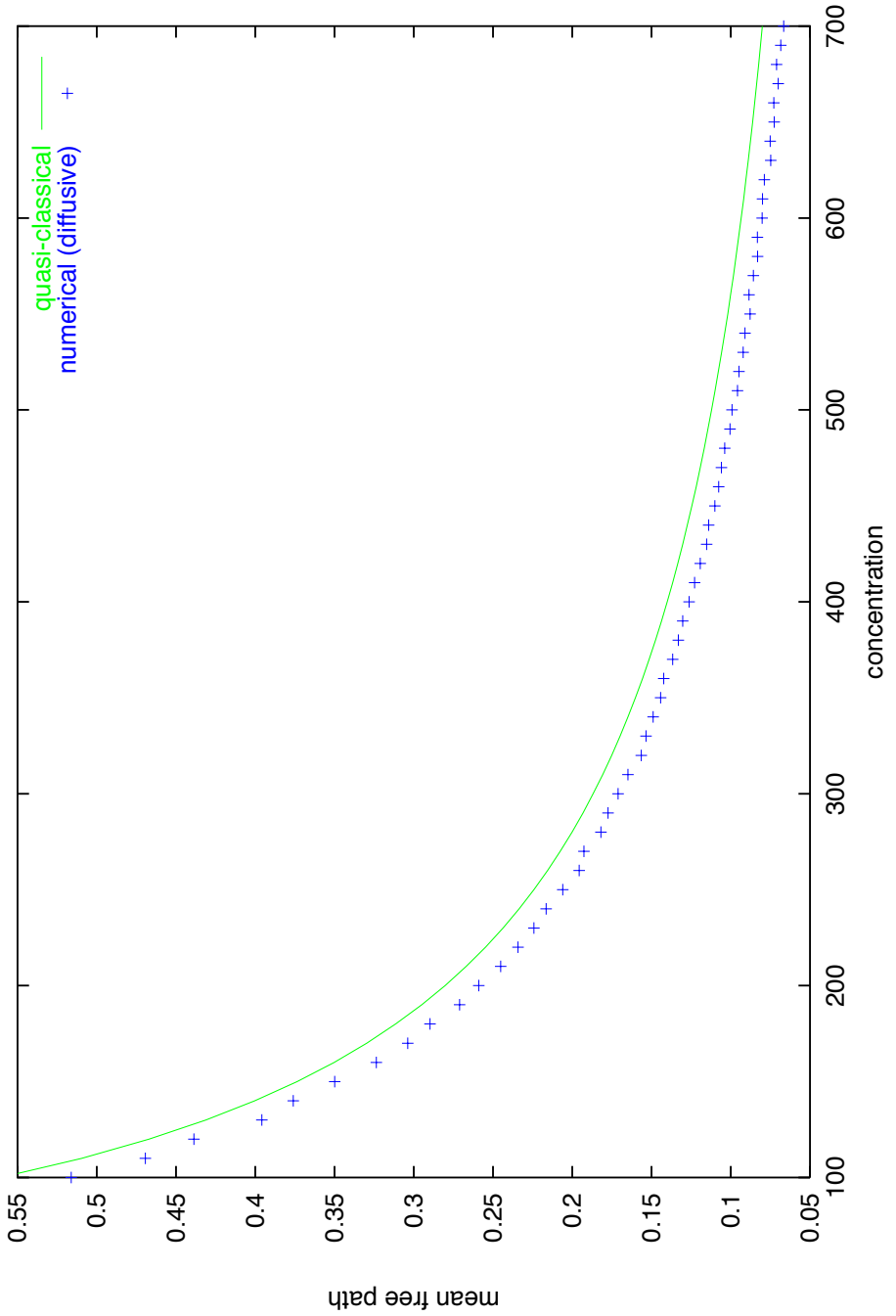

Figure 8.2: Numerically observed mean free path and the classical expectation.

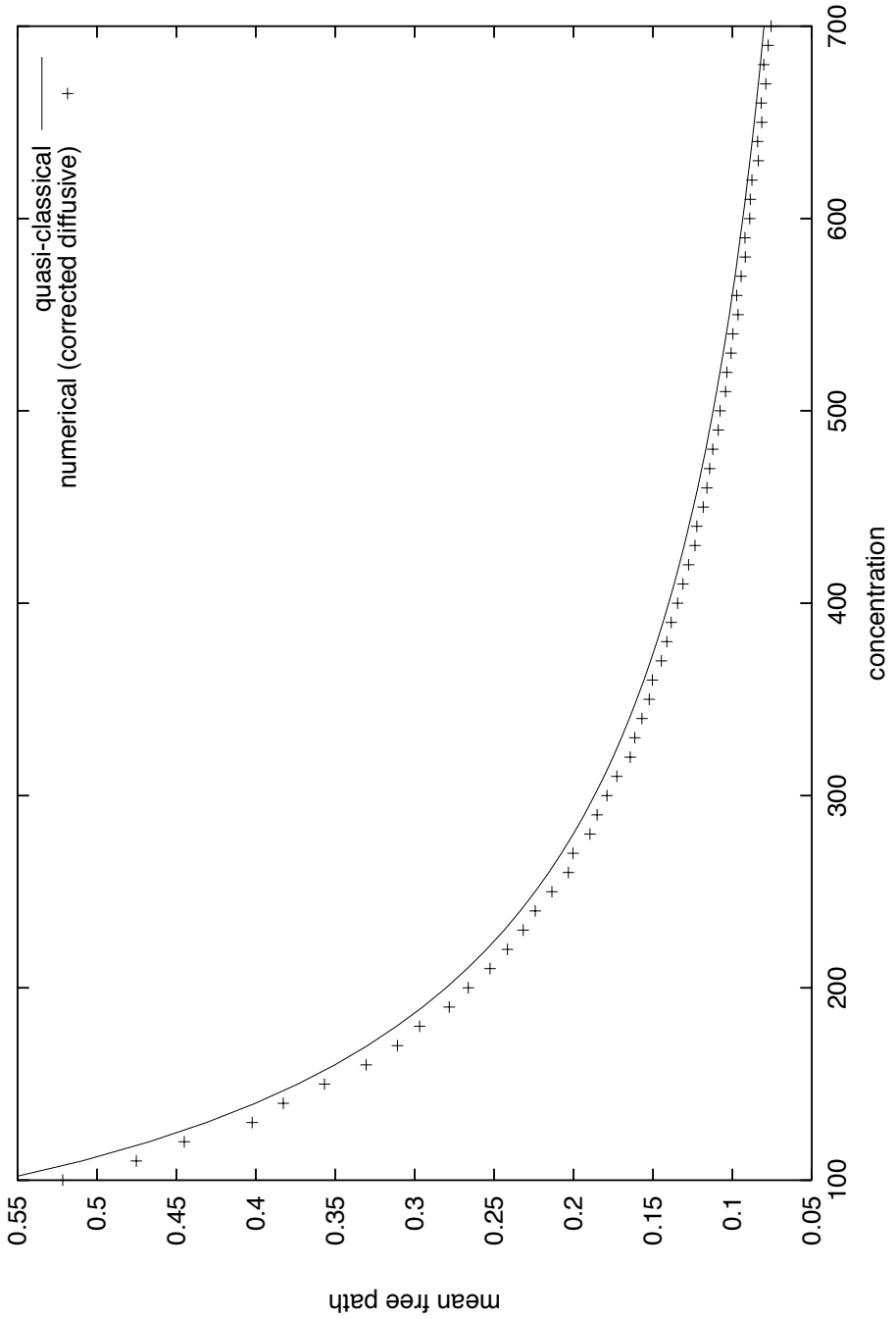

Figure 8.3: Numerically observed mean free path after first-order coherent back-scattering correction and the classical expectation.

is not completely diffusive. As we saw at the beginning of this chapter, ballistic scattering leads to a larger reflection coefficient than diffusive ones. This leads to an apparently smaller mean free path. More interestingly, there is coherent back-scattering at all concentrations (see section 7.5), though its effect is larger at higher concentration since the change in conductance due to weak localization is proportional to λ/ℓ. We correct the conductance, via (7.54), to first order in λ/ℓ and then plot the corrected mean free path and the classical expectation in figure 8.3. The agreement is clearly better, though there is clearly some other source of reduced conductance. At the lowest concentrations there is still a ballistic correction as noted above but this cannot account for the lower than expected conductance at thigher concentrations where the motion is clearly diffusive.

As λ/ℓ increases, the difference between the classical and quantum behavior does as well. For large enough λ/ℓ this will lead to localization. In order to verify that the transport is still not localized, we compute the transmission coefficient vs. the length of the disordered region for fixed concentration. If the transport is diffusive, T will satisfy (8.5) which predicts $T \sim 1/L$ for large L. If instead the wavefunctions in the disordered region are exponentially localized, T will fall exponentially with distance, i.e., $T \sim e^{-L/\xi}$. In figure 8.4 we plot T versus L for two different concentrations and energies. In both plots, 5 realizations of the disorder potential are averaged at each point. In figure 8.4a there are 35 wavelengths across the width of the wire, as in the previous plot, and the concentration is 250 scatterers per unit area. T is clearly more consistent with the diffusive expectation than the strong localization prediction.

We compare this to figure 8.4b where the wavelength and mean free path are comparable and the wire is only a few wavelengths wide. What we see is probably quasi-one dimensional strong localization. Consequently, T does not satisfy (8.5) but rather has an exponential form. We note that the data in figure 8.4b is rather erratic but still much more strongly consistent with strong localization than diffusion. Numerical observation of exponential localization in a true two dimensional system would be very difficult since the two dimensional localization length is exponentially long in the mean free path.

8.1.3 Numerical Considerations

Numerical computation using the techniques outlined in chapters 3 and 5 is quite simple. For each set of parameters computation proceeds as follows:

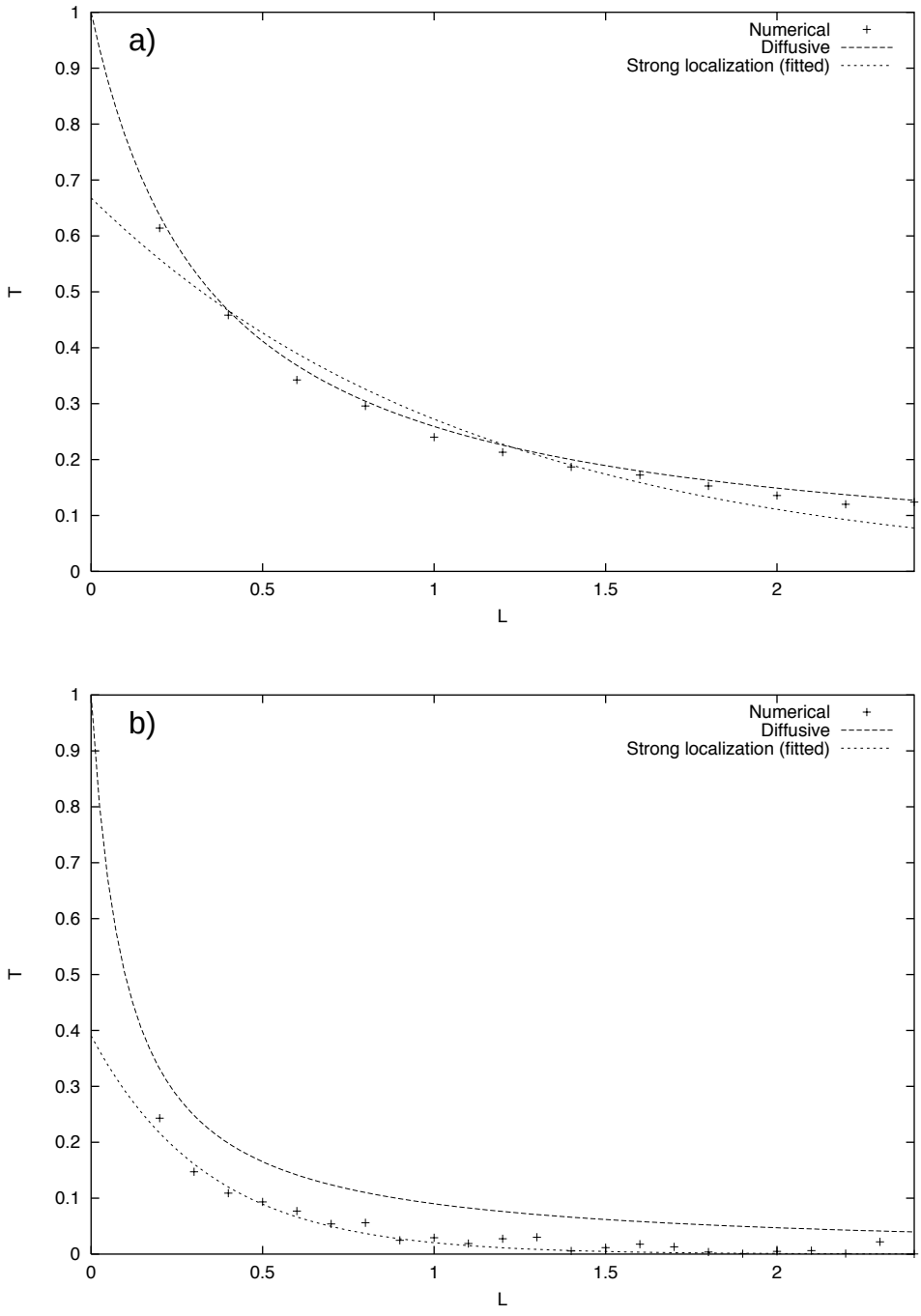

Figure 8.4: Transmission versus disordered region length for (a) diffusive and (b) localized wires.

1. Compute the random locations of N scatterers.
2. Compute the renormalized t-matrix of each scatterer.
3. Compute the scatterer-scatterer Green functions for all pairs of scatterers.
4. Construct the inverse multiple scattering matrix, T^{-1}.
5. Invert T^{-1}, giving T, using the Singular Value Decomposition.
6. Use formula (5.37) to compute the channel-to-channel Green function.
7. Use (5.31) and the Fisher-Lee formula to find the conductance Γ.
8. Repeat for as many realizations as required to get $\langle\Gamma\rangle$.

The bottleneck in this computation can be either the $\mathcal{O}(N^3)$ SVD or the $\mathcal{O}(N^2 N_c^2)$ application of (5.37) depending the concentration and the energy. The computations appearing above were done in one to four hours on a fast desktop workstation (DEC Alpha 500/500).

There are faster matrix inversion techniques than the SVD but few are as stable when operating on near-singular matrices. Though that is crucial for the finite system eigenstate calculations of the next chapter, it is non-essential here. If one were to switch to an LU decomposition or a QR decomposition (see appendix C) we could speed up the inversion stage by a factor of four or two respectively. For most of the calculations we performed, the computation of the channel-to-channel Green function computation was more time consuming and so such a switch was never warranted.

Chapter 9

Quenched Disorder in 2D Rectangles

While analytic approaches to disordered quantum systems abound, certain types of experimental or numerical data is difficult to come by. There is a particular dearth of wavefunction intensity statistics for 2D disordered systems.

Experimentally, wavefunctions are difficult quantities to measure. The application of atomic force microscopy to quantum dot systems is a promising technique [11]. An atomic force microscope (AFM) can be capacitively coupled to a quantum dot in such a way that the at the point in the two-dimensional electron gas below the tip, electrons are effectively excluded. The size of the excluded region depends on a variety of factors but is typically of the order of one wavelength square. One scenario for measuring the wavefunction involves moving the tip around and measuring the shift in conductance of the dot due to the location of the tip. For a small enough excluded region, this conductance shift should be proportional to the square of the wavefunction. Even for a wavelength sized excluded region, this technique should be capable of resolving most of the nodal structure of the wavefunction from which the wavefunction could be reconstructed. Preliminary numerical calculations suggest that this technique could work and at least one experimental group is working on this scheme or a near variant.

One successful experimental approach has been using microwave cavities as an analog computer to solve the Helmholtz equation in disordered and chaotic geometries [24]. This technique has led to some of the only data available on disordered 2D systems. How-

ever, experimental limitations make it difficult to consider enough ensembles to do proper averaging. Instead, the statistics are gathered from states at several different energies. Since the mean free path and wavelength both depend on the energy, the mixing of different distributions makes analysis of the data difficult. Still, the data does suggest that large fluctuations in wavefunction intensities are possible in two dimensional weakly disordered systems.

Numerical methods, which would seem a natural way to do rapid ensemble averaging, have not been applied or, at least, not been successful at reaching the necessary parameter regimes and speed requirements to consider the tails of the intensity distribution. There are some results for the tight-binding Anderson model [30]. However, the nature of the computations required for the Anderson model makes it similarly difficult to gather sufficient intensity statistics to fit the tails of the distribution. It is the purpose of the section to illustrate how the techniques discussed in this thesis can provide the data which is so sorely needed to move the theory (see section 7.7) forward.

We begin with an abstract treatment of the extraction of discrete eigen-energies and corresponding eigenstates from t-matrices. This is a topic worth considering carefully since it is the basis for all the calculations which follow. The t-matrix has a pole at the eigenenergies so the inverse of the t-matrix is nearly singular.

Once the preliminaries are out of the way, we discuss the difficulties of studying intensity statistics in the parameter regime and with the methods of [24]. In particular, we consider the impact of Dirichlet boundaries on systems of this size. We consider the possibility that dynamics in the sides and corners of a Dirichlet rectangle can have a strong effect on the intensity statistics and perhaps mask the effects predicted by the Field-Theory.

We also discuss eigenstate intensity statistics for a periodic rectangle (a torus) with various choices of disorder potential (i.e. various ℓ and λ). We'll briefly discuss the fitting procedure used to show that the distributions are well described by a log-normal form and extract coefficients. We'll then compare these coefficients to the predictions of field theory. The computation of intensity statistics in the diffusive weak disorder regime is the most difficult numerical work in this thesis. It also produces results which are at odds with existing theory. Thus we spend some time exploring the stability of the numerics and possible explanations for the differences between the results and existing theory.

Finally, as in the last chapter, we'll discuss the numerical techniques more specifically and outline the algorithm. Here, some less than obvious ideas are necessary to gather

statistics at the highest possible speed.

9.1 Extracting eigenstates from t-matrices

We want to apply the results of Chapter 3 to finite systems, i. e., systems with discrete spectrum. In some sense this is very similar to section 6.1.5 but in this case we have many scatterers instead of one; what was simply root finding becomes linear algebra.

Suppose $\hat{t}^{-1}(z)$ has a non-trivial null-space when $z = E_n$. Define $\hat{P}_N$ and $\hat{P}_R$ as projectors onto the null-space and range of $\hat{t}^{-1}(E_n)$ respectively. Since we know that E_n is a pole of $\hat{T}(z)$, we know that, for $0 < |\epsilon| << 1$ and $\forall \mathbf{v} \in \mathcal{S}$ we have

$$\hat{T}^{-1}(E_n + \epsilon)\,|v\rangle \approx \hat{T}^{-1}(E_n)\hat{P}_R\,|v\rangle + \frac{\epsilon}{C}\hat{P}_N\,|v\rangle \tag{9.1}$$

We define a pseudo-inverse (on the range of $\mathbf{T}^{-1}$) $\hat{B}_R$, via

$$\hat{t}^{-1}(E_n)\hat{B}_R\hat{P}_R\,|v\rangle = \hat{P}_R\,|v\rangle\,, \tag{9.2}$$

which exists since $\hat{t}^{-1}(E_n)$ is explicitly non-null on $\hat{P}_R\,|v\rangle$. We can now invert $\hat{t}^{-1}(z)$ in the neighborhood of $z = E_n$:

$$\hat{t}(E_n + \epsilon)\,|v\rangle \approx \hat{B}_R\hat{P}_R\,|v\rangle + \frac{C}{\epsilon}\hat{P}_N\,|v\rangle\,. \tag{9.3}$$

Thus, the residue of $\hat{t}(z)$ at $z = E_n$ projects any vector onto the null-space of $\hat{t}^{-1}(E_n)$.

Recall that the full wavefunction is written

$$|\psi\rangle\,|\phi\rangle + \hat{G}_B\hat{t}\,|\phi\rangle\,. \propto \lim_{\epsilon\to 0}\hat{G}_B\frac{C}{\epsilon}\hat{P}_N\,|\phi\rangle \tag{9.4}$$

Since the t-matrix term has a pole, the incident wave term is irrelevant and the wavefunction is (up to a constant) $\hat{G}_B\hat{P}_N\,|\phi\rangle$.

When the state at E_n is non-degenerate (which is generic in disordered systems), there exists a vector $|\alpha\rangle$ the projector may be written $\hat{P}_N = |\alpha\rangle\,\langle\alpha|$ and thus

$$|\psi_n\rangle = \mathcal{N}\hat{G}_B(E_n)\,|\alpha\rangle\,, \tag{9.5}$$

where $\mathcal{N}$ is a normalization constant. In position representation,

$$\psi_n(\mathbf{r}) = \mathcal{N}\int_{\mathcal{S}} G_B(\mathbf{r},\mathbf{r}';E_n)\alpha(\mathbf{r}')\,d\mathbf{r}'. \tag{9.6}$$

If the state is m-fold degenerate, $\hat{P}_N = \sum_{j=1}^{m} |\alpha_j\rangle \langle\alpha_j|$ and we have the solutions $\left|\psi_n^{(j)}\right\rangle = \mathcal{N}_j \hat{G}_B |\alpha_j\rangle$

Thus, the task of finding eigenenergies of a multiple scattering system is equivalent to finding E_n such that $\hat{t}^{-1}(E_n)$ has a non-trivial null space. Finding the corresponding eigenstates is done by finding a basis for that null space.

Suppose that our t-matrix is generated by the multiple scattering of N zero range scatterers (see 3.1). In this case, the procedure outlined above can be done numerically using the Singular Value Decomposition (SVD). We have

$$\hat{t}^{-1} = \sum_{ij} |\mathbf{r}_i\rangle (\mathbf{A})_{ij} \langle\mathbf{r}_j| \tag{9.7}$$

We can decompose $\mathbf{A}$ via $\mathbf{A} = \mathbf{U}\mathbf{\Sigma}\mathbf{V}^T$ where $\mathbf{U}$ and $\mathbf{V}$ are orthogonal and $\mathbf{\Sigma}$ is diagonal. The elements of $\mathbf{\Sigma}$ are called the "singular values" of $\mathbf{A}$. We can detect rank deficiency (the existence of a null-space) in $\mathbf{A}$ by looking for zero singular values. Far more detail on numerical detection of rank-deficiency is available in [17].

Once zero singular values are found, the vector, α (where $|alpha\rangle = \sum_i = \alpha_i |\mathbf{r}_i\rangle$), needed to apply (9.5), sits in the corresponding column of $\mathbf{V}$. It is important to note that we have extracted the eigenstate without ever actually inverting $\mathbf{A}$ which would incur tremendous numerical error. Thus our wavefunction is written

$$\psi(\mathbf{r}) = \mathcal{N} \sum_i G_B(\mathbf{r}, \mathbf{r}_i; E_n)\alpha_i. \tag{9.8}$$

We normalize the wavefunction by sampling at many points and determining $\mathcal{N}$ numerically.

In practice, we may use this procedure in a variety of ways. Perhaps the simplest is looking at parts of the spectra of specific configurations of scatterers. We define $S_N(E)$ as the smallest singular value of $\hat{t}^{-1}(E)$ (standard numerical techniques for computing the SVD give the smallest singular value as $(\mathbf{\Sigma})_{NN}$). Computing $S_N(E)$ is $\mathcal{O}(N^3)$. Then we use standard numerical techniques (e.g., Brent's method, see [33]) to minimize $S_N^2(E)$. We then check that minimum found is actually zero (within our numerical tolerance of zero, to be precise). These standard numerical techniques are more efficient when the minima are quadratic which is why we square the smallest singular value. We have to be careful to consider $S_N(E)$ at many energies per average level spacing so we catch all the levels in the spectrum. Since we know the average level spacing (see 2.27) is

$$\frac{1}{\mathcal{V}\varrho_2(E)} = \frac{\hbar^2}{2m} \cdot \frac{4\pi}{\mathcal{V}}, \tag{9.9}$$

we know approximately how densely to search in energy. The generic level repulsion in disordered systems [14] helps here, since the possibility of nearby levels is smaller.

9.2 Intensity Statistics in Small Disordered Dirichlet Bounded Rectangles

Our first attempt to gather intensity statistics will be performed on systems with relatively few scatterers (72) and thus large mean free paths. This regime is chosen for comparison with the experimental results of [24].

When gathering intensity statistics we need to find eigenstates near a particular energy. This is most simply done by choosing an energy and then hunting for a zero singular value in some window about that energy. For windows smaller than the average level spacing, we will frequently get no eigenstate at all. This method works but is very inefficient since we frequently perform the time-consuming SVD on matrices which will not yield a state. However, for this number of scatterers, this inefficiency is tolerable. In the next section we will consider improvements on this technique.

In figure 9.1 we plot $|\psi|^2$ on a gray-scale (black for high intensity and white for low) in a 72 scatterer system along with the scatterers plotted as black dots for a set of typical low energy wavefunctions in order to give the reader a picture of the sort of scatterer density and wavelength of the system we are considering.

In the experiments of [24], higher energies than those depicted in figure 9.1 are used. Some sample wavefunctions in the relevant energy range are shown in figure 9.2. In the original work, this energy range was chosen because λ must be significantly smaller than the system size for various field-theoretic techniques to be applicable. Unfortunately, there are not enough scatterers in the system to make the motion diffusive. This is clear from the large mean free paths in the states in 9.2, where ℓ/L_o varies from 1/4 to 1/2. This problem was overlooked in the original work due to a confusion about the relevant mean free path.

So, rather than $\lambda \ll \ell \ll L_o$, we have $\lambda < \ell < L_o$. This means that we expect the boundaries to play a large role in the dynamics of the system. In figure 9.3 we plot the intensity statistics for a 1×1 square with Dirichlet boundaries, $\ell = .31$ and $\lambda = .07$. In these and subsequent intensity statistics plots, we find $P(t)$ by computing wavefunctions, accumulating a histogram of values of $|\psi|^2$ and then dividing the number of counts in each

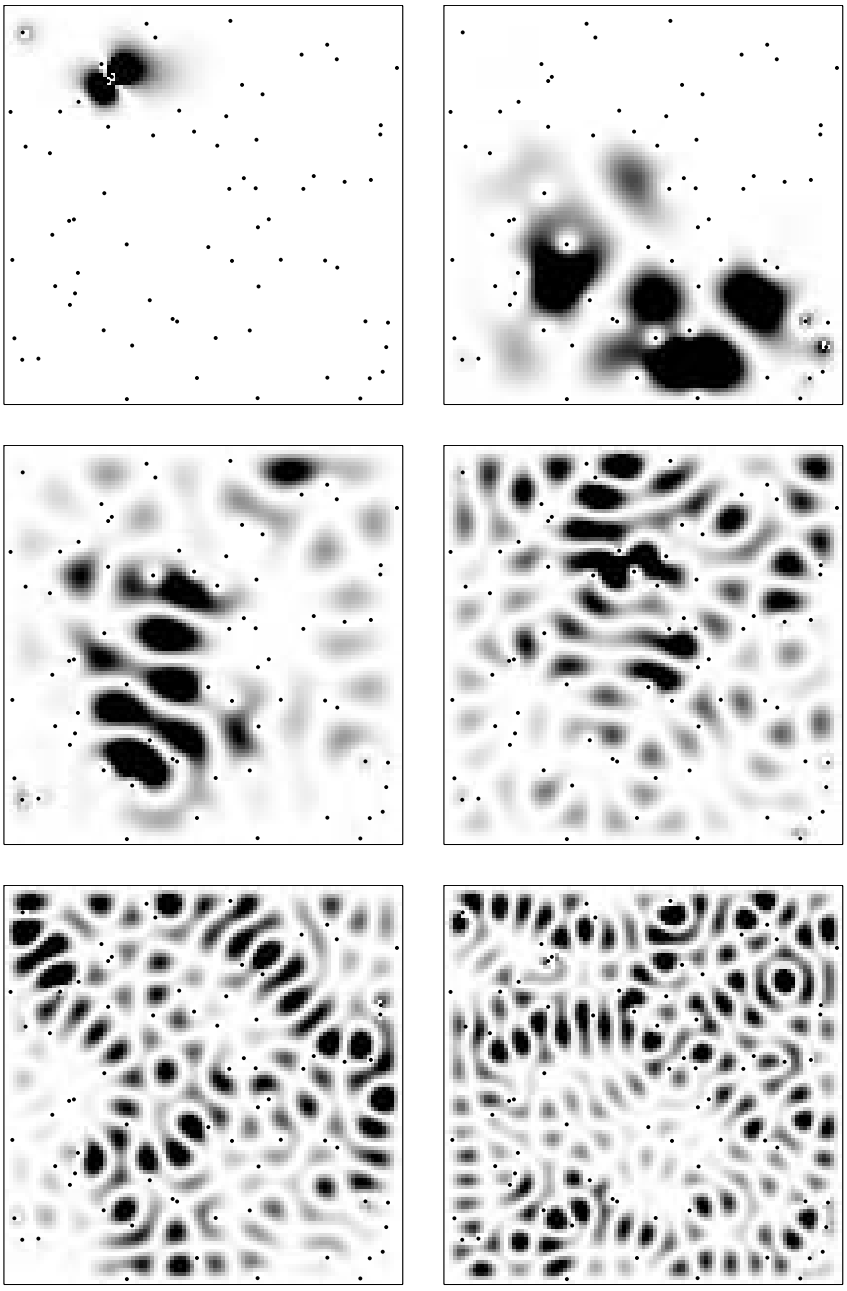

Figure 9.1: Typical low energy wavefunctions ($|\psi|^2$ is plotted) for 72 scatterers in a 1×1 Dirichlet bounded square. Black is high intensity, white is low. The scatterers are shown as black dots.For the top left wavefunction $\ell = .12$, $\lambda = .57$ whereas $\ell = .23$, $\lambda = .11$ for the bottom wavefunction. ℓ increases from left to right and top to bottom whereas λ decreases in the same order.

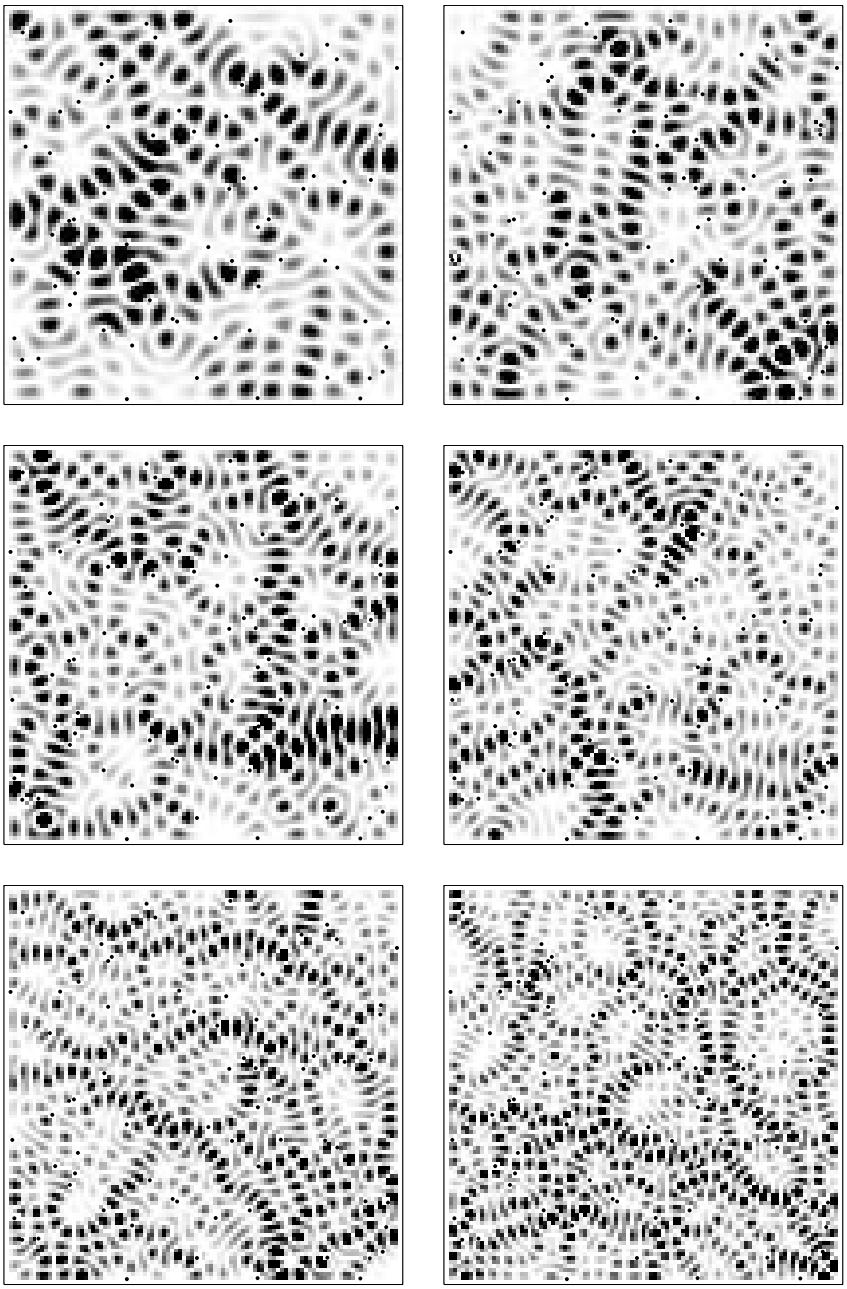

Figure 9.2: Typical medium energy wavefunctions ($|\psi|^2$ is plotted) for 72 scatterers in a 1×1 Dirichlet bounded square. Black is high intensity, white is low. The scatterers are shown as black dots. For the top left wavefunction $\ell = .25$, $\lambda = .09$ whereas $\ell = .48$, $\lambda = .051$ for the bottom wavefunction. ℓ increases from left to right and top to bottom whereas λ decreases in the same order.

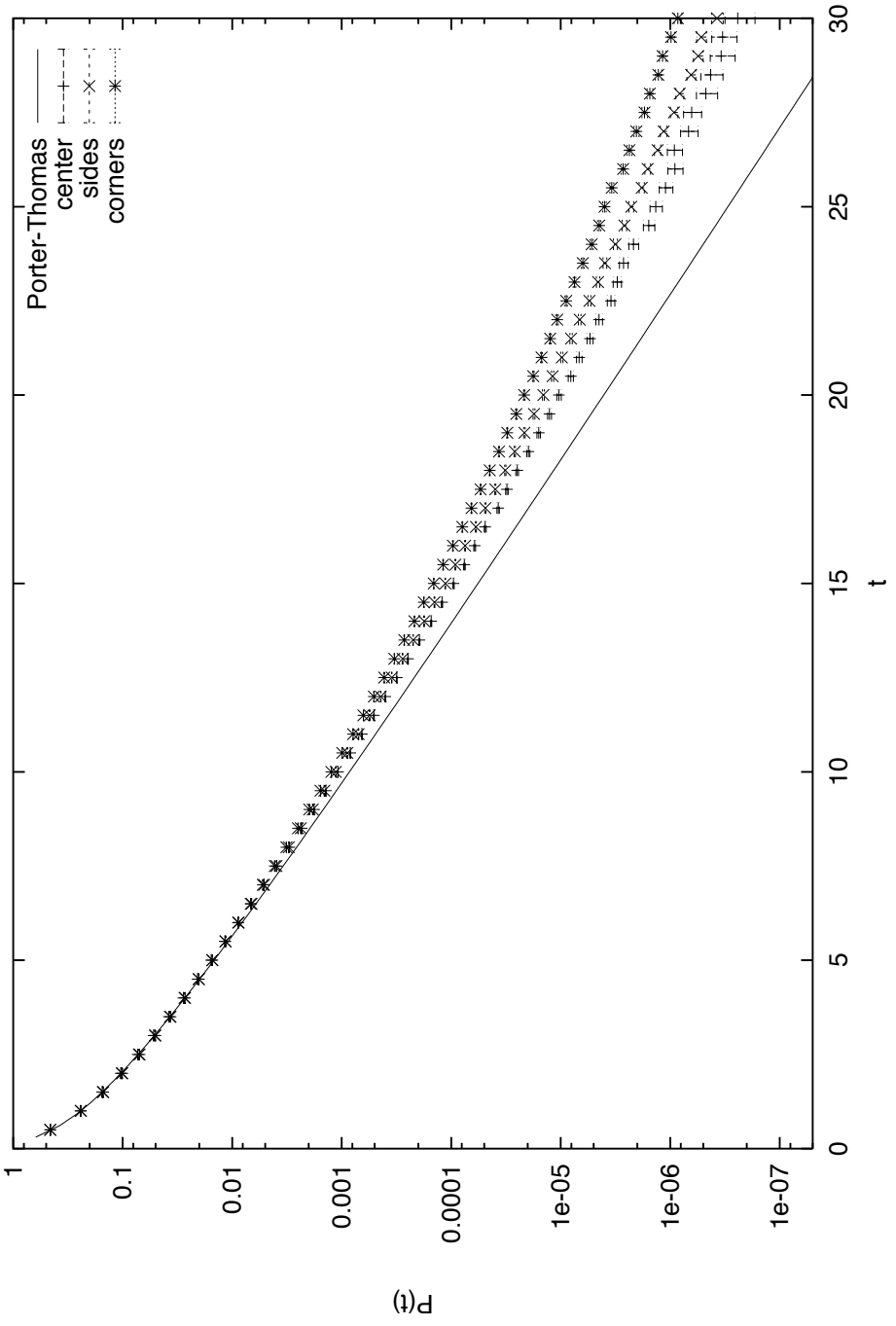

Figure 9.3: Intensity statistics gathered in various parts of a Dirichlet bounded square. Clearly, larger fluctuations are more likely in at the sides and corners than in the center. The (statistical) error bars are different sizes because four times as much data was gathered in the sides and corners than in the center.

bin by the total number of counts and the width of each bin.

As is clear from the figure, anomalous peaks are more likely near the sides and most likely near the corners. This large boundary effect makes it unlikely that existing theory can be fit to data which is, effectively, an average over all regions of the rectangle.

9.3 Intensity Statistics in Disordered Periodic Rectangle

In order to minimize the effect of boundary conditions, we change to periodic boundary conditions and decrease ℓ/L_o while holding λ/L_o constant. While periodic boundary conditions won't eliminate finite size system effects they do remove the enhanced localization near the Dirichlet boundary.

Decreasing ℓ/L_o at constant λ/L_o comes at a cost. Since the number of scatterers required to hold the concentration constant scales as the volume of the system, a larger system means more scatterers and a larger multiple scattering matrix. The method used in the previous section will not work quickly enough to be of practical use here (at least not on a workstation). This leads us to some very specific numerical considerations which we address below.

9.3.1 Numerical Considerations

The most serious inefficiency in computing wavefunctions are all the wasted SVD's which do not result in a state. However, we can overcome this bottleneck by looking more closely at the small singular values. We will see that small singular values correspond to states of a system with slightly different size scatterers.

First, we recall that the renormalized scattering strength of a ZRI in a periodic rectangle is independent of position and thus the scattering strengths of all the scatterers are the same, just as they were in free-space. This means that the denominator of the multiple scattering t-matrix, $1 - S(E)\bar{\mathbf{G}}_B$, is symmetric since $S(E)$, the real scalar renormalized scattering strength, is the same for all scatterers.

If there is an eigenstate at energy E, there exists some vector, $\mathbf{w}$, such that

$$\left(1 - S(E)\bar{\mathbf{G}}_B\right)\mathbf{w} = 0. \tag{9.10}$$

If we have no zero eigenvalue but instead a small one, $\epsilon \ll 1$, then there exists

vector $\mathbf{w}$ such that

$$(\mathbf{1} - S(E)\bar{\mathbf{G}}_B)\mathbf{w} = \epsilon\mathbf{w}, \tag{9.11}$$

which implies

$$\bar{\mathbf{G}}_B\mathbf{w} = \frac{1-\epsilon}{S(E)}\mathbf{w}, \tag{9.12}$$

and so

$$\left(1 - \frac{S(E)}{1-\epsilon}\bar{\mathbf{G}}_B\right)\mathbf{w} = 0. \tag{9.13}$$

Thus there exists a nearby $\tilde{S}(E) = S(E)/(1-\epsilon)$ such that we do have an eigenstate at E. Since $S(E)$ parameterizes the renormalized scatterer strength, $\tilde{S}(E)$ corresponds to a nearby scatterer strength. Thus, in order to include states corresponding to small eigenvalues α we must choose an initial scattering strength such that $S(E)/(1-\alpha)$ is still a possible scattering strength.

As discussed in section C.3, for a symmetric matrix, the singular values are, up to a sign, the eigenvalues. Thus we may use the columns of $\mathbf{V}$ corresponding to small singular values to compute eigenstates.

This provides a huge gain in efficiency. We pick a particular energy, choose a realization of the potential, find the SVD of the t-matrix and then compute a state from every vector corresponding to a small singular value. Small here means small enough that the resultant scatterer strength is in some specified range. We frequently get more than one state per realization.

With this technique in place, there is little we can do to further optimize each use of the SVD. The other bottleneck in state production is the computation of the background Green function. Each Green function requires performing a large sum of trigonometric and hyperbolic trigonometric functions. Thus for moderate size systems (e.g., 500 scatterers), filling the inverse multiple scattering matrix takes far longer than inverting it. Green function computation time is also a bottleneck when computing the wavefunction from the multiple scattering t-matrix.

We could try to improve the convergence of the sums and thus require fewer terms per Green function. That would bring a marginal improvement in performance. Of course, when function computation time is a bottleneck a frequent approach is to tabulate function values and then use lookups into the table to get function values later. A naive application of this is of no use here since our scatterers move in every realization and thus tabulated Green functions for one realization are useless for the next. There is a simple way to get

the advantages of tabulated functions and changing realizations. Instead of tabulating the Green functions for one realization of scatterers, we tabulate them for a larger number of scatterers and then choose realizations from the large number of precomputed locations. For example, if we need 500 scatterers per realization, we pre-compute the Green functions for 1000 scatterers and choose 500 of them at a time for each realization.

In order to check that this doesn't lead to any significant probability of getting physically similar ensembles, we sketch here an argument from [4]. Consider a random potential of size L with mean free path ℓ. A particle diffusing through this system typically undergoes L^2/ℓ^2 collisions. The probability that a *particular* scatterer is involved in one of these collisions is roughly this number divided by the total number of scatterers, nL^d, where n is the concentration and d is the dimension of the system. Thus a shift of one scatterer can, e.g., shift an energy level by about a level spacing when

$$\frac{\delta E}{\Delta} = \left(\frac{L}{\ell}\right)^2 \frac{1}{nL^d} = \frac{1}{n\ell^2 L^{d-2}}, \tag{9.14}$$

is of order one. That is, we must move $n\ell^2 L^{d-2}$ scatterers. In particular, in two dimensions we must move $n_o = n\ell^2$ scatterers to completely change a level.

There are $\begin{pmatrix} M \\ N \end{pmatrix}$ ways to choose N scatterers from M possible locations and $\begin{pmatrix} M \\ N \end{pmatrix}^2$ ways to independently choose two sets. Of those pairs of sets

$$\begin{pmatrix} M \\ N - n_o \end{pmatrix} \begin{pmatrix} M - N + n_o \\ n_o \end{pmatrix}^2, \tag{9.15}$$

have $N - n_o$ or more scatterers in common. The first factor is the number of ways to choose the common $N - n_o$ scatterers and the second is the number of ways to choose the rest independently. Thus the probability, p_2, that two independently chosen sets of scatterers have $N - n_o$ or more in common is

$$p_2 = \frac{\begin{pmatrix} M \\ N - n_o \end{pmatrix} \begin{pmatrix} M - N + n_o \\ n_o \end{pmatrix}^2}{\begin{pmatrix} M \\ N \end{pmatrix}^2}. \tag{9.16}$$

We will be looking at thousands or millions of realizations. The probability that no pair among R realizations shares as many as n_o scatterers is

$$p_R = 1 - (1 - p_2)^{R(R-1)}. \tag{9.17}$$

For large M and N, this probability is extremely small. For example, the fewest scatterers we use will be 500 which we'll choose from 1000 possible locations. Our simulations are in a 1×1 square and the mean free path is .08 implying that $n_o < 4$. The chance that all but 4 scatterers are common between any of one million realizations 500 scatterers chosen from a pool of 1000 is less than 10^{-268}. Thus we need not really concern ourselves with the possibility of oversampling a particular configuration of the disorder potential.

The combination of getting one or more states from nearly very realization and pre-computing the Green functions, leads to an improvement of more than three orders of magnitude over the method used for the smaller systems of 9.2. This allows us to consider systems with more scatterers and thus get closer to the limit $\lambda \ll \ell \ll L_o$.

With this improvement we can proceed to look at the distribution of scatterer intensities for various values of ℓ and λ in a $L_o = 1$ square.

9.3.2 Observed Intensity Statistics

In figure 9.4 we plot the numerically observed $P(t)$ for various λ with $\ell = .081$ in a 1×1 square ($L_o = 1$). It is clear that large values of $|\psi|^2$ are more likely at larger λ/ℓ.

In order to compare these distributions with theoretical calculations we must fit them to various functional forms. Since we are counting independent events, the expected distribution of events in each bin is Poisson. This needs to be taken into account when fitting the numerically computed $P(t)$ to various analytic forms.

While there may be many forms of $P(t)$ which the data could fit, among the various ones motivated by existing theory only some product of log-normal and power-law fit reasonably well. That is, we will fit $P(t)$ to

$$e^{-C_o - C_1 \ln t - C_2 \ln^2 t}, \tag{9.18}$$

where C_o is just a normalization constant, C_1 is the power in the power-law and C_2 is the log-normal coefficient. We note that the expectation is that log-normal behavior will occur in the *tail* of the distribution. In order to account for this we fit each numerically computed

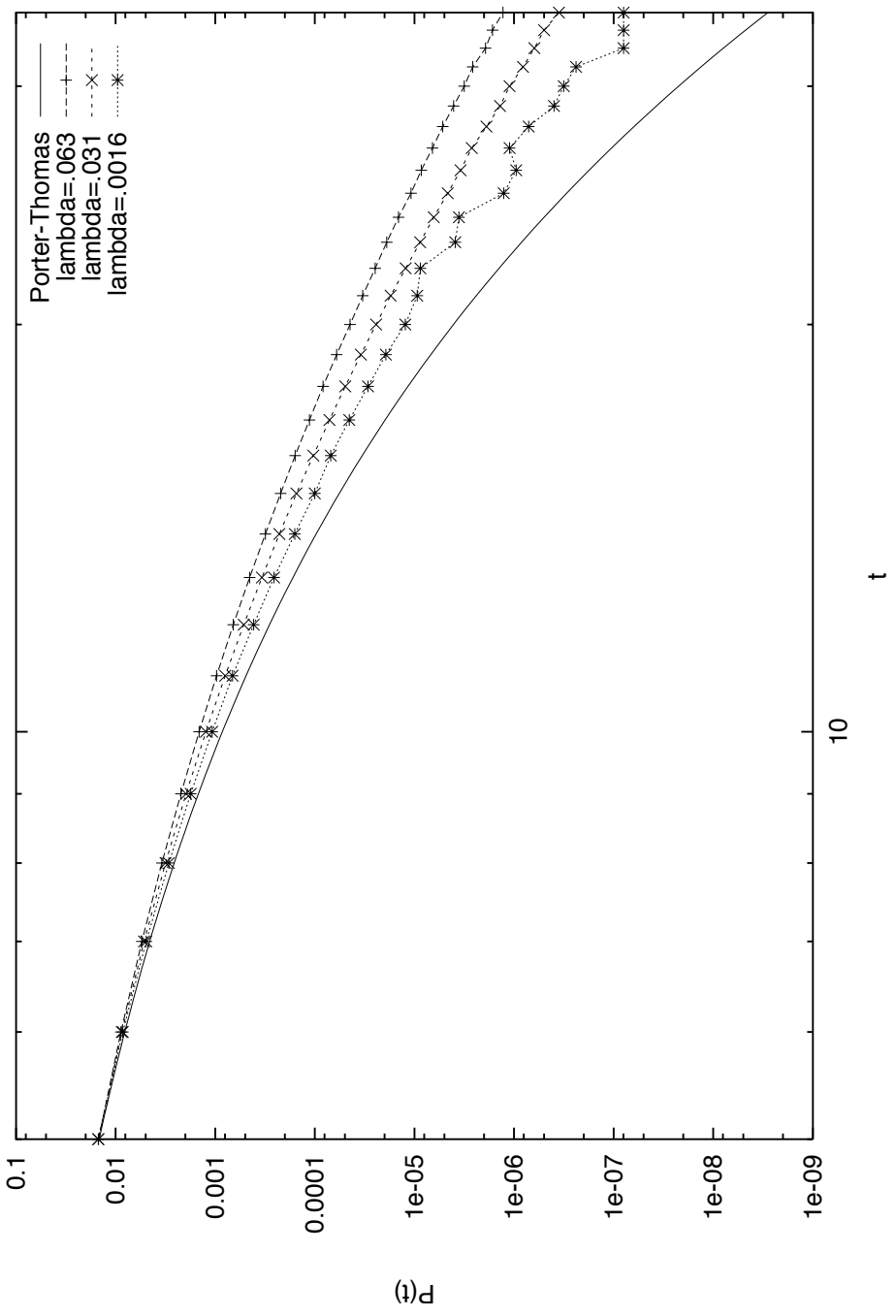

Figure 9.4: Intensity statistics gathered in various parts of a Periodic square (torus). Larger fluctuations are more likely for larger λ/ℓ. The erratic nature of the smallest wavelength data is due to poor statistics.

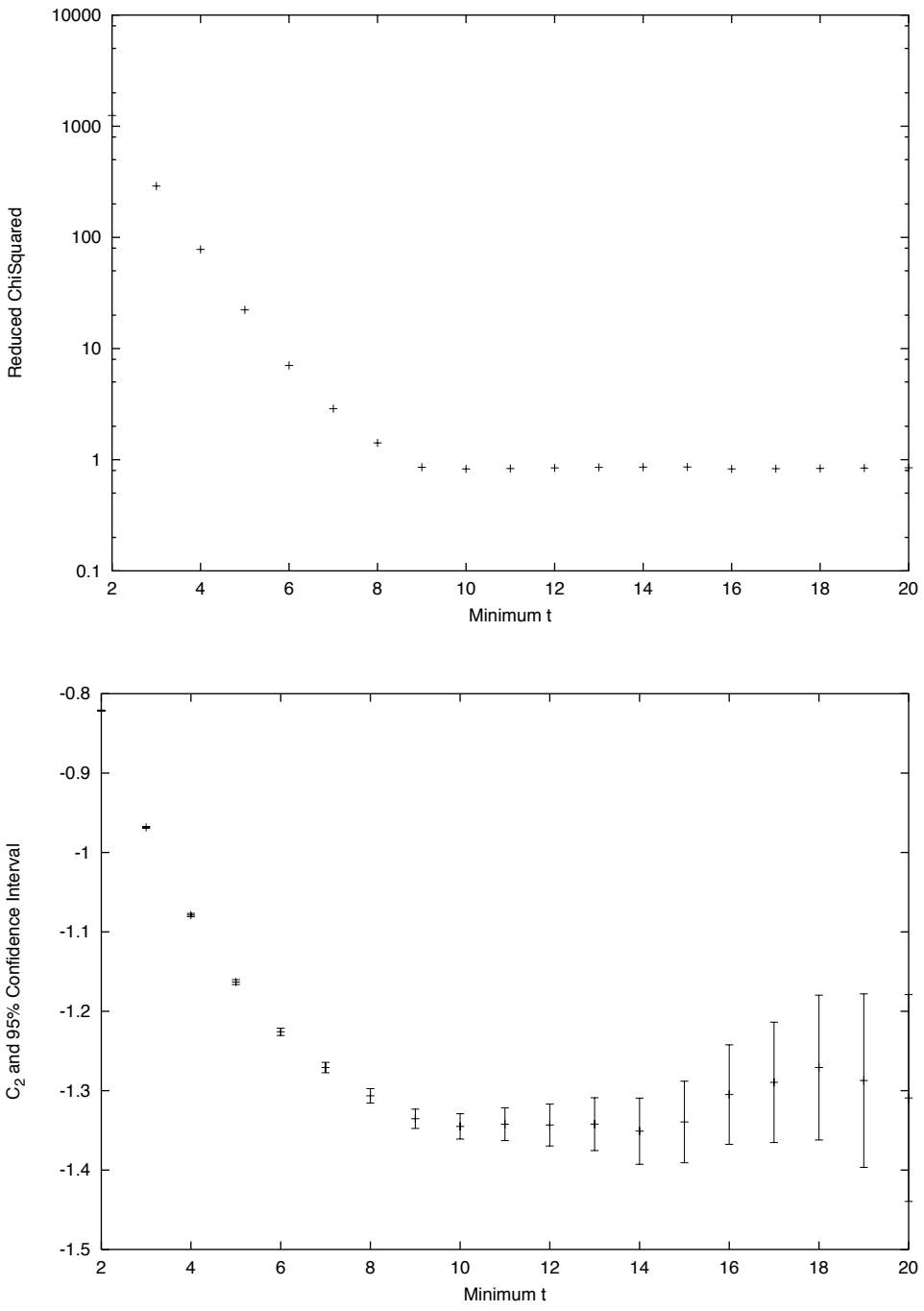

Figure 9.5: Illustrations of the fitting procedure. We look at the reduced χ^2 as a function of the starting value of t in the fit (top, notice the log-scale on the y-axis) then choose the C_2 with smallest confidence interval (bottom) and stable reduced χ^2. In this case we would choose the C_2 from the fit starting at $t = 10$.

$P(t)$ beginning at various values of t. We then look at the reduced χ^2, $\bar{\chi}^2 = (\chi^2 - D)/N_d$ (where there are D fitting parameters and N_d data points) for each fit. A plot of a typical sequence of $\bar{\chi}^2$ values is plotted in figure 9.5 (top). Once $\bar{\chi}^2$ settles down to a near constant value, we choose the fit with the smallest confidence interval for the fitted C_2. A typical sequence of C_2's and confidence intervals for one fit is plotted in figure 9.5 (bottom). The behavior of $\bar{\chi}^2$ is consistent with the assumption that $P(t)$ does not have the form (9.18) until we reach the tail of the distribution.

As discussed in section 7.7 there are two field theoretic computations which give two different forms for C_2:

$$C_2^{(1)} = \frac{\pi k \ell}{4 \ln(F_1 k L_o)}, \tag{9.19}$$

and

$$C_2^{(2)} = \frac{\beta \pi k \ell}{4 \ln(F_2 L_o / \ell)}. \tag{9.20}$$

We can attempt to fit our observed C_2's to these two forms. We find that neither form works very well at all. In figure 9.6 we compare these fits to the observed values of C_2 as we vary k at fixed $\ell = .081$ (top) and vary ℓ at fixed $k = 200$ ($\lambda = .031$).

Thus, while the numerically computed intensity statistics are well fitted by a log-normal distribution as predicted by theory, the coefficients of the log-normal do not seem to be explained by existing theory.

9.3.3 Anomalous Wavefunctions

It is interesting to look at the anomalous wavefunctions themselves. In figures 9.7 we plot two typical wavefunctions and in 9.8 we plot two anomalously peaked wavefunctions. For each we show a contour plot of ψ and a density plot of $|\psi|^2$. The scale is different on each wavefunction so that each is shown with maximum visual dynamic range. This necessarily obscures the fact that the typical wavefunction have a maximum $|\psi^2|$ of 20 as opposed to 40 or 60 for the anomalous states.

It is difficult to determine much information from the entire wavefunction. In order to simplify things a bit we look at the average scaled intensity at various distances from the peak, $\mathbf{r}_o$, via

$$R(r) = \frac{1}{|\psi(\mathbf{r}_o)|^2} \frac{1}{r} \int_0^{2\pi} |\psi\left(\mathbf{r}_o + r[\hat{x}\cos\theta + \hat{y}\sin\theta]\right)|^2 \, d\theta. \tag{9.21}$$

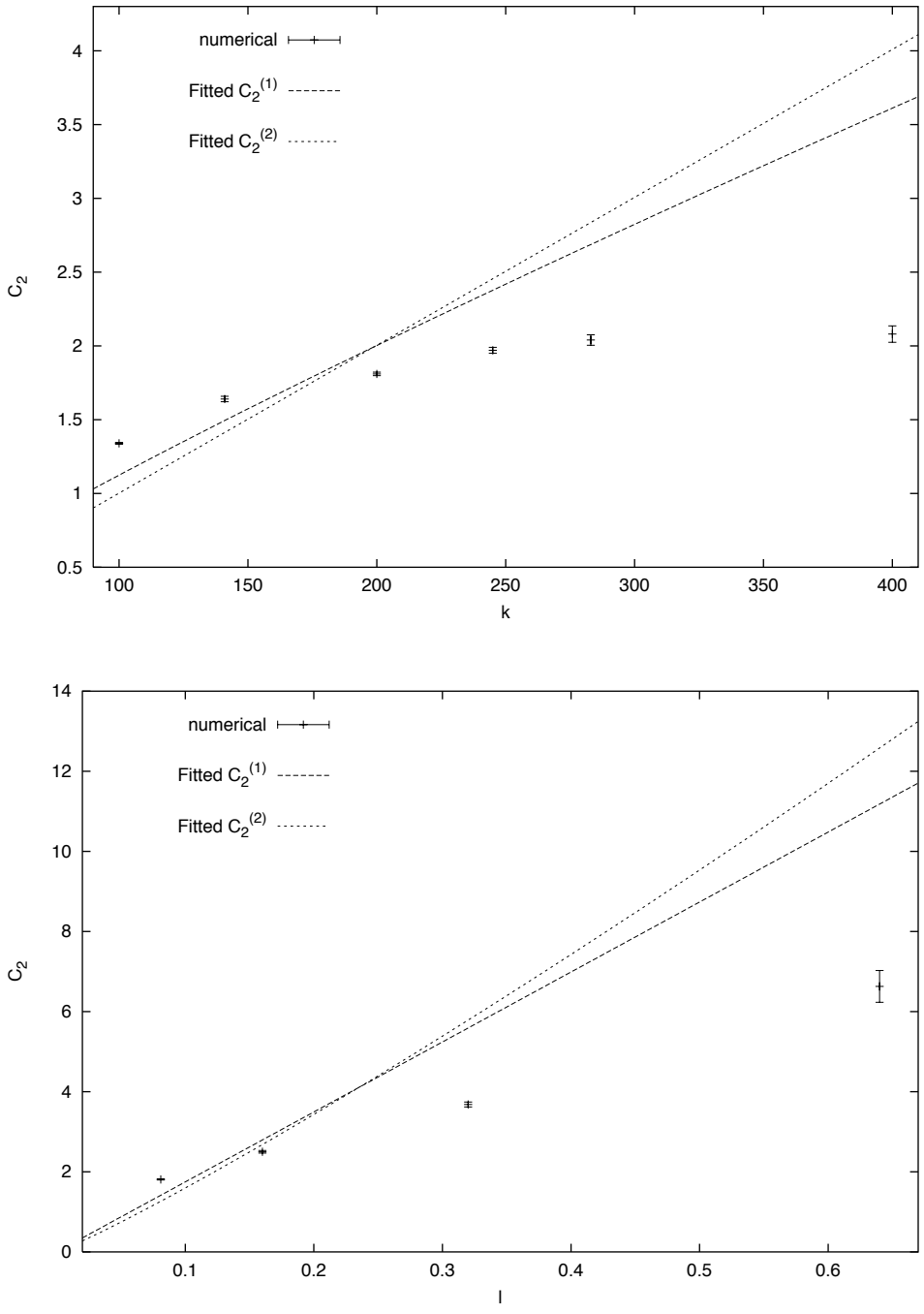

Figure 9.6: Numerically observed log-normal coefficients (fitted from numerical data) and fitted theoretical expectations plotted (top) as a function of wavenumber, k at fixed $\ell = .081$ and (bottom) as function of ℓ at fixed $k = 200$.

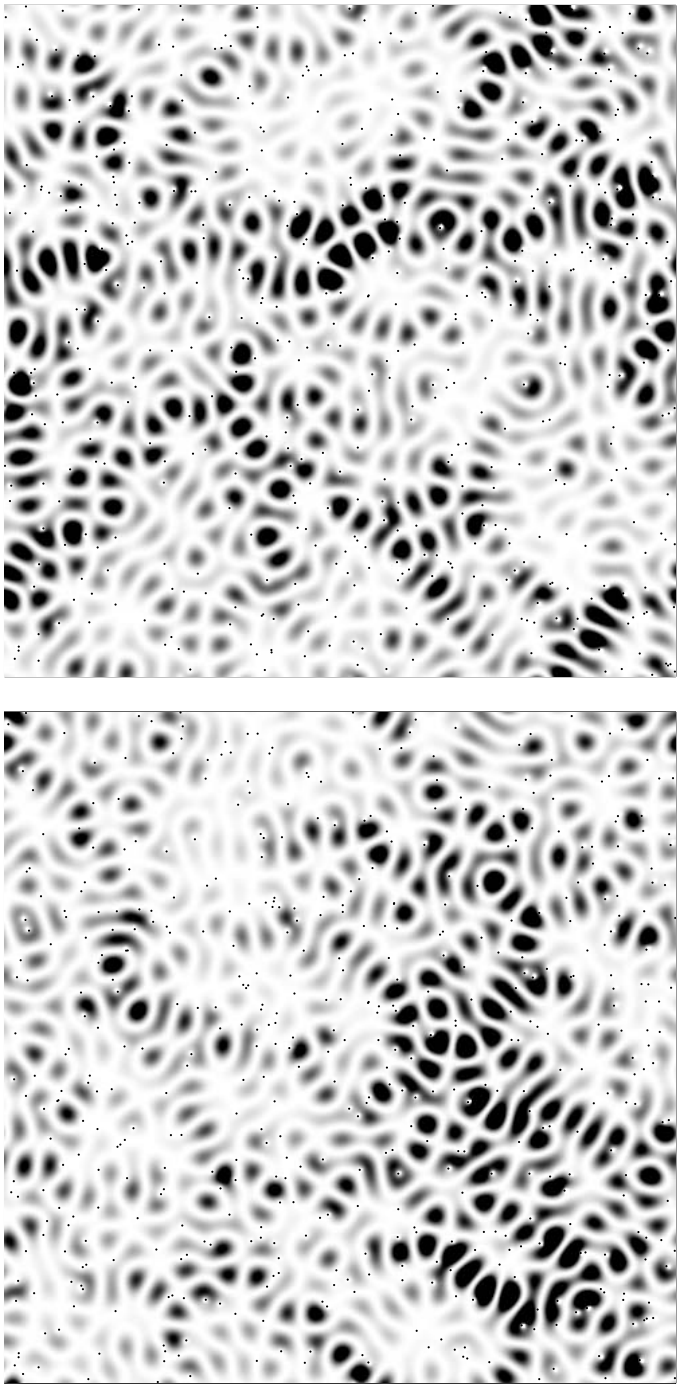

Figure 9.7: Typical wavefunctions ($|\psi|^2$ is plotted) for 500 scatterers in a 1×1 periodic square (torus) with $\ell = .081$, $\lambda = .061$. The density of $|\psi|^2$ is shown.

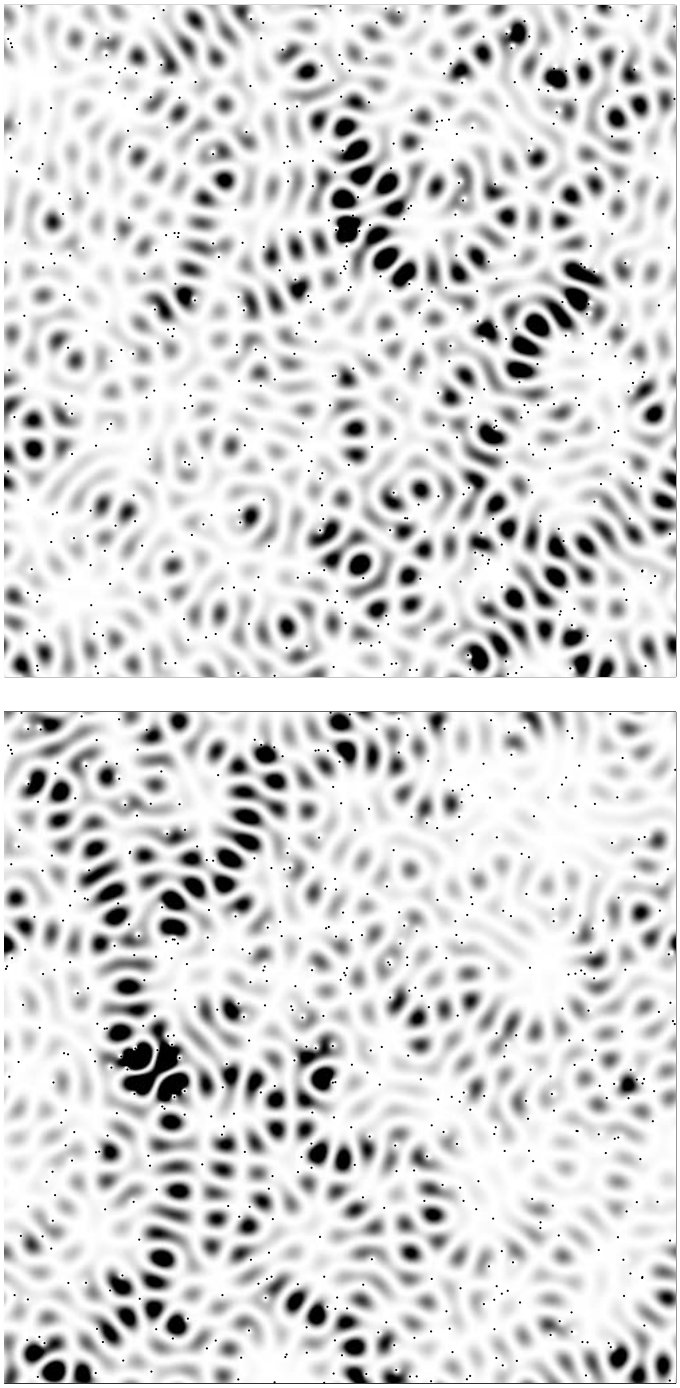

Figure 9.8: Anomalous wavefunctions ($|\psi|^2$ is plotted) for 500 scatterers in a 1×1 periodic square (torus) with $\ell = .081$, $\lambda = .061$. The density of $|\psi|^2$ is shown. We note that the scale here is different from the typical states plotted previously.

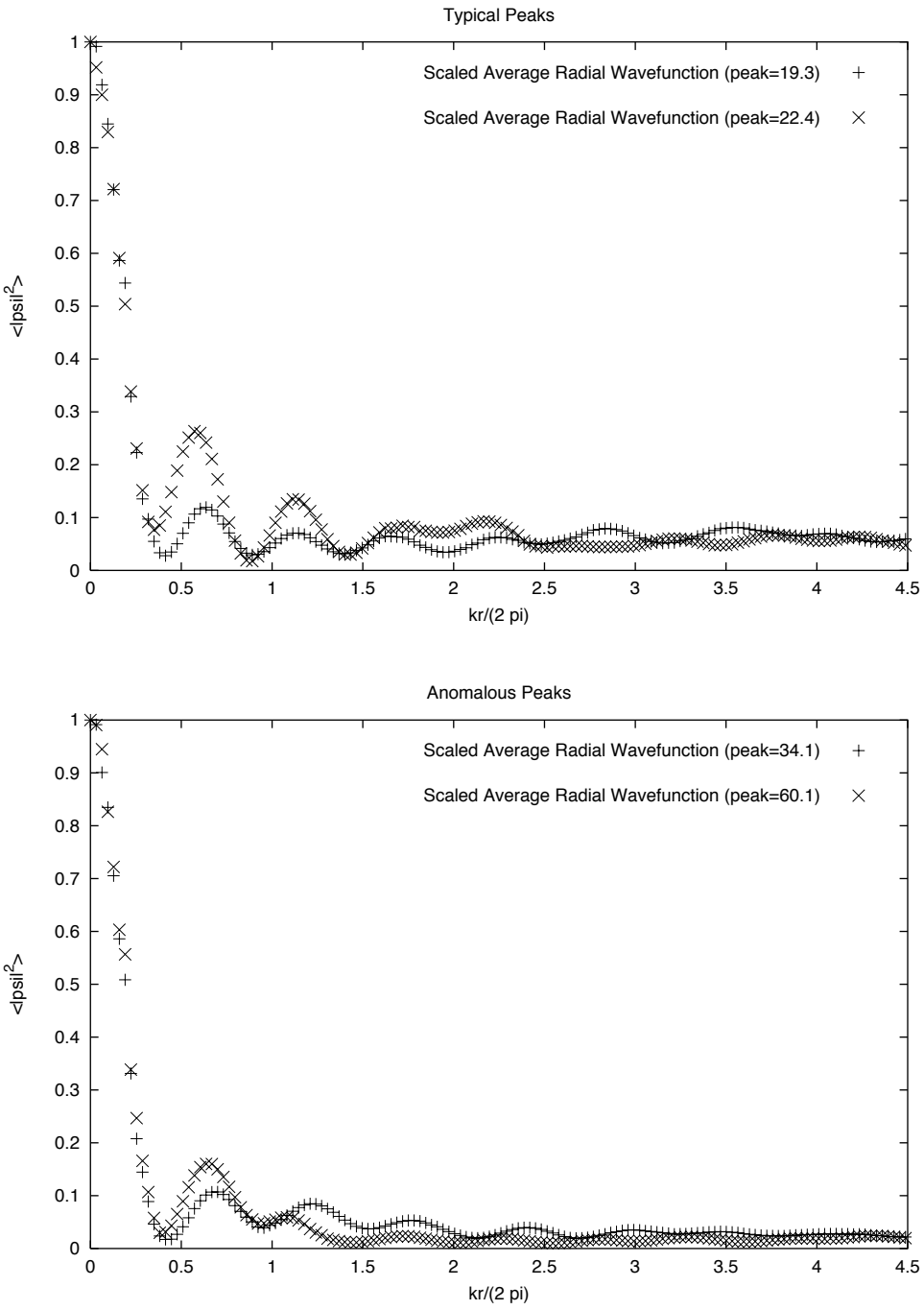

Figure 9.9: The average radial intensity centered on two typical peaks (top) and two anomalous peaks (bottom).

In figure 9.9 we plot $R(r)$ for two typical peaks (one from each wavefunction in figure 9.7) and the two anomalous peaks from the wavefunctions in figure 9.8. Here we see that each set of peaks have a very similar behavior in their average decay and oscillation. The anomalous peaks have a more quickly decaying envelope as they must to reach the same Gaussian random background value. This is predicted in [39], although we have not yet confirmed the quantitative prediction of those authors. Again we note

9.3.4 Numerical Stability

Throughout this work we have checked the accuracy and stability of our numerics in several ways. In chapter 5 we checked that the numerical procedure we use gives the correct classical limit cross-section for one scatterer. In chapter 8 we checked that for an appropriate choice of parameters, many scatterers in a wire give the classically expected mean free path.

In chapter 6, we checked that the analytic structure of renormalized t-matrices correctly predicts ground state energies in Dirichlet bounded squares. However, we do not have a direct way to check higher energy eigenenergies or eigenstates. Thus we do the next best thing and check the stability of the numerical procedure which produces them. That is, we check that small perturbations of the input to the method (scatterer locations, scatterer strengths, Green functions, etc.) do not result in large changes to the computed wavefunction.

As a simple perturbation we will consider random changes in scatterer location. We consider one realization of the scattering potential, compute the wavefunction, ψ, and then proceed to move the scatterers each by some small amount in a random direction. We then compute the new wavefunction, $\tilde{\psi}$, and compare the two wavefunctions. We repeat this for ever larger perturbations of the scatterers until we have completely de-correlated the wavefunctions. We consider two measures for comparison. We define $\delta\psi(\mathbf{r}) = \psi(\mathbf{r}) - \tilde{\psi}(\mathbf{r})$ and we consider both

$$\sqrt{\mathcal{V}\,\langle|\delta\psi(\mathbf{r})|^2\rangle}, \tag{9.22}$$

where we average over $\mathbf{r}$ and

$$\sqrt{\frac{\max\{(\delta\psi)^2\}}{\max\{|\psi|^2\}}}. \tag{9.23}$$

The former is a standard measure of the difference of functions and the latter we expect to be more sensitive to changes in anomalously large peaks.

In order to see if a small perturbation in scatterer locations produces a small change in the wavefunction, we need an appropriate scale for the scatterer perturbation. If Random Matrix Theory applies, we know that a single state can be shifted by one level (and thus completely de-correlated) by moving one scatterer with cross-section approximately the wavelength by one wavelength. From that argument and that the fact that the motion of each scatterer is uncorrelated with the motion of the others, we can see that the appropriate parameter is approximately

$$\epsilon = \sqrt{N}\frac{\delta x}{\lambda}, \tag{9.24}$$

where δx is average distance moved by a single scatterer. That is, if the error in the wavefunction is comparable to ϵ we can assume it comes from physical changes in the wavefunction not numerical error.

In figure 9.10 we plot our two measures of wavefunction deviation against ϵ (on a log-log scale) for several ϵ between 3.6×10^{-7} and 3 for a state with an anomalously large peak. Since our deviations are no larger then expected from Random Matrix Theory, we can assume that the numerical stability is sufficiently high for our purposes.

Though not exactly a source of numerical error, we might worry that including states that result from small but non-zero singular values has an influence on the statistics. If this were the case, we would need to carefully choose our singular value cutoff in order to match the field theory. However, the influence on the statistics is minimal as summarized in table 9.1.

	Maximum Singular Value	.1	.01
C_1		$-2.05 \pm .03$	$-2.2 \pm .1$
C_2		$1.335 \pm .006$	$1.38 \pm .03$

Table 9.1: Comparison of log-normal tails of $P(t)$ for different maximum allowed singular value.

9.3.5 Conclusions

In contrast to the well understood phenomena observed in disordered wires, we have observed some rather more surprising things in disordered squares. While the various theoretical computations of the expected intensity distribution appear to correctly predict the shape of the tail of the distribution, none of them seem to correctly predict the dependence of that shape on wavelength or mean free path.

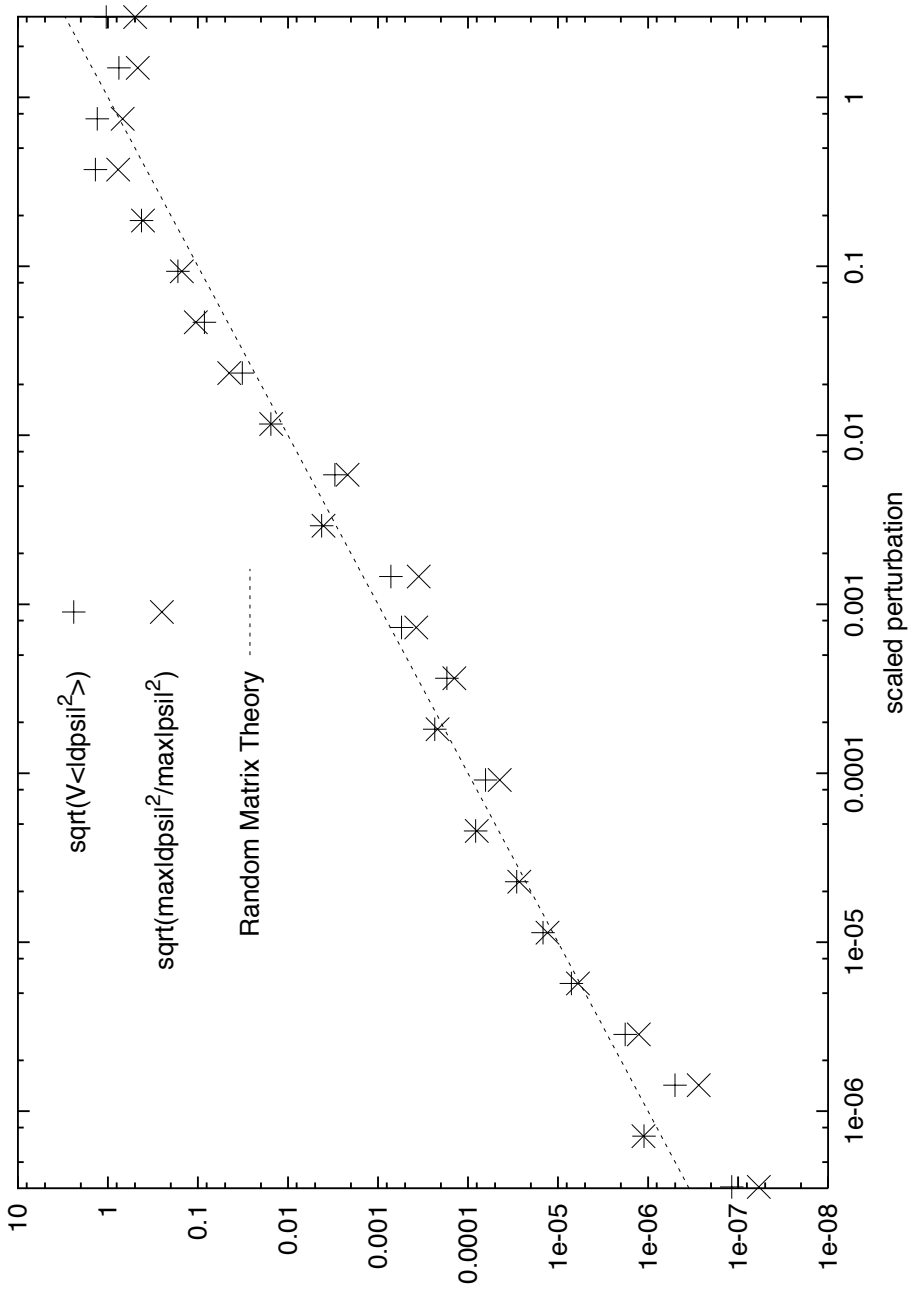

Figure 9.10: Wavefunction deviation under small perturbation for 500 scatterers in a 1×1 periodic square (torus). $\ell = .081$, $\lambda = .061$.

We have considered a variety of explanations for the discrepancies between the field theory and our numerical observations. There is one way in which our potential differs drastically from the potential which the field theory assumes. We have a finite number of discrete scatterers whereas the field theory takes the concentration to infinity while taking the scatterer strength to zero while holding the mean free path constant. Thus it seems possible that there are processes which can cause large fluctuations in $|\psi|^2$ which depend on there being finite size scatterers. In order to explore this possibility we consider the dependence of $P(t)$ on the scatterer strength at constant wavelength and mean free path. Specifically, at two different wavelengths ($\lambda = .06$ and $\lambda = .03$) and fixed $\ell = .08$ we double the concentration and halve the cross-section of the scatterers. The results are summarized in table 9.2. While changes in concentration and scatterer strength do influence the coefficients of the distribution, they do not do so enough to explain the discrepancy with the field theory.

		Strong Scatterers	Weak Scatterers
$\lambda = .061$			
	C_1	$-2.05 \pm .03$	$-1.96 \pm .09$
	C_2	$1.335 \pm .006$	$1.27 \pm .01$
$\lambda = .031$			
	C_1	$-4.1 \pm .1$	$-4.1 \pm .34$
	C_2	$1.84 \pm .02$	$1.83 \pm .066$

Table 9.2: Comparison of log-normal tails of $P(t)$ for strong and weak scatterers at fixed λ and ℓ.

9.4 Algorithms

We have used several different algorithms in different parts of this chapter. We have gathered spectral information about particular realizations of scatterers, gathered statistics in small systems where we only used realizations with a state in a particular energy window, gathered statistics from nearly every realization by allowing the scatterer size to change and computed wavefunctions for particular realizations and energies. Below, we sketch the algorithms used to perform these various tasks.

We will frequently use the smallest singular value of a particular realization at a particular energy which we denote $S_N^{(i)}(E)$ where i labels the realization. When only one realization is involved, the i will be suppressed. To compute $S_N^{(i)}(E)$ we do the following:

1. Compute the renormalized t-matrix of each scatterer.
2. Compute the scatterer-scatterer Green functions for all pairs of scatterers.
3. Construct the inverse multiple scattering matrix, T^{-1}.
4. Find the singular value decomposition of T^{-1} and assign $S_N^{(i)}(E)$ the smallest singular value.

In order to find spectra from E_i to E_f for a particular realization of scatterers

1. Load the scatterer locations and sizes.
2. choose a δE less than the average level spacing.
3. Set $E = E_i$
   (a) If $E < E_f$ find $S_N(E)$, $S_N(E + \delta E)$ and $S_N(E + 2\delta E)$, otherwise end.
   (b) If the smallest singular value at $E + \delta E$ is not smaller than for E and $E = 2\delta E$, increase E by δE and repeat from (a).
   (c) Otherwise, apply a minimization algorithm to $S_N(E)$ in the region near $E + \delta E$. Typically, minimization algorithms will begin from a triplet as we have calculated above.
   (d) If the minimum is not near zero, increment E and repeat from (a).
   (e) If the minimum coincides with an energy where the renormalized t-matrices are extremely small, it is probably a spurious zero brought on by a state of the empty background. Increment E and repeat from (a).
   (f) The energy E_o at which the minimum was found is an eigenenergy. Save it, increment E by δE and repeat from (a).

The bottleneck in this computation is the filling of the inverse multiple scattering matrix and computation of the $\mathcal{O}(N^3)$ SVD. Performance can be improved by a clever choice of δE but too large a δE can lead to states being missed altogether. The optimal δE can only be chosen by experience or by understanding the width of the minima in $S_m(E)$. The origin of the width of these minima is not clear.

The simpler method for computing intensity statistics by looking for states in an energy window of size $2\delta E$ about an energy E goes as follows:

1. Choose a realization of scatterer locations.

2. Use the method above to check if there is an eigenstate in the desired energy window about E. If not, choose a new realization and repeat.

3. If there is an eigenstate, use the singular vector corresponding to the small singular value to compute the eigenstate. Make a histogram of the values of $|\psi|^2$ sampled on a grid in position space with spacing approximately one half-wavelength in each direction.

4. Combine this histogram with previously collected data and repeat with a new realization.

The bottlenecks in this computation are the same as the previous computation. In this case, a clever choice of window size can improve performance.

The more complex method for computing intensity statistics by looking only at energy E is a bit different:

1. Randomly choose a number of locations (approximately twice the number of scatterers).

2. Compute and store all renormalized t-matrices and the Green functions from each scatterer to each other scatterer.

3. Choose a grid on which to compute the wavefunction.

4. Compute and store the Green function from each scatterer to each location on the wavefunction grid.

5. Choose a subset of the precomputed locations, construct the inverse multiple scattering matrix, T^{-1} and find the SVD of T^{-1}.

6. For each singular value smaller than some cutoff (we've tried both .1 and .01), compute the associated eigenstate on the grid, count the values of $|\psi|^2$ and combine with previous data. Choose a new subset and repeat.

For this computation the bottlenecks are somewhat different. The $\mathcal{O}(N^3)$ SVD is one bottleneck as is computation of individual wavefunctions which is $\mathcal{O}(SN^2)$ where S is the number of points on the wavefunction grid.

For all of these methods, near singular matrices are either sought, frequently encountered or both. This requires a numerical decomposition which is stable in the presence of small eigenvalues. The SVD is an ideal choice. The SVD is usually computed via transformation to a symmetric form and then a symmetric eigendecomposition. Since the matrix we are decomposing can be chosen to be symmetric, we could use the symmetric eigendecomposition directly. We imagine some marginal improvement might result by the substitution of such a decomposition for the SVD.

Chapter 10

Conclusions

Scattering theory can be applied to some unusual problems and in some unexpected ways. Several ideas of this sort have been developed and applied in this work. All the methods developed here are related to the fundamental idea of scattering theory, namely the separation between propagation and collision. The applications range from the disarmingly simple single scatterer in a wire to the obviously complex problem of intensity statistics in weakly disordered two dimensional systems.

These ideas allow calculation of some quantities which are difficult to compute other ways, for example the scattering strength of a scatterer in a narrow two dimensional wire as discussed in section 5.6. It also allows simpler calculation of some quantities which have been computed other ways, e.g., the eigen-states of one zero range interaction in a rectangle, also known as the "Šeba billiard."

The methods developed here also lead to vast numerical improvements in calculations which are possible but difficult other ways, for example the calculation of intensity statistics in closed weakly disordered two dimensional systems as demonstrated in section 9.3.

The results of these intensity statistics calculations are themselves quite interesting. They appear to contradict previous theoretical predictions about the likelihood of large fluctuations in the wavefunctions in such systems. At the same time some qualitative features of these theoretical predictions have been verified for the first time.

There are a variety of foreseeable applications of these techniques. One of the most exciting, is the possible application to superconductor normal-metal junctions. For instance, a disordered normal metal region with a superconducting wall will have different

dynamics because of the Andre'ev reflection from the superconductor. The superconductor energy gap can be used to probe various features of the dynamics in the normal metal. Also, the field of quantum chaos has, so far, been focused on systems with an obvious chaotic classical limit. Systems with purely quantum features very likely have different and interesting behavior. A particle-hole system like the superconductor is only one such example.

A different sort of application is to renormalized scattering in atomic traps. The zero range interaction is a frequently used model for atom-atom interactions in such traps. The trap itself renormalizes the scattering strengths as does the presence of other scatterers. Some of this can be handled, at least in an average sense, with the techniques developed here.

We would also like to extend some of the successes with point scatterers to other shapes. There is an obvious simplicity to the zero range interaction which will not be shared with any extended shape. However, other shapes, e.g., finite length line segments, have simple scattering properties which can be combined in much the way we have combined single scatterers in this work.

Bibliography

[1] M. Abramowitz and I.A. Stegun, editors. *Handbook of Mathematical Functions*. Dover, London, 1965.

[2] S. Albeverio, F. Geszetsky, R. Høegh-Krohn, and H. Holden. *Solvable models in quantum mechanics*. Springer-Verlag, Berlin, 1988.

[3] S. Albeverio and P. Šeba. Wave chaos in quantum systems with point interaction. *J. Stat. Phys.*, 64(1/2):369–83, 1991.

[4] Boris L. Altshuler and B.D. Simons. Universalities: From anderson localization to quantum chaos. In E. Akkermans, G. Montambaux, J.-L. Pichard, and J. Zinn-Justin, editors, *Les Houches 1994: Mesoscopic Quantum Physics (LXI)*, Les Houches, pages 1–98, Sara Burgerhartstraat 25, P.O. Box 211, 1000 AE Amsterdam, The Netherlands, 1994. Elsevier Science B.V.

[5] G.E. Blonder, M. Tinkham, and T.M. Klapwijk. Transition from metallic to tunneling regimes in superconducting microconstrictions: Excess current, charge imbalance, and supercurrent conversion. *Phys. Rev. B*, 25(7):4515–32, April 1982.

[6] M. Born. Zur quantenmechanik der stossvorgänge. *Zeitschrift für Physik*, 37:863–67, 1926. Translated into English by Wheeler, J.A. and Zurek W.H. (1981) and reprinted in *Quantum Theory and Measurement*, Wheeler, J.A. and Zurek W.H. eds., Princeton Univeristy Press (1983).

[7] A. Cabo, J. L. Lucio, and H. Mercado. On scale invariance and anomalies in quantum mechanics. *ajp*, 66(6):240–6, March 1998.

[8] S. Datta. *Electronic Transport in Mesoscopic Systems*. Number 3 in Cambridge Stud-

ies in Semiconductor Physics and Microelectronic Engineering. Cambridge University Press, The Pitt Building, Trumpington Street, Cambridge CB2 1RP, 1995.

[9] S. Doniach and E.H. Sondheimer. *Green's Functions for Solid State Physicists*. Number 44 in Frontiers in Physics Lecture Note Series. The Benjamin/Cummings Publishing Company, Inc., 1982.

[10] E.N. Economou. *Green's Functions in Quantum Physics*. Number 7 in Solid-State Sciences. Springer-Verlag, 175 Fifth Ave., New York, NY 10010, USA, 2nd edition, 1992.

[11] J.D. Edwards, Lupu-Sax A.S., and Heller E.J. Imaging the single electron wavefunction in mesoscopic structures. *To Be Published*, 1998.

[12] F. Evers, D. Belitz, and Wansoo Park. Density expansion for transport coefficients: Long-wavelength versus fermi surface nonanalyticities. *prl*, 78(14):2768–2771, April 1997.

[13] P. Exner and P. Šeba. Point interactions in two and three dimensions as models of small scatterers. *Phys. Rev. A*, 222:1–4, October 1996.

[14] Haake F. *Quantum Signatures of Chaos*, volume 54 of *Springer Series in Synergetics*. Springer-Verlag, SV-addr, 1992.

[15] V.I. Fal'ko and K.B. Efetov. Statistics of prelocalized states in disordered conductors. *Physical Review B*, 52(24):17413–29, December 1995.

[16] Daniel S. Fisher and Patrick A. Lee. Relation between conductivity and transmission matrix. *Phys. Rev. B*, 23(12):6851–4, June 1981.

[17] Gene H. Golub and Charles F. Van Loan. *Matrix Computations*. Johns Hopkins University Press, 2715 North Charles Street, Baltimore, MD 21218-4319, 3 edition, 1996.

[18] I.S. Gradshteyn and I.M. Ryzhik. *Table of Integrals, Series, and Products*. Academic Press, Inc., 1250 Sixth Avenue, San Diego, CA 92101-4311, 5th edition, 1994.

[19] C. Grosche. Path integration via summation of perturbation expansions and applications to totally reflecting boundaries, and potential steps. *Phys. Rev. Lett.*, 71(1), 1993.

[20] E.J. Heller. Bound-state eigenfunctions of classically chaotic hamiltonian systems: scars of periodic orbits. *Phys. Rev. Lett.*, 55:1515–8, 1984.

[21] E.J. Heller, M.F. Crommie, C.P. Lutz, and D.M. Eigler. Scattering and absorption of surface electron waves in quantum corrals. *Nature*, 369:464, 1994.

[22] K. Huang. *Statistical Mechanics.* Wiley, New York, 1987.

[23] J.A. Katine, M.A. Eriksson, A.S. Adourian, R.M. Westervelt, J.D. Edwards, A.S. Lupu-Sax, E.J. Heller, K.L. Campman, and A.C. Gossard. Point contact conductance of an open resonator. *prl*, 79(24):4806–9, December 1997.

[24] A. Kudrolli, V. Kidambi, and S. Sridhar. Experimental studies of chaos and localization in quantum wave functions. *Phys. Rev. Lett.*, 75(5):822–5, July 1995.

[25] L.D. Landau and Lifshitz E.M. *Mechanics.* Pergamon Press, Pergamon Press Inc., Maxwell House, Fairview Park, Elmsford, NY 10523, 3rd edition, 1976.

[26] L.D. Landau and Lifshitz E.M. *Quantum Mechanics.* Pergamon Press, Pergamon Press Inc., Maxwell House, Fairview Park, Elmsford, NY 10523, 3rd edition, 1977.

[27] C. Livermore. *Coulomb Blocakade Spectroscopy of Tunnel-Coupled Quantum Dots.* PhD thesis, Harvard University, May 1998.

[28] A Messiah. *Quantum Mechanics*, volume II. John Wiley & Sons, 1963.

[29] A.D. Mirlin. Spatial structure of anomalously localized states in disordered conductors. *J. Math. Phys.*, 38(4):1888–917, April 1997.

[30] K. Müller, B. Mehlig, F. Milde, and M. Schreiber. Statistics of wave functions in disordered and in classically chaotic systems. *prl*, 78(2):215–8, January 1997.

[31] M. Olshanii. Atomic scattering in the presence of an external confinement and a gas of impenetrable bosons. *prl*, 81(5):938–41, August 1998.

[32] R.K Pathria. *Statistical Mechanics*, volume 45 of *International Series in Natural Philosophy*. Pergamon Press, Elsevier Science Inc., 660 White Plains Road, Tarrytown, NY, 10591-5153, 1972.

[33] W.H. Press, S.A. Teukolsky, W.T. Vetterling, and B.P. Flannery. *Numerical recipes in C: The art of scientific computing*. Cambridge University Press, The Pitt Building, Trumplington Street, Cambridge CB2 1RP, 40 West 20th Street, New York, NY 10011-4211, USA, 2nd edition, 1992.

[34] G. Rickayzen. *Green's Functions and Condensed Matter*. Number 5 in Techniques of Physics. Academic Press, Academic Press Inc. (London) Ltd., 24/28 Oval Road, London NW1, 1980.

[35] L.S. Rodberg and R.M. Thaler. *Introduction to the quantum theory of scattering*. Academic Press, Inc., 111 Fifth Avenue, New York, NY 10003, USA, 1st edition, 1970.

[36] J.J. Sakurai. *Modern Quantum Mechanics*. Addison Wesley, 1st edition, 1985.

[37] P. Sheng. *Introduction to Wave Scattering , Localization, and Mesoscopic Phenomena*. Academic Press, Inc., 525 B Street, Suite 1900, San Diego, CA 92101-4495, 1995.

[38] T. Shigehara. Conditions for the appearance of wave chaos in quantum singular systems with a pointlike scatterer. *Phys. Rev. E*, 50(6):4357–70, December 1994.

[39] I.E. Smolyarenko and B.L. Altshuler. Statistics of rare events in disordered conductors. *Phys. Rev. B*, 55(16):10451–10466, April 1997.

[40] Douglas A. Stone and Aaron Szafer. What is measured when you measure a resistance?–the landauer formula revisited. *IBM Journal of Research Development*, 32(3):384–412, May 1988.

[41] D. Zwillinger. *Handbook of Integration*. Jones & Bartlett, One Exeter Plaza, Boston, MA 02116, 1992.

Appendix A

Green Functions

A.1 Definitions

Green functions are solutions to a particular class of inhomogeneous differential equations of the form

$$[z - \mathcal{L}(\mathbf{r})]\, G(\mathbf{r}, \mathbf{r}'; z) = \delta(\mathbf{r} - \mathbf{r}'). \tag{A.1}$$

G is determined by (A.1) *and* boundary conditions for $\mathbf{r}$ and $\mathbf{r}'$ lying on the surface S of the domain Ω. Here z is a complex variable while $\mathcal{L}(\mathbf{r})$ is a differential operator which is time-independent, linear and Hermitian. $\mathcal{L}(\mathbf{r})$ has a complete set of eigenfunctions $\{\psi_n(\mathbf{r})\}$ which satisfy

$$\mathcal{L}(\mathbf{r})\psi_n(\mathbf{r}) = \lambda_n \psi_n(\mathbf{r}). \tag{A.2}$$

Each of the $\psi_n(\mathbf{r})$ satisfy the same boundary conditions as $G(\mathbf{r}, \mathbf{r}'; z)$. The functions $\{\psi_n(\mathbf{r})\}$ are orthonormal,

$$\int_\Omega \psi_n(\mathbf{r})\psi_m^*(\mathbf{r}) = \delta_{nm}, \tag{A.3}$$

and complete,

$$\sum_n \psi_n(\mathbf{r})\psi_n^*(\mathbf{r}') = \delta(\mathbf{r} - \mathbf{r}'). \tag{A.4}$$

In Dirac notation we can write

$$(z - \mathcal{L})\hat{G}(z) = 1 \tag{A.5}$$

$$\hat{\mathcal{L}}\,|\psi_n\rangle = \lambda_n\,|\phi_n\rangle \tag{A.6}$$

$$\langle\psi_n\,|\psi_m\,\rangle = \delta_{nm} \tag{A.7}$$

$$\sum_n |\psi_n\rangle\,\langle\psi_n| = 1. \tag{A.8}$$

In all of the above, sums over n may be integrals in continuous parts of the spectrum.

For $z \neq \lambda_n$ we can formally solve equation A.5 to get

$$\hat{G}(z) = \frac{1}{z - \hat{\mathcal{L}}}. \tag{A.9}$$

Multiplying by A.8 we get

$$\hat{G}(z) = \frac{1}{z - \hat{\mathcal{L}}} \sum_n |\psi_n\rangle \langle\psi_n| = \sum_n \frac{1}{z - \hat{\mathcal{L}}} |\psi_n\rangle \langle\psi_n| = \sum_n \frac{|\psi_n\rangle \langle\psi_n|}{z - \lambda_n}. \tag{A.10}$$

We recover the $\mathbf{r}$-representation by multiplying on the left by $\langle\mathbf{r}|$ and on the right by $|\mathbf{r}'\rangle$

$$G(\mathbf{r}, \mathbf{r}'; z) = \sum_n \frac{\psi_n(\mathbf{r})\psi_n^*(\mathbf{r}')}{z - \lambda_n}. \tag{A.11}$$

In order to find (A.11) we had to assume that $z \neq \lambda_n$. When $z = \lambda_n$ we can write a limiting form for $\hat{G(z)}$:

$$\hat{G}^{\pm}(z) = \frac{1}{z - \hat{\mathcal{L}} \pm i\epsilon}, \tag{A.12}$$

and it's corresponding form in position space,

$$G^{\pm}(\mathbf{r}, \mathbf{r}'; z) = \lim_{\epsilon \to 0} \sum_n \frac{\psi_n(\mathbf{r})\psi_n^*(\mathbf{r}')}{z - \lambda_n \pm i\epsilon}, \tag{A.13}$$

where $\hat{G}^+(z)$ is called the "retarded" or "causal" Green function and $\hat{G}^-(z)$ is called the "advanced" Green function.

These names are reflections of properties of the corresponding time-domain Green functions. Consider the Fourier transform of (A.13) with respect to z:

$$G^{\pm}(\mathbf{r}, \mathbf{r}'; \tau = t - t') = \lim_{\epsilon \to 0} \frac{1}{2\pi} \int_{-\infty}^{\infty} \sum_n \frac{\psi_n(\mathbf{r})\psi_n^*(\mathbf{r}')}{E - \lambda_n \pm i\epsilon} e^{-iEt/\hbar}\, dE. \tag{A.14}$$

We switch the order of the energy sums (integrals) and have

$$G^{\pm}(\mathbf{r}, \mathbf{r}'; \tau) = \frac{1}{2\pi} \lim_{\epsilon \to 0} \sum_n \psi_n(\mathbf{r})\psi_n^*(\mathbf{r}') \int_{-\infty}^{\infty} \frac{}{E - \lambda_n \pm i\epsilon} e^{-iE\tau/\hbar}\, dE. \tag{A.15}$$

We can perform the inner integral with contour integration by closing the contour in either the upper or lower half plane. We are forced to choose the upper or lower half plane by the sign of τ. For $\tau > 0$ we must close the contour in the lower half-plane so that the exponential forces the integrand to zero on the part of the contour not in the original integral. However, if the contour is closed in the lower half plane, only poles in the lower half plane will be picked up by the integral. Thus $G^+(\mathbf{r}, \mathbf{r}'; \tau)$ is zero for $tau < 0$ and therefore corresponds only to propagation forward in time. $G^-(\mathbf{r}, \mathbf{r}'; \tau)$, on the other hand, is zero for $\tau > 0$ and corresponds to propagation backwards in time. $\hat{G}^-$ is frequently useful in formal calculations.

A.2 Scaling $\mathcal{L}$

We will find it useful to relate the Green function of the operator $\alpha\hat{\mathcal{L}}$ to the Green function of $\hat{\mathcal{L}}$ where α is a complex constant.

Suppose

$$\left[z - \alpha\hat{\mathcal{L}}\right] \hat{G}_\alpha(z) = 1 \tag{A.16}$$

We note that $\hat{\mathcal{L}}$ and $\alpha\hat{\mathcal{L}}$ have the same eigenfunctions but different eigenvalues. i.e.,

$$\alpha\hat{\mathcal{L}} \left|\psi_n\right\rangle = \alpha\lambda_n \left|\psi_n\right\rangle \tag{A.17}$$

so

$$\hat{G}_\alpha(z) = \sum_n \frac{\left|\psi_n\right\rangle \left\langle\psi_n\right|}{z - \alpha\lambda_n} = \frac{1}{\alpha}\sum_n \frac{\left|\psi_n\right\rangle \left\langle\psi_n\right|}{\frac{z}{\alpha} - \lambda_n} = \frac{1}{\alpha}\hat{G}_1\left(\frac{z}{\alpha}\right) \tag{A.18}$$

So we have

$$\hat{G}_\alpha(z) = \frac{1}{\alpha}\hat{G}_1\left(\frac{z}{\alpha}\right) \tag{A.19}$$

A.3 Integration of Energy Green functions

Claim:

$$\int G(\mathbf{r}_1, \mathbf{r}; z) G(\mathbf{r}, \mathbf{r}_2; z)\, d\mathbf{r} = -\frac{d}{dz} G(\mathbf{r}_1, \mathbf{r}_2; z). \tag{A.20}$$

Proof:

$$I = \int G(\mathbf{r}_1, \mathbf{r}; z) G(\mathbf{r}, \mathbf{r}_2; z)\, d\mathbf{r} = \int \left\langle\mathbf{r}_1\right| \hat{G}(z) \left|\mathbf{r}\right\rangle \left\langle\mathbf{r}\right| \hat{G}(z) \left|\mathbf{r}_2\right\rangle \, d\mathbf{r}, \tag{A.21}$$

or

$$I = \left\langle\mathbf{r}_1\right| \hat{G}(z) \left[\int \left|\mathbf{r}\right\rangle \left\langle\mathbf{r}\right| \, d\mathbf{r}\right] \hat{G}(z) \left|\mathbf{r}_2\right\rangle, \tag{A.22}$$

but

$$\int \left|\mathbf{r}\right\rangle \left\langle\mathbf{r}\right| \, d\mathbf{r} = \mathbf{1}, \tag{A.23}$$

so

$$I = \left\langle\mathbf{r}_1\right| \hat{G}(z)\hat{G}(z) \left|\mathbf{r}_2\right\rangle. \tag{A.24}$$

We expand the Green functions:

$$\hat{G}(z) = \sum_n^\infty \frac{\left|n\right\rangle \left\langle n\right|}{z - E_n}, \tag{A.25}$$

so

$$I = \langle \mathbf{r}_1 | \sum_n^\infty \frac{|n\rangle \langle n|}{z - E_n} \sum_m^\infty \frac{|m\rangle \langle m|}{z - E_m} |\mathbf{r}_2\rangle . \tag{A.26}$$

But, since $\langle n | m \rangle = \delta_{nm}$,

$$I = \langle \mathbf{r}_1 | \sum_n^\infty \frac{|n\rangle \langle n|}{(z - E_n)^2} |\mathbf{r}_2\rangle , \tag{A.27}$$

which is very like the Green function except that the denominator is squared. We can get around this by taking a derivative:

$$I = \langle \mathbf{r}_1 | \sum_n^\infty -\frac{d}{dz} \frac{|n\rangle \langle n|}{z - E_n} |\mathbf{r}_2\rangle . \tag{A.28}$$

We move the derivative outside the sum and matrix element to get

$$I = -\frac{d}{dz} \langle \mathbf{r}_1 | \hat{G}(z) |\mathbf{r}_2\rangle = -\frac{d}{dz} \hat{G}(\mathbf{r}_1, \mathbf{r}_2; z), \tag{A.29}$$

as desired.

A.4 Green functions of separable systems

Suppose we have a system which is separable. That is, the eigenstates are products of functions in each of the domains into which the system can separated. For example, a system in which an electron can move freely in the x-direction but is confined to the region $|y| < h/2$ has eigenfunctions which are products of plane waves in x and quantized modes in y. The Green function of such a system is written

$$\hat{G}^{(\pm)}(z) = \sum_\alpha \sum_\beta \frac{|\alpha\rangle \otimes |\beta\rangle \langle \alpha| \otimes \langle \beta|}{z - \varepsilon_\alpha - \varepsilon_\beta \pm i\epsilon}. \tag{A.30}$$

We can move either of the sums inside to get

$$\hat{G}^{(\pm)}(z) = \sum_\alpha |\alpha\rangle \langle \alpha| \otimes \sum_\beta \frac{|\beta\rangle \langle \beta|}{z - \varepsilon_\alpha - \varepsilon_\beta \pm i\epsilon}, \tag{A.31}$$

but now the inner sum is just another Green function (albeit of lower dimension), so we have

$$\hat{G}^{(\pm)}(z) = \sum_\alpha |\alpha\rangle \langle \alpha| \otimes \hat{G}^{(\pm)}_\beta(z - \varepsilon_\alpha) = \sum_\beta |\beta\rangle \langle \beta| \otimes \hat{G}^{(\pm)}_\alpha(z - \varepsilon_\beta) \tag{A.32}$$

Consider the example mentioned at the beginning of this section. We'll label the eigenstates in the x-direction by their wavenumber, k and label the transverse modes by a channel index, n. So we have

$$\hat{G}^{(\pm)}(z) = \int_{-\infty}^{\infty} |k\rangle \langle k| \otimes \hat{G}_n(E - \varepsilon(k)) \pm i\epsilon)\, dk = \sum_n |n\rangle \langle n| \otimes \hat{g}_o^{(\pm)}(E - \varepsilon_n) \tag{A.33}$$

where $\hat{g}_o^{(\pm)}(z)$ is the one dimensional free Green function. In the position representation this latter equality is rewritten as

$$G^{(\pm)}(x, y, x', y'; z) = \sum_n \chi_n(y)\chi_n(y') g^{(\pm)}(x, x'; E - \varepsilon_n). \tag{A.34}$$

A.5 Examples

Below we examine two examples of the explicit computation of Green functions. We begin with the mundane but useful free space Green function in two dimensions. Then we consider the more esoteric Gor'kov Green function; the Green function of a single electron in a superconductor.

A.5.1 The Free-Space Green Function in Two Dimensions

In two-dimensions, we can derive the free-space Green function of the operator $\mathcal{L} = -\nabla^2$ (corresponding to 2D free quantum mechanics with $\hbar^2/2m = 1$) using symmetry and limiting properties. See, e.g., [10]. The Green function, G_o satisfies

$$\left(z + \nabla^2\right) G_o(\mathbf{r}, \mathbf{r}'; z) = \delta\left(\mathbf{r} - \mathbf{r}'\right). \tag{A.35}$$

By translational symmetry of $\mathcal{L}$, $G_o(\mathbf{r}, \mathbf{r}'; z)$ is a function only of $\rho = |\mathbf{r} - \mathbf{r}'|$. For $\rho \neq 0$, $G(\rho; z)$ satisfies the *homogeneous* differential equation

$$\left(z + \nabla^2\right) G(\rho; z) = 0. \tag{A.36}$$

Recall that

$$\delta(\mathbf{r} - \mathbf{r}') = \frac{1}{2\pi\rho}\delta(\rho), \tag{A.37}$$

so we may re-write (A.35) as

$$2\pi z \int_0^\rho G_o \rho'\, d\rho' \; + \int_0^\rho 2\pi\rho' \nabla^2 G_o(\rho'; z)\, d\rho' = 1. \tag{A.38}$$

In radial polar coordinates (ρ, θ)

$$\nabla^2 = \frac{1}{\rho}\frac{\partial}{\partial\rho}\rho\frac{\partial}{\partial\rho} + \frac{1}{\rho^2}\frac{\partial^2}{\partial\theta^2}, \tag{A.39}$$

so

$$\rho\nabla^2 f(\rho) = \frac{\partial}{\partial\rho}\left(\rho\frac{\partial f}{\partial\rho}\right). \tag{A.40}$$

Thus

$$\int_0^\rho 2\pi\rho'\nabla^2 G_o(\rho';z)\,d\rho' = 2\pi\int_0^\rho \frac{\partial}{\partial\rho'}\left(\rho' G_o(\rho';z)\right)\,d\rho' = 2\pi\rho\frac{\partial G_o}{\partial\rho}, \tag{A.41}$$

where the last equality follows from Gauss' Theorem (in this case, the fundamental theorem of calculus). So we have

$$2\pi z\int_0^\rho G_o\rho'\,d\rho' \; + 2\pi\rho\frac{\partial G_o}{\partial\rho} = 1, \tag{A.42}$$

which, as $\rho \to 0$, gives

$$2\pi\rho\frac{\partial G_o(\rho;z)}{\partial\rho} = 1 \Rightarrow G_o(\rho;z) \to \frac{1}{2\pi}\ln(\rho) + \text{const.} \tag{A.43}$$

Also,

$$\lim_{\rho\to\infty} G_o(\rho;z) = 0 \tag{A.44}$$

General solutions of (A.35) are linear combinations of Hankel functions of the first and second kind of the form (See e.g., [1]).

$$\left[A_n H_n^{(1)}(\sqrt{z}\rho) + B_n H_n^{(2)}(\sqrt{z}\rho)\right] e^{\pm in\theta}. \tag{A.45}$$

Since we are looking for a θ independent solution we must have $n = 0$. Since $H_0^{(2)}(\sqrt{z}\rho)$ blows up as $\rho \to \infty$, $B_0 = 0$. The boundary condition (A.43) fixes $A_0 = \frac{-i}{4}$. So we have

$$G_o(\mathbf{r},\mathbf{r}';z) = -\frac{i}{4}H_o^{(1)}(\sqrt{z}|\mathbf{r}-\mathbf{r}'|), \tag{A.46}$$

where $H_o^{(1)}$ is the Hankel function of zero order of the first kind:

$$H_o^{(1)}(x) = [J_o(x) + iY_o(x)] \tag{A.47}$$

where $J_o(x)$ is the zero order Bessel function and $Y_o(x)$ is the Neumann function of zero order.

It will be useful to identify some properties of $Y_o(x)$ for use elsewhere. We will often be interested in $Y_o(x)$ for small x. As $x \to 0$

$$Y_o(x) = Y_o^{(R)}(x) + \frac{2}{\pi}J_o(x)\ln(x) \tag{A.48}$$

$Y_o^{(R)}(x)$ is called the "regular" part of $Y_o(x)$. We note that $Y_o^{(R)}(0) \neq 0$. Ordinarily, the specific value of this constant is irrelevant since it is overwhelmed by the logarithm. However, we will have occasion to subtract the singular part of G_o and the constant, $Y_o^{(R)}(0)$, will be important.

A.6 The Gor'kov (bulk superconductor) Green Function

In this appendix we will derive the Green Function for particles and holes in a superconductor. We plan to use this Green function to simulate Andre'ev scattering systems. We will find an explicit solution in the case of a uniform bulk superconductor.

Andre'ev scattering takes place at normal-metal superconductor boundaries (NS). When an electron in the normal metal hits the superconductor boundary it can scatter as a hole with the time-reversed momentum of the electron. That is, the electron disappears at the boundary and a hole appears which goes back along the electron's path at the same speed as the electron came in. This type of scattering leads to a class of trajectories which interfere strongly (even in chaotic/disordered systems) and produce weak-localization effects.

The simplest way to deal with the co-existence of particles and holes is to solve a set of coupled Schrödinger-like equations known as the Bogoliubov equations (see, e.g., [5]):

$$i\hbar\frac{\partial}{\partial t}|f\rangle = \left[\hat{H}_o - \hat{\mu}\right]|f\rangle + \hat{\Delta}\,|g\rangle\,, \tag{A.49}$$

$$i\hbar\frac{\partial}{\partial t}|g\rangle = -\left[\hat{H}_o - \hat{\mu}\right]|g\rangle + \hat{\Delta}^\dagger\,|f\rangle\,, \tag{A.50}$$

$$\tag{A.51}$$

where $\hat{H}_o$ is the single particle Hamiltonian, $\hat{\mu} = \int |\mathbf{r}\rangle\,\mu(\mathbf{r})\,\langle\mathbf{r}|$ is the (possibly position dependent) chemical potential and $\hat{\Delta} = \int |\mathbf{r}\rangle\,\Delta(\mathbf{r})\,\langle\mathbf{r}|$ is the (possibly position dependent) superconductor energy gap. In the $\hat{\Delta} = 0$ case, we have the Schrödinger equation for $|f\rangle$ (the electron state) and the time-reversed Schrödinger equation for $|g\rangle$ (the hole state).

If we form the spinor

$$|\Psi\rangle = \begin{pmatrix} |f\rangle \\ |g\rangle \end{pmatrix}, \tag{A.52}$$

we can write the Bogoliubov equations as

$$i\hbar\frac{\partial}{\partial t}\left|\Psi\right\rangle = \begin{pmatrix} \left(\hat{H}_o - \hat{\mu}\right) & \hat{\Delta} \\ \hat{\Delta}^\dagger & -\left(\hat{H}_o - \hat{\mu}\right) \end{pmatrix} \left|\Psi\right\rangle = \mathcal{H}\left|\Psi\right\rangle . \tag{A.53}$$

In order to compute the Green function operator, $\hat{G}(z)$, for this system we form

$$\hat{G}^{-1}(z) = z - \hat{\mathcal{H}} = \begin{pmatrix} z - \left(\hat{H}_o - \hat{\mu}\right) & -\hat{\Delta} \\ -\hat{\Delta}^\dagger & z + \left(\hat{H}_o - \hat{\mu}\right) \end{pmatrix}, \tag{A.54}$$

which, at first, looks difficult to invert. However, there are some nice techniques we can apply to a matrix with this form. To understand this, we need a brief review of 2×2 quantum mechanics.

Recall the Pauli spin matrices are defined

$$\begin{aligned} \sigma_1 &= \begin{pmatrix} 0 & 1 \\ 1 & 0 \end{pmatrix}, \\ \sigma_2 &= \begin{pmatrix} 0 & -i \\ i & 0 \end{pmatrix}, \\ \sigma_3 &= \begin{pmatrix} 1 & 0 \\ 0 & -1 \end{pmatrix}, \end{aligned}$$

and that the set $\{\mathcal{I}, \sigma_1, \sigma_2, \sigma_3\}$ is a basis for the vector space of complex 2×2 matrices.

The Pauli matrices satisfy

$$[\sigma_i, \sigma_j] = \sigma_i\sigma_j - \sigma_j\sigma_i = \epsilon_{ijk}\sigma_k \tag{A.55}$$

$$\{\sigma_i, \sigma_j\} = \sigma_i\sigma_j + \sigma_j\sigma_i = I\delta_{ij} \tag{A.56}$$

where ϵ_{ijk} is the ϵ three-symbol (ϵ_{ijk} is 1 if ijk is a cyclic permutation of 123, -1 if ijk is a non-cyclic permutation of 123 and 0 otherwise) and δ_{ij} is the Kronecker delta.

To simplify the later manipulations we rewrite $\hat{G}^{-1}$:

$$\hat{G}^{-1}(z) = \hat{g}^{-1}(z)\sigma_3 \Rightarrow \hat{G}(z) = \sigma_3^{-1}\hat{g}(z) \tag{A.57}$$

where

$$\hat{g}^{-1}(z) = \begin{pmatrix} z - \left(\hat{H}_o - \hat{\mu}\right) & \hat{\Delta} \\ -\hat{\Delta}^\dagger & -z - \left(\hat{H}_o - \hat{\mu}\right) \end{pmatrix}. \tag{A.58}$$

We now write

$$\hat{g}^{-1}(z) = \hat{a}\mathcal{I} + i\hat{\mathbf{b}} \cdot \sigma, \tag{A.59}$$

where

$$\begin{aligned} \hat{a} &= -\left(\hat{H}_o - \hat{\mu}\right), \\ \hat{\mathbf{b}} &= \left(\mathrm{Im}(\hat{\Delta}), \mathrm{Re}(\hat{\Delta}), -iz\right), \\ \sigma &= (\sigma_1, \sigma_2, \sigma_3). \end{aligned}$$

Let's make the additional assumptions that

$$\begin{aligned} \left[\hat{a}, \hat{b}_i\right] &= 0 \ \forall i, \\ \left[\hat{b}_i, \hat{b}_j\right] &= 0 \ \forall i, j. \end{aligned}$$

For our problem, as long as $\hat{\Delta} = \mathcal{I} \times \text{const}$, we satisfy these assumptions. That is, we are in a uniform superconductor.

So

$$\hat{g}^{-1}(z) = \begin{pmatrix} \hat{a} - i\hat{b}_3 & i(\hat{b}_1 - i\hat{b}_2) \\ i(\hat{b}_1 + i\hat{b}_2) & \hat{a} + i\hat{b}_3 \end{pmatrix} \tag{A.60}$$

Since all the operators commute, we can invert this like a 2×2 matrix of scalars:

$$\hat{g}(z) = \frac{1}{\hat{a}^2 + \hat{b}_3^2 + \hat{b}_1^2 + \hat{b}_2^2} \begin{pmatrix} \hat{a} + i\hat{b}_3 & -i(\hat{b}_1 - i\hat{b}_2) \\ -i(\hat{b}_1 + i\hat{b}_2) & \hat{a} - i\hat{b}_3 \end{pmatrix} = \frac{1}{\hat{a}^2\mathcal{I} + \hat{\mathbf{b}}^2} \left(\hat{a}\mathcal{I} - i\hat{\mathbf{b}} \cdot \sigma\right). \tag{A.61}$$

We clarify this by explicit multiplication

$$\hat{g}(z)\hat{g}^{-1}(z) = \frac{\mathcal{I}}{\hat{a}^2 + \hat{\mathbf{b}}^2} \left(\hat{a}\mathcal{I} - i\hat{\mathbf{b}} \cdot \sigma\right) \left(\hat{a}\mathcal{I} + i\hat{\mathbf{b}} \cdot \sigma\right) = \frac{\mathcal{I}}{\hat{a}^2 + \hat{\mathbf{b}}^2} \left[\hat{a}^2\mathcal{I} + \left(\hat{\mathbf{b}} \cdot \sigma\right)^2\right]. \tag{A.62}$$

Now we use the relation (A.56) to simplify $\hat{\mathbf{b}} \cdot \sigma$:

$$\hat{\mathbf{b}} \cdot \sigma = \sum_{i,j=1}^{3} \hat{b}_i \sigma_i \hat{b}_j \sigma_j = \sum_{\substack{i,j=1 \\ i<j}}^{3} \hat{b}_i \hat{b}_j \{\sigma_i, \sigma_j\} = \hat{\mathbf{b}}^2 \mathcal{I}. \tag{A.63}$$

So we have

$$\hat{g}(z)\hat{g}^{-1}(z) = \frac{\mathcal{I}}{\hat{a}^2 + \hat{\mathbf{b}}^2} \left[\hat{a}^2\mathcal{I} + \left(\hat{\mathbf{b}} \cdot \sigma\right)^2\right] = \frac{\mathcal{I}}{\hat{a}^2 + \hat{\mathbf{b}}^2} \left(\hat{a}^2\mathcal{I} + \hat{\mathbf{b}}^2\mathcal{I}\right) = \mathcal{I}. \tag{A.64}$$

At this point we have an expression for $\hat{g}(z)$ but it's not obvious how we evaluate $\frac{\mathcal{I}}{\hat{a}^2+\hat{\mathbf{b}}^2}$. We use another trick, and factor $\hat{g}(z)$ as follows (defining $\hat{b} = |\hat{\mathbf{b}}|$):

$$\hat{g}(z) = \frac{\mathcal{I}}{\hat{a}^2 + \hat{\mathbf{b}}^2}\left(\hat{a}\mathcal{I} - i\hat{\mathbf{b}}\cdot\sigma\right) = \frac{1}{2}\sum_{s=\pm 1}\frac{\mathcal{I} + s\frac{\hat{\mathbf{b}}\cdot\sigma}{\hat{b}}}{\hat{a} + is\hat{b}}. \tag{A.65}$$

Why does this help? We've replaced the problem of inverting $\hat{a}^2 + \hat{b}^2$ with the problem of inverting $\hat{a} \pm i\hat{b}$. We recall that $a = -(\hat{\mathcal{H}}_o - \hat{\mu})$ and $b = \sqrt{b_1^2 + b_2^2 + b_3^2} = \sqrt{|\Delta|^2 - z^2}$. So

$$\hat{a} \pm i\hat{b} = -\left[\hat{H}_o - \hat{\mu} \mp i\sqrt{|\Delta|^2 - z^2}\right], \tag{A.66}$$

which means

$$(\hat{a} \pm i\hat{b})^{-1} = \hat{G}_\mu\left(\pm i\sqrt{|\Delta|^2 - z^2}\right), \tag{A.67}$$

where

$$\hat{G}_\mu(z) = \frac{1}{z - \left(\hat{H}_o - \hat{\mu}\right)}. \tag{A.68}$$

We note that if $\hat{\mu} = E_{\text{fermi}} = \text{const.}$, $\hat{G}_\mu(z) = \hat{G}_o(E_{\text{fermi}} + z)$. We define

$$\begin{aligned} \eta &= \sqrt{z^2 - |\Delta|^2} \\ f_\pm(z,\Delta) &= \frac{1}{2}\left(1 \pm \frac{z}{\sqrt{z^2 - |\Delta|^2}}\right) \\ \delta &= \frac{\Delta}{2\sqrt{z^2 - |\Delta|^2}} \end{aligned}$$

and then write

$$g(z) = \begin{pmatrix} \hat{G}_\mu(\eta)f_+(z,\Delta) + \hat{G}_\mu(-\eta)f_-(z,\Delta) & \delta^\dagger\left[\hat{G}_\mu(\eta) - \hat{G}_\mu(-\eta)\right] \\ \delta\left[\hat{G}_\mu(\eta) - \hat{G}_\mu(-\eta)\right] & \hat{G}_\mu(-\eta)f_+(z,\Delta) + \hat{G}_\mu(\eta)f_-(z,\Delta) \end{pmatrix}. \tag{A.69}$$

So, finally, we have a simple closed form expression for $G(z)$:

$$\hat{G}(z) = \sigma_3^{-1}\hat{g}(z) = \begin{pmatrix} \hat{G}_\mu(\eta)f_+(z,\Delta) + \hat{G}_\mu(-\eta)f_-(z,\Delta) & \delta^\dagger\left[\hat{G}_\mu(\eta) - \hat{G}_\mu(-\eta)\right] \\ -\delta\left[\hat{G}_\mu(\eta) - \hat{G}_\mu(-\eta)\right] & -\hat{G}_\mu(-\eta)f_+(z,\Delta) - \hat{G}_\mu(\eta)f_-(z,\Delta) \end{pmatrix}. \tag{A.70}$$

Various Limits

- $\Delta = 0$

When $\Delta = 0$ we have

$$\begin{aligned} f_+(z, \Delta = 0) &= 1 \\ f_-(z, \Delta = 0) &= 0 \\ \delta &= 0 \end{aligned}$$

and thus

$$\hat{G}(z) = \begin{pmatrix} \hat{G}_\mu(\eta) & 0 \\ 0 & -\hat{G}_\mu(-\eta) \end{pmatrix}. \tag{A.71}$$

as we would expect for a normal metal.

Appendix B

Generalization of the Boundary Wall Method

Handling the general boundary condition

$$\alpha(s)\,\psi(\mathbf{r}(s))\Big|_{\mathcal{C}} + [1-\alpha(s)]\;\partial_{\mathbf{n}(s)}\,\psi(\mathbf{r}(s))\Big|_{\mathcal{C}} = 0, \tag{B.1}$$

requires a more complex potential,

$$V(\mathbf{r}) = \int_{\mathcal{C}} ds\,\lambda(s)\,\delta\left(\mathbf{r}-\mathbf{r}(s)\right)\left\{\alpha(s) - [1-\alpha(s)]\,\partial_{\mathbf{n}(s)}\right\}, \tag{B.2}$$

and thus is somewhat more difficult than the case of Dirichlet boundary conditions considered in section 4.2. First, we assume $\mathbf{n}(s)$ a unit vector normal to $\mathcal{C}$ at each point s, and

$$\partial_{\mathbf{n}(s)} f(\mathbf{r}(s)) = \mathbf{n}(s)\cdot\nabla f(\mathbf{r}(s)). \tag{B.3}$$

Second, we insert (B.2) into (4.3) to get

$$\psi(\mathbf{r}) = \phi(\mathbf{r}) + \int_{\mathcal{C}} ds'\,\lambda(s')\,G_0(\mathbf{r},\mathbf{r}(s'))\left\{\alpha(s') - [1-\alpha(s')]\,\partial_{\mathbf{n}(s')}\right\}\psi(\mathbf{r}(s')), \tag{B.4}$$

which then we consider at a point $\mathbf{r}(s'')$ on $\mathcal{C}$ (with the same notational abbreviation used in Section 4.2)

$$\psi(s'') = \phi(s'') + \int ds'\,\lambda(s')\,G_0(s'',s')\left\{\alpha(s') + [1-\alpha(s')]\,\partial_{n(s')}\right\}\psi(s'). \tag{B.5}$$

As it stands, (B.5) is *not* a linear equation in ψ. To fix this, we multiply both sides by $\left\{\alpha(s'') + [1-\alpha(s'')]\,\partial_{n(s'')}\right\}$ and define

$$\psi^B(s'') \quad = \quad \left\{\alpha(s'') + [1-\alpha(s'')]\,\partial_{n(s'')}\right\}\psi(s'')$$

$$\begin{aligned} \phi^B(s'') &= \left\{\alpha(s'') + [1-\alpha(s'')]\,\partial_{n(s'')}\right\}\phi(s'') \\ G_0^B(s'',s') &= \left\{\alpha(s'') + [1-\alpha(s'')]\,\partial_{n(s'')}\right\}G_0(s'',s'). \end{aligned} \tag{B.6}$$

This yields

$$\psi^B(s'') = \phi^B(s'') + \int ds'\,\lambda(s')\,G_0^B(s'',s')\,\psi^B(s'), \tag{B.7}$$

a linear equation in ψ^B, and solved by

$$\tilde{\psi}^B = \left[\tilde{\mathrm{I}} - \tilde{G}_0^B\,\tilde{\Lambda}\right]^{-1}\tilde{\phi}^B, \tag{B.8}$$

where again the tildes emphasize that the equation is defined only on $\mathcal{C}$. The diagonal operator $\tilde{\Lambda}$ is

$$\left(\tilde{\Lambda}f\right)(s) = \lambda(s)f(s). \tag{B.9}$$

We define

$$T^B = \tilde{\Lambda}\left[\tilde{\mathrm{I}} - \tilde{G}_0^B\,\tilde{\Lambda}\right]^{-1}, \tag{B.10}$$

that solves the original problem

$$\psi(\mathbf{r}) = \phi(\mathbf{r}) + \int ds'\,G_0(\mathbf{r},\mathbf{r}(s'))\,T^B_{\phi^B}(\mathbf{r}(s')), \tag{B.11}$$

for

$$T^B_{\phi^B}(\mathbf{r}(s')) = \int ds\,T^B(s',s)\,\phi^B(s). \tag{B.12}$$

As in Section 4.2, in the limit $\lambda(s) = \lambda \to \infty$, T^B converges to $-\left[\tilde{G}_0^B\right]^{-1}$ which, when inserted into (B.7), gives

$$\left\{\alpha(s) + [1-\alpha(s)]\,\partial_{n(s)}\right\}\psi(s) = \psi^B(s) = \left(\left[\tilde{\mathrm{I}} - \tilde{G}_0^B\,\left[\tilde{G}_0^B\right]^{-1}\right]\tilde{\phi}^B\right)(s) = 0, \tag{B.13}$$

the desired boundary condition (B.1).

For completeness, we expand T^B in a power series

$$T^B = \tilde{\Lambda} + \tilde{\Lambda}\left(\sum_{j=1}^{\infty}\left[\tilde{G}_0^B\,\tilde{\Lambda}\right]^j\right), \tag{B.14}$$

so

$$T^B(s'',s') = \lambda(s'')\,\delta(s''-s') + \lambda(s'')\left(\sum_{j=1}^{\infty}[T^B]^{(j)}(s'',s')\right), \tag{B.15}$$

where

$$[T^B]^{(j)}(s'',s') = \int ds_1\ldots ds_j\,G_0^B(s'',s_j)\,\lambda(s_j)\,\ldots\,G_0^B(s_2,s_1)\,\lambda(s_1)\,\delta(s_1-s'), \tag{B.16}$$

allowing one, at least in principle, to compute $T^B(s'',s')$, and thus the wavefunction everywhere.

Appendix C

Linear Algebra and Null-Space Hunting

In this appendix we deal with the linear algebra involved in implementing various methods discussed above. We begin with the standard techniques for solving $\mathbf{Ax} = \mathbf{v}$ type equations when A is of full rank. We do this mostly to establish notation.

In many of the techniques above, we had a matrix which was a function of a real parameter (usually a scaled energy), $\mathbf{A}(t)$ and we wanted to look for t such that $\mathbf{A(t)x} = 0$ has non-trivial solutions ($\mathbf{x} \neq 0$). The standard technique for handling this sort of problem is the Singular Value Decomposition (SVD). We'll discuss this in (C.3).

There are other methods to extract null-space information from a matrix and they are typically faster than the SVD. We'll discuss one such method, the QR Decomposition (QRD). [17] is a wonderful reference for all that follows.

C.1 Standard Linear Solvers

A system of N linear equations in N unknowns:

$$\sum_{i=1}^{N} a_{ij} x_i = b_j \text{ for } j \in \{1...N\} \tag{C.1}$$

may be written as the matrix equation

$$\mathbf{Ax} = \mathbf{b}, \tag{C.2}$$

where $(\mathbf{A})_{ij} = a_{ij}$. This implies that a formal solution is available if the matrix inverse A^{-1} exists. Namely,

$$\mathbf{x} = \mathbf{A}^{-1}\mathbf{b}. \tag{C.3}$$

Most techniques for solving (C.2) do not actually invert $\mathbf{A}$ but rather "decompose" $\mathbf{A}$ in a form where we can compute $\mathbf{A}^{-1}\mathbf{b}$ efficiently for a given $\mathbf{b}$. One such form is the LU decomposition,

$$\mathbf{A} = \mathbf{LU}, \tag{C.4}$$

where $\mathbf{L}$ is a lower triangular matrix and $\mathbf{U}$ is an upper-triangular matrix. Since it is simple to solve a triangular system (see [17], section 3.1) we can solve our original equations with a two step process. We find a $\mathbf{y}$ which solves $\mathbf{Uy} = \mathbf{b}$ and then find $\mathbf{x}$ which solves $\mathbf{Lx} = \mathbf{y}$. This is an abstract picture of the familiar process of Gaussian elimination. Essentially, there exists a product of (unit diagonal) lower triangular matrices which will make $\mathbf{A}$ upper-triangular. Each of these lower triangular matrices is a gauss transformation which zeroes all the elements below the diagonal in $\mathbf{A}$ one column at a time. The LU factorization returns the inverse of the product of the lower triangular matrices as $\mathbf{L}$.and the resulting upper triangular matrix in $\mathbf{U}$. It is easy to show that the product of a lower(upper) triangular matrices is lower(upper) triangular and the same for the inverse. That is, $\mathbf{L}$ represents a sequence of gauss transformations and $\mathbf{U}$ represents the result of those transformations. For large matrices, the LUD requires approximately $2N^3/2$ flops (floating point operations) to compute.

The LUD has several drawbacks. The computation of the gauss transformations involves division by a_{ii} as the i_{th} column is zeroed. This means that if a_{ii} is zero for any i the computation will fail. This can happen two ways. If the "leading principal submatrix" of A is singular, i.e., $\det(\mathbf{A}(1:i, 1:i)) = 0$ then a_{ii} will be zero when the i_{th} column is zeroed. If $\mathbf{A}$ is non-singular, pivoting techniques can successfully find an LUD of a row-permuted version of $\mathbf{A}$. Row permutation of $\mathbf{A}$ is harmless in terms of finding the solution. However, if $\mathbf{A}$ is singular then we can only chase the small pivots of $\mathbf{A}$ down r columns where $r = \text{rank}\,(A)$. At this point we will encounter small pivots and numerical errors will destroy the solution. Thus we are led to look for methods which are stable even when $\mathbf{A}$ is singular.

C.2 Orthogonalization and the QR Decomposition

Suppose we wanted to keep the basic idea of the LU decomposition, zeroing the columns of **A** but avoid the pivot problem. We have to be careful because the inverse of the transformation matrix (the L in LU) has to be easy to invert or the decomposition won't be much help. One class of transformations which might work are orthogonal transformations. Orthogonal transformations include reflections and rotations. Orthogonal transformations do not re-scale (so they are stable in the presence of small pivots) and they are easy to invert (the inverse of an orthogonal transformation is its transpose). The simplest such method is the QR decomposition,

$$\mathbf{A} = \mathbf{QR} \tag{C.5}$$

where **Q** is orthogonal and **R** is upper-triangular. Performing this decomposition is straightforward. Consider the first column of **A**. A rotation (or reflection about a correctly chosen plane) will zero all but the first element (simply rotate a basis vector into the first column of **A** and then invert that rotation). Now go to the second column. To zero everything below the diagonal it is sufficient to consider a problem of 1 dimension smaller and rotate in that smaller space. This leaves the previously zeroed elements alone (since those vectors are null in the smaller space). We do this one column at a time and accomplish our goal.

A wonderful consequence of the QRD is that the eigenvalues of **A** are the diagonal elements of **R**. Since **Q** is orthogonal, it does not change eigenvalues, it just rotates the eigenvectors. This makes it ideal for null-space hunting since we can do QRDs and look for small eigenvalues. Typically the eigenvalues in a QRD are in generated in order of their absolute value as a side effect of the transformation.

If **A** is singular with rank N-1, a typical QRD algorithm will leave the zero eigenvalue in the last row of **R**. That is, the last row of **R** is all zeroes. A modified back-substitution algorithm will immediately return a vector in the null space. Since the null space is one dimensional, this vector spans it. A similar approach will work with multi-dimensional null-spaces but requires a bit more work.

The QRD is not magic. It does not provide a solution where none-exists. While the algorithm is stable, the attempt to solve the $\mathbf{Ax} = \mathbf{b}$ will still fail for singular **A** and non-zero **b**, it will simply do so in the back-substitution phase rather than during decomposition.

There is a fix for this back-substitution problem. We can pivot the columns of

A as we do the QRD and then, though we still cannot solve an ill-posed problem we *can* extract a least squares solution from this column pivoted QRD (QRD_CP).

For large N, the QRD requires approximately $4N^3/3$ flops (twice as many as LU) and QRD_CP requires $4N^3$ flops to compute.

C.3 The Singular Value Decomposition

It is possible to further reduce $\mathbf{R}$ by post-multiplying it by a sequence of orthogonal transformations. The SVD is one such "complete orthogonalization" It reduces $\mathbf{R}$ to a diagonal matrix with positive entries. That is, the SVD gives

$$\mathbf{A} = \mathbf{U}\mathbf{\Sigma}\mathbf{V}^T \tag{C.6}$$

where $\mathbf{U}$ and $\mathbf{V}$ are orthogonal and $\mathbf{\Sigma} = \text{diag}(\sigma_1, \ldots, \sigma_N)$. In this formulation, zero singular values correspond to zero eigenvalues and the corresponding vectors may be extracted from $\mathbf{V}$. Since the SVD is computed entirely with orthogonal transformations, it is stable even when applied to singular matrices.

The SVD of a symmetric matrix is an eigendecomposition. That is, the singular values of a symmetric matrix are the absolute values of the eigenvalues and the singular vectors are the eigenvectors. If a symmetric matrix has two eigenvalues with the same absolute value but opposite sign, the SVD cannot distinguish these eigenvalues and may mix them. For non-degenerate eigenvalues, the sign information is encoded in $\mathbf{U}\mathbf{V}^T$ which is a diagonal matrix made up of ± 1. All of this follows from a careful treatment of the uniqueness of the decomposition.

The SVD can be applied to computing only the singular values (SVD_S), the singular values and the matrix V (SVD_SV) and the singular values, the matrix V, and the matrix U (SVD_USV). The flop count is different for these three versions (we include LUD and QRD for comparison) and we summarize this in table C.3.

Algorithm	flops	seconds
SVD_USV	$20N^3$	13.51
SVD_SV	$12N^3$	9.55
SVD_S	$4N^3$	2.13
QRD_CP	$4N^3$	1.73
QRD	$4N^3/3$	.43
LUD	$2N^3/3$	N/A

Table C.1: Comparison of flop counts and timing for various matrix decompositions. The timing test was the decomposition of a 500×500 matrix on a DEC Alpha 500/500 workstation.

We include this table to point out that choice of algorithm can have a dramatic effect on computation time. For instance, when looking for a t such that $\mathbf{A}(t)$ is singular, we may use either the SVD_S or the QRD to examine the rank of $\mathbf{A}(t)$. However, using the QRD will be at least 4 times faster than using the SVD_S.

Appendix D

Some important infinite sums

D.1 Identites from $\sum \frac{x^n}{n}$

Recall that

$$\sum_{n=1}^{\infty} \frac{x^n}{n} = \ln\left(\frac{1}{1-x}\right) \text{ for } |x| < 1. \tag{D.1}$$

Thus

$$\sum_{n=1}^{\infty} \frac{e^{in\alpha}e^{-n\beta}}{n} = \ln\left(\frac{1}{1-e^{i\alpha-\beta}}\right) \text{ for } \alpha, \beta \text{ real}, \beta > 0. \tag{D.2}$$

So

$$\sum_{n=1}^{\infty} \frac{\cos(n\alpha)e^{-n\beta}}{n} = \mathrm{Re}\left\{\ln\left(\frac{1}{1-\exp(i\alpha-\beta)}\right)\right\} = \frac{1}{2}\ln\left(\frac{e^{\beta}}{2\cosh\beta - 2\cos\alpha}\right), \tag{D.3}$$

and

$$\sum_{n=1}^{\infty} \frac{\sin(n\alpha)e^{-n\beta}}{n} = \mathrm{Im}\left\{\ln\left(\frac{1}{1-\exp(i\alpha-\beta)}\right)\right\} = -\arctan\left(\frac{e^{-\beta}\sin\alpha}{1-e^{-\beta}\cos\alpha}\right). \tag{D.4}$$

Since

$$\sin n\alpha \ \sin n\alpha' = \frac{1}{2}\left[\cos n(\alpha-\alpha') - \cos n(\alpha+\alpha')\right], \tag{D.5}$$

we find

$$\begin{aligned}\sum_{n=1}^{\infty} \frac{\sin n\alpha \ \sin n\alpha'}{n} e^{-\beta n} &= \frac{1}{4}\left\{\ln\left[\frac{e^{\beta}}{2\cosh\beta - 2\cos(\alpha-\alpha')}\right] - \ln\left[\frac{e^{\beta}}{2\cosh\beta - 2\cos(\alpha+\alpha')}\right]\right\} \\ &= \frac{1}{4}\ln\left[\frac{\cosh\beta - \cos(\alpha+\alpha')}{\cosh\beta - \cos(\alpha-\alpha')}\right]\end{aligned}$$

$$= \frac{1}{4}\ln\left[\frac{\cosh\beta - 1 + 1 - \cos(\alpha+\alpha')}{\cosh\beta - 1 + 1 - \cos(\alpha-\alpha')}\right]$$

$$= \frac{1}{4}\ln\left[\frac{\sinh^2\frac{\beta}{2} + \sin^2\frac{\alpha+\alpha'}{2}}{\sinh^2\frac{\beta}{2} + \sin^2\frac{\alpha-\alpha'}{2}}\right]$$

We also note that for $\alpha, \beta << 1$

$$\ln\left(\frac{e^{\beta}}{2\cosh\beta - 2\cos\alpha}\right) = -\ln\left(1 + e^{-2\beta} - e^{i\alpha-\beta} - e^{-i\alpha-\beta}\right)$$
$$\approx \ln\left(\beta^2 + \alpha^2\right), \tag{D.6}$$

since, in the small argument expansion of the exponentials, the constant and linear terms cancel. Similarly, for $\beta, |\alpha - \alpha'| << 1$

$$\ln\left[\frac{\sinh^2\frac{\beta}{2} + \sin^2\frac{\alpha+\alpha'}{2}}{\sinh^2\frac{\beta}{2} + \sin^2\frac{\alpha-\alpha'}{2}}\right] \approx \ln\left[\sin^2\frac{\alpha+\alpha'}{2}\right] - \ln\left[\frac{\beta^2 + (\alpha-\alpha')^2}{4}\right] \tag{D.7}$$

D.2 Convergence of Green Function Sums

D.2.1 Dirichlet Boundary Green Function Sums

Consider

$$a_n(\xi) = \sin(nx)\sin(nx')\left(1 - \exp\left(-2\kappa_n h\right)\right)^{-1}\left(n^2\pi^2/l^2 - E\right)^{-1/2}\exp\left(-\kappa_n\xi\right), \tag{D.8}$$

where $\kappa_n = \sqrt{\frac{n^2\pi^2}{l} - E}$, and

$$b_n(\xi) = \sin(nx)\sin(nx')\frac{l}{n\pi}\exp\left(-\frac{n\pi}{l}\xi\right), \tag{D.9}$$

In this case, we may perform $\sum_{n=1}^{\infty} b_n(\xi)$ for $\xi \geq 0$ using the identities above (section D.1).

We need to show that $\sum_{n=1}^{\infty} a_n(\xi) - b_n(\xi)$ converges and that it converges uniformly with respect to ξ for all $\xi \geq 0$. Since $|\sin(nx)\sin(nx')| \leq 1$, we have

$$|a_n(\xi) - b_n(\xi)| =$$
$$\frac{l}{n\pi}\left[\left(1 - e^{-2\kappa_n h}\right)^{-1}\left(1 - \frac{El^2}{n^2\pi^2}\right)^{-1/2}\exp\left(-\frac{n\pi}{l}\xi\sqrt{1 - \frac{El^2}{\pi^2 n^2}}\right) - \exp\left(-\frac{n\pi}{l}\xi\right)\right].$$

For $x < 1$, $\frac{1}{\sqrt{x}} < \frac{1}{x}$ and $\exp(-\sqrt{x}a) < \exp(-xa)$ so

$$|a_n(\xi) - b_n(\xi)| <$$

$$\frac{l}{n\pi}\left[\left(1-e^{-2\kappa_n h}\right)^{-1}\left(1-\frac{El^2}{n^2\pi^2}\right)^{-1}\exp\left(-\frac{n\pi}{l}\xi\right)\exp\left(\frac{El}{\pi n}\xi\right)-\exp\left(-\frac{n\pi}{l}\xi\right)\right]$$
$$<\frac{l}{n\pi}\exp\left[-\frac{n\pi}{l}\xi\left(1-\frac{El^2}{n^2\pi^2}\right)\right]\left[\left(1-e^{-2\kappa_n h}\right)^{-1}\left(1-\frac{El^2}{n^2\pi^2}\right)^{-1}-\exp\left(-\frac{El}{\pi n}\xi\right)\right]$$

Since

1. $n>\frac{l}{\pi}\sqrt{2E}$ implies

$$\exp\left[-\frac{n\pi}{l}\xi\left(1-\frac{El^2}{n^2\pi^2}\right)\right]<\exp\left(-\frac{n\pi}{2l}\xi\right), \tag{D.10}$$

2. and, since $x<\frac{1}{2}\Rightarrow\frac{1}{1-x}<1+2x$, $n>\frac{l}{\pi}\sqrt{2E}$ implies

$$\left(1-\frac{El^2}{n^2\pi^2}\right)^{-1}<\left(1+\frac{2El^2}{n^2\pi^2}\right), \tag{D.11}$$

3. $n>\frac{l}{\pi}\sqrt{\left(\frac{\ln 2}{2h}\right)^2+E}$ implies

$$\left(1-e^{-2\kappa_n h}\right)^{-1}<\left(1+2e^{-2\kappa_n h}\right), \tag{D.12}$$

4. $x\geq 0\Rightarrow e^{-x}\geq 1-x$,

we have, for $n>\max\left\{\frac{l}{\pi}\sqrt{2E},\frac{l}{\pi}\sqrt{\left(\frac{\ln 2C}{2h}\right)^2+E}\right\}$,

$$|a_n(\xi)-b_n(\xi)|<\frac{l}{n\pi}\exp\left[-\frac{n\pi}{2l}\xi\right]\left[\left(1+2Ce^{-2\kappa_n h}\right)\left(1+\frac{2El^2}{n^2\pi^2}\right)-\left(1-\frac{El}{\pi n}\xi\right)\right]. \tag{D.13}$$

Further, for $n>\frac{l}{\pi}\sqrt{E+\left[\frac{1}{2h}\ln\left(\frac{El^2}{\pi^2}\right)^2\right]}$,

$$|a_n(\xi)-b_n(\xi)|<\frac{l}{n\pi}\exp\left[-\frac{n\pi}{2l}\xi\right]\left[\frac{El}{n\pi}\xi+\frac{5El^2}{n^2\pi^2}\right]. \tag{D.14}$$

Therefore, for $M>\max\left\{\frac{l}{\pi}\sqrt{2E},\frac{l}{\pi}\sqrt{E+\left[\frac{1}{2h}\ln\left(\frac{El^2}{\pi^2}\right)^2\right]}\right\}$,

$$\sum_{n=M}^{\infty}a_n(\xi)-b_n(\xi)<\exp\left[-\frac{M\pi}{2l}\xi\right]\left[\frac{2El^3}{\pi^3M^2}\frac{\frac{\pi}{2l}\xi}{1-\exp\left(-\frac{\pi}{2l}\xi\right)}+\frac{5El^3}{M^2\pi^2}\right]. \tag{D.15}$$

But $\frac{x}{1-e^{-x}}$ is a monotonically increasing function of x so $\frac{\frac{\pi}{2l}\xi}{1-\exp\left(-\frac{\pi}{2l}\xi\right)} < \frac{\frac{\pi}{2l}h}{1-\exp\left(-\frac{\pi}{2l}h\right)}$ and thus

$$\sum_{n=M}^{\infty}\left[a_n(\xi)-b_n(\xi)\right] < \exp\left[-\frac{M\pi}{2l}\xi\right]\left[\frac{El^2}{\pi^2M^2}\frac{h}{1-\exp\left(-\frac{\pi}{2l}h\right)}+\frac{5El^3}{3M^2\pi^2}\right]. \tag{D.16}$$

Thus $\sum_{n=M}^{\infty}\left[a_n(\xi)-b_n(\xi)\right]$ converges for all $\xi \geq 0$.

Further, since $\frac{El}{n\pi}\xi\exp\left[-\frac{n\pi}{2l}\xi\right] < \frac{2El^2}{n^2\pi^2}$,

$$|a_n(\xi)-b_n(\xi)| < \frac{7El^3}{n^3\pi^3} = f_n, \tag{D.17}$$

and $\sum_{n=M}^{\infty} f_n$ converges. Therefore $\sum_{n=M}^{\infty}\left[a_n(\xi)-b_n(\xi)\right]$ converges *uniformly* with respect to ξ for $\xi \geq 0$

D.2.2 Periodic Boundary Green Function Sums

Consider

$$a_n(\xi) = \cos(n|x-x'|)\left(n^2\pi^2/l^2-E\right)^{-1/2}\exp\left(-\kappa_n\xi\right), \tag{D.18}$$

where $\kappa_n = \sqrt{\frac{n^2\pi^2}{l}-E}$, and

$$b_n(\xi) = \cos(n|x-x'|)\frac{l}{n\pi}\exp\left(-\frac{n\pi}{l}\xi\right), \tag{D.19}$$

In this case, we may perform $\sum_{n=1}^{\infty} b_n(\xi)$ for $\xi \geq 0$ using the identities above (section D.1).

We need to show that $\sum_{n=1}^{\infty} a_n(\xi)-b_n(\xi)$ converges and that it converges uniformly with respect to ξ for all $\xi \geq 0$. Since $|\cos(n|x-x'|)| \leq 1$, we have

$$|a_n(\xi)-b_n(\xi)| = \frac{l}{n\pi}\left[\left(1-\frac{El^2}{n^2\pi^2}\right)^{-1/2}\exp\left(-\frac{n\pi}{l}\xi\sqrt{1-\frac{El^2}{\pi^2n^2}}\right)-\exp\left(-\frac{n\pi}{l}\xi\right)\right].$$

For $x < 1$, $\frac{1}{\sqrt{x}} < \frac{1}{x}$ and $\exp(-\sqrt{x}a) < \exp(-xa)$ so

$$\begin{aligned}|a_n(\xi)-b_n(\xi)| &< \frac{l}{n\pi}\left[\left(1-\frac{El^2}{n^2\pi^2}\right)^{-1}\exp\left(-\frac{n\pi}{l}\xi\right)\exp\left(\frac{El}{\pi n}\xi\right)-\exp\left(-\frac{n\pi}{l}\xi\right)\right] \\ &< \frac{l}{n\pi}\exp\left[-\frac{n\pi}{l}\xi\left(1-\frac{El^2}{n^2\pi^2}\right)\right]\left[\left(1-\frac{El^2}{n^2\pi^2}\right)^{-1}-\exp\left(-\frac{El}{\pi n}\xi\right)\right]\end{aligned}$$

Since

1. $n > \frac{l}{\pi}\sqrt{2E}$ implies

$$\exp\left[-\frac{n\pi}{l}\xi\left(1-\frac{El^2}{n^2\pi^2}\right)\right] < \exp\left(-\frac{n\pi}{2l}\xi\right), \tag{D.20}$$

2. and, since $x < \frac{1}{2} \Rightarrow \frac{1}{1-x} < 1+2x$, $n > \frac{l}{\pi}\sqrt{2E}$ implies

$$\left(1-\frac{El^2}{n^2\pi^2}\right)^{-1} < \left(1+\frac{2El^2}{n^2\pi^2}\right), \tag{D.21}$$

3. $x \geq 0 \Rightarrow e^{-x} > 1-x$, **(proof?)**

we have, for $n > \frac{l}{\pi}\sqrt{2E}$

$$|a_n(\xi) - b_n(\xi)| < \frac{l}{n\pi}\exp\left[-\frac{n\pi}{2l}\xi\right]\left[\left(1+\frac{2El^2}{n^2\pi^2}\right) - \left(1-\frac{El}{\pi n}\xi\right)\right]. \tag{D.22}$$

So

$$|a_n(\xi) - b_n(\xi)| < \frac{l}{n\pi}\exp\left[-\frac{n\pi}{2l}\xi\right]\left[\frac{El}{n\pi}\xi + \frac{2El^2}{n^2\pi^2}\right]. \tag{D.23}$$

Therefore, for $M > \frac{l}{\pi}\sqrt{2E}$

$$\sum_{n=M}^{\infty} a_n(\xi) - b_n(\xi) < \exp\left[-\frac{M\pi}{2l}\xi\right]\left[\frac{2El^3}{\pi^3M^2}\frac{\frac{\pi}{2l}\xi}{1-\exp\left(-\frac{\pi}{2l}\xi\right)} + \frac{El^3}{M^2\pi^3}\right]. \tag{D.24}$$

But $\frac{x}{1-e^{-x}}$ is a monotonically increasing function of x so $\frac{\frac{\pi}{2l}\xi}{1-\exp\left(-\frac{\pi}{2l}\xi\right)} < \frac{\frac{\pi}{2l}h}{1-\exp\left(-\frac{\pi}{2l}h\right)}$ and thus

$$\sum_{n=M}^{\infty}\left[a_n(\xi) - b_n(\xi)\right] < \exp\left[-\frac{M\pi}{2l}\xi\right]\left[\frac{El^2}{\pi^2M^2}\frac{h}{1-\exp\left(-\frac{\pi}{2l}h\right)} + \frac{El^3}{M^2\pi^3}\right]. \tag{D.25}$$

Thus $\sum_{n=M}^{\infty}\left[a_n(\xi) - b_n(\xi)\right]$ converges for all $\xi \geq 0$.

Further, since $\frac{El}{n\pi}\xi\exp\left[-\frac{n\pi}{2l}\xi\right] < \frac{2El^2}{n^2\pi^2}$,

$$|a_n(\xi) - b_n(\xi)| < \frac{4El^3}{n^3\pi^3} = f_n, \tag{D.26}$$

and $\sum_{n=M}^{\infty} f_n$ converges. Therefore $\sum_{n=M}^{\infty}\left[a_n(\xi) - b_n(\xi)\right]$ converges *uniformly* with respect to ξ for $\xi \geq 0$

Appendix E

Mathematical Miscellany for Two Dimensions

E.1 Polar Coordinates

$$\nabla = \frac{\partial}{\partial r}\hat{r} + \frac{\partial}{\partial \theta}\hat{\theta} \tag{E.1}$$

$$\nabla^2 = \frac{1}{r}\frac{\partial}{\partial r} r \frac{\partial}{\partial r} + \frac{1}{r^2}\frac{\partial^2}{\partial \theta^2} \tag{E.2}$$

E.2 Bessel Expansions

$$e^{ikr} = \sum_{l=-\infty}^{\infty} (i)^l \, J_l(kr) \tag{E.3}$$

$$e^{iky} = e^{ikr\sin\theta} = \sum_{l=-\infty}^{\infty} J_l(kr) e^{il\theta} \tag{E.4}$$

$$e^{ikx} = e^{ikr\cos\theta} = \sum_{l=-\infty}^{\infty} (i)^l \, J_l(kr) \, \cos l\theta \tag{E.5}$$

$$\sin ky = \sin(kr\sin\theta) = \sum_{l=-\infty}^{\infty} J_{2l+1}(kr) \, \sin([2l+1]\theta) \tag{E.6}$$

$$\sin kx = \sin(kr\cos\theta) = \sum_{l=-\infty}^{\infty} (-1)^l \, J_{2l+1}(kr) \, \cos([2l+1]\theta) \tag{E.7}$$

$$\tag{E.8}$$

E.3 Asymptotics as $kr \to \infty$

$$J_n(kr) \approx \sqrt{\frac{2}{\pi kr}} \cos\left(kr - \frac{n\pi}{2} - \frac{\pi}{4}\right) \tag{E.9}$$

$$Y_n(kr) \approx \sqrt{\frac{2}{\pi kr}} \sin\left(kr - \frac{n\pi}{2} - \frac{\pi}{4}\right) \tag{E.10}$$

$$H_n^{(1)}(kr) \approx \sqrt{\frac{2}{\pi kr}}\, e^{i\left(kr - \frac{n\pi}{2} - \frac{\pi}{4}\right)} \tag{E.11}$$

$$H_n^{(1)}(kr)^* = H_n^{(2)}(kr) \approx \sqrt{\frac{2}{\pi kr}}\, e^{-i\left(kr - \frac{n\pi}{2} - \frac{\pi}{4}\right)} \tag{E.12}$$

(E.13)

E.4 Limiting Form for Small Arguments ($kr \to 0$)

$$J_n(kr) \sim \frac{\left(\frac{1}{2}kr\right)^n}{\Gamma(n)} \text{ for } n \neq -1, -2, -3 \cdots \tag{E.14}$$

$$Y_o(kr) \sim (2/\pi) \ln kr \tag{E.15}$$

$$H_o^{(1)}(kr) \sim (2i/\pi) \ln kr \tag{E.16}$$

$$Y_n(kr) \sim -\frac{1}{\pi}\Gamma(n)\left(\frac{kr}{2}\right)^{-n} \text{ for } \mathrm{Re}\{n\} > 0 \tag{E.17}$$

$$H_n^{(1)}(kr) \sim -\frac{i}{\pi}\Gamma(n)\left(\frac{kr}{2}\right)^{-n} \text{ for } \mathrm{Re}\{n\} > 0 \tag{E.18}$$